

Exploring the process window for production of itaconic, 2-hydroxyparaconic, and itatartaric acid with engineered *Ustilago* strains

Philipp Ernst

Schlüsseltechnologien / Key Technologies

Band / Volume 293

ISBN 978-3-95806-825-4

Forschungszentrum Jülich GmbH
Institut für Bio- und Geowissenschaften (IBG)
Biotechnologie (IBG-1)

Exploring the process window for production of itaconic, 2-hydroxyparaconic, and itatartaric acid with engineered *Ustilago* strains

Philipp Ernst

Schriften des Forschungszentrums Jülich
Reihe Schlüsseltechnologien / Key Technologies

Band / Volume 293

ISSN 1866-1807

ISBN 978-3-95806-825-4

Bibliografische Information der Deutschen Nationalbibliothek.
Die Deutsche Nationalbibliothek verzeichnet diese Publikation in der
Deutschen Nationalbibliografie; detaillierte Bibliografische Daten
sind im Internet über <http://dnb.d-nb.de> abrufbar.

Herausgeber
und Vertrieb: Forschungszentrum Jülich GmbH
Zentralbibliothek, Verlag
52425 Jülich
Tel.: +49 2461 61-5368
Fax: +49 2461 61-6103
zb-publikation@fz-juelich.de
www.fz-juelich.de/zb

Umschlaggestaltung: Grafische Medien, Forschungszentrum Jülich GmbH

Druck: Grafische Medien, Forschungszentrum Jülich GmbH

Copyright: Forschungszentrum Jülich 2025

Schriften des Forschungszentrums Jülich
Reihe Schlüsseltechnologien / Key Technologies, Band / Volume 293

D 61 (Diss. Düsseldorf, Univ., 2024)

ISSN 1866-1807
ISBN 978-3-95806-825-4

Vollständig frei verfügbar über das Publikationsportal des Forschungszentrums Jülich (JuSER)
unter www.fz-juelich.de/zb/openaccess.



This is an Open Access publication distributed under the terms of the [Creative Commons Attribution License 4.0](https://creativecommons.org/licenses/by/4.0/),
which permits unrestricted use, distribution, and reproduction in any medium, provided the original work is properly cited.

In der Mitte von Schwierigkeiten liegen die Möglichkeiten.

- Albert Einstein -

The research presented in this dissertation has been published in the following manuscripts:

J. Becker*, H. Hosseinpour Tehrani*, **P. Ernst***, L. M. Blank, and N. Wierckx (2021). An Optimized *Ustilago maydis* for Itaconic Acid Production at Maximal Theoretical Yield. *J Fungi (Basel)*, 7(1), 20. doi: 10.3390/jof7010020

*These authors contributed equally to this work.

P. Ernst, K. M. Saur, R. Kiefel, P.-J. Niehoff, R. Weskott, J. Büchs, A. Jupke, and N. Wierckx (2024). Balancing pH and Yield: Exploring Itaconic Acid Production in *Ustilago cynodontis* from an Economic Perspective. *Biotechnol Biofuels Bioprod*, 17(1), 103. doi: 10.1186/s13068-024-02550-0

P. Ernst, A. Wirtz, B. Wynands, and N. Wierckx (2024). Establishing an Itaconic Acid Production Process with *Ustilago* species on the Low-cost Substrate Starch. *FEMS Yeast Res*, 24, foae023. doi: 10.1093/femsyr/foae023

P. Ernst, F. Zlati, L. Kever, A. Wirtz, R. Goldbaum, J. Pietruszka, B. Wynands, J. Frunzke, and N. Wierckx (2024). Selective Production of the Itaconic Acid-derived Compounds 2-Hydroxyparaconic and Itatartaric Acid. *Metab Eng Commun*, 19, e00252. doi: 10.1016/j.mec.2024.e00252

Further published manuscripts not included in this dissertation:

P.-J. Niehoff, W. Müller, J. Pastoors, K. Miebach, **P. Ernst**, J. Hemmerich, S. Noack, N. Wierckx, and J. Büchs (2023). Development of an Itaconic Acid Production Process with Ustilaginaceae on Alternative Feedstocks. *BMC Biotechnol*, 23(1), 34. doi: 10.1186/s12896-023-00802-9

K. M. Saur, R. Kiefel, P.-J. Niehoff, J. Hofstede, **P. Ernst**, J. Brockkötter, J. Gätgens, J. Viell, S. Noack, N. Wierckx, J. Büchs, and A. Jupke (2023). Holistic Approach to Process Design and Scale-Up for Itaconic Acid Production from Crude Substrates. *Bioengineering (Basel)*, 10(6), 723. doi: 10.3390/bioengineering10060723

J. de Witt, **P. Ernst**, J. Gätgens, S. Noack, D. Hiller, B. Wynands, and N. Wierckx (2023). Characterization and Engineering of Branched Short-chain Dicarboxylate Metabolism in *Pseudomonas* reveals Resistance to Fungal 2-Hydroxyparaconate. *Metab Eng*, 75, 205-216. doi: 10.1016/j.ymben.2022.12.008

T. Helm, T. Stausberg, M. Prevati, **P. Ernst**, B. Klein, T. Busche, J. Kalinowski, W. Wiechert, L. Claerhout, N. Wierckx, and S. Noack (2024). Itaconate Production from Crude Substrates with *U. maydis*: Scale-up of an Industrially Relevant Bioprocess. *Microb Cell Factories*, 23, 29. doi: 10.1186/s12934-024-02295-3

Abbreviations

2-HP	2-hydroxyparaconate
AOX	alternative oxidase
CaCO ₃	calcium carbonate
Ca(OH) ₂	calcium hydroxide
CAZy	carbohydrate-active enzyme
CDW	cell dry weight
cf.	confer
DAD	diode array detector
ddH ₂ O	deionized water
DO	dissolved oxygen
DOE	Department of Energy
DS-FIA-MS/MS	dilute-and-shoot flow-injection-analysis tandem mass spectrometry
DSP	downstream processing
e.g.	exempli gratia
et al.	et alii
GC-ToF-MS	gas chromatography coupled to time-of-flight mass spectrometry
Glc	glucose
Gly	glycerol
GOI	gene of interest
HPLC	high performance liquid chromatography
ISPR	<i>in situ</i> product removal
ITA	itaconate
ITT	itatarate
KPIs	key performance indicators
MAPK	Ras/mitogen-activated protein kinase
MES	2-(<i>N</i> -morpholino)ethanesulfonic acid
Mg(OH) ₂	magnesium hydroxide
MTM	modified Tabuchi medium
NaOH	sodium hydroxide
NAD(P)	nicotinamide adenine (phosphate) dinucleotide
NDH-2	type 2 NADH:quinone oxidoreductase (alternative NADH dehydrogenase)
OD ₆₀₀	optical density at 600 nm
pH	negative logarithm of the hydronium ion concentration
pK _a	acid dissociation constant at logarithmic scale
(q)NMR	(quantitative) nuclear magnetic resonance spectroscopy
(q)PCR	(quantitative) polymerase chain reaction
RI	refraction index
TCA	tricarboxylic acid
Tet	tetracycline
U	units
vvm	volume of air per volume of medium per minute
WT	wildtype
YEPS	yeast extract, peptone, sucrose medium

Further abbreviations not included in this section can be found in the JCB abbreviation list under the following hyperlink: [Standard Abbreviations | Journal of Cell Biology | Rockefeller University Press \(rupress.org\)](https://www.jcb.org/standard-abbreviations/)

List of figures

Figure 1: Effects of an increasing world population and fossil-fuel overexploitation on climate development, and opportunities provided by the transition towards a sustainable, circular bioeconomy.	4
Figure 2: Key properties of itaconic acid. Data was taken from Willke and Vorlop (2001).	5
Figure 3: List of top value-added chemicals from biomass according to the DOE in 2004 and multifaceted applications of itaconic acid, divided into industrial applications and therapeutic properties.	7
Figure 4: Life cycle and cell morphology of <i>Ustilago</i> species.	9
Figure 5: Itaconate, 2-hydroxyparaconate, and itatartarate metabolism in <i>Ustilago</i> species and annotation of the respective enzymes.	12
Figure 6: System Duetz cultivations of morphology-engineered <i>U. maydis</i> MB215 strains in MTM with 15 mM NH ₄ Cl, 100 mM MES pH 6.5, and 50 g L ⁻¹ glucose.	27
Figure 7: System Duetz cultivations of <i>U. maydis</i> MB215 strains expressing <i>mttA</i> in MTM with 15 mM NH ₄ Cl, 100 mM MES pH 6.5, and 50 g L ⁻¹ glucose.	29
Figure 8: System Duetz cultivations of six <i>U. maydis</i> MB215 mutants in MTM with 15 mM NH ₄ Cl, 66 g L ⁻¹ CaCO ₃ pH 7.5, and 100 g L ⁻¹ glucose.	30
Figure 9: Production parameters of <i>U. maydis</i> MB215 $\Delta cyp3 \Delta MEL \Delta UGA \Delta dga1 \Delta P_{ria1}::P_{etef} \Delta fuz7$ transformants with different <i>mttA</i> copy numbers incubated in MTM with (A) 15 mM NH ₄ Cl, 100 mM MES pH 6.5, and 50 g L ⁻¹ glucose and (B) 15 mM NH ₄ Cl, 66 g L ⁻¹ CaCO ₃ pH 7.5, and 100 g L ⁻¹ glucose (n = 3 biological replicates).	31
Figure 10: High cell-density pulsed fed-batch fermentations of <i>U. maydis</i> strain K14.	32
Figure 11: High cell-density fed-batch fermentations with continuous feed of <i>U. maydis</i> strain K14.	33
Figure 12: Low cell-density fed-batch fermentations with continuous feed of <i>U. maydis</i> strain K14.	33
Figure 13: Graphical abstract showing the relationship of cell dry weight, yield, productivity, titer, and NaOH consumption during ITA production at different pH values in <i>U. cynodontis</i> ITA MAX pH (not submitted as part of the manuscript).	37

Figure 14: Fed-batch fermentations with continuous feed of <i>U. maydis</i> K14 with high ammonium concentration (A) and <i>U. cynodontis</i> ITA MAX pH with high (B) and low (C) ammonium concentration.....	41
Figure 15: High cell-density fed-batch fermentations with continuous feed of <i>U. cynodontis</i> ITA MAX pH at pH 3.6 (A) and pH 6.5 (B).	43
Figure 16: Fed-batch fermentations for the determination of the pH optimum for itaconate production with <i>U. cynodontis</i> ITA MAX pH.....	45
Figure 17: High cell-density fed-batch fermentations with a prolonged feeding phase of <i>U. cynodontis</i> ITA MAX pH.	46
Figure 18: Specific operational costs for fed-batch fermentations at different pH values.....	48
Figure 19: Graphical abstract displaying the amylolytic capabilities of <i>U. cynodontis</i> ITA MAX pH.	53
Figure 20: Shake flask cultivations of <i>U. cynodontis</i> ITA MAX pH and <i>U. maydis</i> K14 on gelatinized potato starch (A and B) and α -amylase pretreated potato starch (C) as a sole carbon source.....	56
Figure 21: High cell-density batch fermentations on gelatinized potato starch (A and C) and α -amylase pretreated potato starch (B and D) as a sole carbon source.	57
Figure 22: SDS-PAGE and LC-MS/MS analysis of <i>U. cynodontis</i> ITA MAX pH and <i>U. maydis</i> K14 culture supernatants.	60
Figure 23: Shake flask cultivations of <i>U. cynodontis</i> ITA MAX pH deletion mutants on gelatinized potato starch as a sole carbon source.	62
Figure 24: Amylolytic activity in supernatants of <i>U. cynodontis</i> ITA MAX pH and <i>U. maydis</i> K14 grown on gelatinized potato starch as a sole carbon source.....	63
Figure 25: Shake flask cultivations of <i>U. cynodontis</i> ITA MAX pH constitutively expressing the native α -amylase gene on gelatinized potato starch as a sole carbon source.....	65
Figure 26: Graphical abstract displaying strategies employed to increase product specificity. 73	
Figure 27: Screening of different <i>U. cynodontis</i> ITA MAX pH_ <i>P_{eteI}cyp3</i> clones regarding production of 2-HP and ITT as the two downstream products of ITA.....	76
Figure 28: System Duetz microcultivations of <i>U. cynodontis</i> 2-HP on two different carbon sources.	78

Figure 29: High cell-density batch fermentations of <i>U. cynodontis</i> 2-HP on two different carbon sources.	79
Figure 30: Schematic representation showing the purification procedure of 2-HP and ITT from culture supernatants.	81
Figure 31: ^{13}C NMR spectra and corresponding structures of 2-HP and ITT. Each peak with different chemical shift and unique shape corresponds to a carbon atom.	82
Figure 32: System Duetz microcultivations of <i>U. cynodontis</i> 2-HP_Δ <i>itp1</i> and <i>U. cynodontis</i> 2-HP_Δ <i>itp1::mfsA</i> (henceforth named <i>U. cynodontis</i> 2-HP MfsA) on two different carbon sources for analyzing ITA, 2-HP and ITT production.....	83
Figure 33: System Duetz microcultivations of <i>U. cynodontis</i> 2-HP and <i>U. cynodontis</i> 2-HP MfsA on glucose using CaCO_3 as buffer.....	85
Figure 34: Fermentation approaches of <i>U. cynodontis</i> 2-HP MfsA to optimize 2-HP and ITT production.	89
Figure 35: Overview of feedstock generations for bio-based production. Images of first to third generation feedstocks were taken from Lips (2022).....	107

List of supplementary figures

Figure S1: Low cell-density pulsed fed-batch fermentations of <i>U. maydis</i> strain K14.....	134
Figure S2: Scatter plot of yield versus volumes of 5 M NaOH.	135
Figure S3: Carbon balance of all fermentations.	135
Figure S4: Crystallization of ITA from batch fermentations conducted at pH 3.6 and pH 2.8.	136
Figure S5: High cell-density batch fermentation of <i>U. cynodontis</i> ITA MAX pH with thick juice as a sole carbon source.....	137
Figure S6: Block flow diagram of multiple crystallization process (simplified from Saur et al. (2023).	137
Figure S7: Amino acid sequence of putative glucoamylase encoded by the gene with the GenBank accession number CAKMX010000014 (region: 83686 to 85185) in <i>U. cynodontis</i> ITA MAX pH identified by LC-MS/MS.....	139
Figure S8: Amino acid sequence of putative exo- α -1,5-L-arabinofuranosidase encoded by the gene with the GenBank accession number CAKMX010000018 (region 665749 to 665919, 666077 to 666352, and 666447 to 667148) in <i>U. cynodontis</i> ITA MAX pH identified by LC-MS/MS.	139
Figure S9: Amino acid sequence of putative aryl-alcohol oxidase encoded by the gene with GenBank accession number CAKMX010000011 (region 416218 to 416544 and 416702 to 418270) in <i>U. cynodontis</i> ITA MAX pH identified by LC-MS/MS.....	139
Figure S10: Initial screening of 22 clones in System Duetz plates – endpoint measurement after 240 h.....	141
Figure S11: pH values during System Duetz microcultivations of <i>U. cynodontis</i> 2-HP, <i>U. cynodontis</i> 2-HP_Δ <i>itp1</i> , and <i>U. cynodontis</i> 2-HP MfsA.....	141
Figure S12: Non-enzymatic equilibration between 2-HP and ITT under acidic conditions (pH 2.3) at room temperature.	141

List of tables

Table 1: Selected fermentation performances of wildtype and genetically engineered strains of <i>A. terreus</i> , <i>U. maydis</i> , and <i>U. cynodontis</i> with regard to ITA production.....	15
Table 2: <i>U. maydis</i> MB215 strains used in this study.....	24
Table 3: Plasmids used in this study.	26
Table 4: Itaconate production parameters of engineered strains of the <i>U. maydis</i> MB215 ITA chassis $\Delta cyp3 \Delta MEL \Delta U A \Delta d g a t \Delta P_{ria1}::P_{etef}$ (n = 3 biological replicates).....	28
Table 5: Determination of $P_{etef} mttA$ copy number in five <i>U. maydis</i> MB215 $\Delta cyp3 \Delta MEL \Delta U A \Delta d g a t \Delta P_{ria1}::P_{etef} \Delta f u z 7 P_{etef} mttA$ transformants by qPCR (n = 3 biological replicates).....	31
Table 6: Putative enzymes present in <i>Ustilago</i> species cleaving α -1,4 and α -1,6-bonds between glucose molecules.....	56
Table 7: <i>Ustilago</i> strains used in this study.	66
Table 8: Plasmids used in this study.	71
Table 9: Elemental analysis of the purified 2-HP.....	82
Table 10: KPIs of the different fermentation approaches, calculated for the endpoint titers..	91
Table 11: <i>U. cynodontis</i> strains used in this study.	92
Table 12: Plasmids used in this study.	96
Table 13: KPIs obtained during optimized continuous low cell-density fed-batch fermentations.	99

List of supplementary tables

Table S1: Oligonucleotides used for deletion and overexpression constructs.	133
Table S2: Production parameters of two engineered <i>U. maydis</i> MB215 strains in two different types of fed-batch fermentations.	134
Table S3: Feeding profile with 70 % w/v glucose solution during high cell-density fed-batch fermentation with a prolonged feeding phase of <i>U. cynodontis</i> ITA MAX pH (Figure 17).	138
Table S4: Oligonucleotides used for the generation of deletion and overexpression constructs.	140
Table S5: Oligonucleotides used for deletion, exchange and overexpression constructs.	142

Table of contents

Abbreviations.....	ii
List of figures.....	iii
List of supplementary figures.....	vi
List of tables.....	vii
List of supplementary tables.....	viii
1. Abstracts.....	1
1.1. Summary.....	1
1.2. Zusammenfassung.....	2
2. Scientific context.....	3
2.1. Towards a sustainable bioeconomy	3
2.2. Itaconic acid: A value-added platform chemical	4
2.2.1. Versatile applications: Industrial building block and therapeutic agent.....	5
2.2.2. Microbial itaconic acid production: A historical perspective	7
2.3. <i>Ustilago</i> as microbial production host for itaconic acid.....	8
2.3.1. Regulation of itaconic acid production in <i>Ustilago</i> species.....	10
2.3.2. Genetic and process engineering towards increased itaconic acid production..	13
2.4. Scope of this thesis.....	17
3. Publications and manuscripts	18
3.1. An Optimized <i>Ustilago maydis</i> for Itaconic Acid Production at Maximal Theoretical Yield	20
3.1.1. Introduction.....	21
3.1.2. Materials and methods.....	23
3.1.3. Results and discussion	26
3.1.4. Conclusion	35
3.2. Balancing pH and Yield: Exploring Itaconic Acid Production in <i>Ustilago cynodontis</i> from an Economic Perspective.....	36
3.2.1. Introduction.....	38
3.2.2. Results and discussion	40
3.2.3. Conclusion	48
3.2.4. Materials and methods.....	49

3.3. Establishing an Itaconic Acid Production Process with <i>Ustilago</i> species on the Low-cost Substrate Starch	52
3.3.1. Introduction	53
3.3.2. Results and discussion	55
3.3.3. Conclusion	65
3.3.4. Material and methods	66
3.4. Production and Characterization of the Itaconic Acid-derived Compounds 2-Hydroxyparaconic and Itatartaric Acid.....	72
3.4.1. Introduction	74
3.4.2. Results and discussion	75
3.4.3. Conclusion	90
3.4.4. Materials and methods.....	92
4. General discussion and perspectives	98
4.1. Itaconic acid hyper-producing <i>Ustilago</i> strains: Current limits and optimization approaches	98
4.2. Implementation of itaconic acid production in a circular bioeconomy concept	104
4.3. Production of value-added compounds beyond itaconic acid	108
4.4. Bioactivity of <i>Ustilago</i> -derived organic acids: An ecological perspective	111
5. Conclusion	114
6. References	115
7. Appendix	133
7.1. Appendix to 3.1: An Optimized <i>Ustilago maydis</i> for Itaconic Acid Production at Maximal Theoretical Yield	133
7.2. Appendix to 3.2: Balancing pH and Yield: Exploring Itaconic Acid Production in <i>Ustilago cynodontis</i> from an Economic Perspective	135
7.3. Appendix to 3.3: Establishing an Itaconic Acid Production Process with <i>Ustilago</i> species on the Low-cost Substrate Starch	139
7.4. Appendix to 3.4: Production and Characterization of the Itaconic Acid-derived Compounds 2-Hydroxyparaconic and Itatartaric Acid	141
Acknowledgements	143
Eidesstattliche Erklärung.....	145

1. Abstracts

1.1. Summary

To combat the current challenges of overpopulation, global warming and the limited availability of fossil resources, the linear petrochemical-based industry needs to be replaced by a more sustainable bioeconomy. Therefore, economic production of bio-based platform chemicals such as itaconic acid is an emerging research topic. Itaconic acid is a versatile monomer in the polymer industry and has also high relevance in the medical and pharmaceutical sectors due to its anti-microbial and anti-inflammatory properties. Up to now, itaconic acid is commercially produced by the fungus *Aspergillus terreus*, but its filamentous morphology poses major limitations on bioprocess technology developments and elevates production costs. Thus, current efforts are focusing on the dimorphic basidiomycete *Ustilago* as an alternative, natural itaconic acid producer, which offers several advantages including a stable yeast-like morphology, robustness and biosafety.

In previous studies, *Ustilago maydis* und *Ustilago cynodontis* have already been deeply engineered to optimize itaconate production. In frame of this thesis, established modifications from two different itaconate-hyperproducing *U. maydis* strains were consolidated into one strain named *U. maydis* K14. This strain 1) features stable yeast-like growth due to deletion of *fuz7* involved in filamentous development, 2) produces less by-products due to deletion of competing pathways (Δ MEL, Δ UA, Δ dgat, Δ cyp3), and 3) circumvents enzymatic bottlenecks by overproduction of the itaconate cluster regulator *Ria1* and the mitochondrial *cis*-aconitate transporter *MttA* from *A. terreus*. A lower osmotolerance of *U. maydis* K14 as a side effect of this engineering was counteracted by a continuous glucose feeding strategy in high and low cell-density fed-batch fermentations. With the latter strategy, high product titers with the maximum theoretical substrate-to-product yield of $0.72 \pm 0.02 \text{ g}_{\text{ITA}} \text{ g}_{\text{GLC}}^{-1}$ during the production phase were obtained, thereby mastering one of the main challenges during fungal itaconate production.

However, improving economics is not just about optimizing individual parameters such as yield, titer and productivity, but also about minimizing main cost drivers such as base and acid consumption during fermentation and downstream processing, respectively. Using the previously engineered and naturally acid-tolerant *U. cynodontis* ITA MAX pH (Δ fuz7 Δ cyp3 *P_{etef}mttA P_{ria1}fia1*), the process window of itaconate production with regard to pH was systematically explored in continuous fed-batch fermentations aiming at a rational analysis of operational costs. A subsequent techno-economic analysis exposed that a production pH of 3.6 provided the best trade-off between yield, titer and productivity on the one hand, and the use of base and acid and associated salt waste production on the other hand.

While such process optimizations are usually carried out using the conventional feedstock glucose, long-term solutions for bio-based production processes envisage the usage of unprocessed, low-cost feedstocks in order to further reduce production costs and meet the circular bioeconomy concept. In this context, this thesis revealed the natural production of the amylolytic enzymes glucoamylase and α -glucosidase by *U. cynodontis* ITA MAX pH, enabling the utilization of starch as feedstock for itaconate production. Production was optimized by overexpression of an α -amylase gene otherwise not expressed under the applied conditions.

In addition to itaconate, *Ustilago* species produce the two itaconate derivatives 2-hydroxyparaconate and itatartarate, which are potential novel anti-microbial drug candidates. To restore 2-hydroxyparaconate and itatartarate production in *U. cynodontis* ITA MAX pH, the itaconate-oxidizing P450 monooxygenase gene *cyp3* was overexpressed under a constitutive promotor, yielding a product mixture of itaconate, 2-hydroxyparaconate and itatartarate. Derivatives specificity was increased by using glycerol as alternative carbon source, exchanging the native itaconate transporter *Itp1* with the one from *A. terreus* (*MfsA*), and low pH conditions. In batch fermentations on glycerol, this strain was able to produce 2-hydroxyparaconate and itatartarate with $100 \pm 0.0 \%$ derivatives specificity, allowing subsequent purification of both, not yet commercially available products for structural and biochemical characterization.

In conclusion, this thesis demonstrates that an integrated approach of strain and process engineering can provide major advances for optimizing economic feasibility of itaconate, 2-hydroxyparaconate and itatartarate production with *Ustilago* species in a biorefinery context, thereby enabling an expanded production of bio-based building blocks of industrial and potentially also pharmaceutical relevance.

1.2. Zusammenfassung

Um aktuelle Herausforderungen wie Überbevölkerung, globale Erwärmung und die begrenzte Verfügbarkeit fossiler Ressourcen zu bewältigen, muss die lineare petrochemische Industrie durch eine nachhaltigere Bioökonomie ersetzt werden. In diesem Zusammenhang ist die ökonomische Produktion von biobasierten Plattformchemikalien wie Itaconsäure ein wichtiges Forschungsthema. Itaconsäure ist ein vielseitiges Molekül in der Polymerindustrie und hat aufgrund seiner anti-mikrobiellen und entzündungshemmenden Eigenschaften auch große Bedeutung im medizinischen und pharmazeutischen Sektor. Bisher wird Itaconsäure kommerziell durch den Pilz *Aspergillus terreus* hergestellt. Jedoch stellt seine filamentöse Morphologie eine große Einschränkung für die Entwicklung von Bioprozesstechnologien dar und trägt zu erhöhten Produktionskosten bei. Daher konzentrieren sich aktuelle Studien auf den dimorphen Basidiomyceten *Ustilago* als alternativen, natürlichen Itaconsäureproduzenten, der mehrere Vorteile bietet, darunter eine stabile hefeartige Morphologie, Robustheit und biologische Sicherheit.

In früheren Projekten wurden *Ustilago maydis* und *Ustilago cynodontis* bereits stark modifiziert, um die Itaconat-Produktion zu optimieren. Im Rahmen dieser Arbeit wurden etablierte Modifikationen von zwei verschiedenen Itaconat-hyperproduzierenden *U. maydis* Stämmen in einem Stamm namens *U. maydis* K14 konsolidiert. Dieser Stamm zeigt 1) ein stabiles hefeartiges Wachstum durch die Deletion von *fuz7*, dass an der Filament-Entwicklung beteiligt ist, 2) produziert weniger Nebenprodukte aufgrund der Deletion konkurrierender Stoffwechselwege (Δ MEL, Δ UA, Δ dgt, Δ cyp3) und 3) umgeht enzymatische Engpässe durch Überproduktion des Itaconat-Cluster-Regulators *Ria1* und des mitochondrialen *cis*-Aconitat Transporters *MttA* aus *A. terreus*. Einer geringeren Osmotoleranz von *U. maydis* K14 als Nebeneffekt dieser Modifizierungen wurde durch eine kontinuierliche Glukosezufuhr in Fed-Batch Fermentationen unter Hoch- und Niedrigzelldichte-Bedingungen entgegengewirkt. Mit der letztgenannten Strategie konnten hohe Produkttiter mit der maximal möglichen Substrat-zu-Produkt Ausbeute von $0,72 \pm 0,02$ g_{ITA} g_{GLC}⁻¹ während der Produktionsphase erzielt werden, wodurch eine der wichtigsten Herausforderungen der Pilz-basierten Itaconat-Produktion gemeistert wurde.

Bei der Verbesserung der Wirtschaftlichkeit geht es jedoch nicht nur um die Optimierung einzelner Parameter wie Ausbeute, Titer und Produktivität, sondern auch um die Minimierung von Kostentreibern wie Base- und Säureverbrauch während der Fermentation bzw. der nachgeschalteten Produktaufarbeitung. Unter Verwendung des zuvor für die Itaconat-Produktion optimierten und von Natur aus säuretoleranten *U. cynodontis* ITA MAX pH (Δ fuz7 Δ cyp3 *P_{ete}mmtA P_{ria1}ria1*) wurde das Prozessfenster für die Produktion von Itaconat in Bezug auf den pH-Wert in kontinuierlichen Fed-Batch Fermentationen systematisch untersucht, um eine rationale Analyse der Produktionskosten zu ermöglichen. Eine anschließende techno-ökonomische Analyse ergab, dass ein Produktions-pH-Wert von 3,6 den optimalen Kompromiss zwischen Ausbeute, Titer und Produktivität auf der einen Seite, und dem Verbrauch von Basen und Säuren und der damit verbundenen Produktion von Salzabfällen auf der anderen Seite, darstellt.

Während solche Prozessoptimierungen in der Regel mit dem konventionellen Substrat Glukose durchgeführt werden, sehen langfristige Lösungen für biobasierte Produktionsprozesse die Verwendung unverarbeiteter, industrieller Nebenströme vor, um die Produktionskosten weiter zu senken und dem Konzept der zirkulären Bioökonomie zu entsprechen. In diesem Zusammenhang wurde in dieser Arbeit gezeigt, dass *U. cynodontis* ITA MAX pH natürlicherweise amylolytische Enzyme wie Glucoamylasen und α -Glucosidasen sekretiert, was die Verwertung von Stärke als Ausgangsmaterial für die Itaconat-Produktion ermöglicht. Durch die Überexpression eines α -Amylase-Gens, welches unter den angewandten Bedingungen normalerweise nicht exprimiert wird, konnte die Produktion optimiert werden.

Ustilago produziert neben Itaconat auch die beiden Itaconat-Derivate 2-Hydroxyparaconat und Itatartarat, welche potenziell vielversprechende, neue anti-mikrobielle Wirkstoffe darstellen. Zur Wiederherstellung der Produktion von 2-Hydroxyparaconat und Itatartarat in *U. cynodontis* ITA MAX pH wurde das Itaconat-oxidierende P450-Monooxygenase Gen *cyp3* unter einem konstitutiven Promotor überexprimiert, was zur Bildung eines Gemischs aus Itaconat, 2-Hydroxyparaconat und Itatartarat führte. Die Spezifität der Derivate konnte durch die Verwendung von Glycerin als alternative Kohlenstoffquelle, den Austausch des nativen Itaconat-Transporters *Itp1* mit dem aus *A. terreus* (MfsA) und niedriger pH-Bedingungen gesteigert werden. In Batch-Fermentationen mit Glycerin war dieser Stamm in der Lage, 2-Hydroxyparaconat und Itatartarat mit einer Derivatspezifität von $100 \pm 0,0\%$ zu produzieren, was eine anschließende Aufarbeitung der beiden noch nicht kommerziell erhältlichen Produkte zur strukturellen und biochemischen Charakterisierung ermöglichte.

Zusammenfassend zeigt diese Arbeit, dass durch einen integrierten Ansatz von Stamm- und Prozessentwicklung wichtige Fortschritte erzielt werden können, um die wirtschaftliche Machbarkeit der Produktion von Itaconat, 2-Hydroxyparaconat und Itatartarat mittels *Ustilago* im Kontext einer Bioraffinerie zu optimieren. Dies ermöglicht eine erweiterte Herstellung von biobasierten Chemikalien mit industrieller und möglicherweise auch pharmazeutischer Relevanz.

2. Scientific context

2.1. Towards a sustainable bioeconomy

The world's population has grown considerably over the last century, from around 2 billion people at the beginning of the 20th century to more than 8 billion at the end of 2022. According to projections, this population growth will continue - albeit at a slower pace - and approach the 10 billion mark by 2050 (Gerland et al., 2022), thereby raising the global energy and food demand and challenging global economy.

To date, our economy relies mainly on oil, gas and coal as fossil fuels for power generation, electricity, heat, transportation and industrial production, accounting for more than 80 % of the global energy mix in 2020 (Khan et al., 2022). However, combustion of fossil fuel emits high amounts of CO₂ and massively contributes to the current climate crises. Increasing global temperatures have led to extreme weather events, challenging food production and threatening human existence (Duchenne-Moutien & Neetoo, 2021). Global warming together with the limited availability of these resources highlights the importance to reduce their anthropogenic overexploitation and to develop sustainable, climate-friendly alternatives in order to meet the Paris climate agreement and the 2-degree target (Kircher, 2021; Watson et al., 2016). Facing this necessity, the initiated transition towards a sustainable, circular bioeconomy is considered a core concept of the European Green Deal policy launched in 2019 (Figure 1) (European Commission, 2019; Liobikienė & Miceikienė, 2023). It aims at the utilization of renewable biological energy and carbon sources for sustainable production of value-added, bio-based products and bioenergy (referred to as bioeconomy), and at minimizing or valorizing waste (referred to as circular economy) (Tan & Lamers, 2021).

Besides the electric power and transport sector (EIA, 2023), the chemical industry is considered as one of the largest consumer of fossil fuels, as it uses fossil fuels both as energy source and as feedstock for chemical production processes, causing approximately 5 % of the global CO₂ emission. However, with more than 70,000 products, the chemical industry plays an essential role in our daily life by directly touching almost all manufactured goods (Gabrielli et al., 2023; Levi & Cullen, 2018; Philp, 2023; Rissman et al., 2020). The strong dependence of organic chemistry on carbon-containing resources, coupled with the integration of chemical building blocks in numerous supply chains of the manufacturing industry, has led to intensive research on defossilization by microbial biosynthesis of commercially important chemicals from renewable resources (Gabrielli et al., 2020). Yet, biotechnology faces several challenges when trying to compete with the fossil-based chemical industry. This is not at least conditioned by 1) decades of

process optimization in the petrochemical sector allowing rapid production of highly concentrated chemicals and 2) the necessity to prevent interference of the utilized bio-based feedstock with food supply chains to ensure food and nutrition security (Klement & Büchs, 2013; Philp, 2023). On the contrary, the required feedstock transition offers opportunities to obtain novel, sustainable products with improved properties (Klement & Büchs, 2013). In 2004, the Department of Energy (DOE) has identified the twelve most promising platform chemicals from over 300 bio-based building blocks, including itaconic acid (Werpy & Petersen, 2004).

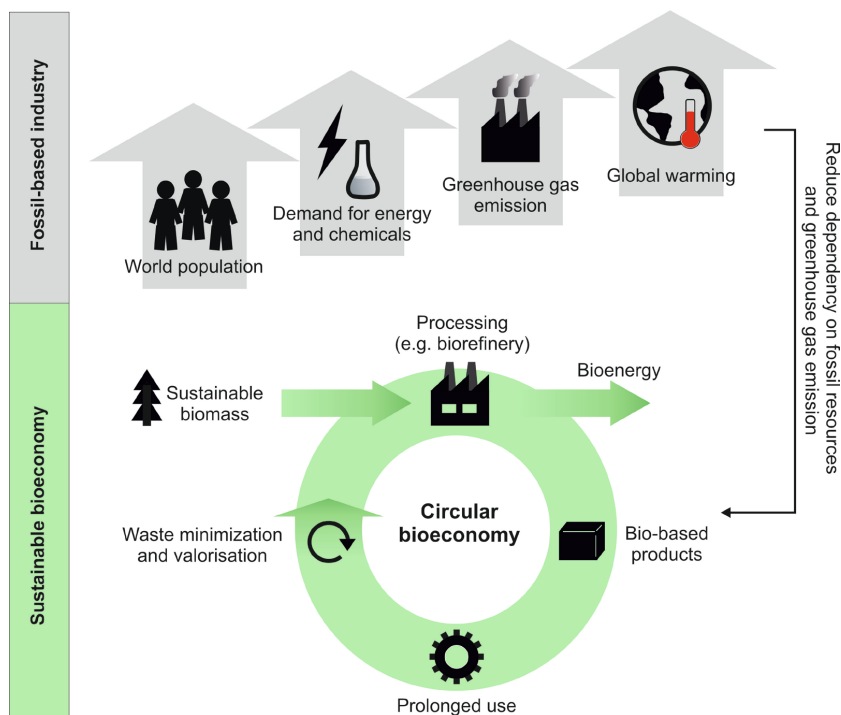


Figure 1: Effects of an increasing world population and fossil-fuel overexploitation on climate development, and opportunities provided by the transition towards a sustainable, circular bioeconomy. Schematic illustration of circular economy was designed based on Stegmann et al. (2020).

2.2. Itaconic acid: A value-added platform chemical

Itaconic acid (also known as methylenesuccinic acid or methylenebutanedioic acid) is a 5-C dicarboxylic acid with one methylene group and an α,β -unsaturated double bond, that can be chemically or biochemically synthesized (Kuenz & Krull, 2018). Due to its two carboxyl groups, itaconic acid has two pK_a values ($pK_{a1} = 3.84$ and $pK_{a2} = 5.55$ at 20 °C). As a result, the degree of acid dissociation is significantly influenced by pH (Rychtera & Wase, 2007). At pH values below 3.8, predominantly the non-dissociated acid is present, while at a pH above 5.6, mostly the

double-dissociated acid is prevalent. In the range of pH 3.8 to pH 5.6, a mixture of all dissociation forms occurs. All key properties of itaconic acid are summarized in Figure 2.

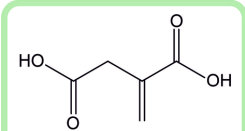
 <p>Itaconic acid (C₅H₆O₄)</p>	Molar mass	pK _a values	Appearance	
	130.1 g mol ⁻¹	3.84 and 5.55	White crystalline powder	
	Solubility in H ₂ O	Density	Melting point	Boiling point
	83 g L ⁻¹ (20 °C)	1.63 g (cm ³) ⁻¹	162 - 167 °C	268 °C

Figure 2: Key properties of itaconic acid. Data was taken from Willke and Vorlop (2001).

Although it was excluded from an updated list of the top value-added platform chemicals in 2010 due to a lack of studies (Bozell & Petersen, 2010), research on itaconic acid production and usage has increased substantially within the last years, as indicated by the number of itaconic acid-related publications (Web of Science Core Collection). While exact numbers about the current and projected market value for the next years vary dependent on the source used, they all agree in an increasing upward trend. According to the Verified Market Research (2022), this is reflected by a current market value of US\$ 98.4 million in 2022, predicted to grow to US\$ 168.7 million in 2030.

2.2.1. Versatile applications: Industrial building block and therapeutic agent

Due to its structural features and its biodegradability (de Witt et al., 2023), itaconic acid is a valuable monomer for a wide range of chemical reactions such as anhydride formation, esterification with alcohols, or homo- and copolymerization (Sollka & Lienkamp, 2021). Its application fields are diverse and continuously growing, with the potential to develop green analogs of existing fossil-derived materials (Figure 3). In particular, itaconic acid is considered as a potential substitute for acrylic and methyl acrylic acid in polyesters used for coatings, paints, fibers, resins, plastics etc. (Teleky & Vodnar, 2019). This addresses not only the inevitable reduction of fossil fuel consumption by the chemical industry, but also the demand for a higher biodegradation rate to combat plastic and microplastic pollution and its environmental impacts (Kim et al., 2023). Besides being used as a co-monomer for the production of styrene-butadiene rubber (SBR) and latex for paper coatings (Teleky & Vodnar, 2019), several fully bio-based itaconic acid containing elastomer (e.g. PDBIB: poly(dibutyl itaconate-co-butadiene); PDMIB: poly(dimethyl itaconate-co-butadiene)) have been developed, which even showed improved mechanical properties compared to conventional synthetic rubbers (Ji et al., 2023; Li et al., 2020). In addition, itaconic acid-containing polymers are utilized to produce hydrogels that serve as

superabsorbents for water decontamination, intelligent food packaging, drug delivery and other applications (Teleky & Vodnar, 2019). Just recently, polyitaconic acid was reported to be a bio-based, sustainable superabsorbent polymer with potential applications for ice packs, hygiene products and environmental packaging (Choi et al., 2022). Apart from that, itaconic acid serves as a precursor for 3-methyltetrahydrofuran, a promising biofuel candidate and an eco-friendly solvent (Hegde et al., 2016).

Besides its industrial applications, itaconic acid also has significant value in the medical and pharmaceutical sectors. It is of great interest due to its therapeutic properties, such as its ability to alleviate inflammatory diseases as recently reviewed by Shi et al. (2022) (Figure 3). It was discovered to be an immunometabolite massively produced upon inflammatory and pathogen-associated macrophage activation by decarboxylation of the TCA cycle intermediate *cis*-aconitate via IRG1 (immune responsive gene 1) (Michelucci et al., 2013; Strelko et al., 2011). Through its ability to reprogram immune cells at a transcriptional, metabolic or post-translational level, itaconic acid is considered as a key player in linking immune response, metabolism and inflammation (Shi et al., 2022). Its anti-inflammatory effects in mammals include for example the activation of anti-inflammatory transcription factors, inhibition of succinate dehydrogenase and regulation of TLR-mediated inflammatory cytokine production (Bambouskova et al., 2018; Lampropoulou et al., 2016; Mills et al., 2018). Furthermore, itaconic acid shows also promising anti-microbial properties. For instance, inhibition of the isocitrate lyase of the glyoxylate shunt strongly impairs bacterial growth during infection (McFadden & Purohit, 1977). Moreover, the cell-permeable derivative 4-octyl-itaconate showed anti-viral capacity by blocking for instance influenza virus A and SARS-CoV-2 replication (Olagnier et al., 2020; Ribó-Molina et al., 2023; Sohail et al., 2022), thereby representing a potent anti-viral drug candidate. Another itaconic acid derivative, hexylitaconic acid, even showed antitumor activity. It prevents cells from becoming cancerous by inhibiting the degradation of the tumor suppressor p53 (Tsukamoto et al., 2006).

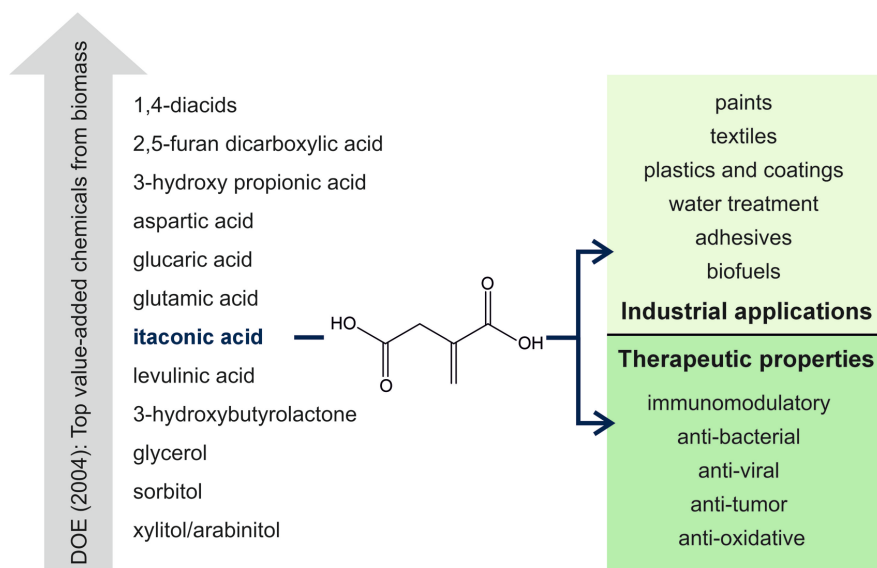


Figure 3: List of top value-added chemicals from biomass according to the DOE in 2004 and multifaceted applications of itaconic acid, divided into industrial applications and therapeutic properties.

2.2.2. Microbial itaconic acid production: A historical perspective

Itaconic acid was first described in 1836 as the product of citric acid pyrolysis and subsequent hydrolysis of the anhydrides formed and was therefore named “itaconic acid” as an anagram of “aconitic acid” (Baup, 1836; Goldberg & Rokem, 2009). In these early days, chemical synthesis by distillation of citric acid, decarboxylation of aconitic acid (Luskin, 1974), oxidation of isoprenes to citraconic acid with subsequent isomerization (Berg and Hetzel, 1978), or carboxylation of acetylene derivatives, was the only known way to obtain itaconic acid (Cunha da Cruz et al., 2018). More than 90 years later, Kinoshita reported the first biosynthesis of itaconate (ITA) during the fermentation of a filamentous fungus coining its name *Aspergillus itaconicus* (Kinoshita, 1931). In 1939, *Aspergillus terreus* was identified as a further, even better microbial production host and its submerged cultivation process for industrial-scale ITA production was subsequently patented and added to the product portfolio of Charles Pfizer & Co (Calam et al., 1939; Kane et al., 1945). Since the 1960s, the biotechnological process for ITA production with *A. terreus* has been continuously optimized, making it more economical than the chemical production processes (Tate, 1981) (Gopaliya et al., 2021). Currently, the biotechnological process accounts for an annual production of 80,000 tons (Okabe et al., 2009). Corresponding production facilities are highly concentrated in the Asia-Pacific area with major companies such as Qingdao Kehai Biochemistry Co., Ltd and Zhejiang Guoguang Biochemistry Co., Ltd. (Cunha da Cruz et al., 2018).

The biotechnological production of ITA by *A. terreus* was intensively studied with respect to nutrients, pH values, oxygen supply, and cultivation systems. Using a controlled pH of 3.4 during fed-batch fermentation of *A. terreus* wildtype on glucose, titers of up to 160 g L⁻¹ were achieved with an overall productivity of 0.56 to 0.99 g L⁻¹ h⁻¹ and a yield of 0.46 to 0.58 g_{ITA} g_{GLC}⁻¹ (Krull et al., 2017a) (Table 1, chapter 2.3.2). On the industrial scale, ITA is produced from pretreated molasses and starch hydrolysates as an alternative to glucose (Kuenz & Krull, 2018). However, despite decades of optimization efforts, the production cost of ITA remains higher than that of its petrochemical-derived counterparts acrylic and methacrylic acid, hindering a more extended usage of ITA (Kuenz & Krull, 2018; Okabe et al., 2009). According to the DOE report from 2004, production cost for ITA needs to be reduced to 0.5 US\$ kg⁻¹ to be competitive with its fossil-based analogs (Werpy & Petersen, 2004), although the exact number may have changed due to current economic circumstances. Considering the already high yield (up to 80 % of the theoretical maximum), high product titer, and decent productivity of the industrially established ITA production process with *A. terreus* (Klement & Büchs, 2013), further process improvement possibilities appear to be limited. This is due to several drawbacks when using *A. terreus* as production host. In this filamentous growing fungus, ITA production is dependent on a specific pellet-like morphology (Gyamerah, 1995), which showed a high sensitivity to medium impurities like metal ions. This makes the usage of alternative low-costs feedstocks like lignocellulosic biomass without expensive pretreatment challenging (Kuenz & Krull, 2018). Also, its filamentous growth is usually associated with an increased viscosity of cultivation broth and impaired local oxygen supply (Kuenz & Krull, 2018). Thus, a compromise between sufficient oxygen supply and minimum mechanical stress due to increasing stirring intensities is required for morphological control, overall entailing a more complicated handling and increased production cost (Klement & Büchs, 2013). As a result, innovation is required in other aspects of the process window. Non-conventional ITA-producing yeasts such as *Ustilago*, *Candida*, or *Pseudozyma* (Krull et al., 2020; Levinson et al., 2006; Tabuchi et al., 1981) have the potential to revolutionize ITA production. This is attributed to 1) their unicellular morphology providing a higher degree of freedom in handling of the fermentation broth and 2) their reduced sensitivity to medium impurities, which is outlined in more detail in the following chapters.

2.3. *Ustilago* as microbial production host for itaconic acid

Ustilago species are fungal plant pathogens belonging to phylum Basidiomycota (Banuett, 1995). Their life cycle is characterized by a yeast-mycelium dimorphism, which is associated to its pathogenicity. The life cycle starts with the germination of a diploid teliospore and meiotic

division leading to haploid basidiospores. These basidiospores multiply by cell budding and represent the yeast-like, non-pathogenic growth phase of *Ustilago*. Pheromone signaling triggers the formation of conjugation tubes that extend in the direction of the gradient to reach compatible mating partners (Bölker, 2001; Vollmeister et al., 2012). The fusion of two haploid basidiospores differing at both mating loci, *a* and *b*, initiates transition to filamentous, pathogenic dikaryotes. Infection of plants is mediated by specialized cell structures at the hyphal tips facilitating plant penetration, which finally leads to tumor formation upon enormous proliferation of intracellular mycelial structures. Further morphological development results in the formation of teliospores, which are released upon tumor rupture, completing the fungal life cycle (Bölker, 2001; Vollmeister et al., 2012) (Figure 4A and B).

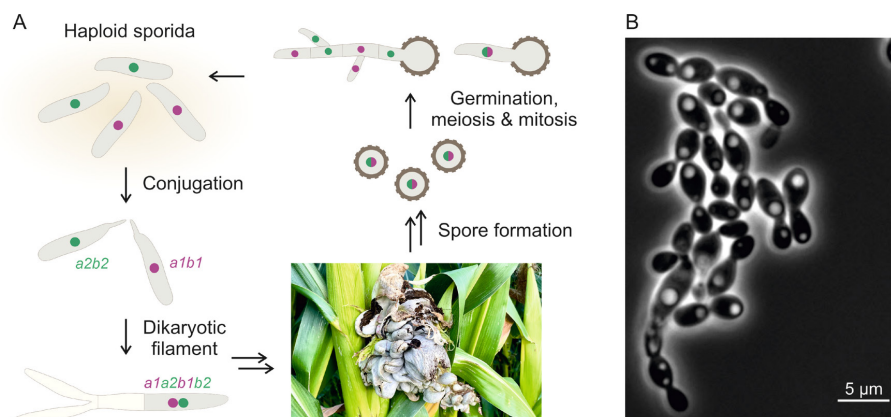


Figure 4: Life cycle and cell morphology of *Ustilago* species.

(A) Life cycle of *Ustilago* species showing the yeast-mycelium dimorphism. Whereas haploid cells show yeast-like growth, fusion of two cells with opposite mating types initiates transition towards pathogenic, filamentous growth causing severe disease symptoms upon plant infection, as exemplified by the maize smut caused by *Ustilago maydis*. The rupture of tumors releases mature spores into the environment, which can germinate under favorable conditions to begin a new life cycle. Design of the figure was inspired by Feldbrügge et al. (2004) and Saville et al. (2012). (B) Microscopic image of haploid *Ustilago cynodontis* cells showing yeast-like growth.

Studies about these basidiomycetes focus mainly on the model species *U. maydis*, but there is also a growing interest in *U. cynodontis* when it comes to ITA production. Their names were coined by their pathogenic behavior causing maize smut and Bermuda grass smut, respectively (Banuett, 1995; García-Guzmán & Burdon, 1997). In addition to their dimorphism, *Ustilago* species harbor several features making them suitable production hosts for a broad variety of compounds. In the haploid form, the unicellular, yeast-like morphology is accompanied by high robustness to medium impurities and hydromechanical stress, a moderate doubling time of about two hours, and the capability to achieve high cell-densities on glucose (Becker et al., 2023).

Members of the family Ustilaginaceae harbor the natural ability to synthesize a broad portfolio of valuable molecules including glycolipids, triacylglycerols, polyols like erythritol as well as organic acids covering broad application fields (Paulino et al., 2017). However, while almost all tested isolates are capable of producing malate and succinate, ITA production appears to be more specific for single strains like for instance *U. maydis*, *U. cynodontis* or *U. rabenhorstiana* (Geiser et al., 2014; Krull et al., 2020). The broad product spectrum is as favorable as it is challenging when aiming at a high product specificity. Yet, *U. maydis*, *U. cynodontis*, and other species are genetically accessible and modifiable allowing construction of chassis strains to overcome enzymatic bottlenecks and reduce metabolic flux in competing by-product pathways (Bösch et al., 2016; Kämper et al., 2006; Ullmann et al., 2022a; Wege et al., 2021; Wierckx et al., 2021). Moreover, *Ustilago* species benefit from a broad substrate spectrum, including glucose, fructose, glycerol, sucrose, and xylose, among others (Liebal et al., 2022). Together with its genetic repertoire for the production of secretory hydrolytic enzymes, this offers the potential to use low-cost feedstocks like lignocellulosic and pectin-containing biomass or starch-containing side streams from the food industry (Geiser et al., 2013; Helm et al., 2023; Mueller et al., 2008; Stoffels et al., 2020), as discussed in further detail in chapter 4.2. Lastly, the biosafety level 1 of *Ustilago* species in contrast to level 2 of *A. terreus* offers a substantial advantage for industrial production in Europe in terms of handling and regulatory requirements (Nascimento et al., 2022).

2.3.1. Regulation of itaconic acid production in *Ustilago* species

As commercial ITA production began to emerge, the first studies of ITA biosynthesis in *A. terreus* were undertaken. Using tracer studies with ^{14}C labeled substrates, ITA was shown to be the product of *cis*-aconitate decarboxylation via *cis*-aconitate decarboxylase (Bentley & Thiessen, 1957). The subcellular compartmentalization of ITA synthesis and a direct involvement of the TCA cycle in precursor supply was described almost 40 years later. The TCA cycle intermediate *cis*-aconitate was revealed to be synthesized by the mitochondrial aconitase, and was found to be subsequently exported via the mitochondrial tricarboxylate transporter MttA into the cytosol for further conversion to ITA (Bonnarme et al., 1995; Jaklitsch et al., 1991).

According to the recently described biosynthetic pathway in *U. maydis* (Figure 5), conversion of *cis*-aconitate to ITA involves two steps in this fungus. After Mtt1-mediated transport into the cytosol in antiport with malate, *cis*-aconitate is isomerized to *trans*-aconitate via aconitate- Δ -isomerase Adi1 prior to decarboxylation via *trans*-aconitic acid decarboxylase Tad1 (Geiser et al., 2016c). Since the negative charge of ITA prevents its passive diffusion through the cell envelop, active transport via the specific transporter Itp1 is required. However, low extracellular pH milieus

favor protonation of ITA (cf. pK_a values in Figure 2), which is able to re-enter the cell by passive diffusion and returns to its dissociated form again in a process called weak acid uncoupling. To prevent intracellular acidification, protons are removed out of the cell by ATP-dependent proton pumps allowing pH homeostasis. The respective energy requirement is met by a surplus of NADH formed during conversion of glucose to ITA (reviewed by Wierckx et al., 2020).

Expression of the complete core gene cluster – *tad1*, *itp1*, *adi1*, *mtt1* – is activated by the transcription factor Ria1, whose expression level strongly correlate with ITA production (Geiser et al., 2018; Geiser et al., 2016c). Moreover, ITA cluster regulation via Ria1 showed an evolutionary conservation among the Ustilaginaceae family, which was verified by *ria1* overexpression and successful ITA production in otherwise non-producing *Ustilago* species harboring silent ITA clusters (Geiser et al., 2018). In addition to the core genes, two other genes called *cyp3* encoding a cytochrome P450 family 3 monooxygenase and *rdo1* originally assumed to encode a ring-cleaving dioxygenase are located in close proximity (Geiser et al., 2016c). Cyp3 catalyzes the oxidation of ITA to the chiral molecule 2-hydroxyparaconate (2-HP), which can be further converted to itatartarate (ITT), either abiotically or enzymatically catalyzed (Geiser et al., 2016b; Guevarra & Tabuchi, 1990a, 1990b). The Cyp3-catalyzed reaction is assumed to regenerate NAD(P)H, thereby contributing to NAD(P) redox homeostasis (Geiser et al., 2016b).

Besides conversion to 2-HP, there is an increasing evidence for alternative degradation pathways of ITA. Such pathway was already described for the natural ITA producer *A. terreus* and involves three enzymatic reactions, including conversion of ITA into itaconyl-CoA via itaconyl-CoA transferase (IctA), hydration of itaconyl-CoA to citramalyl-CoA by itaconyl-CoA hydratase (IchA), and cleavage of citramalyl-CoA into acetyl-CoA and pyruvate by citramalyl-CoA lysase (CclA) (Chen et al., 2016). According to Geiser et al. (2016b), similar proteins are encoded on the *U. maydis* genome pointing towards the existence of an analogous pathway in *Ustilago* species.

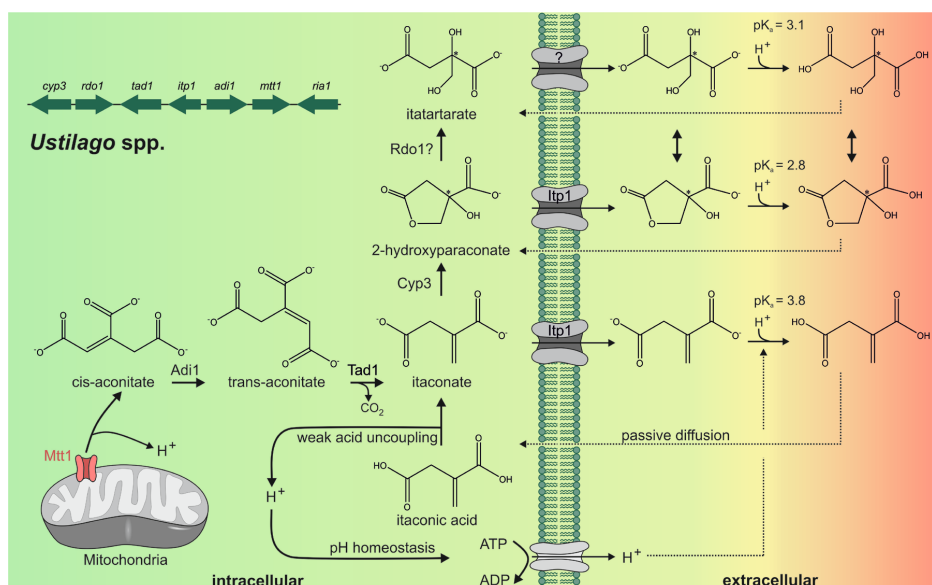


Figure 5: Itaconate, 2-hydroxyparaconate, and itatartarate metabolism in *Ustilago* species and annotation of the respective enzymes.

The figure design was inspired by Wierckx et al. (2020). The color gradient indicates the pH milieu with greenish color representing neutral pH conditions and reddish color representing acidic conditions. Re-uptake by passive diffusion and weak acid uncoupling is shown exemplarily for ITA ($pK_{a1} = 3.84$ and $pK_{a2} = 5.55$ at 20 °C), but also applies to 2-HP and ITT depending on the extracellular pH (2-HP: $pK_a = 2.78$; ITT: $pK_{a1} = 3.14$ and $pK_{a2} = 4.92$ at 20 °C). Rounded pK_a values are shown in the figure. (Ria1: pathway-specific transcription factor; Mtt1: mitochondrial tricarboxylate transporter; Adi1: aconitate- Δ -isomerase; Tad1: *trans*-aconitate decarboxylase; Ltp1: itaconate transport protein; Cyp3: cytochrome P450 monooxygenase; Rdo1: putative ring-cleaving dioxygenase).

Production of ITA, 2-HP and ITT occurs with delay to biomass production. Once nitrogen as the growth-limiting nutrient is completely consumed, the specific promoters in the ITA cluster become activated and initiate ITA synthesis (Zambanini et al., 2017c). Here, high expression levels of *mtt1* are of special importance since transport of *cis*-aconitate via Mtt1 into the cytosol is the rate-limiting step in ITA biosynthesis (Zambanini et al., 2017c). During the production phase, glucose is funneled into ITA production via continuous supply of *cis*-aconitate from the TCA cycle. By varying the carbon/nitrogen (C/N) ratio, yield and productivity can be balanced with higher nitrogen levels resulting in increasing biomass densities. Although this is expected to lead to a higher productivity, it comes at the expense of a lower yield as less carbon is available for ITA production (Maassen et al., 2014; Zambanini et al., 2017c).

2.3.2. Genetic and process engineering towards increased itaconic acid production

Elucidation of the ITA pathway by Geiser et al. (2016c) opened the door to genetic engineering approaches in order to optimize ITA production. So far, studies on ITA synthesis in *Ustilago* species have mainly focused on the model species *U. maydis*, using haploid, yeast-like cells of one mating type. A pH-controlled high cell-density pulsed fed-batch fermentation of the wildtype strain *U. maydis* MB215 exposed moderate ITA production of 14 g L^{-1} , but yield and productivity were extremely low. Instead, up to 21.3 g L^{-1} 2-HP was measured in the fermentation broth, resulting from ITA oxidation via Cyp3 and consequently lowering the final ITA titer. Accordingly, first genetic engineering approaches aimed at the deletion of *cyp3*, which prevents further conversion of ITA, and upregulation of the entire ITA core cluster by exchanging the native promoter of the transcriptional regulator Ria1 with a strong, constitutive one (*P_{etef}*). This already led to an up to 4.5 fold increase in final ITA titers and an improved productivity and yield, the latter being twice as high when reducing carbon and nitrogen concentrations (Geiser et al., 2016b) (Table 1).

Based on these results, Hosseinpour Tehrani et al. (2019c) continued to develop the producer strain by further rational genetic engineering. Although *U. maydis* normally exhibits stable, yeast-like growth, certain stress conditions such as low pH or nitrogen limitation can provoke filamentous growth (Lovely et al., 2011; Lovely & Perlin, 2011; Martinez-Espinoza et al., 2004), potentially by inducing formation of conjugation tubes. This in turn complicates process handling and is associated with several drawbacks that have already been discussed for *A. terreus*-based ITA production (cf. chapter 2.2.2) (Wierckx et al., 2021). One protein essentially involved in transition to filamentous growth is Fuz7. It is part of the Ras/mitogen-activated protein kinase (MAPK) pathway and participates in conjugation tube and filament formation, but also in tumor induction and teliospore formation during plant infection (Banuett & Herskowitz, 1994). Its deletion was found to allow maintenance of yeast-like growth without negatively influencing ITA production under process-relevant conditions (Hosseinpour Tehrani et al., 2019b). In addition to the *fuz7* deletion, overexpression of the mitochondrial transporter *mttA* from *A. terreus* transporting *cis*-aconitate in antiport with oxaloacetate into the cytosol increased ITA production in *U. maydis* (Hosseinpour Tehrani et al., 2019a; Scarcia et al., 2020; Steiger et al., 2016). Combining all the explained mutations in the strain *U. maydis* $\Delta cyp3 \Delta P_{ria1}::P_{etef} \Delta fuz7 P_{etef} mttA$ markedly improved ITA production during controlled low cell-density pulsed fed-batch fermentation. By addition of CaCO_3 for pH control and *in situ* product removal via ITA precipitation, 140 g L^{-1} ITA were produced with an overall yield $0.39 \text{ g}_{\text{ITA}} \text{ g}_{\text{GLC}}^{-1}$ and a productivity of $0.32 \text{ g L}^{-1} \text{ h}^{-1}$. By increasing the biomass density, the final ITA titers could be further increased

to 220 g L⁻¹ with a higher, overall productivity of 0.45 g L⁻¹ h⁻¹, even though at the expense of a slightly reduced yield of 0.33 g_{ITA} g_{GLC}⁻¹ (Hosseinpour Tehrani et al., 2019c) (Table 1). Accordingly, higher ITA titers have been achieved compared to *A. terreus* fermentations, although the productivity and yield are still not competitive (Krull et al., 2017a).

Besides ITA, *U. maydis* also produces lipidic products like extracellular glycolipids and intracellular triacylglycerol (Aguilar et al., 2017; Hewald et al., 2006; Teichmann et al., 2007). In an alternative approach to optimize ITA production, Becker et al. (2020) abolished lipid by-product formation to channel metabolic flux towards ITA synthesis. For this purpose, the ustilagic acid (UA) cluster and the mannosylerythritol lipids (MEL) cluster were genetically disrupted. To further reduce intracellular triacylglycerol (TAG) formation, a single gene deletion encoding a putative diacylglycerol acyltransferase was introduced as well. Shake flask cultivations with *in situ* product removal with CaCO₃ enabled a 1.2-fold improved ITA production in terms of final titer, yield and productivity of the final ITA chassis strain *U. maydis* $\Delta cyp3 \Delta MEL \Delta UA \Delta dgat \Delta P_{ria1}::P_{etef}$ compared to its progenitor strain *U. maydis* $\Delta cyp3 \Delta P_{ria1}::P_{etef}$ (Becker et al., 2020) (Table 1).

In addition to *U. maydis*, *U. cynodontis* has also been found to produce ITA. Contrary to *U. maydis* requiring pH values above 5.0 for ITA production, *U. cynodontis* has a high tolerance to acidic conditions and the wildtype strain NRBC9727 does not produce any glycolipids (Geiser et al., 2014; Morita et al., 2008). These properties could make industrial ITA production more economical by reducing the costs for pH adjustment and saline waste disposal as well as by facilitating a more streamlined DSP due to fewer by-products. Lower process pH values would also enable autosterility, leading to further cost reductions (Hosseinpour Tehrani et al., 2019b; Roa Engel et al., 2011). However, *U. cynodontis* NRBC9727 showed strong filamentous growth during high cell-density pulsed fed-batch fermentations and only low production of 5.1 g L⁻¹ ITA at pH 6.0. At pH 3.8, ITA production was almost completely absent, most likely due to strong filamentous growth triggered through the low pH conditions. Morphological engineering by deletion of *fuz7* enabled stable, unicellular growth and resulted in markedly increased product titers of 21.2 g L⁻¹ ITA at the pH of 3.8. Further metabolic engineering by introducing analogous mutations as in the ITA hyper-producing *U. maydis* strain led to the construction of the *U. cynodontis* ITA MAX pH strain ($\Delta fuz7 \Delta cyp3 P_{etef} mttA P_{ria1} ria1$) (Hosseinpour Tehrani et al., 2019b). This strain showed 2.1-fold increased production of ITA as well as an improved productivity (0.23 g L⁻¹ h⁻¹) and yield (0.39 g_{ITA} g_{GLC}⁻¹) compared to the morphology-engineered strain *U. cynodontis* $\Delta fuz7$ during pH-controlled low cell-density pulsed fed-batch fermentations. Comparable fermentations under high cell-density conditions even resulted in a further increase in product titer (83.0 g L⁻¹) and productivity (0.59 g L⁻¹ h⁻¹), but came at the expense of a reduced

yield of $0.30 \text{ g}_{\text{ITA}} \text{ g}_{\text{GLC}}^{-1}$. The best ITA production in terms of yield ($0.45 \text{ g}_{\text{ITA}} \text{ g}_{\text{GLC}}^{-1}$) was achieved in a high cell-density fed-batch fermentation with a constant glucose feed controlled by an inline glucose sensor (Hosseinpour Tehrani et al., 2019d) (Table 1).

Table 1: Selected fermentation performances of wildtype and genetically engineered strains of *A. terreus*, *U. maydis*, and *U. cynodontis* with regard to ITA production.

Obtained key performance indicators (KPIs) are color-coded with the green coloration increasing as performances improves.

Strain modification	Cultivation condition		Titer g L ⁻¹	Prod. g L ⁻¹ h ⁻¹	Yield g _{ITA} g _{GLC} ⁻¹	Reference
A. terreus DSM-23081						
Wildtype	pulsed fed-batch fermentation, pH control at pH 3.4 after second day	200 g L ⁻¹ glucose _{start} , 5.9 mM KH ₂ PO ₄	160	0.99	0.46	(Krull et al., 2017a)
	pulsed fed-batch fermentation, pH control at pH 3.4 after second day	180 g L ⁻¹ glucose _{start} , 0.7 mM KH ₂ PO ₄	160	0.56	0.58	
U. maydis MB215						
Wildtype	High cell-density pulsed fed-batch fermentation, pH control between pH 6.0-6.5	200 g L ⁻¹ glucose _{start} , 75 mM NH ₄ Cl	14	0.09	0.05	(Geiser et al., 2016b)
Δcyp3 ΔP _{ria1} ::P _{etef}	High cell-density pulsed fed-batch fermentation, pH control between pH 6.0-6.5	200 g L ⁻¹ glucose _{start} , 75 mM NH ₄ Cl	63.2	0.38	0.23	
	Low cell-density pulsed fed-batch fermentation, pH control between pH 6.0-6.5	50 g L ⁻¹ glucose _{start} , 15 mM NH ₄ Cl	54.8	0.33	0.48	
Δcyp3 ΔP _{ria1} ::P _{etef} Δfuz7 P _{etef} mttA	Low cell-density pulsed fed-batch fermentation with 66 g L ⁻¹ CaCO ₃ for <i>in situ</i> product removal, pH control at pH 6.0-6.5	50 g L ⁻¹ glucose _{start} , 30 mM NH ₄ Cl	140	0.32	0.39	(Hosseinpour Tehrani et al., 2019c)
	High cell-density pulsed fed-batch fermentation with 66 g L ⁻¹ CaCO ₃ for <i>in situ</i> product removal, pH control at pH 6.0-6.5	200 g L ⁻¹ glucose _{start} , 75 mM NH ₄ Cl	220	0.45	0.33	
Δcyp3 ΔP _{ria1} ::P _{etef}	shake flask cultivation with 66 g L ⁻¹ CaCO ₃ for <i>in situ</i> product removal, pH control at pH 6.0-7.0	100 g L ⁻¹ glucose, 15 mM NH ₄ Cl	43.7	0.22	0.39	(Becker et al., 2020)
Δcyp3 ΔMEL ΔUA Δdga1 ΔP _{ria1} ::P _{etef}	shake flask cultivation with 66 g L ⁻¹ CaCO ₃ for <i>in situ</i> product removal, pH control at pH 6.0-7.0	100 g L ⁻¹ glucose, 15 mM NH ₄ Cl	53.5	0.28	0.47	

Continuation of Table 1:

Strain modification	Cultivation condition	Titer g L ⁻¹	Prod. g L ⁻¹ h ⁻¹	Yield g _{ITA} g _{GLC} ⁻¹	Reference	
U. cynodontis NRBC9727						
Wildtype	High cell-density pulsed fed-batch fermentation, pH control at pH 6.0	200 g L ⁻¹ glucose _{start} , 75 mM NH ₄ Cl	5.1	0.03	-	(Hosseinpour Tehrani et al., 2019b)
	High cell-density pulsed fed-batch fermentation, pH control at pH 3.8	200 g L ⁻¹ glucose _{start} , 75 mM NH ₄ Cl	-	-	-	
Δfuz7	Low cell-density pulsed fed-batch fermentation, pH control at pH 3.8	50 g L ⁻¹ glucose _{start} , 15 mM NH ₄ Cl	21.2	0.07	0.22	
Δfuz7 Δcyp3 P _{etef} mttA P _{rio1} ria1	Low cell-density pulsed fed-batch fermentation, pH control at pH 3.6	50 g L ⁻¹ glucose _{start} , 15 mM NH ₄ Cl	44.5	0.23	0.39	(Hosseinpour Tehrani et al., 2019d)
	High cell-density pulsed fed-batch fermentation, pH control at pH 3.6	200 g L ⁻¹ glucose _{start} , 75 mM NH ₄ Cl	83.0	0.59	0.30	
	Continuous high cell-density fed-batch fermentation, pH control at pH 3.6	20 g L ⁻¹ glucose _{constant} , 75 mM NH ₄ Cl	78.6	0.42	0.45	

2.4. Scope of this thesis

The aim of this thesis was to explore and expand the process window in which the *Ustilago*-based ITA production process operates. This was tackled by strain engineering to push yields to the theoretical maximum, through process engineering to balance yield, titer, productivity against pH and associated titrant use and salt waste co-production, through expansion of the substrate range, and through expansion of the product range to potentially higher-value derivatives.

- For the model species *U. maydis*, two previously engineered ITA hyper-producing strains are described in literature (Table 1). In order to further optimize ITA production, established modifications of both strains were consolidated into one strain to stabilize the yeast-like morphology, to alleviate enzymatic bottlenecks and to reduce by-product formation at the same time. The performance of this strain was investigated under industrially relevant conditions in high and low cell-density fed-batch bioreactor experiments and compared with respect to the KPIs (chapter 3.1).
- In recent years, *U. cynodontis* has emerged as an additional ITA producing non-conventional yeast, mainly due to its high acid tolerance, which significantly reduces base and acid use as well as saline waste co-production during fermentation and downstream processing. Based on the knowledge from previous engineering of *U. maydis*, several genetic modifications were also integrated into *U. cynodontis*. However, the optimal pH value for ITA biosynthesis as well as additional key parameters of the ITA production process have not been determined for this strain. Thus, chapter 3.2 focused on the investigation of the ITA production capabilities of this acid-tolerant strain through controlled fed-batch fermentations, combined with an operational cost analysis to evaluate the impact of different production pH values on overall process economics.
- In addition to improving the ITA production from pure glucose, this thesis also dealt with the cultivation of *Ustilago* species on alternative carbon sources (chapter 3.3). Since starch is a low-cost and relatively clean carbon source, we selected this substrate and evaluated the amylolytic properties of *U. maydis* and *U. cynodontis*. This evaluation included initial enzyme characterizations and bioreactor cultivations on starch.
- Besides ITA, *Ustilago* species produce other value-added chemicals such as the two ITA downstream products 2-HP and ITT. In order to allow efficient production of these novel chemicals, the pH-tolerant, ITA hyper-producing *U. cynodontis* strain was subjected to further genetic engineering approaches. The resulting strains were characterized on glucose, but also on the alternative carbon source glycerol, a waste product from biodiesel production (chapter 3.4). This chapter also focused on the downstream process development as well as on the structural characterization of the two compounds.

3. Publications and manuscripts

Research presented in this thesis was mainly funded by the following projects:



“Glaukos will develop bio-based textile fibers and textile coatings that are adapted to the needs of the 21st century. The complete life cycle of clothing and fishing gear will be redesigned, their sustainability performance will be enhanced significantly, while their technical performance will be matched to end-user requirements. The ambition is to significantly reduce the carbon and plastic footprint of clothing and fishing gear.”

(taken from glaukos-project.eu)



Upcycling organischer Reststoffe für die chemische Industrie (UpRePP): „Die stoffliche Aufwertung von organischen Reststoffströmen aus der Land- und Lebensmittelwirtschaft des Rheinischen Reviers steht im Mittelpunkt des Innovationslabors UpRePP. In Kooperation mit lokalen Unternehmen werden Upcycling-Prozesse entwickelt, die als Schlüsseltechnologien die wettbewerbsfähige Herstellung von hochwertigen biobasierten Plattformchemikalien und Komponenten (z. B. Zuckertensiden) ermöglichen.“

(taken from [BioökonomieREVIER: UpRePP](#))

Contributions of the listed authors to the manuscripts were described using the Contributor Roles Taxonomy (CRediT) ([CRediT – Contributor Roles Taxonomy \(niso.org\)](https://www.niso.org/standards/crediting)):

CONTRIBUTOR ROLE	DEFINITION
CONCEPTUALIZATION	Ideas; formulation or evolution of overarching research goals and aims
DATA CURATION	Management activities to annotate (produce metadata), scrub data and maintain research data (including software code, where it is necessary for interpreting the data itself) for initial use and later re-use
FORMAL ANALYSIS	Application of statistical, mathematical, computational, or other formal techniques to analyze or synthesize study data
FUNDING ACQUISITION	Acquisition of the financial support for the project leading to this publication
INVESTIGATION	Conducting a research and investigation process, specifically performing the experiments, or data/evidence collection
METHODOLOGY	Development or design of methodology; creation of models
PROJECT ADMINISTRATION	Management and coordination responsibility for the research activity planning and execution
RESOURCES	Provision of study materials, reagents, materials, patients, laboratory samples, animals, instrumentation, computing resources, or other analysis tools
SOFTWARE	Programming, software development; designing computer programs; implementation of the computer code and supporting algorithms; testing of existing code components
SUPERVISION	Oversight and leadership responsibility for the research activity planning and execution, including mentorship external to the core team
VALIDATION	Verification, whether as a part of the activity or separate, of the overall replication/reproducibility of results/experiments and other research outputs
VISUALIZATION	Preparation, creation and/or presentation of the published work, specifically visualization/data presentation
WRITING – ORIGINAL DRAFT	Preparation, creation and/or presentation of the published work, specifically writing the initial draft (including substantive translation)
WRITING – REVIEW AND EDITING	Preparation, creation and/or presentation of the published work by those from the original research group, specifically critical review, commentary or revision – including pre- or post-publication stages

3.1. An Optimized *Ustilago maydis* for Itaconic Acid Production at Maximal Theoretical Yield

J. Becker*, H. Hosseinpour Tehrani*, P. Ernst*, L. M. Blank, and N. Wierckx

*These authors contributed equally to this work.

Journal of Fungi (Basel), 2021. doi: 10.3390/jof7010020

Contributor role	Contributor
Conceptualization	N. Wierckx, L. M. Blank
Data curation	N. Wierckx, J. Becker, H. Hosseinpour Tehrani, P. Ernst
Formal analysis	J. Becker, H. Hosseinpour Tehrani, P. Ernst
Funding acquisition	N. Wierckx, L. M. Blank
Investigation	J. Becker, H. Hosseinpour Tehrani, P. Ernst
Methodology	J. Becker, H. Hosseinpour Tehrani, P. Ernst
Project administration	N. Wierckx, L. M. Blank
Resources	N. Wierckx, L. M. Blank
Software	-
Supervision	N. Wierckx, L. M. Blank
Validation	J. Becker, H. Hosseinpour Tehrani, P. Ernst
Visualization	J. Becker, H. Hosseinpour Tehrani, P. Ernst
Writing – original draft	J. Becker
Writing – review and editing	N. Wierckx, P. Ernst

Overall contribution: 30 %

J. Becker performed the strain engineering and the System Duetz cultivations associated to Figure 6-9. H. Hosseinpour Tehrani performed the high cell-density pulsed fed-batch fermentation associated to Figure 10 and Figure S1. I performed the high and low cell-density fed-batch fermentations with continuous feed associated to Figure 11 and Figure 12. J. Becker wrote the original draft. J. Becker and I were significantly involved in the visualization of the figures. All authors, but especially N. Wierckx and I, were involved in the review and editing process.

An Optimized *Ustilago maydis* for Itaconic Acid Production at Maximal Theoretical Yield

Johanna Becker^{§1}, Hamed Hosseinpour Tehrani^{§1}, Philipp Ernst^{§2}, Lars Mathias Blank¹ and Nick Wierckx^{*1}

¹ iAMB – Institute of Applied Microbiology, ABBt – Aachen Biology and Biotechnology, RWTH Aachen University, Worringerweg 1, 52074, Aachen, Germany; johanna.becker@rwth-aachen.de; hamed.tehrani@rwth-aachen.de; lars.blank@rwth-aachen.de

² Institute of Bio- and Geosciences IBG-1: Biotechnology, Forschungszentrum Jülich, 52425, Jülich, Germany; p.ernst@fz-juelich.de; n.wierckx@fz-juelich.de

* Correspondence: n.wierckx@fz-juelich.de

[§] These authors contributed equally to this manuscript

Received: 22 November 2020; Accepted: 29 December 2020; Published: 31 December 2020

Abstract: *U. maydis*, member of the Ustilaginaceae family, is a promising host for the production of several metabolites including itaconic acid. This dicarboxylate has great potential as a bio-based building block in the polymer industry, and is of special interest for pharmaceutical applications. Several ITA-overproducing *Ustilago* strains have been generated by metabolic and morphology engineering. This yielded stabilized unicellular morphology through *fuz7* deletion, reduction of by-product formation through deletion of genes responsible for ITA oxidation and (glyco)lipid production, and the overexpression of the regulator of the ITA cluster *ria1* and the mitochondrial tricarboxylate transporter encoded by *mttA* from *A. terreus*. In this study, ITA production was further optimized by consolidating these different optimizations into one strain. The combined modifications resulted in ITA production at theoretical maximal yield, which was achieved under biotechnologically relevant fed-batch fermentations with continuous feed.

Keywords:

Itaconic acid; *Ustilago maydis*; Metabolic engineering, Fungi, Yeast

3.1.1. Introduction

Itaconic acid and its derivatives are found in many application fields, such as the production of paper, paints, and fibers, or in waste water treatment (Klement et al., 2012; Okabe et al., 2009; Steiger et al., 2017; Willke & Vorlop, 2001), providing a stable market for this bio-based chemical. In 2004, the organic acid was classified as one of the top 12 value-added platform chemicals derived from biomass (Werpy & Petersen, 2004). There is also a strong interest in this molecule in the medical and pharmaceutical sectors, both as an anti-bacterial compound (Michelucci et al., 2013) and as an immunoregulator for the treatment of autoimmune diseases (Mills et al., 2018) and viral infections including SARS-CoV2 (Olaghier et al., 2020). However, its relatively high production cost compared to fossil counterparts like acrylic acid prevents an even more expanded usage range (Hosseinpour Tehrani et al., 2019c; Klement & Büchs, 2013). Given the already high yield, titer, and productivity of the industrially established ITA production process with *A. terreus*

(Hevekerl et al., 2014), a qualitative breakthrough in other dimensions of the process window is needed. Non-conventional ITA producing yeasts like *Ustilago*, *Candida*, or *Pseudozyma* (Krull et al., 2020; Levinson et al., 2006; Tabuchi et al., 1981) may offer such a breakthrough because of their unicellular morphology as well as their lower sensitivity to medium impurities. It also enables easier handling and scale-up using cheaper raw substrates or even waste streams (Hosseinpour Tehrani et al., 2019c; Regestein et al., 2018; Wierckx et al., 2020). However, compared to the filamentous ascomycete *A. terreus*, the substrate-to-product yield has to be improved to make *U. maydis* competitive, and this yield also needs to be achievable under industrially relevant conditions (Straathof et al., 2019).

In nature, *U. maydis* is known for its pathogenicity towards maize (*Zea mays*) causing corn smut disease (Kahmann et al., 2000; Kämper et al., 2006). To penetrate and invade maize tissue, *U. maydis* switches from a yeast-like, non-pathogenic to a filamentous, pathogenic cell form (Christensen, 1963). This switch is governed by a complex regulatory pathway which has been investigated in detail (see for extensive reviews Kahmann and Kämper (2004) and Brefort et al. (2009). Although predominantly growing in its yeast form in fermentation processes, *U. maydis* can switch to filamentous growth under stress conditions such as the presence of hydrophobic lipids, low pH, or nitrogen deficiency (Klose et al., 2004; Lovely et al., 2011; Lovely & Perlin, 2011). Filamentous growth causes issues such as high viscosity, reduced oxygen supply, and cell adherence to reactor walls (Klement & Büchs, 2013). This can be avoided through the deletion of *fuz7*, the product of which plays an essential role in regulating pathogenicity and the switch to filamentous growth (Klose et al., 2004). This deletion stabilizes the yeast-like morphology of *U. maydis* and *U. cynodontis* without impacting the fitness of the cells under biotechnologically relevant stresses (Hosseinpour Tehrani et al., 2019d; Hosseinpour Tehrani et al., 2019b).

U. maydis produces ITA as one product from a potpourri of metabolites including organic acids such as malate, succinate, 2-HP, and ITT, polyols such as erythritol and mannitol, and different lipidic products including glycolipids and triglycerides (Aguilar et al., 2017; Bölker et al., 2008; Feldbrügge et al., 2013; Geiser et al., 2014; Guevarra & Tabuchi, 1990a; Moon et al., 2010). It can also metabolize a range of renewable carbon sources, which besides sugar also include glycerol (Zambanini et al., 2017b), galacturonic acid (Müller et al., 2018), cellulose (Schlembach et al., 2020), xylan (Geiser et al., 2016a), and pectin (Stoffels et al., 2020). Although these features make *U. maydis* an attractive candidate for industrial applications (Klement & Büchs, 2013; Maassen et al., 2014; Olicón-Hernández et al., 2019), it also poses a drawback because often multiple products are produced simultaneously. This hinders handling and downstream processing, and it also reduces yield on substrate by diverting carbon flux away from the main product (Becker et

al., 2020). If ITA is to become a bulk chemical, yield is one of the most relevant production parameter because substrate cost is the decisive price-determining factor. For ITA production from glucose, the reported maximal theoretical yield is $0.72 \text{ g}_{\text{ITA}} \text{ g}_{\text{GLC}}^{-1}$, which equals $1 \text{ mol}_{\text{ITA}} \text{ mol}_{\text{GLC}}^{-1}$. The yield achieved in practice is affected by different factors such as cell-density, the metabolic pathway leading up to ITA (i.e., anaplerosis), bottlenecks in the ITA biosynthesis pathway itself, side product formation, redox cofactor balancing, and cell-maintenance demand (Karaffa & Kubicek, 2019; Kuenz & Krull, 2018).

In previous studies several knockouts, promotor replacements and overexpression of genes were implemented to increase ITA production, reduce by-product formation, and stabilize the unicellular morphology (Becker et al., 2020; Geiser et al., 2016b; Hosseinpour Tehrani et al., 2019c; Hosseinpour Tehrani et al., 2019b; Zambanini et al., 2017a). Those metabolic engineering approaches resulted in several ITA hyper-producing *Ustilago* strains with individual modifications. In this study, these modifications are consolidated into one strain, based on the previously engineered *U. maydis* ITA chassis (Becker et al., 2020). The resulting strain K14 produces ITA from glucose at maximum theoretical yield. The catalytic vigor of the strain was demonstrated in fed-batch cultures.

3.1.2. Materials and methods

Media and culture conditions

All strains used in this work are listed in Table 2. *U. maydis* strains were grown in YEPS medium containing 10 g L^{-1} yeast extract, 10 g L^{-1} peptone, and 10 g L^{-1} sucrose. As screening medium for production experiments, *U. maydis* was cultivated in modified Tabuchi medium (MTM) according to Geiser et al. (2014). Besides varying glucose concentrations and different buffers 2-(*N*-morpholino)ethanesulfonic acid (MES) or calcium carbonate (CaCO_3), this medium contained $15 \text{ mM NH}_4\text{Cl}$, $0.2 \text{ g L}^{-1} \text{ MgSO}_4 \cdot 7\text{H}_2\text{O}$, $0.01 \text{ g L}^{-1} \text{ FeSO}_4 \cdot 7\text{H}_2\text{O}$, $0.5 \text{ g L}^{-1} \text{ KH}_2\text{PO}_4$, 1 mL L^{-1} vitamin solution, and 1 mL L^{-1} trace element solution. The vitamin solution contained (per liter) 0.05 g D-biotin , $1 \text{ g D-calcium pantothenate}$, $1 \text{ g nicotinic acid}$, $25 \text{ g myo-inositol}$, $1 \text{ g thiamine hydrochloride}$, $1 \text{ g pyridoxol hydrochloride}$, and $0.2 \text{ g para-aminobenzoic acid}$. The trace element solution contained (per liter) 1.5 g EDTA , $0.45 \text{ g ZnSO}_4 \cdot 7\text{H}_2\text{O}$, $0.10 \text{ g MnCl}_2 \cdot 4\text{H}_2\text{O}$, $0.03 \text{ g CoCl}_2 \cdot 6\text{H}_2\text{O}$, $0.03 \text{ g CuSO}_4 \cdot 5\text{H}_2\text{O}$, $0.04 \text{ g Na}_2\text{MoO}_4 \cdot 2\text{H}_2\text{O}$, $0.45 \text{ g CaCl}_2 \cdot 2\text{H}_2\text{O}$, $0.3 \text{ g FeSO}_4 \cdot 7\text{H}_2\text{O}$, $0.10 \text{ g H}_3\text{BO}_3$, and 0.01 g KI . When using CaCO_3 , medium components were added relative to the total volume of solids plus liquid, leading to a higher aqueous concentration of soluble components. Shaking cultures of *U. maydis* were performed in 24-well System Duetz plates with a filling volume of 1.5 mL (shaking diameter = 50 mm , $n = 300 \text{ rpm}$, $T = 30^\circ\text{C}$ and

$\Phi = 80\%$) (Duetz et al., 2000) or in 500 mL shaking flasks with a filling volume of 50 mL (shaking diameter = 25 mm, $n = 200$ rpm, $T = 30^\circ\text{C}$ and $\Phi = 80\%$). When using System Duetz, cultures were inoculated in parallel into multiple plates in order to ensure continuous oxygenation by taking a complete plate as sacrificial sample for each sample point.

Table 2: *U. maydis* MB215 strains used in this study.

Strain designation	Resistance	Reference
<i>U. maydis</i> MB215		(Hewald et al., 2005)
<i>U. maydis</i> MB215 $\Delta cyp3 \Delta P_{ria1::P_{etef}}$		(Hosseinpour Tehrani et al., 2019c)
<i>U. maydis</i> MB215 $\Delta U\text{MAG}_{05079} P_{etef} mttA$	Hyg ^R , Cbx ^R	(Hosseinpour Tehrani et al., 2019a)
<i>U. maydis</i> MB215 $\Delta cyp3 \Delta fuz7 \Delta P_{ria1::P_{etef} P_{etef} mttA_K14}$	Hyg ^R , Cbx ^R	(Hosseinpour Tehrani et al., 2019c)
<i>U. maydis</i> MB215 $\Delta cyp3 \Delta MEL \Delta U\Delta \Delta dgat \Delta P_{ria1::P_{etef}}$ (= ITA chassis)		(Becker et al., 2020)
<i>U. maydis</i> MB215 $\Delta cyp3 \Delta MEL \Delta U\Delta \Delta dgat \Delta P_{ria1::P_{etef} \Delta fuz7}$		this study
<i>U. maydis</i> MB215 $\Delta cyp3 \Delta MEL \Delta U\Delta \Delta dgat \Delta P_{ria1::P_{etef} \Delta fuz7 P_{etef} mttA_K3}$	Cbx ^R	this study
<i>U. maydis</i> MB215 $\Delta cyp3 \Delta MEL \Delta U\Delta \Delta dgat \Delta P_{ria1::P_{etef} \Delta fuz7 P_{etef} mttA_K8}$	Cbx ^R	this study
<i>U. maydis</i> MB215 $\Delta cyp3 \Delta MEL \Delta U\Delta \Delta dgat \Delta P_{ria1::P_{etef} \Delta fuz7 P_{etef} mttA_K9}$	Cbx ^R	this study
<i>U. maydis</i> MB215 $\Delta cyp3 \Delta MEL \Delta U\Delta \Delta dgat \Delta P_{ria1::P_{etef} \Delta fuz7 P_{etef} mttA_K10}$	Cbx ^R	this study
<i>U. maydis</i> MB215 $\Delta cyp3 \Delta MEL \Delta U\Delta \Delta dgat \Delta P_{ria1::P_{etef} \Delta fuz7 P_{etef} mttA_K14}$ (= K14 strain)	Cbx ^R	this study

Pulsed fed-batch fermentations were performed in New Brunswick BioFlo 115 bioreactors (Eppendorf, Germany) as described in Hosseinpour Tehrani et al. (2019c). Fed-batch fermentations with continuous feed were performed in a 2.3 L DASGIP Bioblock bioreactor (Eppendorf, Germany) with a starting volume of 1.0 L. The medium contained 120 g L⁻¹ glucose, 15 mM or 75 mM NH₄Cl, 0.2 g L⁻¹ MgSO₄·7H₂O, 0.01 g L⁻¹ FeSO₄·7H₂O, 0.5 g L⁻¹ KH₂PO₄, 1 mL L⁻¹ vitamin solution as specified above, 1 mL L⁻¹ trace element solution as specified above, and 1 g L⁻¹ yeast extract. When the glucose concentration reached approximately 50 g L⁻¹, a constant feed of a 50 % glucose solution was started. Feeding rates of 2.8 and 0.75 g h⁻¹ were estimated from the glucose consumption rates of previous pulsed fed-batch fermentations under similar conditions. During cultivation, the pH was controlled by automatic addition of 5 M NaOH and 1 M HCl. 0.5 mL Antifoam 204 (Sigma Life Science, USA) was added manually every 24 h to avoid foam formation. The dissolved oxygen (DO) was controlled at 30 % by using a cascade mode including stirring 800-1200 rpm, air flow 1-2 vvm and the addition of pure oxygen. The CO₂

formation was determined with the DASGIP GA4 module, employing infrared (IR) sensors (BlueSens). The cultivations were performed at 30 °C. Bioreactors were inoculated to an optical density measured at a wavelength of 600 nm (OD_{600}) of 0.75 from a 48 h preculture in 50 mL MTM.

Analytical methods

When using $CaCO_3$ as buffer, 1 mL culture broth was taken for OD_{600} and high performance liquid chromatography (HPLC) analysis. The $CaCO_3$ was dissolved 1:1 with 4 M HCl prior to further measurements as described in (Zambanini et al., 2016a). Cell-densities were measured by determining the absorption at 600 nm with an Ultrospec 10 Cell-Density Meter (Amersham Biosciences, UK).

For HPLC analysis, all samples were filtered with Rotilabo (CA, 0.2 μ m, \varnothing 15 mm) or Acrodisc (GHP, 0.2 μ m, \varnothing 13 mm) syringe filters and diluted 1:5 or 1:10 with 5 mM H_2SO_4 or ddH $_2O$. Products in the supernatant were analyzed using a DIONEX UltiMate 3000 HPLC System (Thermo Scientific, Waltham, Massachusetts, USA) or a Agilent 1260 Infinity HPLC system (Agilent, Waldbronn, Germany) with an ISERA Metab-AAC column 300 x 7.8 mm column (ISERA, Düren, Germany). As mobile phase, 5 mM H_2SO_4 with a constant flow rate of 0.6 mL min⁻¹ and a temperature of 40 °C was used. When using the DIONEX UltiMate 3000 HPLC System, detection was carried out by a DIONEX UltiMate 3000 Variable Wavelength Detector set to 210 nm and a SHODEX RI-101 detector (Showa Denko Europe GmbH, Munich, Germany). When using the Agilent 1260 Infinity HPLC system, detection was undertaken by a diode array detector (DAD) at 210 nm and a refraction index (RI) detector. Analytes were identified via retention time and UV/RI ratio compared to corresponding standards. All values are the arithmetic mean of at least two biological replicates. For n = 2, error bars indicate the deviation from the mean and for n > 2 error bars indicate the standard error of the mean. Statistical significance was evaluated by t test (two-tailed distribution, heteroscedastic, $p \leq 0.05$).

Plasmid cloning and strain engineering

Plasmids were constructed by Gibson assembly (Gibson et al., 2009) using the NEBuilder HiFi DNA Assembly Cloning Kit (New England Biolabs (NEB), Ipswich, MA, USA). Primers were ordered as DNA oligonucleotides from Eurofins Genomics (Ebersberg, Germany). As polymerase, Q5 High-Fidelity DNA Polymerase (NEB) was used. Detailed information about utilized primers and plasmids are listed in Table 3 and supplementary Table S1. Competent *E. coli* DH5 α were used for standard cloning and plasmid maintenance according to Sambrook and Russell (2006). Plasmids were confirmed by polymerase chain reaction (PCR) or sequencing. Generation of protoplasts and transformation of *U. maydis* were performed according to Brachmann et al. (2004). Genomic DNA

of *U. maydis* was isolated according to Hoffman and Winston (1987). For the deletion of *fuz7*, homologous recombination with 1000 bp flanking regions including FRT-sites and a hygromycin resistance cassette were used (Khrunyk et al., 2010). Successful integration and deletion was verified by PCR and sequencing. For the overexpression of *mttA*, the plasmid *P_{etef}-Cbx-AT_mttA* was used (Hosseinpour Tehrani et al., 2019a).

Table 3: Plasmids used in this study.

Plasmid	Description	Reference
pJET1.2/blunt	Ori ColE1; Amp ^R	Thermo Scientific, Germany
pFLPexpC	<i>P_{erg1}</i> promoter; synthetic FLP recombinase gene; Cbx ^R ; ARS; Amp ^R	Prof. M. Feldbrügge, Heinrich-Heine University Düsseldorf, Germany
pUMa1523	FRTm1-Hyg ^R -FRTm1 cassette; Gent ^R	Kerstin Schipper, Heinrich-Heine University Düsseldorf, Germany
pJET1.2- <i>fuz7</i> 5'-UTR flank -FRTm1-Hyg ^R -FRTm1- <i>fuz7</i> 3'-UTR flank	pJET1.2 with 5'- and 3'-UTR flank of UMAG_01514 as deletion construct; Hyg ^R ; FRT m1 recombination sites	this study
<i>P_{etef}-Cbx-AT_mttA</i>	constitutive <i>P_{etef}</i> promoter, dicodon-optimized version of <i>A. terreus</i> ATEG_09970 (<i>mttA</i>), Cbx ^R , Amp ^R	(Hosseinpour Tehrani et al., 2019a)

Quantitative PCR (qPCR) was applied to determine the copy number of *mttA* integrated into the *U. maydis* genome using Luna Universal qPCR Master Mix (NEB, Frankfurt, Germany). Primers were designed using “GenScript Real-Time PCR (TaqMan) Primer Design” tool (Gen Script, Piscataway, New Jersey, USA). Primer sequences are given in Table S1. As reference genes, UMAG_02592 and UMAG_03726 were amplified with the primer pairs JB-126/JB-127 and JB-128/JB-129. Primers JB-132/JB-133 specifically bound within the *mttA* sequence (supplementary Table S1). Amplification curves were taken by Bio-Rad CFX Connect™ Real-Time PCR Detection system and data were analyzed by using Bio-Rad CFX Manager™ 3.1 software (Bio-Rad Laboratories, Hercules, CA, USA) using the ΔC_t method according to Pfaffl (2001).

3.1.3. Results and discussion

Prevention of filamentous growth by *fuz7* deletion and its influence on itaconate production

In previous work, ITA production with *Ustilago* has been significantly improved. The characterization and upregulation of the ITA gene cluster (Geiser et al., 2018; Geiser et al., 2016b; Geiser et al., 2016c) as well as the engineering of the mitochondrial carrier for *cis*-aconitate (Hosseinpour Tehrani et al., 2019a) has laid the foundation for this improvement. Those

achievements were combined with further modifications including the deletion of genes responsible for ITA oxidation (*cyp3*) and (glyco)lipid production (MEL, UA, *dgat*), resulting in the *U. maydis* MB215 ITA chassis ($\Delta cyp3 \Delta MEL \Delta UA \Delta dgat \Delta P_{ria1}::P_{etef}$) with reduced by-product formation (Becker et al., 2020). Filamentous growth was observed for this strain, similar to other engineered *U. maydis* variants (Hosseinpour Tehrani et al., 2019c). The morphology switch is likely induced by the additional stress imposed by the metabolic engineering itself, and the resulting high ITA titers and associated low pH. This drawback can be overcome by the deletion of *fuz7* (UMAG_01514) (Hosseinpour Tehrani et al., 2019d; Hosseinpour Tehrani et al., 2019b). The influence of this knockout in the *U. maydis* MB215 ITA chassis was assessed in System Duetz cultivations in MTM containing 15 mM NH₄Cl, 100 mM MES pH 6.5, and 50 g L⁻¹ glucose (Figure 6). Under these conditions, the $\Delta fuz7$ strain produced 1.3-fold more ITA than the reference ITA chassis strain (Figure 6A, Table 4). Full consumption of glucose by both strains resulted in an equivalently improved yield of the $\Delta fuz7$ strain to 0.45 ± 0.01 g_{ITA} g_{GLC}⁻¹. The overall productivity was increased by 12 % and the maximal productivity even by 26 % (Table 4).

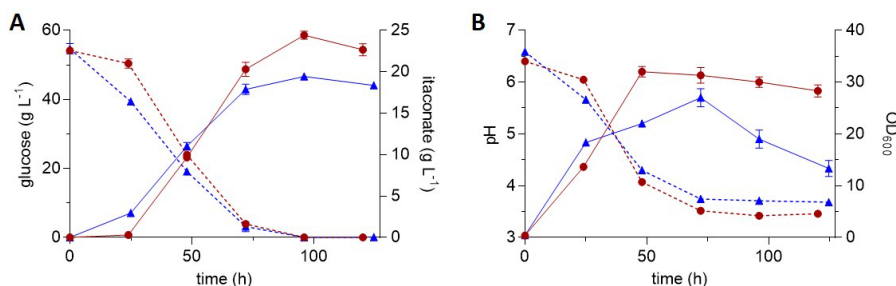


Figure 6: System Duetz cultivations of morphology-engineered *U. maydis* MB215 strains in MTM with 15 mM NH₄Cl, 100 mM MES pH 6.5, and 50 g L⁻¹ glucose.

(A) Concentration of itaconate (continuous lines) and glucose (dotted lines) and (B) OD₆₀₀ (continuous lines) and pH (dotted lines) of *U. maydis* MB215 $\Delta cyp3 \Delta MEL \Delta UA \Delta dgat \Delta P_{ria1}::P_{etef}$ (▲) and the same strain with additional *fuz7* deletion (●) (n = 3 biological replicates).

These results clearly illustrate the benefit of preventing filamentous growth. In these deeply engineered strains of *U. maydis*, cells start to adhere to the walls of the culture plates during the production phase, likely as a result of the combined stress of ammonium limitation, low pH and increasing product concentrations (Klose et al., 2004; Lovely et al., 2011; Lovely & Perlin, 2011). This adhesion has been described in detail in Hosseinpour Tehrani et al. (2019c). The resulting cell accumulations likely encounter oxygen, buffer, and nutrition heterogeneities, leading to limitations for cells deeper within the clumps. The accumulation on the walls was reflected in decreasing optical density values after 72 h (Figure 6B) and a decreasing ITA productivity (Figure

6A). This is in contrast to the *fuz7* mutant, which showed a constant ITA productivity in the production phase until glucose was depleted.

Overexpression of *mttA* from *A. terreus* and its impact on itaconate production

The transport of *cis*-aconitate from the mitochondria to the cytosol is the rate-limiting step in the ITA production pathway of *U. maydis* (Geiser et al., 2016b; Geiser et al., 2016c). In the ITA chassis this bottleneck is addressed through the overexpression of *mtt1* caused by the promoter exchange of the ITA cluster regulator encoded by *ria1* (Becker et al., 2020; Geiser et al., 2016c). However, the *mttA* transporter from *A. terreus* was shown to cause a higher metabolic flux towards ITA than its *U. maydis* counterpart *mtt1* (Hosseinpour Tehrani et al., 2019c; Hosseinpour Tehrani et al., 2019a). Overexpression of both *mtt1* and *mttA* further enhances ITA production. Therefore, a P_{etef} *mttA* construct was targeted to the *ip*-locus on the genome of the novel $\Delta fuz7$ strain.

Targeted integration of Cbx^R constructs into the *ip*-locus is not perfect. Often, multi-copy integration and/or ectopic insertion into random genomic sites occurs. Therefore, several clones were picked to identify the best ITA producer. Insertion of at least one *mttA* copy was verified by PCR for five clones resulting in the strains listed in Table 4. The strains significantly differed from each other regarding ITA production, glucose consumption, and growth. Corresponding cultivations are depicted in Figure 7 and Figure 8.

Table 4: Itaconate production parameters of engineered strains of the *U. maydis* MB215 ITA chassis

$\Delta cyp3 \Delta MEL \Delta UGA \Delta dgt \Delta P_{ria1::P_{etef}}$ (n = 3 biological replicates).

Symbols refer to Figures 6, 7, and 8. a) overall ITA productivity; b) maximum ITA productivity; c) yield ITA per consumed glucose.

Condition	Symbol	Strain modification	Titer _{max} (g L ⁻¹)	q _p ^a (g L ⁻¹ h ⁻¹)	q _{p, max} ^b (g L ⁻¹ h ⁻¹)	Y _{P/S} ^c (g _{ITA} g _{GLC} ⁻¹)
15 mM NH ₄ Cl, 100 mM MES, pH 6.5 50 g L ⁻¹ glucose	▲	control	19.4 ± 0.3	0.25 ± 0.01	0.35 ± 0.02	0.36 ± 0.02
	●	$\Delta fuz7$	24.4 ± 0.5	0.28 ± 0.01	0.44 ± 0.03	0.45 ± 0.01
	■	P_{etef} <i>mttA</i> _K3	23.5 ± 0.6	0.20 ± 0.00	0.46 ± 0.02	0.53 ± 0.01
	■	P_{etef} <i>mttA</i> _K8	29.1 ± 0.1	0.35 ± 0.01	0.49 ± 0.03	0.54 ± 0.01
	■	P_{etef} <i>mttA</i> _K9	28.9 ± 0.3	0.24 ± 0.00	0.44 ± 0.01	0.57 ± 0.01
	■	P_{etef} <i>mttA</i> _K10	32.3 ± 0.8	0.37 ± 0.00	0.54 ± 0.01	0.60 ± 0.02
15 mM NH ₄ Cl, 66 g L ⁻¹ CaCO ₃ pH 7.5 100 g L ⁻¹ glucose	■	P_{etef} <i>mttA</i> _K14	29.9 ± 0.7	0.25 ± 0.00	0.44 ± 0.01	0.64 ± 0.03
	○	$\Delta fuz7$	48.8 ± 1.3	0.42 ± 0.01	0.70 ± 0.07	0.47 ± 0.01
	□	P_{etef} <i>mttA</i> _K3	33.8 ± 0.5	0.29 ± 0.00	0.43 ± 0.06	0.58 ± 0.04
	□	P_{etef} <i>mttA</i> _K8	56.5 ± 1.7	0.48 ± 0.01	0.74 ± 0.09	0.51 ± 0.02
	□	P_{etef} <i>mttA</i> _K9	48.1 ± 2.9	0.41 ± 0.02	0.52 ± 0.02	0.56 ± 0.03
	□	P_{etef} <i>mttA</i> _K10	49.0 ± 3.8	0.42 ± 0.03	0.64 ± 0.07	0.44 ± 0.03
	□	P_{etef} <i>mttA</i> _K14	54.4 ± 0.2	0.46 ± 0.00	0.82 ± 0.01	0.57 ± 0.00

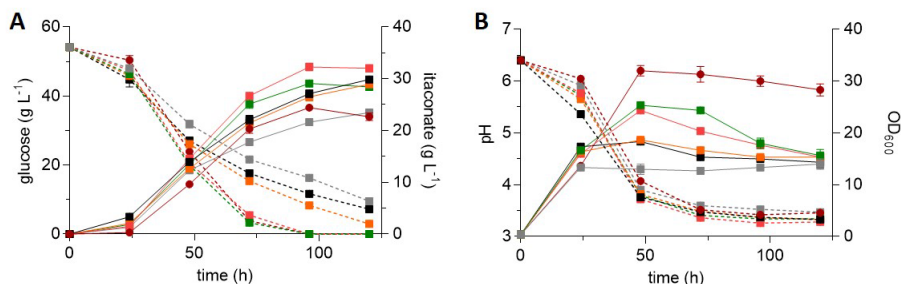


Figure 7: System Duetz cultivations of *U. maydis* MB215 strains expressing *mttA* in MTM with 15 mM NH₄Cl, 100 mM MES pH 6.5, and 50 g L⁻¹ glucose.

(A) Concentration of itaconate (continuous lines) and glucose (dotted lines) and (B) OD₆₀₀ (continuous lines) and pH (dotted lines) of *U. maydis* MB215 $\Delta cyp3 \Delta MEL \Delta UA \Delta dgt \Delta P_{ria1::P_{tef}} \Delta fuz7$ (●) and five *PtefmttA* transformants named K3 (■), K8 (■), K9 (■), K10 (■), and K14 (■) (n = 3 biological replicates).

With the exception of K3, all *mttA* transformants outperformed the reference strain with 18-32 % improvements in titer (Figure 7A, Table 4). Clones K3, K9, and K14 did not consume all glucose during 120 h of cultivation (Figure 7A), which further boosted the yield. All *mttA* transformants achieved a higher yield than the reference (Table 4), with K14 reaching $0.64 \pm 0.03 \text{ g}_{ITA} \text{ g}_{GLC}^{-1}$, which is 89 % of the theoretical maximum. Strains K8 and K10 had the highest rates, which were 25 % and 32 % higher, respectively, compared to the reference. Overexpression of *mttA* also had a strong impact on the growth (Figure 7B). While *U. maydis* MB215 $\Delta cyp3 \Delta MEL \Delta UA \Delta dgt \Delta P_{ria1::P_{tef}} \Delta fuz7$ reached OD₆₀₀ values above 30, all *mttA* transformants remained well below this value. A similar effect was observed in other *mttA* overexpressing strains, where growth and glucose consumption were also strongly decreased (Hosseinpour Tehrani et al., 2019a). The constitutive *Ptef* promoter causes expression of *mttA* during the growth phase (Zambanini et al., 2017c). It is assumed that this forces *cis*-aconitate export from the mitochondria to the cytosol, leading to the observed growth defects.

The trends regarding OD₆₀₀, yield, and productivity were similar under screening conditions with a higher substrate concentration and CaCO₃ as buffer (Figure 8, Table 4). Much higher titers of up to $56.5 \pm 1.7 \text{ g L}^{-1}$ were reached compared to the MES-buffered cultivation due to the higher buffer capacity of CaCO₃, higher substrate concentration, and *in situ* precipitation of calcium ITA, which alleviates product inhibition.

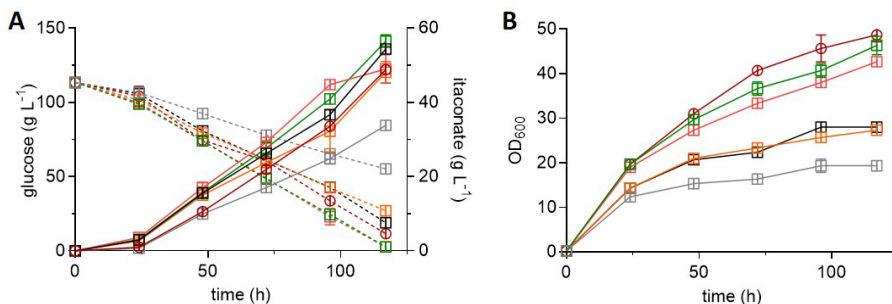


Figure 8: System Duetz cultivations of six *U. maydis* MB215 mutants in MTM with 15 mM NH₄Cl, 66 g L⁻¹ CaCO₃ pH 7.5, and 100 g L⁻¹ glucose.

(A) Concentration of itaconate (continuous lines) and glucose (dotted lines) and (B) OD₆₀₀ of *U. maydis* MB215 $\Delta cyp3 \Delta MEL \Delta UGA \Delta dgat \Delta P_{ria1}::P_{eteftmtA} \Delta fuz7$ (○) and five *P_eteftmtA* transformants of *U. maydis* MB215 $\Delta cyp3 \Delta MEL \Delta UGA \Delta dgat \Delta P_{ria1}::P_{eteftmtA} \Delta fuz7$ *P_eteftmtA*, K3 (□), K8 (□), K9 (□), K10 (□), and K14 (□) (n = 3 biological replicates).

Correlation between copy number of *P_eteftmtA* and impact on itaconate production

In order to test whether these differences in production parameters and growth are a result of differences in the copy number of *P_eteftmtA*, the copy number was determined by qPCR. Primer efficiencies and C_t values of *mttA* and two reference genes, UMG_02595 and UMG_03726, were 2.014 for JB-126/JB-127 ($R^2 = 0.999$), 1.994 for JB-128/JB-129 ($R^2 = 0.999$), and 1.976 for JB-132/JB-133 ($R^2 = 1.0$). Ratios between *mttA* and each reference gene were calculated independently according to Pfaffl (2001) and the resulting mean of both ratios was rounded to an integer value. As positive control, *U. maydis* MB215 $\Delta UMG_05079 P_{eteftmtA}$ was used. This strain was previously proven to be a single-copy *mttA* transformant by Southern blot (Hosseinpour Tehrani et al., 2019a), which was confirmed by the qPCR method. For the *mttA* transformants, copy numbers between 1 and 4 were determined (Table 5).

Table 5: Determination of $P_{etef}mttA$ copy number in five *U. maydis* MB215 $\Delta cyp3 \Delta MEL \Delta UA \Delta dgat \Delta P_{ria1}::P_{etef} \Delta fuz7 P_{etef}mttA$ transformants by qPCR (n = 3 biological replicates).

<i>U. maydis</i> strain	C _t value UMAG_ 02595	C _t value UMAG_ 03726	C _t value <i>mttA</i>	Ratio <i>mttA</i> to UMAG_ 02595	Ratio <i>mttA</i> to UMAG_ 03726	Rounded mean
wildtype	27.6 ± 0.10	27.9 ± 0.29	35.9 ± 1.20	0.0	0.0	0
$\Delta UMAG_05079::P_{etef}mttA$	25.7 ± 0.14	25.8 ± 0.24	25.7 ± 0.32	1.0	1.0	1
$P_{etef}mttA_K3$	28.3 ± 0.12	28.4 ± 0.31	26.7 ± 0.36	3.2	3.1	3
$P_{etef}mttA_K8$	27.8 ± 0.10	27.9 ± 0.11	28.5 ± 0.21	0.7	0.6	1
$P_{etef}mttA_K9$	28.2 ± 0.27	28.5 ± 0.16	26.4 ± 0.18	3.7	3.9	4
$P_{etef}mttA_K10$	26.8 ± 0.17	26.6 ± 0.35	26.6 ± 0.10	1.2	0.9	1
$P_{etef}mttA_K14$	26.6 ± 0.03	27.0 ± 0.13	25.2 ± 0.13	2.8	3.3	3

Cells of strain K8 with a single *mttA* copy reached the highest OD₆₀₀ and ITA productivity (Figure 9). The transformants with higher copy numbers showed lower OD₆₀₀ and production rates, but significantly higher yields. Transformant K3 represents an outlier, which is most apparent in the direct comparison to K14 having the same copy number of 3. Possibly, one or more copies of the *mttA* construct were inserted into a different locus, which may lead to different expression levels or to defects in growth due to gene disruption. Overall, transformant K14 showed the best balance of high yield with minimal reduction in growth and production rates. Therefore, this strain was selected for further characterization.

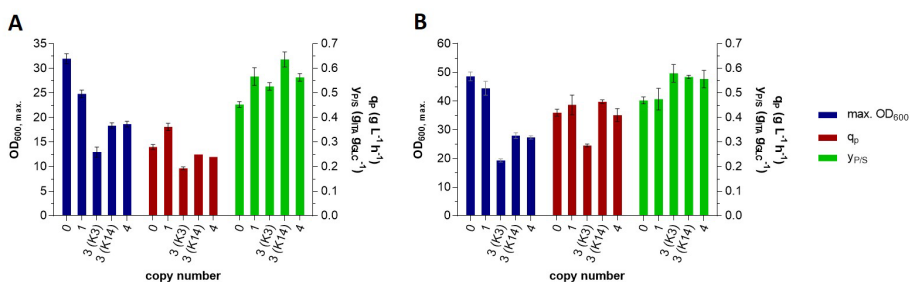


Figure 9: Production parameters of *U. maydis* MB215 $\Delta cyp3 \Delta MEL \Delta UA \Delta dgat \Delta P_{ria1}::P_{etef} \Delta fuz7$ transformants with different *mttA* copy numbers incubated in MTM with (A) 15 mM NH_4Cl , 100 mM MES pH 6.5, and 50 g L⁻¹ glucose and (B) 15 mM NH_4Cl , 66 g L⁻¹ $CaCO_3$ pH 7.5, and 100 g L⁻¹ glucose (n = 3 biological replicates).

Evaluation of itaconate production with the novel engineered strain K14 in a bioreactor

The final consolidated *U. maydis* MB215 $\Delta cyp3 \Delta MEL \Delta UA \Delta dgat \Delta P_{ria1}::P_{etef} \Delta fuz7 P_{etef}mttA_K14$, henceforth named strain K14 for ease of reference, was deeply engineered to reduce by-product formation, to stabilize the yeast-like morphology, and to alleviate bottlenecks in the ITA production pathway. This engineering strongly impacted growth, and thus might also affect its

catalytic vigor under stress. To assess the performance of the novel engineered strain K14 under more industrially relevant conditions, fed-batch bioreactor experiments were performed.

Previously, *in situ* precipitation of calcium ITA was successfully used to achieve very high titers with *U. maydis* MB215 $\Delta cyp3 \Delta P_{ria1}::P_{etef} \Delta fuz7 P_{etef} mttA$ (Hosseinpour Tehrani et al., 2019c). Under similar conditions with 200 g L⁻¹ glucose and 75 mM NH₄Cl in the presence of CaCO₃, strain K14 achieved very similar yield, titer, and productivity of ITA production (supplementary Table S2). A titer of 205.6 ± 1.1 g L⁻¹ ITA was achieved within 481 h with an overall productivity of 0.43 ± 0.00 g L⁻¹ h⁻¹ and a yield of 0.32 ± 0.00 g_{ITA} g_{GLC}⁻¹ (Figure 10). Although a very high titer was reached under these conditions due to the alleviation of product inhibition, the yield is relatively low compared to the shaken cultures. After the fermentation, extensive clumping of solids attached to reactor walls and components was discovered, indicating that the shown ITA production from broth samples during cultivation may be an underestimation. Although the *in situ* precipitation of ITA is a very promising strategy, it clearly requires extensive optimization of solids feeding and reactor mixing in order to realize the full potential of the engineered strain.

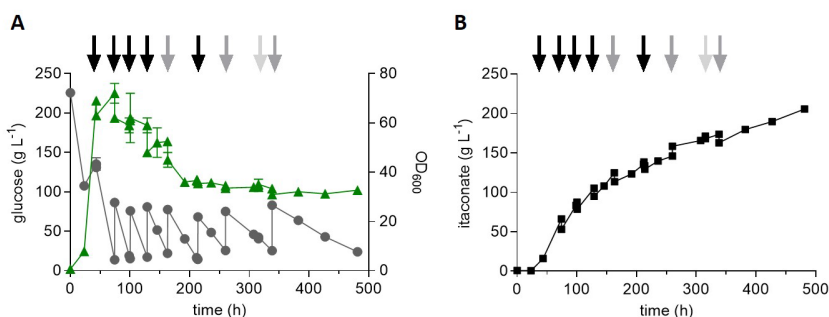


Figure 10: High cell-density pulsed fed-batch fermentations of *U. maydis* strain K14.

(A) Concentration of glucose (●) and OD₆₀₀ values (▲) and (B) concentration of itaconate (■) during fermentation in bioreactors containing batch medium with 75 mM NH₄Cl, CaCO₃ as buffer, and 200 g L⁻¹ glucose (n = 2 biological replicates). The stirrer was equipped with a pitched blade impeller on the top and a Rushton impeller on the bottom. Arrows indicate the addition of 80 g glucose + 50 g CaCO₃ (black arrow), 80 g glucose (grey arrow), or 50 g CaCO₃ (light grey arrow).

The intermittent stress imposed by the pulsed feeding strategy likely also negatively affected production. This is especially apparent in NaOH-titrated pulsed fed-batch fermentations, where only 60.0 g L⁻¹ ITA was produced with a yield of 0.42 g_{ITA} g_{GLC}⁻¹ (supplementary Figure S1). Although this is a considerable improvement compared to a similar fermentation with *U. maydis* MB215 $\Delta cyp3 \Delta P_{ria1}::P_{etef} \Delta fuz7 P_{etef} mttA$ (Hosseinpour Tehrani et al., 2019c) (supplementary Table S2), the achieved yield is still far lower from that obtained in shake flasks. This indicates that the strain modifications, especially the overexpression of *mttA*, reduced the tolerance of the engineered

strains to osmotic stress. Consequently, the novel engineered strain was cultivated in fed-batch fermentations with continuous feed to achieve a lower baseline glucose concentration. High cell-density fermentations with 75 mM NH_4Cl (Figure 11) as well as low cell-density fermentations with 15 mM NH_4Cl (Figure 12) were performed. A starting glucose concentration of 120 g L^{-1} was allowed to drop to approximately 50 g L^{-1} during growth, at which point a constant feed of 2.8 or 0.75 g h^{-1} was started, for the high and low cell-density fermentation, respectively.

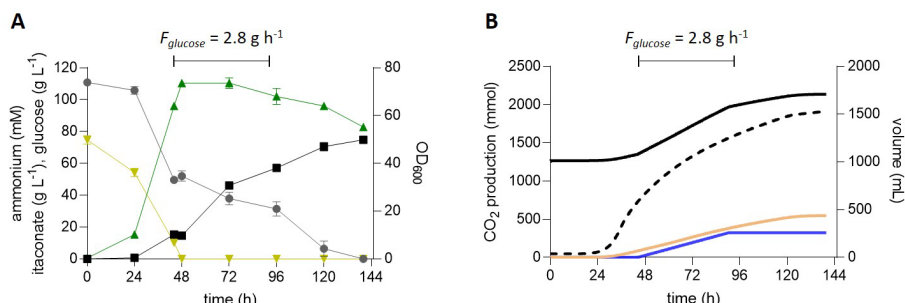


Figure 11: High cell-density fed-batch fermentations with continuous feed of *U. maydis* strain K14.

(A) Concentration of glucose (●), itaconate (■), ammonium (▼), and OD₆₀₀ values (▲) and (B) filling volume (continuous black line), CO₂ production (dotted black line), and the added volumes of 5 M NaOH (orange line) and 50 % glucose (blue line) during fermentation in bioreactors containing batch medium with 75 mM NH_4Cl and 120 g L^{-1} glucose ($n = 2$ biological replicates). The pH was kept at 6.5 by automatic titration with 5 M NaOH. Cultures were fed with an additional 130 g glucose at a rate of 2.8 g h^{-1} during the indicated time interval.

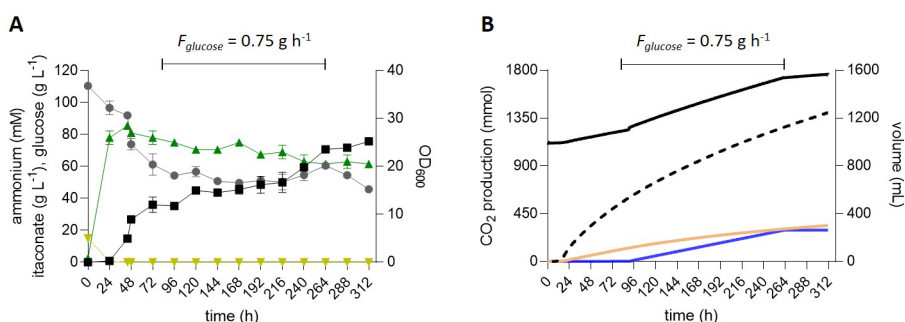


Figure 12: Low cell-density fed-batch fermentations with continuous feed of *U. maydis* strain K14.

(A) Concentration of glucose (●), itaconate (■), ammonium (▼), and OD₆₀₀ values (▲) and (B) filling volume (continuous black line), CO₂ production (dotted black line), and the added volumes of 5 M NaOH (orange line) and 50 % glucose (blue line) during fermentation in bioreactors containing batch medium with 15 mM NH_4Cl and 120 g L^{-1} glucose ($n = 2$ biological replicates). The pH was kept at 6.5 by automatic titration with NaOH. Cultures were fed with an additional 130 g glucose at a rate of 0.75 g h^{-1} during the indicated time interval.

In the high cell-density fermentation, $74.9 \pm 1.3 \text{ g L}^{-1}$ ITA was produced by *U. maydis* strain K14 within 140 h with an overall productivity of $0.53 \pm 0.01 \text{ g L}^{-1} \text{ h}^{-1}$ and a yield of $0.54 \pm 0.02 \text{ g}_{\text{ITA}} \text{ g}_{\text{GLC}}^{-1}$ (Figure 11). The low cell-density fermentation resulted in a similar ITA titer of $75.7 \pm 1.3 \text{ g L}^{-1}$ (Figure 12). The five-fold reduction in NH_4Cl as growth limiting nutrient only resulted in an approximately two-fold reduction of the maximum OD_{600} value as well as of the overall productivity (supplementary Table S2). A similar trend was observed previously for both ITA and malate producing strains (Geiser et al., 2016b; Zambanini et al., 2016a). The lower substrate requirement for biomass formation enabled a higher yield of $0.66 \pm 0.02 \text{ g}_{\text{ITA}} \text{ g}_{\text{GLC}}^{-1}$ (Figure 12). Compared to the low cell-density pulsed fed-batch (supplementary Figure S1), the fed-batch with continuous feed increased the titer by 27 %, the overall productivity by 14 % and the yield by 57 %. These results clearly illustrate the benefit of the lower glucose concentration, probably due to a reduced osmotic stress and the absence of osmo shocks caused by glucose pulses. A similar trend was observed for an engineered *U. cynodontis* strain, where a constant glucose feed controlled by an in-line glucose sensor significantly increased the production parameters, while lowering the production of erythritol as an osmoprotectant (Hosseinpour Tehrani et al., 2019d). Erythritol production was not observed in our *U. maydis* cultures, which is in good accordance with previous studies (Geiser et al., 2014; Guevarra & Tabuchi, 1990a). However, this species can tolerate over 2.5 osmol L^{-1} (Klement et al., 2012) and is known to produce other osmotically active compounds when exposed to such extreme osmotic conditions. Salmerón-Santiago et al. (2011) reported that *U. maydis* cells treated with 1 M sorbitol accumulated an increased level of trehalose, probably functioning as an osmoprotectant. The trehalase activity in these cells was increased at the same time, indicating cellular mechanisms for a rapid adaption of the trehalose content. Cervantes-Chávez et al. (2016) found that *U. maydis* mutants with a disrupted trehalose biosynthesis pathway were more sensitive to osmotic stress than the wildtype. Assuming that the ITA produced and the 0.5-1.0 M glucose pulses had a similar effect, it is reasonable to assume that the *U. maydis* cells were stressed during the pulsed fed-batch fermentations. This stress, combined with the drain of carbon posed by the synthesis of compatible solutes, likely caused the lower itaconate yield.

The yield of $0.66 \pm 0.02 \text{ g}_{\text{ITA}} \text{ g}_{\text{GLC}}^{-1}$ is the highest yield ever reported for *U. maydis*, and it is also higher than most reported yields achieved with *A. terreus* (Kuenz & Krull, 2018). In fact, the low cell-density fermentation achieved the theoretical maximal yield during the production phase. When disregarding the glucose consumed during the first 24 h in the growth phase, the yield was $0.72 \pm 0.02 \text{ g}_{\text{ITA}} \text{ g}_{\text{GLC}}^{-1}$, or $1.00 \pm 0.03 \text{ mol}_{\text{ITA}} \text{ mol}_{\text{GLC}}^{-1}$.

3.1.4. Conclusion

This study explored the limits of microbial ITA production with *U. maydis* by combinatorial metabolic and morphological engineering. These modifications, especially the overexpression of *mttA*, had a major effect on growth of the final strain *U. maydis* K14. This reduction in growth did affect its performance in fed-batch fermentations, but this effect could be avoided by reducing the glucose concentration with a continuous feeding strategy. Under these conditions, ITA was produced from glucose at 100 % of the theoretical maximum yield during the production phase in a low cell-density fermentation. Looking forward, osmotolerance of *U. maydis* may be enhanced by laboratory evolution. Further, production of ITA at low pH values is also paramount. Although *U. maydis* grows relatively poorly at low pH, the shaken cultures clearly indicate that the K14 strain is able to produce ITA at pH levels below 4. A pH shift between growth and production may therefore enable low-pH production. Since substrate cost is usually the main price-determining factor for commodity products, the high yield achieved in this work will significantly contribute to the establishment of an *Ustilago*-based industrial ITA production process, further enabled by the facile, yeast-like growth of this strain.

Funding

The work of J. Becker and H. Hosseinpour Tehrani was funded by the German Federal Ministry of Food and Agriculture (BMEL), through the Specialist agency renewable raw materials e. V. (FNR) as part of the ERA-IB project 'TTRAFFIC' (FKZ 22030515). The work of P. Ernst was funded by the German Federal Ministry of Education and Research (BMBF) as part of the 'BioökonomieRevier_INNO' project "UpRePP" (FKZ 031B0918A). N. Wierckx acknowledges funding from the Bio Based Industries Joint Undertaking under the European Union's Horizon 2020 research and innovation program under grant agreement No 887711 for the project Glaukos. The lab of L. M. Blank was partially funded by the German Research Foundation (DFG) under Germany's Excellence Strategy - Exzellenzcluster 2186 'The Fuel Science Center' (ID:390919832).

Acknowledgements

We thank Kerstin Schipper and Michael Feldbrügge (Institute of Microbiology, Heinrich-Heine University Düsseldorf) for pUMa1523 and pFLPexpC.

Conflicts of Interest

N. Wierckx, L. M. Blank and H. Hosseinpour Tehrani are inventors of patent applications on morphological engineering and organic acid production with *Ustilago* and related fungi. The other authors declare no conflict of interest.

3.2. Balancing pH and Yield: Exploring Itaconic Acid Production in *Ustilago cynodontis* from an Economic Perspective

P. Ernst, K. M. Saur, R. Kiefel, P.-J. Niehoff, R. Weskott, J. Büchs, A. Jupke, and N. Wierckx

Submitted for publication (January 2024).

Contributor role	Contributor
Conceptualization	N. Wierckx
Data curation	N. Wierckx, P. Ernst, K. M. Saur, R. Kiefel, P.-J. Niehoff
Formal analysis	P. Ernst, K. M. Saur, R. Kiefel, P.-J. Niehoff
Funding acquisition	N. Wierckx
Investigation	P. Ernst, K. M. Saur, R. Kiefel, P.-J. Niehoff, R. Weskott
Methodology	P. Ernst, K. M. Saur, R. Kiefel, P.-J. Niehoff
Project administration	N. Wierckx
Resources	N. Wierckx, J. Büchs, A. Jupke
Software	-
Supervision	N. Wierckx, J. Büchs, A. Jupke
Validation	P. Ernst, K. M. Saur, R. Kiefel, P.-J. Niehoff
Visualization	P. Ernst, K. M. Saur, R. Kiefel
Writing – original draft	P. Ernst
Writing – review and editing	N. Wierckx, P. Ernst, K. M. Saur

Overall contribution: 70 %

I performed all batch and fed-batch fermentations on glucose, partly supported by R. Weskott. K. M. Saur performed the crystallization experiments associated to Figure S4. R. Kiefel performed the specific operational cost analysis associated to Figure 18. P.-J. Niehoff performed the batch fermentation on thick juice associated to Figure S5. I was significantly involved in the visualization of the figures and wrote the original draft. All authors, but especially N. Wierckx, I, and K. M. Saur, were involved in the review and editing process.

A peer-reviewed version of the following manuscript was finally published in Biotechnology for Biofuels and Bioproducts (July 2024). doi: 10.1186/s13068-024-02550-0

Balancing pH and Yield: Exploring Itaconic Acid Production in *Ustilago cynodontis* from an Economic Perspective

Philipp Ernst¹, Katharina Maria Saur², Robert Kiefel², Paul-Joachim Niehoff³, Ronja Weskott¹, Jochen Büchs³, Andreas Jupke², Nick Wierckx^{*1}

¹ Institute of Bio- and Geosciences IBG-1: Biotechnology, Forschungszentrum Jülich GmbH, Wilhelm-Johnen-Straße, 52425 Jülich, Germany

² Fluid Process Engineering (AVT.FVT), RWTH Aachen University, Forckenbeckstraße 51, 52074 Aachen, Germany

³ Biochemical Engineering (AVT.BioVT), RWTH Aachen University, Forckenbeckstraße 51, 52074 Aachen, Germany

* Corresponding author: n.wierckx@fz-juelich.de

Background: Itaconic acid is a promising bio-based building block for the synthesis of polymers, plastics, fibers, and other materials. In recent years, *U. cynodontis* has emerged as an additional ITA producing non-conventional yeast, mainly due to its high acid tolerance, which significantly reduces base and acid use and associated saline waste co-production during fermentation and downstream processing. As a result, this could likely improve the economic viability of the ITA production process with Ustilaginaceae.

Results: In this study, we characterized a previously engineered ITA hyper-producing *U. cynodontis* strain in controlled fed-batch fermentations to determine the minimal and optimal pH for ITA production. Under optimal fermentation conditions, the hyper-producing strain can achieve the theoretical maximal ITA yield during the production phase in a low cell-density fermentation at pH 3.6, but at the expense of considerable base addition. Base consumption is strongly reduced at the pH of 2.8, but at cost of production yield, titer, and rate. A techno-economic analysis based on the entire process demonstrated that cost savings due to an additional decrease in pH control reagents and saline waste cannot compensate the yield loss observed at the highly acidic pH value 2.8.

Conclusions: Overall, this work provides novel data regarding the individual strain properties and production capabilities, contributing to a better understanding of the ITA production process with *U. cynodontis*, especially from an economic perspective.

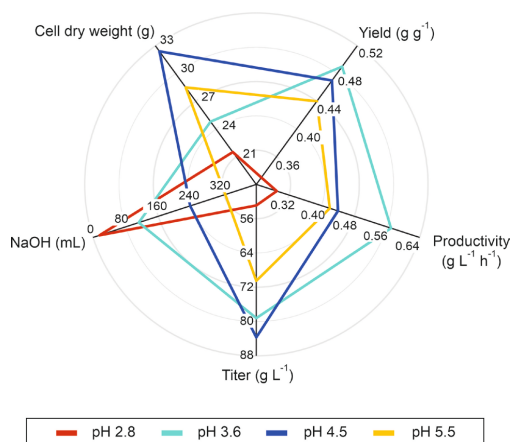


Figure 13: Graphical abstract showing the relationship of cell dry weight, yield, productivity, titer, and NaOH consumption during ITA production at different pH values in *U. cynodontis* ITA MAX pH (not submitted as part of the manuscript).

Keywords

Ustilago cynodontis, itaconic acid, low pH fermentations, downstream processing, techno-economic analysis

3.2.1. Introduction

Itaconic acid is considered as a promising renewable building block for the synthesis of plastics, synthetic resins, fibers and other materials (Klement et al., 2012; Okabe et al., 2009; Steiger et al., 2017; Willke & Vorlop, 2001). While ITA and its derivatives also hold great potential in the medical and pharmaceutical sectors (Michelucci et al., 2013; Mills et al., 2018; Olgagnier et al., 2020), a major opportunity exist in replacing acrylic acid and methacrylic acid in the polymer industry. However, this is only possible if the efficiency of the fermentation process can be increased to a point where it can compete with the petrochemical production (Bafana & Pandey, 2018; Klement & Büchs, 2013). In view of the already high yield, high titer, and high productivity of the industrially well-established ITA production process with the filamentous fungi *A. terreus* (Hevekerl et al., 2014), the possibilities for further process improvements seem to be largely exhausted, requiring a qualitative breakthrough in other dimensions of the process window. Therefore, we focus on *Ustilago*, which with its stable yeast-like morphology, may enable such further efficiency gains in scaled up fermentation processes by providing greater degrees of freedom in handling of the fermentation broth (Krull et al., 2020; Tabuchi et al., 1981). These gains may be further boosted by utilizing untreated industrial feedstocks (Regestein et al., 2018), as the substrate cost remains a critical factor in ITA production (Saur et al., 2023). Moreover, the long history of safe use and lower biosafety level of *Ustilago* simplifies the ITA production process in Europe compared to *A. terreus*.

In previous work, ITA production with a deeply engineered *U. maydis* strain was optimized in terms of glucose feeding strategies (Becker et al., 2021). A continuous fed-batch fermentation with a reduced glucose baseline concentration enabled ITA production at 100 % of the theoretical maximal yield during the production phase in a low cell-density fermentation. Since *U. maydis*'s pH sensitivity is largely uninvestigated, these fermentations were performed at a neutral pH. However, acidic pH values are beneficial for organic acid production (Roa Engel et al., 2011; van Maris et al., 2004). Therefore, we investigated *U. cynodontis*, an additional natural ITA producer that has recently been engineered to higher efficiencies (Hosseinpour Tehrani et al., 2019d; Hosseinpour Tehrani et al., 2019b). The advantage of this strain lies in the amalgamation of yeast-like morphology with high acid tolerance, thus enabling both easier handling and the utilization of the benefits from lower process pH values. On the one hand, low pH values reduce bacterial

growth, which generally reduces the risk of process contamination and may also allow to use a semi-sterile process, reducing costs. On the other hand, a low pH is crucial for downstream processing (DSP) efficiency (Magalhães et al., 2019; Okabe et al., 2009). Like other carboxylic acids, ITA can be purified by various unit operations such as crystallization (Okabe et al., 2009), extraction (Eggert et al., 2019), adsorption, chromatography (González et al., 2006; Ortíz-de-Lira et al., 2022), and membrane separation. Most of the ITA purification techniques require the free acid. Therefore, the fully protonated state is required to obtain high yields during DSP (Biselli et al., 2022; Eggert et al., 2019; Holtz et al., 2021; López-Garzón & Straathof, 2014; Ortíz-de-Lira et al., 2022; Saur et al., 2023). As a result, the pH needs to be lowered after fermentation by acid addition. In the industrially used crystallization, this leads to the formation of a co-salt with the base from the fermentation. While for *A. terreus*, this is not an issue due to its low fermentation pH, the concentration and composition of the co-salt limits the yield and increases the cost of waste disposal for *U. maydis* (Gausmann et al., 2021; Saur et al., 2023). A techno-economic analysis already revealed that a slightly lower fermentation yield with *U. cynodontis* could be compensated by its low fermentation pH of 3.6 when compared to *U. maydis* (Saur et al., 2023). According to previous research, it is known that *U. cynodontis* is capable of producing ITA even at pH values below 3.6 (Hosseinpour Tehrani et al., 2019d). Considering the pK_a values of ITA (3.84 and 5.55 at 20 °C), further reduction of the fermentation pH would shift ITA dissociation towards the fully protonated species, significantly reducing the addition of pH control reagents and therefore costs. As a result, this could likely improve the economic viability of the ITA production process with Ustilaginaceae.

A major factor in the establishment of *U. cynodontis* as a non-conventional ITA producer was the deletion of *fuz7*, which arrested the cells in a yeast-like morphology thereby avoiding filamentous growth. Hosseinpour Tehrani et al. (2019d) determined the pH optimum for ITA production at 3.6 with this morphology-engineered strain, but additional modifications were later performed to enhance ITA production. These genetic modifications include the deletion of the P450 monooxygenase encoding *cyp3*, the overexpression of the transcription regulator *ria1*, and the heterologous overexpression of the mitochondrial tricarboxylate transporter *mttA* from *A. terreus*. Since this metabolic engineering altered the product spectrum and interfered with the regulation of the ITA gene cluster, the pH optimum for ITA production with this optimized strain may have shifted. In this study, we therefore investigated the ITA production capabilities of the new ITA hyper-producing *U. cynodontis* strain through controlled fed-batch fermentations. We identified the pH optimum of this strain and explored process window boundaries of key parameters such as the maximum ITA titer and the lowest pH value possible. Additionally, the impact of pH on overall process economics was evaluated in a techno-economic analysis. Our

findings revealed that additional cost savings could be achieved by minimizing pH control reagents and reducing saline waste. Although ITA can be produced with the optimized *U. cynodontis* strain at pH values as low as 2.1, there is a clear optimum balance between the KPIs that is not reached by simply maximizing individual parameters. In summary, this study provides insight into the specific characteristics and production capabilities of the new ITA hyper-producing *U. cynodontis* strain, which improves our understanding of the ITA production process with this microorganism, particularly from an economic standpoint.

3.2.2. Results and discussion

Comparison of *U. maydis* K14 and *U. cynodontis* ITA MAX pH for itaconate production at low pH values

Despite the advantage of acidic pH values for organic acid production, previous fermentations of *U. maydis* MB215 $\Delta cyp3 \Delta MEL \Delta UGA \Delta dga1 P_{ria1::P_{etef} \Delta fuz7 P_{etef} mttA_K14$, henceforth named strain K14 for ease of reference, were performed at a neutral pH of 6.5 due to the largely uninvestigated growth- and production characteristics of this strain at lower pH values. In shake flask cultivations, engineered *U. maydis* hyper-producers do not grow at acidic pH conditions, but still produce significant amounts of ITA at lower pH values (Becker (b. Loevenich), 2019; Hosseinpour Tehrani et al., 2019c). Hence, ITA production of *U. maydis* K14 was assessed in fermentations with different pH values for growth and ITA production phase (Figure 14A). To gain a comprehensive comparison, *U. cynodontis* NBRC9727 $\Delta fuz7 \Delta cyp3 P_{etef} mttA P_{ria1ria1}$, henceforth named strain ITA MAX pH for ease of reference, was cultured under similar conditions (Figure 14B). To study the effect of reduced ammonium concentrations on the product to substrate yield in *U. cynodontis* ITA MAX pH, an additional low cell-density fed-batch fermentation was performed (Figure 14C).

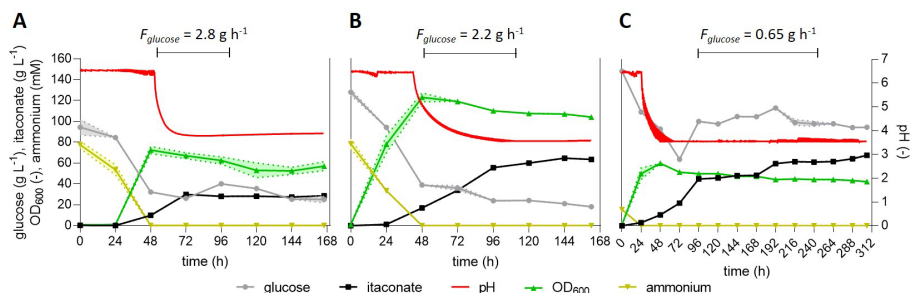


Figure 14: Fed-batch fermentations with continuous feed of *U. maydis* K14 with high ammonium concentration (A) and *U. cynodontis* ITA MAX pH with high (B) and low (C) ammonium concentration.

Bioreactor cultivations were performed in batch medium with 75 mM NH_4Cl and approximately 120 g L^{-1} glucose ($n = 2$ biological replicates). The pH was controlled by automatic titration with 5 M NaOH. After the depletion of nitrogen (24 h and 48 h), the pH was allowed to drop from pH 6.5 to pH 3.6 through the production of ITA. Cultures were fed with an additional 130 g glucose (50 % w/v feeding solution) at a rate of 2.8 g h^{-1} for *U. maydis* K14 and 2.2 g h^{-1} or 0.65 g h^{-1} for *U. cynodontis* ITA MAX pH during the indicated time interval. The feeding rates were estimated from glucose consumption rates of previous fermentations, aimed at keeping the glucose concentration at a relatively constant level of approximately 50 g L^{-1} . The low cell-density cultures were overfed between 72 h and 96 h.

Until 72 h, both high cell-density fermentations behaved similarly (Figure 14A, B). The depletion of nitrogen was achieved and ITA accumulated to approximately 30 g L^{-1} . However, upon reaching lower pH levels, difference became apparent between the two species. In the case of you *U. maydis* K14, production almost completely stopped once the pH reached values below 4.0. On the contrary, *U. cynodontis* ITA MAX pH produced an additional 30 g L^{-1} ITA after reaching acidic pH values. Remarkably, the *U. maydis* K14 culture did not even reach the final pH value 3.6, although the glucose concentration still declined until the end of the fermentation. This continued glucose uptake in the absence of further production indicates a very high metabolic energy demand for maintaining intracellular pH homeostasis. These results show that *U. maydis* K14 is not suitable to produce ITA at lower pH values and is possibly more sensitive towards weak acid stress. Consequently, *U. cynodontis* ITA MAX pH was identified as a preferable candidate for subsequent characterization. If ITA is to become a bulk chemical, yield is one of the most relevant production parameter because substrate cost is a decisive price-determining factor (Saur et al., 2023). The availability of nitrogen and the resulting C/N ratio offer a dimension to optimize the product to substrate yield by controlling the biomass density. Typically, lower nitrogen levels result in higher yields but also lower productivities (Zambanini et al., 2017c). In previous fed-batch fermentations of *U. maydis* K14 with a reduced ammonium concentration, ITA was produced at the maximal theoretical yield of $0.72 \pm 0.02 \text{ g}_{\text{ITA}} \text{ g}_{\text{GLC}}^{-1}$ during the production phase (Becker et al., 2021). A similar trend was observed for *U. cynodontis* ITA MAX pH during the low cell-density fermentation (Figure 14C). This fermentation resulted in a similar ITA titer of $67.8 \pm 0.7 \text{ g L}^{-1}$

compared to the high cell-density fermentation. Interestingly, the 5-fold reduction in ammonium chloride as growth-limiting nutrient only resulted in an approximately 2-fold reduction of the maximum OD_{600} value as well as of the overall productivity ($0.22 \pm 0.01 \text{ g L}^{-1} \text{ h}^{-1}$). A similar phenomenon was observed for *U. maydis* (Becker et al., 2021). The lower substrate requirement for biomass production enabled a higher yield of $0.55 \pm 0.02 \text{ g}_{\text{ITA}} \text{ g}_{\text{GLC}}^{-1}$. When disregarding the glucose consumed during the first 24 hours in the growth phase, this fermentation achieved the theoretical maximal yield of $0.72 \pm 0.01 \text{ g}_{\text{ITA}} \text{ g}_{\text{GLC}}^{-1}$. This yield is the highest yield ever reported for *U. cynodontis*. Compared to previously published low cell-density pulsed fed-batch fermentation with a pH shift from 6.0 to 3.6, the fed-batch with continuous feed increased the titer by 62 % and the yield by 41 %, while the overall productivity remained nearly constant. These results clearly illustrate the benefit of a continuous glucose feed, preventing osmotic shocks caused by pulsed feeding. However, it is to note that the baseline glucose concentration during feeding was significantly higher than in the pulsed fed-batch fermentation. Although a higher osmotic stress due to elevated glucose concentration would be expected, it is also plausible that approximately 100 g L^{-1} glucose represents a threshold concentration for achieving more efficient ITA production while maintaining relatively low osmotic stress. These findings are in line with those reported for ITA production with *A. terreus*, where the highest yields were obtained at glucose concentration between 120 to 200 g L^{-1} (Karaffa et al., 2015). Almost the same is reported for citrate production in *A. niger* (Xu et al., 1989). This phenomenon should be further investigated for ITA production with Ustilaginaceae.

Comparison of the itaconate production capabilities of *U. cynodontis* ITA MAX pH at neutral and acidic pH values

Previous research has demonstrated that *U. cynodontis* is also able to grow at the acidic pH value 3.6 (Hosseinpour Tehrani et al., 2019d). To investigate the impact of reduced pH values throughout the entire fermentation process, additional continuous fed-batch fermentations were conducted as described above. Growth and production capabilities achieved at pH 3.6 were compared to values obtained from fermentations at pH 6.5 (Figure 15).

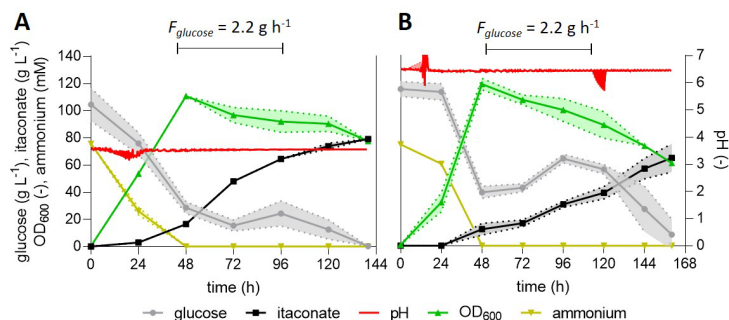


Figure 15: High cell-density fed-batch fermentations with continuous feed of *U. cynodontis* ITA MAX pH at pH 3.6 (A) and pH 6.5 (B).

Bioreactor cultivations were performed in batch medium with 75 mM NH₄Cl and approximately 110 g L⁻¹ glucose ($n = 2$ biological replicates). The pH was controlled by automatic titration with 5 M NaOH. Cultures were fed with an additional 130 g glucose (50 % w/v feeding solution) at a rate of 2.2 g h⁻¹ during the indicated time interval. The feeding rates were estimated from glucose consumption rates of previous fermentations, aimed at keeping the glucose concentration at a constant level of approximately 50 g L⁻¹.

In the neutral pH fermentation, $64.7 \pm 10.5 \text{ g L}^{-1}$ ITA was produced within approximately 160 h with an overall productivity of $0.40 \pm 0.06 \text{ g L}^{-1} \text{ h}^{-1}$ and the yield $0.42 \pm 0.02 \text{ g}_{\text{ITA}} \text{ g}_{\text{GLC}}^{-1}$ (Figure 15B). Previous fed-batch fermentation with a pH-shift from 6.5 to 3.6 achieved similar KPIs (Figure 14B). However, the low pH fermentation resulted in a higher ITA yield of $0.49 \pm 0.01 \text{ g}_{\text{ITA}} \text{ g}_{\text{GLC}}^{-1}$ (Figure 15A). In addition, the overall productivity was increased by 39 % ($0.57 \pm 0.01 \text{ g L}^{-1} \text{ h}^{-1}$) and the titer by 22 % ($79.2 \pm 1.3 \text{ g L}^{-1}$). These results show that *U. cynodontis* ITA MAX pH not only tolerates acidic conditions, it actually produces better at lower pH values. This result is promising, given that the acidic pH fermentation required approximately 3.5-fold less NOH compared to the neutral pH fermentation (112 mL and 398 mL 5 M NaOH solution). The KPIs are in good accordance with those previously achieved with this strain using a constant glucose feed controlled by an inline glucose sensor (78.6 g L^{-1} , $0.45 \text{ g}_{\text{ITA}} \text{ g}_{\text{GLC}}^{-1}$, $0.42 \text{ g L}^{-1} \text{ h}^{-1}$) (Hosseinpour Tehrani et al., 2019d). Less optimal progenitor strains of *U. cynodontis* ITA MAX pH are capable of producing ITA even at pH levels below 3.6 (Hosseinpour Tehrani et al., 2019d). Given the pK_a values of ITA of 3.84 and 5.55 (at 20 °C), further reduction of the fermentation pH is expected to still significantly reduce base consumption (Krull et al., 2017a). Thereby, costs associated with pH adjusting reagents can be further reduced. In addition, less HCl is necessary for DSP. This leads to a lower amount of co-salt in the fermentation broth, which can therefore be further concentrated which increases the crystallization yields. As shown by Saur et al. (2023), this increased yield in DSP is able to compensate for partial yield loss in fermentation (cf. introduction). As a result, this capability holds the potential to improve the economic viability of the ITA production process with *U. cynodontis*.

Identification of the pH optimum for itaconate production with *U. cynodontis* ITA MAX pH

The pH plays a crucial role as it determines the ITA species distribution during the fermentation process. On the one hand, protonated ITA negatively impacts the efficiency of the fermentation as it leads to weak acid uncoupling, which increases maintenance demand through energy-driven export of protons, and it possibly increases product inhibition by raising the intracellular ITA concentration. On the other hand, the protonated acid greatly facilitates DSP as it avoids additional acid use and salt co-production as described above. Therefore, it is crucial to carefully determine the optimum pH value in order to balance these effects and achieve the overall most efficient ITA production. However, the pH optimum for ITA production with *U. cynodontis* has so far only been determined with the sub-optimal production strain containing only the *fuz7* deletion. To examine the pH optimum of the new ITA hyper-producing strain, a series of pH controlled fed-batch fermentations were conducted in standardized conditions (Figure 16). To avoid growth defects due to pH values below 3.6, the initial biomass production phase was performed at pH 3.6 for all fermentations. Following the depletion of the nitrogen source, the pH was allowed to drop to the corresponding lower pH value. To adjust the pH value above values of 3.6, NaOH was added.

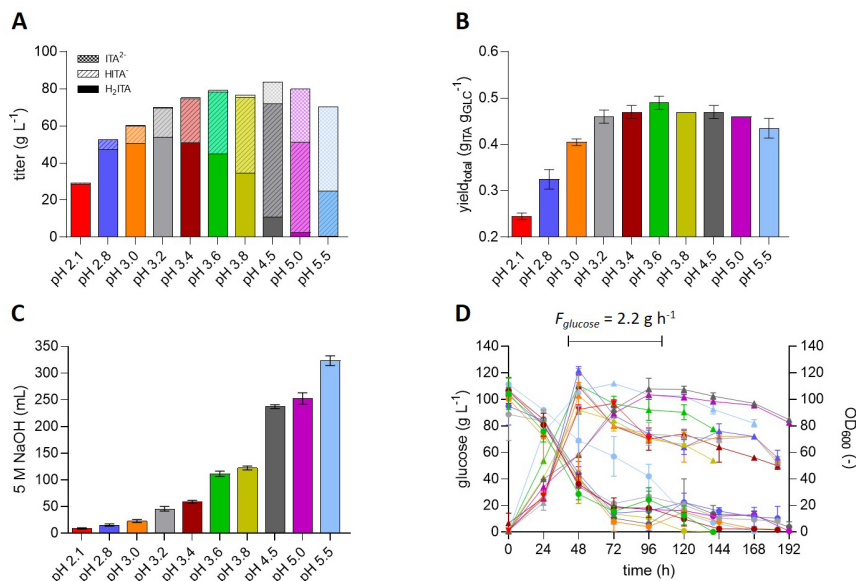


Figure 16: Fed-batch fermentations for the determination of the pH optimum for itaconate production with *U. cynodontis* ITA MAX pH.

(A) Distribution of protonation states of ITA, (B) yield_{total}, (C) added volumes of 5 M NaOH and (D) concentration of glucose (●) and OD₆₀₀ (▲) during fermentation at different pH values in bioreactors containing batch medium with 75 mM NH₄Cl and approximately 110 g L⁻¹ glucose (n = 2 biological replicates). The colors in Figure D indicate fermentations at the pH values as shown in the panels A-C. The pH was controlled by automatic titration with 5 M NaOH. After the depletion of nitrogen (48 h), the pH was allowed to naturally drop to the corresponding lower pH value. pH values above 3.6 were adjusted with 5 M NaOH. pH 2.1 represents the lowest possible pH value that can be achieved with *U. cynodontis* ITA MAX pH. This pH value was determined in a high cell-density batch fermentation with 75 mM NH₄Cl, approximately 200 g L⁻¹ glucose, and an uncontrolled pH value during the production phase. All other cultures were fed with an additional 130 g glucose (50 % w/v feeding solution) at a rate of 2.2 g h⁻¹ during the indicated time interval in B.

During the initial biomass production phase, a similar growth was observed across all experiments. However, after the pH was adjusted to the corresponding value being tested, differences in the cell-densities became apparent. pH values below 3.6 resulted in decreased optical densities (Figure 16D), indicating acid stress of the cells. The stress is most likely caused by weak acid uncoupling, which is more prominent at low pH values due to higher fractions of the double-protonated species (Figure 16A). The increased weak acid uncoupling at these lower pH values is also reflected in reduced yields (Figure 16B). The lowest yield was observed at the minimal pH value of 2.1, which was identified in a batch fermentation without pH control during the ITA production phase. However, the NaOH consumption during this fermentation was 36-fold reduced compared to the fermentation at pH 5.5 (Figure 16C, Figure S2). The highest yield with moderate base addition was achieved at pH 3.6, similar to what was previously determined for

the morphology-engineered strain. The double-protonated form remained relatively constant within the pH range of 2.8 and 3.4, suggesting a potential inhibitory threshold for the cells (Figure 16A). At pH 3.6, there is a significant reduction in H₂ITA. This reduction could explain the high KPIs observed at this pH value, indicating that H₂ITA concentrations are key to achieving maximum KPIs. Considering only the yield, the additional genetic modification did not change the pH optimum. The morphology-engineered strain also achieved the highest ITA titer at 3.6, and showed afterwards declining titer with increasing pH values. Regarding ITA titers, it consequently appears that higher pH values negatively impact the regulation of the ITA cluster genes of the *fuz7* variant. The new ITA hyper-producing strain however, showed increasing titers with increasing pH values until a pH of 5.0 (Figure 16A). This may be due to the interference in the regulatory mechanisms of the ITA cluster genes by the *ria1* overexpression. The overexpression of *ria1* may have contributed to an increased tolerance of the strain towards higher product concentrations. It may also be possible that the overexpression of *ria1* reduced the pH dependency of the regulation of the ITA cluster genes. One of the main potential benefits of production at more neutral pH values lies in the potentially higher titers (Hevekerl et al., 2014; Krull et al., 2017a). In order to determine the maximum ITA titer with this strain, an additional fed-batch fermentation was performed with a prolonged feeding phase (Figure 17).

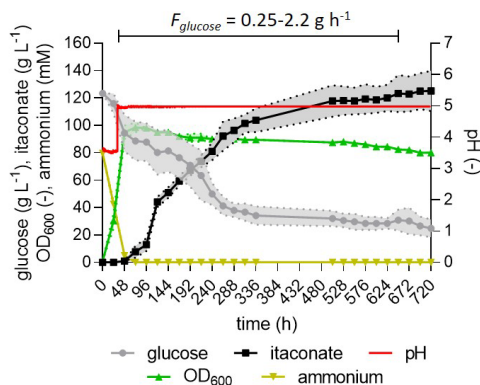


Figure 17: High cell-density fed-batch fermentations with a prolonged feeding phase of *U. cynodontis* ITA MAX pH.

Bioreactor cultivations were performed in batch medium with 75 mM NH₄Cl and approximately 120 g L⁻¹ glucose (n = 2 biological replicates). The pH was controlled by automatic titration with 5 M NaOH. After approximately 48 h, the pH was adjusted to pH 5 and afterwards maintained at this value until the end of the fermentation. Cultures were fed with an additional 540 g glucose (70 % w/v feeding solution) at rates between 0.25-2.2 g h⁻¹ during the indicated time interval. The feeding profile is shown in Table S3. The feeding rates were manually adjusted aimed at keeping the glucose concentration at a constant level of approximately 50 g L⁻¹.

In the fed-batch fermentation with a prolonged feeding phase, the ITA titer kept linearly increasing up to 264 h up to approximately $92.3 \pm 10.7 \text{ g L}^{-1}$ at a productivity of $0.34 \pm 0.01 \text{ g L}^{-1} \text{ h}^{-1}$ and a yield of $0.42 \pm 0.01 \text{ g}_{\text{ITA}} \text{ g}_{\text{GLC}}^{-1}$ (Figure 17). During the remaining fermentation time, a linear increase of the ITA titer could still be observed, however with a strongly reduced productivity as the product inhibition became more and more prominent, taking another 434 h to produce only $32.9 \pm 4.0 \text{ g L}^{-1}$ additional ITA. This fermentation reached a final ITA titer of $125.2 \pm 14.6 \text{ g L}^{-1}$, one of the highest ITA titers reported for Ustilaginaceae with NaOH titration. The ITA concentration remained constant between 696 h and 720 h, indicating that the maximum titer was finally reached after approximately one month of fermentation time. In total, this fermentation resulted in an overall productivity of $0.17 \pm 0.02 \text{ g L}^{-1} \text{ h}^{-1}$ and a yield of $0.36 \pm 0.01 \text{ g}_{\text{ITA}} \text{ g}_{\text{GLC}}^{-1}$. Although a very high titer could be achieved through extended feeding, this came at the major expense of a lower yield end rate. Despite the reduced weak acid stress at the pH value of 5.0 and the higher ITA production per cell, this fermentation highlighted the strong inhibitory effect of elevated product titers on the over KPIs, indicating a major efficiency loss at titers above $92.3 \pm 10.7 \text{ g L}^{-1}$ even at a higher pH value. This result highlights that not only elevated H_2ITA concentrations are inhibitory for the cells, but also higher overall product titers due to increased osmotic stress.

In summary, the engineered *U. cynodontis* ITA MAX pH strain shows an extended operational range for ITA production compared to the previous morphology-engineered strain, particularly in terms of ITA titers. The carbon balance of all fermentations is shown in Figure S3. Analogous to the morphology-engineered strain, the achieved KPIs for the hyper-producing strain exhibited a moderate decrease at pH values below 3.6, which became more prominent at pH values below 3.0 (Figure 16B). However, the volumes of NaOH added during these low-pH fermentations were also significantly reduced (Figure 16C) and associated reductions in acid consumption and saline waste production during DSP can be expected. To assess whether these can economically compensate for the losses in fermentation yield at pH values lower than 3.6, an operational cost analysis was performed. We also added the economic results for fed-batch fermentations at higher pH values than 3.6 to provide a full picture of the cost structure changes.

Identification of the pH optimum by operative cost analysis

The process KPIs from the fed-batch fermentations served as an input parameter for the simulation. Those consist of product titer, fermentation yield, and pH during product formation phase (Figure 16A, B). The results of the cost analysis are displayed in Figure 18.

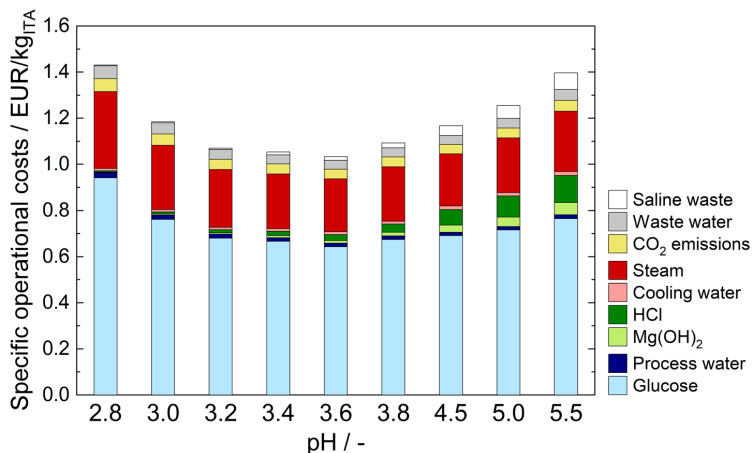


Figure 18: Specific operational costs for fed-batch fermentations at different pH values.

As expected, the simulated costs associated to acid and base use and saline waste disposal decrease with lower fermentation pH. Reduced amounts of HCl and saline waste could also be confirmed in crystallization experiments using real cultivation supernatants from batch fermentations (Figure S4). However, those costs comprise only a small fraction of the total operational costs. Independent of the selected pH, the total operational costs are most strongly influenced by overall substrate yield. The outstanding fermentation yield at pH 3.6 cuts costs significantly while specific operational costs are visibly larger at high and low pH values due to the poor substrate-to-product conversion. This cannot be outweighed by higher DSP yields as at lower pH as discussed in Saur et al. (2023). The specific operational costs of approximately 1.04 EUR kg⁻¹ at pH 3.6 achieved in this work are approximately 0.40 EUR kg⁻¹ lower than those previously obtained for this strain (Saur et al., 2023). Nevertheless, to successfully compete with the petrochemical production of the counterparts acrylic acid and methacrylic acid, it is necessary to further reduce the production costs (Werpy & Petersen, 2004).

3.2.3. Conclusion

From an economic perspective, the process pH should not be controlled below 3.6 as yield deficits cannot be counterbalanced by reduced amounts of salt waste production. However, lower pH values during the production phase may still offer advantages. Due to the further reduced risk of process contamination, semi-sterile industrial feedstocks might be fed during the production phase, reducing costs. The general feasibility to produce ITA at the highly acidic pH value 2.8 using the side stream thick juice from the sugar industry could already be successfully demonstrated (Figure S5). In addition *in situ* product removal is greatly facilitated by direct production of the

protonated ITA at these lower pH values (Eggert et al., 2019; Pastoors et al., 2023). Therefore, the low fermentation pH of 2.8 is expected to significantly enhance product removal efficiency, which may further reduce the DSP costs. These effects should be investigated in the future. Further studies could also comprise a techno-economic analysis excluding the initial biomass production phase since Hosseinpour Tehrani et al. (2019d) showed that *U. cynodontis* ITA MAX pH can be subjected to repeated batch fermentations. In this way, the same biomass could be used multiple times for ITA production, potentially leading to a more improved cost analysis of the ITA production process with Ustilaginaceae.

Overall, this study provides exquisite data regarding the production strain properties and production capabilities, potentially enabling the development and implementation of a more cost-effective ITA production process with Ustilaginaceae in the future.

3.2.4. Materials and methods

Chemicals and strains

All chemicals used in this study were obtained from Sigma-Aldrich (St. Louis, USA), Thermo Fisher Scientific (Waltham, USA), or VWR (Radnor, USA) and were of analytical grade. Thick juice was supplied by Pfeifer & Langen Industrie- und Handels-KG. The strain *U. cynodontis* NBRC9727 $\Delta fuz7 \Delta cyp3 P_{etef}mttA P_{ria1}ria1$ (Hosseinpour Tehrani et al., 2019b) and the strain *U. maydis* MB215 $\Delta cyp3 \Delta MEL \Delta UA \Delta dgt P_{ria1}::P_{etef} \Delta fuz7 P_{etef}mttA_K14$ (Becker et al., 2021) were used in this study.

Bioreactor cultivations

As previously described in Becker et al. (2021), controlled fed-batch cultivations were performed in a DASGIP Bioblock (Eppendorf, Germany). The process was controlled using the Eppendorf DASware control software (Eppendorf, Germany). Vessels with a total volume of 2.3 L and a working volume of 1.0 L were used. All cultivations were performed in batch medium according to Geiser et al. (2014) containing 0.2 g L⁻¹ MgSO₄·7H₂O, 0.01 g L⁻¹ FeSO₄·7H₂O, 0.5 g L⁻¹ KH₂PO₄, 1 g L⁻¹ yeast extract (Merck Millipore, Germany), 1 mL L⁻¹ vitamin solution, 1 mL L⁻¹ trace element solution and varying concentrations of glucose and NH₄Cl, as indicated. The vitamin solution contained (per liter) 0.05 g D-biotin, 1 g D-calcium pantothenate, 1 g nicotinic acid, 25 g myo-inositol, 1 g thiamine hydrochloride, 1 g pyridoxol hydrochloride, and 0.2 g *para*-aminobenzoic acid. The trace element solution contained (per liter) 1.5 g EDTA, 0.45 g of ZnSO₄·7H₂O, 0.10 g of MnCl₂·4H₂O, 0.03 g of CoCl₂·6H₂O, 0.03 g of CuSO₄·5H₂O, 0.04 g of Na₂MoO₄·2H₂O, 0.45 g of CaCl₂·2H₂O, 0.3 g of FeSO₄·7H₂O, 0.10 g of H₃BO₃ and 0.01 g of KI. During cultivation, the pH was kept constant at the corresponding value by automatic addition of 5 M NaOH or 1 M HCl. The DO

was controlled at 30 % by a cascade mode: first agitation 800-1200 rpm (0-40 % DOT controller output); second air flow 1-2 vvm (40-80 % DOT controller output); third oxygen 21-100 % oxygen (80-100 % DOT controller output). The cultivation was performed at 30 °C. The bioreactor was inoculated to a final OD₆₀₀ of 0.75 from an overnight pre-culture grown in screening medium according to Geiser et al. (2014) containing 50 g L⁻¹ glucose and 100 mM MES buffer. 0.5 mL Antifoam 204 (Sigma, A6426) was added in the beginning of the cultivation and afterwards every 24 h.

Analytical methods

Identification and quantification of products and substrates in the supernatants was performed using a HPLC 1260 Infinity system (Agilent, Waldbronn, Germany) with an ISERA Metab AAC column 300 × 7.8 mm column (ISERA, Germany). Separation was achieved by using an isocratic elution program at a flow rate of 0.6 mL min⁻¹ and a temperature of 40 °C with 5 mM sulfuric acid as a solvent (Becker et al., 2021). For detection, a DAD at 210 nm and a RI detector was used. All samples were filtered with Rotilabo syringe filters (CA, 0.20 µm, Ø 15 mm) and afterwards diluted with ddH₂O. Analytes were identified via retention time compared to corresponding standards. Data analysis was performed using the Agilent OpenLAB Data Analysis - Build 2.200.0.528 software (Agilent, Waldbronn, Germany). The ammonium concentration in culture samples was determined using the colorimetric method after Willis et al. (1996). 10 µL culture supernatant was combined with 200 µL reagent (8 g sodium salicylate, 10 g trisodiumphosphate, 0.125 g sodium nitroprusside), followed by the quick addition of 50 µL hypochlorite solution. After color development occurred (at least 15 min at RT), absorbance at 685 nm was measured in a flat-bottomed MTP plate without lid using a spectrophotometer. Ammonium concentrations were calculated using a standard curve of ammonium. Cell-densities were quantified by optical density measurement at 600 nm wavelength by use of cuvettes and a spectrophotometer. Samples were diluted appropriately with the respective medium to fall within the linear measuring range of the photometer between absolute values of 0.2 and 0.4. For CDW determination, 2 mL culture broth was centrifuged at maximum speed followed by drying the pellet for 48 h at 65 °C and afterwards weighing it.

Process design and operative cost analysis

The presented cost analysis is performed based on the process design described by Saur et al. (2023) for ITA production with *Ustilago* species. The according flowsheet is illustrated by a block flow diagram in Figure S6.

The fermenter is fed with a diluted glucose feed of 500 g L⁻¹. During ITA production, the pH is maintained by base addition. The broth is separated from the cells by sterile filtration. Afterward,

the filtered broth is concentrated by evaporation up to an ITA concentration of 350 g L⁻¹. The pH is then lowered by acid addition so that a pH of approximately 2.8 is attained after crystallization. In the cooling crystallizer, the temperature is decreased to 15 °C at atmospheric pressure. To increase the ITA yield in the DSP, the purification sequence is repeated. Water is further removed from the mother liquor by a second evaporator up to a concentration at which a co-crystallization of ITA and inorganic salt in a second cooling crystallizer can just be avoided. The inorganic salt-containing liquid stream is subsequently disposed. However, the ITA solid fractions are dissolved in water at 80 °C to remove residual contaminants and increase the purity of the final ITA crystals. The elevated temperature requires only moderate amounts of water for dilution and avoids large heat requirements for evaporation in succeeding process steps. To decolorize the dissolved ITA stream, an activated carbon treatment is performed. Finally, the solution is fed to an evaporative crystallizer. The mother liquor is recycled and mixed with the filtered fermentation broth while the ITA crystals are fed to a dryer.

The process design requires the use of Mg(OH)₂ as base in the fermenter. The subsequent acidic pH shift in the DSP is performed with HCl to form the highly soluble co-salt MgCl₂. To alleviate the experimental investigation, fed-batch fermentations conducted for this work are pH-controlled by 5 M NaOH solution instead of a Mg(OH)₂ suspension, which easily causes blocking of small-diameter tubing.

The flowsheet is modeled using Aspen Plus (V11) (Aspen Technology, Inc., Bedford, MA, USA). Calculated material streams and energy demands are used for the cost analysis. The details of the modeling framework and pricing are outlined in Saur et al. (2023).

Funding

This project has received funding from the Bio-based Industries Joint Undertaking (JU) under the European Union's Horizon 2020 research and innovation program under grant agreement No 887711. The JU receives support from the European Union's Horizon 2020 research and innovation program and the Bio-based Industries Consortium. Further funding was received by the German Federal Ministry of Education and Research (BMBF, project: "Modellregion, BioRevier-PLUS: InBio, Innovationscluster integrierte Bioraffinerie", grant no. 031B1135A).

Acknowledgements

We thank Pfeifer & Langen Industrie- und Handels-KG for providing the thick juice. We thank all project partners for fruitful discussions.

Conflicts of interest

The authors declare that they have no competing interests.

3.3. Establishing an Itaconic Acid Production Process with *Ustilago* species on the Low-cost Substrate Starch

P. Ernst, A. Wirtz, B. Wynands, and N. Wierckx

Submitted for publication (February 2024).

Contributor role	Contributor
Conceptualization	N. Wierckx
Data curation	N. Wierckx, P. Ernst, A. Wirtz
Formal analysis	P. Ernst, A. Wirtz
Funding acquisition	N. Wierckx
Investigation	P. Ernst, A. Wirtz
Methodology	P. Ernst, A. Wirtz
Project administration	N. Wierckx
Resources	N. Wierckx
Software	-
Supervision	N. Wierckx, B. Wynands
Validation	P. Ernst, A. Wirtz
Visualization	P. Ernst
Writing – original draft	P. Ernst
Writing – review and editing	N. Wierckx, P. Ernst

Overall contribution: 90 %

I performed the strain engineering, all cultivations, and the SDS-PAGE analysis. A. Wirtz performed the LC-MS/MS analysis associated to Figure 22. I prepared all figures and wrote the original draft. All authors, but especially N. Wierckx and I, were involved in the review and editing process.

A peer-reviewed version of the following manuscript was finally published in FEMS Yeast Research (July 2024). doi: 10.1093/femsyr/foae023

Establishing an Itaconic Acid Production Process with *Ustilago* species on the low-cost substrate starch

Philipp Ernst¹, Astrid Wirtz¹, Benedikt Wynands¹, Nick Wierckx^{*1}

¹ Institute of Bio- and Geosciences IBG-1: Biotechnology, Forschungszentrum Jülich GmbH, Wilhelm-Johnen-Straße, 52425 Jülich, Germany

* Corresponding author: n.wierckx@fz-juelich.de

Abstract: *U. maydis* and *U. cynodontis* are natural producers of a broad range of valuable molecules including itaconate, malate, glycolipids and triacylglycerols. Both *Ustilago* species are insensitive towards medium impurities, and have previously been engineered for efficient ITA production and stabilized yeast-like growth. Due to these features, these strains were already successfully used for the production of ITA from different alternative feedstocks such as molasses, thick juice and crude glycerol. Here, we analyzed the amylolytic capabilities of *Ustilago* species for metabolism of starch, a highly abundant and low-cost polymeric carbohydrate widely utilized as a substrate in several biotechnological processes. *U. cynodontis* was found to utilize gelatinized potato starch for both growth and ITA production, confirming the presence of extracellular amylolytic enzymes in *Ustilago* species. Starch was rapidly degraded by *U. cynodontis*, even though no α -amylase was detected. Further experiments indicate that starch hydrolysis is caused by the synergistic action of glucoamylase and α -glucosidase enzymes. The enzymes showed a maximum activity of around 0.5 U mL⁻¹ at the fifth day after inoculation, and also released glucose from additional substrates, highlighting potential broader applications. In contrast to *U. cynodontis*, *U. maydis* showed no growth on starch accompanied with no detectable amylolytic activity.

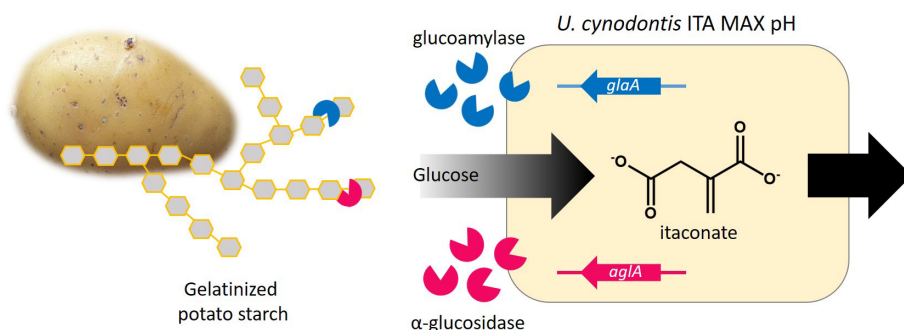


Figure 19: Graphical abstract displaying the amyolytic capabilities of *U. cynodontis* ITA MAX pH.

Keywords

Ustilago cynodontis, starch, itaconic acid, low-cost substrates, glucoamylase, α -glucosidase

3.3.1. Introduction

In view of the growing world population and the overexploitation of fossil fuels, a transition from the fossil-based to bio-based production of chemicals from renewable resources is indispensable

(Stegmann et al., 2020). This has already been successfully done for different carboxylic acids like citric, lactic, succinic or itaconic acid (Chen & Nielsen, 2016; Kuenz & Krull, 2018). ITA belongs to the 12 most promising bio-based platform chemicals defined by the U.S. Department of Energy in 2004 (Werpy & Petersen, 2004). It is of particular interest as an alternative for petrochemical-based acrylic and methacrylic acid in the polymer industry (Teleky & Vodnar, 2019), but also has a variety of biological activities that makes it relevant in medical and pharmaceutical sectors (Michelucci et al., 2013; Mills et al., 2018; Olagnier et al., 2020).

To date, ITA is commercially produced using *A. terreus* achieving titers up to 160 g L⁻¹ and yields of up to 0.58 g_{ITA} g_{GLC}⁻¹ in pulsed batch fermentations on glucose (Krull et al., 2017a). However, to be competitive with the petrochemical sector, production costs need to be further reduced, which are significantly influenced by the feedstock used (Saur et al., 2023). One alternative feedstock offering potential cost reductions is the polysaccharide starch. Starch is highly abundant in nature and the most widely utilized substrate for biofuel production. It can be obtained from a variety of agricultural raw materials such as potatoes, wheat, and corn for industrial production in relatively high purity, simplifying downstream processing (Celińska et al., 2021; Singh et al., 2022). Its metabolization entails the liquefaction by an α -amylase and subsequent saccharification into glucose by a glucoamylase (Ebrahimian et al., 2022). Since the increased cultivation of starch-containing plants for industrial purposes can be negatively perceived in public opinion, there is a growing interest in utilizing starchy side streams from food processing industry (Jagadeesan et al., 2020; Kumar et al., 2023; Rodríguez-Martínez et al., 2023). The usage of such industrial side- and waste streams not only reduces production costs, it also makes it possible to achieve the circular bioeconomy concept without compromising food security (Leong et al., 2021). Since *A. terreus* is highly sensitive to medium impurities, the use of such more complex substrates requires pretreatment in order to remove trace elements, which is in addition to the laborious handling and difficult oxygenation due to its filamentous growth one major drawback of this production organism (Klement & Büchs, 2013).

Therefore, we focus on the basidiomycetes *U. maydis* and *U. cynodontis* as alternative natural ITA producing strains. Both strains have already been metabolically and morphologically engineered to maintain yeast-like growth and to enable high-level ITA production at the maximum theoretical yield of 0.72 ± 0.02 g_{ITA} g_{GLC}⁻¹ in the production phase with a constant glucose feed (Becker et al., 2021; Hosseinpour Tehrani et al., 2019d; Hosseinpour Tehrani et al., 2019b). The robustness of *Ustilago* species to medium impurities and its repertoire of hydrolytic, secretory enzymes makes it a promising candidate for ITA production based on more complex substrate in a consolidated process (Becker et al., 2023; Mueller et al., 2008). This has already been demonstrated by the use

of the untreated, sucrose-containing side streams molasses and thick juice from sugar industry as well as crude glycerol from biodiesel production as feedstock for *Ustilago*-based ITA production (Helm et al., 2023; Niehoff et al., 2023; Saur et al., 2023). Furthermore, activation of intrinsic xylanases, cellulases, and pectinases enabled degradation of the plant cell wall components hemicellulose, cellulose and pectin (Geiser et al., 2016a; Müller et al., 2018; Stoffels et al., 2020), even though direct usage of lignocellulosic biomass usually requires costly pretreatment to destroy its recalcitrant structure (Regestein et al., 2018).

Here, we performed a proof-of-concept study on the amylolytic potential of *U. maydis* and *U. cynodontis* for the direct utilization of potato starch as a feedstock for ITA production in a consolidated bioprocess.

3.3.2. Results and discussion

Genetic inventory of amylolytic enzymes encoded in *Ustilago* species

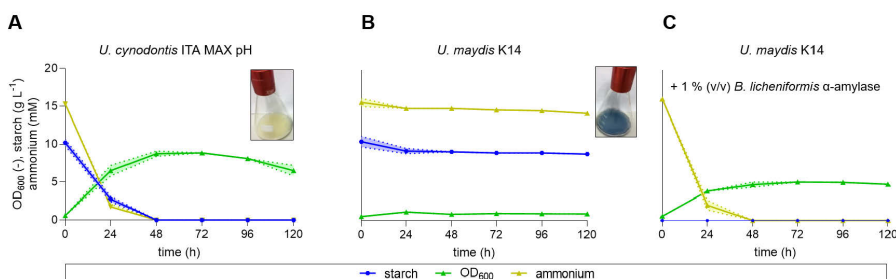
The genome of *U. maydis* 521 encodes four putative amylolytic enzymes which cleave α -1,4 and α -1,6 bonds between glucose molecules (Table 6). A tblastn analysis (Altschul et al., 1997; Gertz et al., 2006) of these protein sequences against the whole-genome shotgun contigs database identified putative orthologues of all enzymes in *U. cynodontis* NBRC9727 with protein sequence similarities ranging between 66.2 and 87.3 % (Table 6). Putative orthologues of all enzymes were also identified in *U. maydis* MB215. Interestingly, while high protein similarities were found for the α -amylase and α -glucosidase, lower similarities were detected for the maltase and glucoamylase.

Table 6: Putative enzymes present in *Ustilago* species cleaving α -1,4 and α -1,6-bonds between glucose molecules.

Enzyme	EC number	Action	<i>U. maydis</i> 521 gene	CAZy family	Reference	Protein similarity (%)	
						<i>U. maydis</i> MB215	<i>U. cynodontis</i> NBRC9727
α -amylase	3.2.1.1	α -1,4 bonds are cleaved within starch to release α -dextrins such as G2, G3, G6, and G7 maltooligomers	UMAG_02300 (putative)	GH13	(Couturier et al., 2012; Kretschmer et al., 2017)	99.8	87.3
Glucoamylase	3.2.1.3	α -1,4 and α -1,6 bonds are cleaved from the non-reducing ends of starch to release glucose	UMAG_04064 (putative)	GH15	(Couturier et al., 2012; Kretschmer et al., 2017)	26.5	66.2
Maltase	3.2.1.20	α -1,4 bonds are cleaved in maltose to release glucose	UMAG_15026 (putative)	GH13	(Couturier et al., 2012)	63.1	79.9
α -glucosidase	3.2.1.20	α -1,4 bonds are cleaved in maltose to release glucose; preferentially α -1,4 bonds are cleaved from the non-reducing ends of starch to release glucose	UMAG_02740 (putative)	GH13 & GH31	(Couturier et al., 2012; Mueller et al., 2008)	98.7	73.3

Shake flask cultivations on potato starch as a sole carbon source

In order to test the expression of these genes *in vivo* in axenic cultures, cultivations of two previously engineered ITA-overproducing *Ustilago* strains (*U. cynodontis* ITA MAX pH and *U. maydis* K14) were performed with potato starch as a sole carbon source. To avoid the energy-intensive initial gelatinization step, the first cultivations were performed with raw starch powder. However, no growth was detected for either strain (data not shown). Consequently, gelatinized starch was applied in the subsequent cultivations (Figure 20).


Figure 20: Shake flask cultivations of *U. cynodontis* ITA MAX pH and *U. maydis* K14 on gelatinized potato starch (A and B) and α -amylase pretreated potato starch (C) as a sole carbon source.

Shake flask cultivations were performed in MTM medium containing 15 mM NH_4Cl , 100 mM MES pH 6.5, and 10 g L^{-1} gelatinized potato starch (n = 2 biological replicates).

Significant differences between *U. cynodontis* ITA MAX pH and *U. maydis* K14 were observed in terms of growth and starch degradation. Whereas *U. cynodontis* ITA MAX pH reached an optical density of 8.9 ± 0.2 and utilized all starch and ammonium within the first 48 h (Figure 20A), *U. maydis* K14 showed almost no growth and no decrease of starch or ammonium (Figure 20B), despite having the same genes present in the genome. Apparently, these genes are silent in *U. maydis* K14 under the applied conditions. The basal expression of amylolytic enzymes may not be sufficient to sense the presence of starch. However, *U. maydis* K14 was able to grow on α -amylase pretreated starch up to OD₆₀₀ values of 5.1 ± 0.1 (Figure 20C), which is consistent with previous literature (Kretschmer et al., 2017).

Lab-scale fermentations on gelatinized potato starch as a sole carbon source

Based on the obtained results, the cultivations were scaled up from shake flasks to bioreactors to analyze ITA production on starch under more industrially relevant conditions (Figure 21).

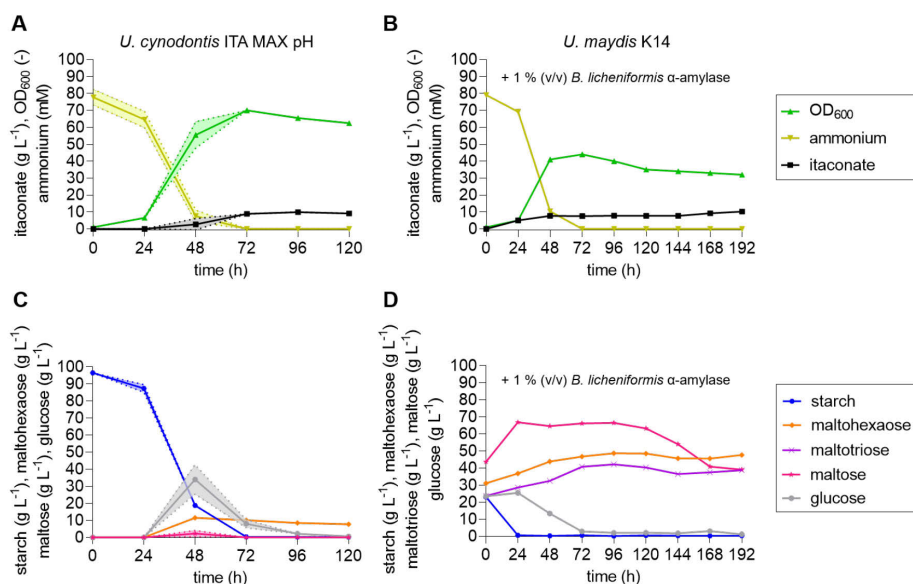


Figure 21: High cell-density batch fermentations on gelatinized potato starch (A and C) and α -amylase pretreated potato starch (B and D) as a sole carbon source.

Bioreactor cultivations were performed in batch medium with 75 mM NH₄Cl and either 100 g L⁻¹ gelatinized potato starch (A and C) ($n = 2$ biological replicates) or 200 g L⁻¹ α -amylase pretreated potato starch (B and D) ($n = 1$ biological replicate). The pH was controlled at pH 3.6 by automatic titration with 5 M NaOH.

In the first 72 h of the *U. cynodontis* ITA MAX pH fermentations on starch, the cell-densities increased up to OD₆₀₀ values of approximately 70 ± 1 (Figure 21A), and starch was converted to sugar mono- and maltooligomers (Figure 21C), which was in line with the shake flask experiments. Starch was mainly hydrolyzed to glucose with a high transient accumulation of approximately $34 \pm 8.6 \text{ g L}^{-1}$ reached after 48 h. In addition, $11.6 \pm 0.6 \text{ g L}^{-1}$ of maltohexaose as well as small amounts of maltose ($2.3 \pm 1.8 \text{ g L}^{-1}$) were detected. Glucose and maltose were constantly metabolized until their complete depletion, whereas the concentration of maltohexaose remained almost constant until the end of the cultivation ($7.8 \pm 0.9 \text{ g L}^{-1}$). This clearly indicates the inability of *U. cynodontis* ITA MAX pH to utilize maltohexaose. In total, this fermentation resulted in the production of $9.1 \pm 1.3 \text{ g L}^{-1}$ ITA at a productivity of $0.08 \pm 0.00 \text{ g L}^{-1} \text{ h}^{-1}$ and a yield of $0.1 \pm 0.01 \text{ g}_{\text{ITA}} \text{ g}_{\text{starch}}$ (unmetabolized sugars not accounted in the yield calculation). These KPIs are significantly lower than the ones achieved on pure glucose as a substrate (Hosseinpour Tehrani et al., 2019d). Together with the carbon loss due to unmetabolized maltohexaose, this clearly emphasizes the need of optimization, for instance by overproduction of additional amylolytic enzymes. Such an approach was already successfully applied for production of ITA from liquefied corn starch with *A. terreus*. While the wildtype strain produced less than 15 g L^{-1} ITA, heterologous overexpression of a glucoamylase gene from *A. niger* increased production to approximately 60 g L^{-1} (Huang et al., 2014). In comparison to *U. cynodontis* ITA MAX pH, the *U. maydis* K14 fermentation on pretreated starch accumulated less biomass with an OD₆₀₀ of 44 after 72 h. Due to the α -amylase pretreatment, most of the starch was already converted to sugar mono- and maltooligomers in the beginning of the fermentation, with a complete hydrolysis obtained after 24 h. The detected glucose concentration was lower than that during the *U. cynodontis* ITA MAX pH fermentation reaching a maximum of 25.5 g L^{-1} after 24 h, which was fully consumed after 72 h. In contrast, higher concentrations of maltose (66.9 g L^{-1}), maltotriose (42.2 g L^{-1}), and maltohexaose (48.7 g L^{-1}) were detected. The latter two remained almost constant until the end of the cultivation. The maltose concentration started to decline after approximately 120 h, however a large amount of this disaccharide remained in the final culture supernatant as well. In total, this fermentation resulted in the production of 10.2 g L^{-1} ITA, while the productivity was reduced to $0.05 \text{ g L}^{-1} \text{ h}^{-1}$ compared to previous fermentation of *U. cynodontis* ITA MAX pH due to the longer fermentation time of 192 h. The yield achieved with *U. maydis* K14 was slightly higher with $0.12 \text{ g}_{\text{ITA}} \text{ g}_{\text{starch}}$, but 125.6 g L^{-1} of unmetabolized sugar (not accounted in the yield calculation) in form of maltose, maltotriose and maltohexaose remained in the culture supernatant. Hence, further optimization is needed to fully degrade accumulated maltooligomers to glucose, as this appears to be the only sugar efficiently utilized by the strains.

Analysis of the amylolytic enzyme activity in *Ustilago* species

To optimize the amylolytic activity by metabolic engineering, enzymes present in the secretome needed to be identified and characterized. This is particularly interesting for *U. cynodontis* ITA MAX pH, as this strain is capable of growing on starch. The distribution of sugar mono- and maltooligomers detected during the fermentations showed relatively high levels of glucose, hinting at the exo-enzymatic degradation of starch by the secretion of a glucoamylase and/or α -glucosidase. Both enzymes have already been frequently reported for a variety of fungi including for example *A. niger*, *A. awamori*, *A. oryzae*, *Neurospora crassa*, *Colletotrichum gloeosporioides* (Kumar & Satyanarayana, 2009; Pandey et al., 2000). Contrary, endo-enzymatic treatment of starch typically results in accumulation of G2 (maltose), G3 (maltotriose), G6 (maltohexaose), and G7 (maltoheptaose) maltooligomers as observed after the α -amylase treatment (Figure 21D), but was less pronounced during *U. cynodontis* ITA MAX pH fermentation. To test the hypothesis regarding the presence of a glucoamylase and/or α -glucosidase and the absence of an α -amylase in the *U. cynodontis* ITA MAX pH secretome, additional shake flask cultivations were performed on starch, and supernatants were analyzed for their α -amylase activity using the commercial α -amylase assay from Phadebas (Kristianstad, Sweden). Indeed, the culture supernatants did not exhibit any α -amylase activity, indicating the absence or very low activity of this enzyme.

For a more detailed analysis of the *U. cynodontis* ITA MAX pH secretome, the supernatants were subjected to SDS-PAGE and LC-MS/MS analysis with *U. maydis* K14 supernatants as comparison (Figure 22). SDS-PAGE analysis of the culture supernatants exposed a set of extracellular proteins, which are exclusively produced by *U. cynodontis* ITA MAX pH when grown on starch as a sole carbon source (Figure 22). This confirms the enzymes as starch-induced proteins absent upon cultivation on the conventional feedstock glucose. In contrast to *U. cynodontis* ITA MAX pH, *U. maydis* K14 culture supernatants showed no detectable proteins when incubated with starch, which was in line with the lack of growth on this carbon source (Figure 20B, Figure 22).

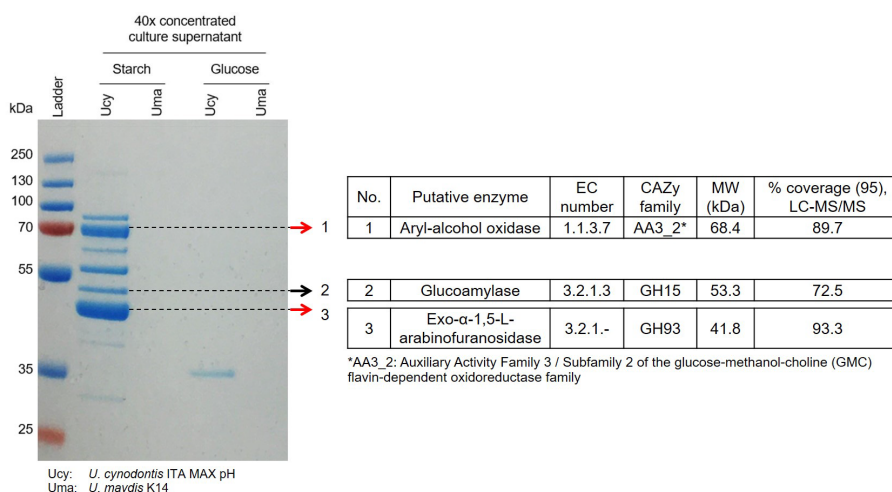


Figure 22: SDS-PAGE and LC-MS/MS analysis of *U. cynodontis* ITA MAX pH and *U. maydis* K14 culture supernatants.

Shake flask cultivations were performed in MTM medium containing 15 mM NH_4Cl , 100 mM MES pH 6.5 and either 10 g L^{-1} gelatinized potato starch or 10 g L^{-1} glucose. Culture supernatants were 40x concentrated using 10 kDa MWCO spin columns and afterwards separated electrophoretically using a 12 % polyacrylamide gel. Two bands (indicated by the red arrows) were excised, trypsin-digested, and subjected to LC-MS/MS analysis. The entire supernatant samples were also analyzed via LC-MS/MS. The predicted signal peptide sequences as indicated in Figure S7-S9 are not accounted in the % coverage (95 %) values.

LC-MS/MS analysis did not identify the genome-encoded α -amylase (60.9 kDa), confirming the absence of this enzyme under the applied conditions. Instead, the genome-encoded glucoamylase could be detected (53.3 kDa, Table 6, Figure 22, Figure S7), supporting the initial hypothesis. In contrast, the genome-encoded α -glucosidase (118.0 kDa) was not identified in the secretome. In addition, a further enzyme belonging to the glycoside hydrolase family 93 (GH93) was detected in high abundance (41.8 kDa, Figure 22, Figure S8). According to the carbohydrate-active-enzymes (CAZy) database, this enzyme shows closest similarity to an exo- α -1,5-L-arabinofuranosidase (Drula et al., 2022). Based on the functional description of a GH93 enzyme in the phytopathogenic fungi *Fusarium graminearum*, this enzyme cleaves L-arabinose side chains from arabinose-substituted oligosaccharides with a strict substrate specificity for linear α -1,5-linked arabinans (Carapito et al., 2009). A similar enzyme activity has been reported for an exo- α -1,5-L-arabinanase (GH93) from both *Chrysosporium lucknowense* C1 (Kühnel et al., 2011) and *Penicillium chrysogenum* 31B (Sakamoto et al., 2004) releasing arabinobiose from the non-reducing end of arabinose oligomers. Since arabinan polymers are an important substitution of hemicellulosic and pectic oligosaccharides in plants (Yeoman et al., 2010), their hydrolysis plays an important role in the complete degradation of the plant cell wall components and is assumed to facilitate enzymatic access of the backbone (Thakur et al., 2019). LC-MS/MS analysis also

revealed the presence of an enzyme with 82.3 % protein sequence similarity to UMAG_03246 (68.4 kDa, Figure 22, Figure S9). UMAG_03246 was previously detected in *U. maydis* when grown on xylan (Geiser et al., 2013). This enzyme is classified as part of the AA3_2 subfamily of the glucose-methanol-choline (GMC) flavin-dependent oxidoreductase family. The subfamily also includes UMAG_04044, which is one of the most abundant enzymes in the secretome of *U. maydis* when grown on maize (Couturier et al., 2012). Further characterization identified UMAG_04044 as an aryl-alcohol oxidase (EC 1.1.3.7) with anisyl alcohol, a methoxylated lignin model compound, as the main substrate. This suggests its functional role in lignocellulose deconstruction through lignin degradation, presumably by producing hydrogen peroxide (Couturier et al., 2016; Hernandez-Ortega et al., 2012). Although these latter two secreted enzymes have no clear relation to starch degradation, a concomitant secretion of amylolytic enzymes, the exo- α -1,5-L-arabinofuranosidase as well as the aryl-alcohol oxidase in *U. cynodontis* ITA MAX pH on starch may be associated to its pythopathogenic lifestyle. Lignocellulose-degrading enzymes are supposed to soft or partly degrade the plant cell wall (Doehlemann et al., 2008), which may facilitate access to starch as the primary storage carbohydrate in plants. The potato starch used in this study might retain trace amounts of lignin and heteropolysaccharides from the potato peels, triggering secretion of these putative enzymes (Rodríguez-Martínez et al., 2023). Additional proteins have been detected through SDS-PAGE, but could not be identified due to their low abundance. This may be caused by the minimal expression of plant cell wall-degrading enzymes to prevent triggering an immune response in the plants (Doehlemann et al., 2008). Accordingly, it is reasonable to assume that further cellulases and/or xylanases required for lignocellulose depolymerization are present in the secretome during growth on starch.

Among the identified enzymes – either via LC-MS/MS in the secretome or via tblastn analysis of the *U. cynodontis* genome – the α -amylase, glucoamylase and α -glucosidase are typically related to starch degradation (Vihinen & Mantsiila, 1989). Since no α -amylase or α -amylase activity could be detected, we deleted the glucoamylase and α -glucosidase-encoding genes in the *U. cynodontis* ITA MAX pH to test their involvement in starch hydrolysis (Figure 23).

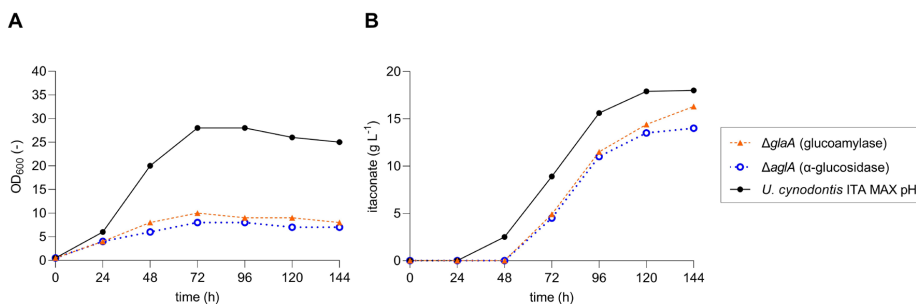


Figure 23: Shake flask cultivations of *U. cynodontis* ITA MAX pH deletion mutants on gelatinized potato starch as a sole carbon source.

Shake flask cultivations were performed in MTM medium containing 15 mM NH₄Cl, 100 mM MES pH 6.5, and 50 g L⁻¹ gelatinized potato starch (n = 1 biological replicate). All modifications were performed in *U. cynodontis* ITA MAX pH. (A) Optical densities and (B) itaconate concentrations throughout the cultivations are shown.

Remarkably, the knockout of either glucoamylase or α -glucosidase resulted in a reduced, but not abolished growth and ITA production, thus indicating a redundancy of both enzymes in starch degradation (Figure 23A and B). It is possible that the accumulation of limit dextrins occurs due to the preferred α -1,4 bond hydrolysis of the α -glucosidase (Lee et al., 2013). Subsequently, glucoamylase may efficiently degrade the remaining α -1,6 linkages. Based on these *in vivo* results and the tblastn analysis (Table 6), the gene with the GenBank accession number CAKMX010000008 (region: 881932 to 885099) encoding the α -glucosidase is designated as *aglA* and the gene with the GenBank accession number CAKMX010000014 (region: 83686 to 85185) encoding the glucoamylase is designated as *glaA*. The genes and enzymes are named according to literature convention described in Murphy et al. (2011). Remarkably, the two highly abundant, yet uncharacterized exo- α -1,5-L-arabinofuranosidase (GenBank accession number CAKMX010000018, region 665749 to 665919, 666077 to 666352, and 666447 to 667148) and aryl-alcohol oxidase (GenBank accession number CAKMX010000011, region 416218 to 416544 and 416702 to 418270) do not appear to be significantly involved in starch degradation.

The amylolytic activity of the secretome was determined using gelatinized potato starch as substrate. To this end, starch degradation and reducing sugar accumulation during *U. cynodontis* ITA MAX pH and *U. maydis* K14 cultivation on starch were monitored throughout the entire cultivation via DNS and iodine assays (Figure 24). These assays enable a differentiation between exo-enzymes, such as glucoamylases and α -glucosidases, and endo-enzymes, such as α -amylases.

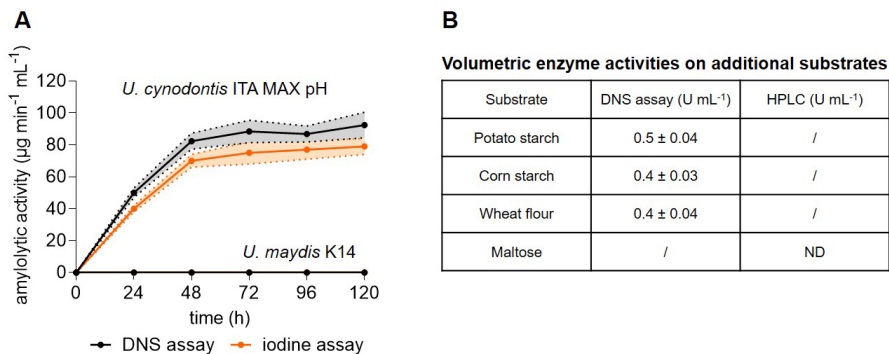


Figure 24: Amylolytic activity in supernatants of *U. cynodontis* ITA MAX pH and *U. maydis* K14 grown on gelatinized potato starch as a sole carbon source.

Shake flask cultivations were performed in MTM medium containing 15 mM NH₄Cl, 100 mM MES pH 6.5, and 10 g L⁻¹ gelatinized potato starch (n = 3 biological replicates). (A) Amylolytic activity in µg min⁻¹ mL⁻¹ during the cultivation, quantified via DNS (black line) and iodine assay (orange line). (B) Volumetric enzyme activities in U mL⁻¹ on potato starch, corn starch, wheat flour, and maltose, calculated based on the molecular weight of glucose.

The activity in the *U. cynodontis* ITA MAX pH culture increased almost linearly during the first 48 h, reaching approximately $82.3 \pm 5 \mu\text{g min}^{-1} \text{mL}^{-1}$ as measured by the DNS assay and $70 \pm 4 \mu\text{g min}^{-1} \text{mL}^{-1}$ as measured by the iodine assay (Figure 24A). Nitrogen limitation after 48 h (cf. Figure 20A) prevented further protein synthesis and led to a stabilization of the amylolytic activity. The activity of the secreted enzymes remained at its maximum level, indicating high stability. Since glucoamylases and α -glucosidases usually lead to a reduction in starch staining capacity along with a significant release of reducing sugars (Glose et al., 1990), the comparable activities measured by both methods serve as a further confirmation for the presence of these two exo-enzymes. Contrary, α -amylase activity typically shows up by a rapid decrease in iodine staining capacity with only a small amount of reducing sugars released. Overall, these results clearly reflect the phytopathogenic lifestyle of *Ustilago* species. For biotrophic growth, fungal plant degradation by carbohydrate-active enzymes needs to be restricted to a minimum level required for penetration (Doehlemann et al., 2008). Higher, unregulated activity would cause severe damage and trigger the plant immune system through sensing of plant cell wall oligomers (Wan et al., 2021), which can be assumed to be also the case for rapid α -amylase-mediated release of starch oligomers. In contrast, exo-enzymes like glucoamylases and α -glucosidases were shown to primarily release glucose in a more controlled fashion, thereby probably circumventing strong activation of the immune response.

To allow better comparison with amylolytic activities in other fungi, the volumetric enzyme activities in $\mu\text{mol min}^{-1} \text{mL}^{-1}$ (U mL⁻¹) were calculated based on the DNS assay using the molecular

weight of glucose (Figure 24B). A maximum enzyme activity of $0.5 \pm 0.04 \text{ U mL}^{-1}$ was detected at the fifth day after inoculation of *U. cynodontis* ITA MAX pH, which is probably a combination of the activity of both identified exo-enzyme. This level of enzymatic activity is consistent with other studies indicating fungal glucoamylase activities between 0.3 U mL^{-1} for culture supernatants (Ogundero & Osunlaja, 1986), although much lower than 200 U mL^{-1} for commercially available glucoamylases (Sigma Aldrich, St. Louis, US). The activities of α -glucosidases are mostly reported as specific activities in U mg^{-1} , which makes the comparison with activities directly measured in culture supernatants without prior enzyme purification difficult.

The hydrolytic activity of the glucoamylase and α -glucosidase was also tested on additional substrates (Figure 24B). With $0.4 \pm 0.03 \text{ U mL}^{-1}$ on gelatinized corn starch and $0.4 \pm 0.04 \text{ U mL}^{-1}$ on gelatinized wheat flour, the activities were comparable to the one observed on potato starch. Interestingly, no activity was determined on maltose, which is one of the preferred substrates of most fungal α -glucosidases (Chiba, 1988; Chiba, 1997; Manjunath et al., 1983). Based on substrate specificity, α -glucosidases can be classified into three main groups. Type-I preferentially degrades heterogeneous linkages (e.g. in sucrose), while types II and III preferentially hydrolyze homogenous linkages (e.g. in maltose, maltooligomers, and starch) with Type-III α -glucosidases being more efficient at degrading polysaccharides such as starch compared to Type-II α -glucosidases (Okuyama et al., 2016). Therefore, it appears that the α -glucosidase present in our culture supernatant is a Type-III α -glucosidase. This is relatively rare among fungal α -glucosidase, as most of them tend to hydrolyze maltose more rapidly than soluble starch (Chiba, 1988; Tanaka et al., 2002). To confirm this tendency, degradation of additional maltooligomers with various chain lengths could be tested, which requires prior purification of the glucosidase to prevent interference with the glucoamylase activity. The purified α -glucosidase could also be examined regarding its transglycosylation activity. This activity has been already reported for the α -glucosidase from *Mortierella alliacea*, which could use glycogen and soluble starch to transfer a glycosyl residue to ethanol, thereby producing ethyl α -D-glucopyranoside, a non-cariogenic sweetening and flavoring agent (Tanaka et al., 2002).

Optimization of the amylolytic activity in *U. cynodontis* ITA MAX pH

The efficient hydrolysis of starch to glucose typically involves the synergetic action of an α -amylase and a glucoamylase. Initially, gelatinized starch is liquefied to maltooligomers, which are then hydrolyzed to glucose by glucoamylases. Since no α -amylase could be detected in *U. cynodontis* ITA MAX pH culture supernatants despite its genomic presence, we constitutively overexpressed the native α -amylase gene with the GenBank accession number CAKMX010000005 (region: 1296343 to 1297953) (Figure 25).

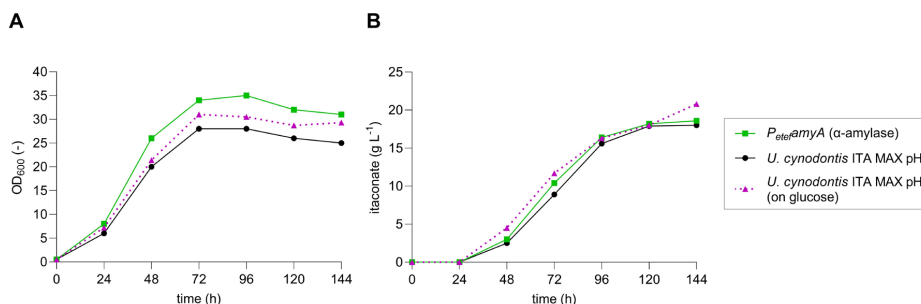


Figure 25: Shake flask cultivations of *U. cynodontis* ITA MAX pH constitutively expressing the native α -amylase gene on gelatinized potato starch as a sole carbon source.

Shake flask cultivations were performed in MTM medium containing 15 mM NH₄Cl, 100 mM MES pH 6.5, and 50 g L⁻¹ gelatinized potato starch (n = 1 biological replicate). (A) Optical densities and (B) itaconate concentrations throughout the cultivations are shown. The OD₆₀₀ values and ITA concentrations of *U. cynodontis* ITA MAX pH from Figure 23 are shown again for comparison. In addition, values from a previous cultivation of *U. cynodontis* ITA MAX pH on 50 g L⁻¹ glucose are shown.

The constitutive overexpression of the native α -amylase gene in *U. cynodontis* ITA MAX pH significantly improved the growth on starch (Figure 25A), presumably due to a more efficient starch degradation. This was accompanied by a slightly improved ITA production compared to the progenitor strain (Figure 25B). Interestingly, similar KPIs were obtained on glucose and starch during shake flask cultivations, whereas they significantly differed during bioreactor batch fermentations (Figure 21). This may be due to variations in the C/N ratio, which could be optimized by low cell-density and/or fed-batch fermentations in follow-up studies.

Since native expression of carbohydrate-active enzymes is expected to be on a low level to minimize plant tissue damage (Doehlemann et al., 2008), conversion of starch to ITA by *U. cynodontis* ITA MAX pH can likely be further optimized by constitutive overexpression of the native amylolytic genes. This might also enable starch degradation by *U. maydis* K14. In addition, the heterologous overexpression of α -amylases containing a starch-binding domain (Janecek et al., 2003) could be tested for the utilization of raw starch. This would eliminate the energy-intensive initial gelatinization step (Robertson et al., 2006) (cf. Figure 20), and has already been successfully demonstrated for *A. terreus* (Wong et al., 2007).

3.3.3. Conclusion

In this work, we investigated the utilization of the low-cost substrate starch by *U. cynodontis* ITA MAX pH and *U. maydis* K14, two *Ustilago* strains that have been previously engineered for efficient ITA production. *U. cynodontis* ITA MAX pH was able to metabolize gelatinized potato starch, reaching ITA titers of up to 10 g L⁻¹ with a yield of approximately 0.1 g_{ITA} g_{starch}⁻¹ during

respective batch fermentations. This could be traced back to the activity of a glucoamylase and an α -glucosidase in its secretome, which were shown to be synergistically involved in starch degradation. In contrast, *U. maydis* K14 required α -amylase pretreated potato starch hydrolysates for growth and ITA production. Although the KPIs are yet lower compared to those achieved with glucose in batch fermentations, the utilization of starch has the advantage of causing less osmotic stress. While high concentrations of monomeric glucose at the start of the fermentation typically result in increased osmotic stress of the deeply engineered *Ustilago* strains, continuous enzymatic liberation of single glucose molecules from glucose polymers and their immediate consumption circumvent higher glucose accumulation. However, to exploit the full potential of starch as a substrate for ITA production, further optimizations such as the constitutive overexpression of the amylolytic genes or the utilization of partly *in situ* hydrolyzed starch are required to achieve higher KPIs. Although further optimization is needed, *U. cynodontis* ITA MAX pH has been successfully demonstrated to be a promising host for ITA production from gelatinized potato starch.

3.3.4. Material and methods

Chemical and strains

The chemicals used in this study were obtained from Sigma-Aldrich, St. Louis, USA. Thermo Fisher Scientific (Waltham, USA), or VWR (Radnor, USA) and were of analytical grade. All strains used in this work are listed in Table 7.

Table 7: *Ustilago* strains used in this study.

Strain designation	Resistance	Reference
<i>U. maydis</i> MB215 $\Delta cyp3$ ΔMEL $\Delta UA \Delta dga1 \Delta P_{ria1}::P_{etef} \Delta fuz7$ $P_{etef}mtta_K14$ (198)	Hyg ^R	(Becker et al., 2021)
<i>U. cynodontis</i> NBRC9727 $\Delta fuz7$ $\Delta cyp3 P_{etef}mtta P_{ria1}ria1$ (223)	Hyg ^R , Cbx ^R	(Hosseinpour Tehrani et al., 2019b)
<i>U. cynodontis</i> NBRC9727 $\Delta fuz7$ $\Delta cyp3 P_{etef}mtta P_{ria1}ria1$ $P_{etef}\alpha\text{-amylase}$ (2699)	Hyg ^R , Cbx ^R , G418 ^R	this study
<i>U. cynodontis</i> NBRC9727 $\Delta fuz7$ $\Delta cyp3 P_{etef}mtta P_{ria1}ria1$ $\Delta UMAG_04064$ (2700)	Hyg ^R , Cbx ^R , G418 ^R	this study
<i>U. cynodontis</i> NBRC9727 $\Delta fuz7$ $\Delta cyp3 P_{etef}mtta P_{ria1}ria1 P_{etef}cyp3$ $\Delta UMAG_02740$ (2701)	Hyg ^R , Cbx ^R , G418 ^R	this study

Media and culture conditions

Ustilago strains were grown in YEPS medium containing 10 g L⁻¹ yeast extract, 10 g L⁻¹ peptone, and 10 g L⁻¹ sucrose. For growth and production experiments, *Ustilago* strains were cultured in 100 mM MES pH 6.5 buffered screening medium (MTM) according to Geiser et al. (2014) with either glucose (10 g L⁻¹) or gelatinized potato starch (10 g L⁻¹ or 50 g L⁻¹). The medium also contained 15 mM NH₄Cl, 0.2 g L⁻¹ MgSO₄·7H₂O, 0.01 g L⁻¹ FeSO₄·7H₂O, 0.5 g L⁻¹ KH₂PO₄, 1 mL L⁻¹ vitamin solution, and 1 mL L⁻¹ trace element solution. The vitamin solution contained (per liter) 0.05 g D-biotin, 1 g D-calcium pantothenate, 1 g nicotinic acid, 25 g myo-inositol, 1 g thiamine hydrochloride, 1 g pyridoxol hydrochloride, and 0.2 g *para*-aminobenzoic acid. The trace element solution contained (per liter) 1.5 g EDTA, 0.45 g of ZnSO₄·7H₂O, 0.10 g of MnCl₂·4H₂O, 0.03 g of CoCl₂·6H₂O, 0.03 g of CuSO₄·5H₂O, 0.04 g of Na₂MoO₄·2H₂O, 0.45 g of CaCl₂·2H₂O, 0.3 g of FeSO₄·7H₂O, 0.10 g of H₃BO₃ and 0.01 g of KI. Cultivations were performed in 500 mL shaking flasks with a filling volume of 50 mL (d=25 mm, n = 200 rpm, T = 30 °C and Φ = 80 %). For growth and production experiments, main cultures were inoculated to an OD₆₀₀ of 0.5 with precultures grown in the same media.

As previously described in Becker et al. (2021), the DASGIP Bioblock system (Eppendorf, Germany) was used to conduct the fermentations, which were controlled using the Eppendorf DASware control software (Eppendorf, Germany). Vessels with a total volume of 2.3 L and a working volume of 1.0 L were used. The cultivations were performed in batch medium according to Geiser et al. 2014 as described above. The medium also contained 1 g L⁻¹ yeast extract (Merck Millipore, Germany) and either 100 g L⁻¹ gelatinized potato starch or 200 g L⁻¹ α-amylase pretreated potato starch. To avoid clumping of starch during autoclaving, a slurry was prepared beforehand by mixing starch in hot water. For the α-amylase pretreatment, a 1 % (v/v) solution of heat-stable *Bacillus licheniformis* α-amylase (Sigma-Aldrich, St. Louis, USA) was added through the septum and incubated for approximately 2 h. The slurry was maintained at 80 °C during the pretreatment. Afterwards, the temperature was adjusted to 30 °C, and the remaining medium compounds were added through the septum. Finally, the bioreactor was inoculated to a OD₆₀₀ of 0.75 from an preculture grown in screening medium according to Geiser et al. (2014) containing 15 mM NH₄Cl, 100 mM MES pH 6.5, and 50 g L⁻¹ gelatinized potato starch. The pH was automatically controlled by adding 5 M NaOH or 1 M HCl, while the DO was maintained at 30 % using a cascade that involved agitation at 800-1200 rpm (0-40 % DOT controller output), air flow at 1-2 vvm (40-80 % DOT controller output), and oxygen at 21-100 % oxygen (80-100 % DOT controller output). Additionally, 0.5 mL of Antifoam 204 (Sigma-Aldrich, St. Louis, USA) was added at the beginning of the cultivation and every 24 h thereafter.

Analytical methods

Identification and quantification of products and substrates present in the supernatants were conducted using a HPLC 1260 Infinity system (Agilent, Waldbronn, Germany) equipped with an ISERA Metab AAC column 300 × 7.8 mm column (ISERA, Germany). Separation was achieved through isocratic elution at a flow rate of 0.6 mL min⁻¹ and a temperature of 40 °C, employing 5 mM sulfuric acid as a solvent (Becker et al., 2021). Detection involved a DAD at 210 nm and a RI detector. Analytes were identified based on their retention time compared to corresponding authentic standards, and data analysis was performed using the Agilent OpenLAB Data Analysis - Build 2.200.0.528 software (Agilent, Waldbronn, Germany). Ammonium concentrations in culture samples were determined using the colorimetric method outlined by Willis et al. (1996). In this method, 50 µL culture supernatant was mixed with 1 mL reagent (8 g sodium salicylate, 10 g trisodiumphosphate, 0.125 g sodium nitroprusside), followed by rapid addition of 250 µL hypochlorite solution. After color development, the absorbance was measured at 685 nm using cuvettes and a spectrophotometer. Ammonium concentrations were calculated using an ammonium calibration. Cell-densities were quantified by measuring the optical density at a wavelength of 600 nm using cuvettes and a spectrophotometer. Samples were diluted appropriately with the respective medium to ensure measurement within the linear range of the photometer, falling between absolute values of 0.2 and 0.4. SDS-PAGE was performed according to the manufacturer's instructions using NuPAGE 12 % Bis-Tris precast gels and MOPS as the running buffer. 10 µL of each sample and 5 µL of the protein ladder were loaded onto the gel. After electrophoresis, the gels were stained with Coomassie (Gel Code Blue). For the detection of residual starch in culture samples, 100 µL of clarified culture broth was combined with 100 µL of Lugol's iodine solution. 150 µL of the iodine-treated sample was transferred to a transparent flat-bottomed 96-well microplate and the absorbance at 580 nm was measured using microplate reader. The amount of starch was calculated using standard curves of starch.

Determination of amylolytic enzyme activity

1) Commercial α -amylase assay from Phadebas (Kristianstad, Sweden) – blue starch polymer

The assays were performed according to the manufacturer's instructions. Briefly, covalently attached dyes were liberated from starch polymers at a speed proportional to the α -amylase activity. The concentration of the free dyes were detected spectrophotometrically at 580 nm and converted into α -amylase activities using manufactures calibration. Both substrates are exclusively designed for measuring α -amylase activity, as no other enzyme can act upon the substrates due to the cross-linkages and the large dye molecules.

2) Decrease of iodine-binding starch material according to Xiao et al. (2006)

40 μL culture supernatant was combined with 40 μL 0.1 M phosphate buffer pH 7.0 containing 0.2 % gelatinized potato starch and incubated at 30 °C for 30 minutes. Reactions were terminated by adding 20 μL 1 M HCl. Following termination, 100 μL of Lugol's iodine solution was added. 150 μL of the iodine-treated sample was transferred to a transparent flat-bottomed 96-well microplate and the absorbance at 580 nm was measured using a microplate reader. The amount of disappeared starch was calculated using standard curves of starch. The activity was defined as the amount of culture supernatant required for the disappearance of an average of 1 μg of iodine-binding starch material per mL and minute in the assay reaction.

$$\mu\text{g min}^{-1} \text{ mL}^{-1} = \frac{A_{580} \text{ control} - A_{580} \text{ sample}}{A_{580} (\mu\text{g starch}) * t * v} * D$$

- A_{580} control: abs. at 580 nm of starch without the addition of culture supernatant [-]
- A_{580} sample: abs. at 580 nm of starch digested with culture supernatant [-]
- A_{580} ($\mu\text{g starch}$): abs. at 580 nm per 1 μg of starch as derived from the standard curve [μg^{-1}]
- t: incubation time [min]
- v: volume of culture supernatant used [mL]
- D: dilution factor [-]

3) Increase of reducing sugar concentration according to Miller (1959)

40 μL culture supernatant was combined with 40 μL 0.1 M phosphate buffer pH 7.0 containing 0.2 % gelatinized potato starch and incubated at 30 °C for 30 minutes. Reactions were terminated by adding 120 μL of DNS reagent and boiling reaction mixtures for 15 minutes at 95 °C. 150 μL of the DNS-treated sample was transferred to a transparent flat-bottomed 96-well microplate and the absorbance at 540 nm was measured using a microplate reader. The activity was defined as the amount of culture supernatant required for the release of 1 μg or 1 μmol glucose per mL and minute in the assay reaction.

$$\mu\text{g min}^{-1} \text{ mL}^{-1} = \frac{A_{580} \text{ control} - A_{580} \text{ sample}}{A_{580} (\mu\text{g glucose}) * t * v} * D$$

$$\text{U mL}^{-1} = \mu\text{mol min}^{-1} \text{ mL}^{-1} = \frac{A_{580} \text{ control} - A_{580} \text{ sample}}{A_{580} (\mu\text{mol glucose}) * t * v} * D$$

- A_{580} control: abs. at 580 nm of sample without the addition of culture supernatant [-]
- A_{580} sample: abs. at 580 nm sample digested with culture supernatant [-]
- A_{580} ($\mu\text{g glucose}$): abs. at 580 nm per 1 μg of glucose as derived from the standard curve [μg^{-1}]
- A_{580} ($\mu\text{mol glucose}$): abs. at 580 nm per 1 μmol of glucose as derived from the standard curve [μmol^{-1}]
- t: incubation time [min]
- v: volume of culture supernatant used [mL]
- D: dilution factor [-]

LC-MS/MS

For in-gel digestion, samples were prepared according to Lavigne et al. (2009). Briefly, the decolorization of the gel pieces was carried out in 3 x 350 μ L in NH_4HCO_3 in 50 % acetonitrile in 1.5 mL Eppendorf LoBind tubes, and were incubated 30 min, gently shaken by 300 rpm at room temperature. For tryptic digestion the vacuum dried slices were treated with the Trypsin Singles Proteomics Grade Kit (Sigma-Aldrich, St. Louis, USA) according to the manufacturer's instructions for in-gel digestion preparation without the reduction and alkylation step. After the incubation at 37 °C overnight, each of the samples were submerged in a new LoBind tube with 100 μ L 20 mM NH_4HCO_3 and were sonicated for 20 min. This step was carried out twice with 50 μ L of 5 % formic acid in 50 % acetonitrile. The samples concentrated in the SpeedVac were taken up in 50 μ L 0.1 % formic acid and were stored at -20 °C before the next sample preparation step. The StageTipping desalting step was carried out as described by Rappsilber et al. (2007). The tryptic peptide samples were stored at -20 °C until use for MS measurements.

For analysis of entire supernatants, protein solutions of 150 μ L were mixed with 0.25 volume of 100 % (w/v) TCA, incubated for 30 min on ice and the precipitated proteins were sedimented for 15 min at 16100 g and 4 °C. The supernatants were removed and the precipitated proteins washed twice in 0.5 mL of ice-cold acetone. After centrifugation again (15 min, 16100 g, 4 °C), the supernatants were discarded, the pellets were air-dried and the proteins were dissolved in 100 μ L TRB buffer (Trypsin Reaction Buffer: 40 mM NH_4HCO_3 pH 8.2, 9 % acetonitrile). Before analyzing the protein samples with LC-MS/MS, they were digested using trypsin to cleave the proteins into peptides using the Trypsin Singles, Proteomics Grade kit (Sigma-Aldrich, St. Louis, USA) according to the manufacturer's instruction. For this, 1 μ g trypsin and 1 μ L of Trypsin Solubilization Reagent (contain 1 mM HCl) was added up to 100 μ g of protein in a total volume of maximum 100 μ L. The tryptic digest was performed at 37 °C in an overnight reaction (18 h). The StageTipping desalting step was carried out as described by Rappsilber et al. (2007). After drying, the sample was resuspended in 30 μ L solvent A (0.1 % formic acid in H_2O).

Subsequent LC-MS/MS analysis of trypsin-digested samples was done as already described previously (Hünnefeld et al., 2021). The IDA data were processed with ProteinPilot (5.02, Sciex) using the Paragon algorithm for protein identification and for building an ion library. This data was then compared with a database consisting of proteins from *U. maydis* 521 and *U. cynodontis* NBRC9727.

Plasmid cloning and strain engineering

Plasmids were constructed via Gibson assembly (Gibson et al., 2009) using the NEBuilder HiFi DNA Assembly Cloning Kit (New England Biolabs (NEB), Ipswich, MA, USA). The DNA oligonucleotides

were purchased from Eurofins Genomics (Ebersberg, Germany), and Q5 High-Fidelity DNA Polymerase (NEB) was used as the polymerase. Table 8 and Table S4 provide details on the plasmids and primers used. Competent *E. coli* DH5 α or PIR2 cells were used for standard cloning and plasmid maintenance, following the protocols described in Sambrook and Russell (2006). Plasmids were confirmed through PCR, restriction analysis, or sequencing. The protocols described in Brachmann et al. (2004) were used for the generation of protoplasts, transformation, and isolation of genomic DNA of *Ustilago* strains. To integrate *P_{etef}amyA* randomly into the genome, the plasmid was linearized with BglI. For the deletion of UMAG_04064 and UMAG_02740, homologous recombination with 1000 bp flanking regions including a geneticin G418 resistance cassette were used. Successful integration and deletion were confirmed by PCR.

Table 8: Plasmids used in this study.

Plasmid	Description	Reference
pJET1.2/blunt	Ori ColE1, Amp ^R	Thermo Scientific, Germany
<i>P_{etef}gfp</i> _G418	Constitutive <i>P_{etef}</i> promotor, <i>gfp</i> gene, G418 ^R	(Przybilla, Roxense BioSC)
<i>P_{etef}amyA</i> _G418	Constitutive <i>P_{etef}</i> promotor, α - <i>amylase</i> gene from <i>U. cynodontis</i> NBRC9727, G418 ^R	this study
Δ UMAG_04064_G418	Deletion of UMAG_04064 in <i>U. cynodontis</i> ITA MAX pH, G418 ^R	this study
Δ UMAG_02740_G418	Deletion of UMAG_02740 in <i>U. cynodontis</i> ITA MAX pH, G418 ^R	this study

Funding

This project has received funding from the Bio-based Industries Joint Undertaking (JU) under the European Union's Horizon 2020 research and innovation program under grant agreement No 887711 for the project Glaukos. The JU receives support from the European Union's Horizon 2020 research and innovation program and the Bio-based Industries Consortium. Further funding was received by the German Federal Ministry of Education and Research (BMBF, project: "Modellregion, BioRevier-PLUS: InBio, Innovationscluster integrierte Bioraffinerie", grant no. 031B1135A).

Acknowledgements

We thank all project partners for fruitful discussions.

Conflicts of interest:

The authors declare that they have no competing interests.

3.4. Production and Characterization of the Itaconic Acid-derived Compounds
2-Hydroxyparaconic and Itatartaric Acid

P. Ernst, F. Zlati, L. Kever, A. Wirtz, R. Goldbaum, J. Pietruszka, B. Wynands, Julia Frunzke, and N. Wierckx

Submitted for publication (February 2024).

Contributor role	Contributor
Conceptualization	N. Wierckx
Data curation	N. Wierckx, P. Ernst, F. Zlati, L. Kever, A. Wirtz, R. Goldbaum
Formal analysis	P. Ernst, F. Zlati, L. Kever, A. Wirtz, R. Goldbaum
Funding acquisition	N. Wierckx
Investigation	P. Ernst, F. Zlati, L. Kever, A. Wirtz, R. Goldbaum
Methodology	P. Ernst, F. Zlati, L. Kever, A. Wirtz, R. Goldbaum
Project administration	N. Wierckx
Resources	N. Wierckx, J. Frunzke, J. Pietruszka
Software	-
Supervision	N. Wierckx, J. Frunzke, B. Wynands, J. Pietruszka
Validation	P. Ernst, F. Zlati, L. Kever, A. Wirtz, R. Goldbaum
Visualization	P. Ernst
Writing – original draft	P. Ernst
Writing – review and editing	N. Wierckx, P. Ernst

Overall contribution: 75 %

I performed the strain engineering and all cultivations, partly supported by F. Zlati. L. Kever performed the qPCR associated to Figure 27F. A. Wirtz supported the metabolite quantification via HPLC. R. Goldbaum measured the ¹H and ¹³C NMR spectra associated to Figure 31. P. Ernst prepared all figures and wrote the original draft. All authors, but especially N. Wierckx and I, were involved in the review and editing process.

A peer-reviewed version of the following manuscript was finally published in Metabolic Engineering Communications (November 2024). doi: 10.1016/j.mec.2024.e00252

Production and Characterization of the Itaconic Acid-derived Compounds 2-Hydroxyparaconic and Itatartaric acid

Philipp Ernst¹, Felicia Zlati¹, Larissa Kever¹, Astrid Wirtz¹, Rainer Goldbaum², Jörg Pietruszka^{1,2}, Benedikt Wynands¹, Julia Frunzke¹, and Nick Wierckx^{*1}

¹ Institute of Bio- and Geosciences IBG-1: Biotechnology, Forschungszentrum Jülich GmbH, Wilhelm-Johnen-Straße, 52425 Jülich, Germany

² Institute of Bioorganic Chemistry, Heinrich-Heine University Düsseldorf in Forschungszentrum Jülich GmbH, Wilhelm-Johnen-Straße, 52428 Jülich, Germany

* Corresponding author: n.wierckx@fz-juelich.de

Abstract: Itaconic acid is used in many application fields such as the production of paper, paints and fibers. There is also a strong interest in this compound in the medical and pharmaceutical sectors, both as an anti-bacterial compound and as an immunoregulator for the treatment of autoimmune diseases and viral infections including SARS-CoV-2. ITA is naturally produced by several fungal hosts including *U. maydis*, *U. cynodontis*, and *A. terreus*. Besides ITA, all hosts also produce the derivatives 2-hydroxyparaconic and itatartaric acid as downstream products of ITA. While the latter has been studied extensively over the years, not much is known about these two derivatives, although their structural characteristics could also open up several applications. In this study, we report the production of these two ITA-derived compounds. By overexpressing the ITA P450 monooxygenase Cyp3 in a previously engineered ITA-overproducing *U. cynodontis* strain, ITA was converted to its lactone 2-hydroxyparaconate. The second product itatartarate is most likely the result of the subsequent lactone hydrolysis. A major challenge in the production of 2-hydroxyparaconate and itatartarate is their co-production with ITA, leading to difficulties in their purification. Achieving high derivatives specificity was therefore the paramount objective. 2-hydroxyparaconate and itatartarate were successfully produced from glucose and glycerol, with the latter resulting in a higher derivatives specificity due to an overall slower metabolism on this non-preferred carbon source. The derivatives specificity could be further increased by metabolic engineering approaches including the exchange of the native ITA transporter Itp1 with the *A. terreus* ITA transporter MfsA. Both 2-hydroxyparaconate and itatartarate were recovered from fermentation supernatants following a pre-existing protocol. 2-hydroxyparaconate was recovered first through a process of evaporation, lactonization, and extraction with ethyl acetate. Subsequently, itatartarate could be obtained in the form of its sodium salt by saponification of the purified 2-hydroxyparaconate. Finally, several analytical methods were used to characterize the resulting products and their structures were confirmed by NMR. This work provides a promising foundation for obtaining 2-hydroxyparaconate and itatartarate in high purity and quantity. This will allow to unravel the full spectrum of potential applications of these novel compounds.

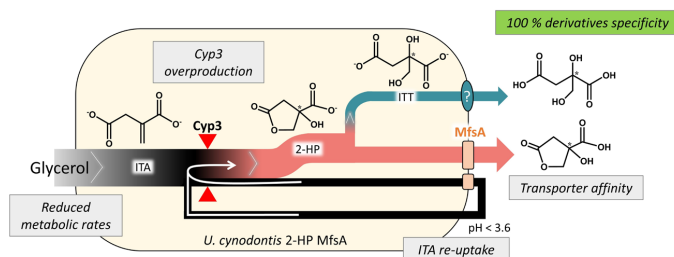


Figure 26: Graphical abstract displaying strategies employed to increase product specificity.

Keywords

Ustilago cynodontis, 2-hydroxyparaconic and itatartaric acid, derivatives specificity, metabolic engineering, fermentation, downstream processing

3.4.1. Introduction

Ustilaginaceae are dimorphic basidiomycetes naturally producing ITA as one of the top 12 value-added platform chemicals derived from biomass with multiple application areas (Geiser et al., 2014; Olicón-Hernández et al., 2019; Werpy & Petersen, 2004; Wierckx et al., 2020). Besides being used for paper, paint and fiber production, ITA is also of increasing interest in the medical and pharmaceutical sectors due to its anti-inflammatory properties (Michelucci et al., 2013; Mills et al., 2018; Olganier et al., 2020). It has been discovered that human macrophages produce ITA to inhibit pathogenic bacteria, however, some bacteria have evolved resistance by ITA degradation (Martin et al., 1961; Sasikaran et al., 2014). A similar arms race may exist between ITA-producing fungi and their natural competitors, which might serve as a simplified model for investigating these interactions. Interestingly, Guevarra and Tabuchi (1990a) identified 2-HP and ITT as two ITA downstream products in *Ustilago* species. Although the detailed functional characterization of these compounds is still pending, initial studies have shown their potential as anti-microbial agents (de Witt et al., 2023). Hypothetically, fungi evolved these compounds to counteract ITA resistance, putting them one step ahead of the human immune system. Accordingly, pharmaceutical use of these compounds may support the human immune system. To confirm this hypothesis and explore potential further applications of 2-HP and ITT, high-purity substances are obligatory.

As shown in the model host *U. maydis*, 2-HP is directly synthesized from ITA via the ITA P450 monooxygenase Cyp3 (Geiser et al., 2016b), which can be further converted to ITT, hypothetically by abiotic lactone hydrolysis. Both acids are suggested to be secreted into the medium by the major facilitator Itp1, which is also responsible for ITA export (Geiser et al., 2018; Hosseinpour Tehrani et al., 2019a). Since low pH values ($pK_a > pH$) allow the re-uptake of ITA facilitating its conversion to 2-HP (Geiser et al., 2016b; Guevarra & Tabuchi, 1990b), highly acid-tolerant *U. cynodontis* is considered as the favorable production host for these downstream compounds. Production of ITA in *U. cynodontis* has already been optimized by morphological and metabolic engineering including the deletion of *fuz7* allowing yeast-like growth and *cyp3* encoding the ITA P450 monooxygenase preventing further conversion of ITA, the heterologous overexpression of the mitochondrial tricarboxylate transporter gene *mttA* from *A. terreus* as well as the overexpression of the ITA cluster regulator encoding gene *ria1* (Hosseinpour Tehrani et al., 2019d;

Hosseinpour Tehrani et al., 2019b). Using this engineered ITA-overproducing strain as a basis for further metabolic engineering, we optimized 2-HP and ITT production and purified both acids in high purity to allow comprehensive characterizations. Conversion of ITA to 2-HP was restored via overproduction of Cyp3 and exchange of the native ITA transporter Itp1 with the *A. terreus* ITA transporter MfsA leading to an accumulation of 2-HP and ITT upon batch fermentations on glucose and glycerol. Highest 2-HP and ITT product yields were achieved in a low cell-density fed-batch fermentation using glucose as a carbon source resulting in $13.5 \pm 0.4 \text{ g L}^{-1}$ 2-HP and $30.5 \pm 0.2 \text{ g L}^{-1}$ ITT. Both products were recovered from the fermentation supernatants according to a protocol adapted from Guevarra and Tabuchi (1990b). Quantitative nuclear magnetic resonance spectroscopy (qNMR) measured a product purity of $85.3 \pm 3.7 \%$ providing the basis for exploring their pharmaceutical relevance in follow-up studies.

3.4.2. Results and discussion

Overexpression of the itaconate-oxidizing P450 monooxygenase Cyp3

Since 2-HP and ITT are metabolically linked to ITA, a previously engineered ITA-overproducing *U. cynodontis* strain (referred to as *U. cynodontis* ITA MAX pH) served as the basis for strain development. Production of the derivatives by this strain was restored through the P_{etef} -driven overexpression of the ITA P450 monooxygenase Cyp3, aiming at the conversion of ITA to 2-HP. To this end, the plasmid designated as $P_{etef}\text{Cyp3}$ was randomly inserted into the genome of *U. cynodontis* ITA MAX pH. Given that random integration of constructs into the genome often results in multi-copy and/or ectopic insertions, several clones of *U. cynodontis* ITA MAX pH_ $P_{etef}\text{Cyp3}$ were characterized to identify the best 2-HP/ITT producer. From this initial screening (Figure S10), six clones were subjected to further characterization regarding 2-HP and ITT production in comparison to the progenitor strain as negative control and *U. cynodontis* Δfuz7 as positive control (Figure 27).

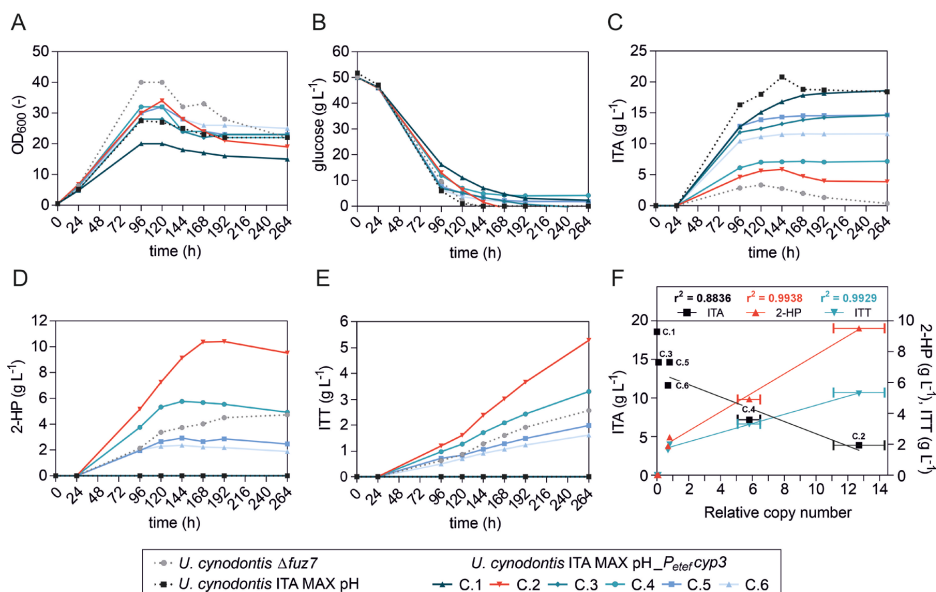


Figure 27: Screening of different *U. cynodontis* ITA MAX pH_ *P_{etef}cyp3* clones regarding production of 2-HP and ITT as the two downstream products of ITA.

(A) Growth, (B) glucose consumption, (C) ITA production, (D) 2-HP production and (E) ITT production of the different clones and the reference strains during cultivation in shake flasks in MTM medium with 15 mM NH₄Cl, 30 mM MES pH 6.5, and 50 g L⁻¹ glucose (n = 1 biological replicate). (F) Correlation between relative *cyp3* copy numbers and product titers of ITA, 2-HP and ITT. Copy numbers of *cyp3* were calculated via qPCR in relation to *tad1* and *rdo1* genes (both single copy) from biological triplicates measured as technical duplicates. The linear fit is shown for the *cyp3*-bearing clones.

Engineered strains exhibited differences in growth in comparison to the Δ fuz7 control (Figure 27A). This can be traced back to the overexpression of *P_{etef}mttA* as previously shown by Hosseinpour Tehrani et al. (2019b). The constitutive promotor *P_{etef}* leads to high expression rates already during the growth phase (Zambanini et al., 2017c), likely causing MttA to export cis-aconitate from the mitochondria before the onset of production of ITA and its derivatives. The *P_{etef}cyp3* overexpression does not seem to have an additional negative impact on growth, with all strains except clone 1 showing similar OD₆₀₀ values and glucose consumption rates as the progenitor strain *U. cynodontis* ITA MAX pH (Figure 27A and B). In contrast, the strains significantly differed from each other regarding 2-HP and ITT production (Figure 27C-E). Clone 2 achieved the highest 2-HP and ITT product titers, which were approximately two-fold higher than the wildtype reference *U. cynodontis* Δ fuz7 (Figure 27D and E) (Hosseinpour Tehrani et al., 2019b). The combined final titers of ITA, 2-HP and ITT of clone 2 add up to 18.7 g L⁻¹, an amount that corresponds well with the production of 18.4 g L⁻¹ ITA by the reference ITA-producing strain. The second best performance regarding 2-HP and ITT production was detected for clone 4 with product titers similar to those of the Δ fuz7 control, whereby the two clones C1 and C3 showed no

conversion of ITA to 2-HP and ITT at all. To investigate whether the variation in product titers can be attributed to differences in the copy number of $P_{etef}cyp3$, a qPCR analysis was performed. The gene copy number of *cyp3* relative to two reference genes *tad1* and *rdo1* (both single copy) strongly correlated with the level of conversion of ITA to 2-HP and ITT for all tested *cyp3*-bearing clones resulting in decreasing ITA ($r^2 = 0.8836$) and increasing 2-HP ($r^2 = 0.9938$) and ITT ($r^2 = 0.9929$) titers with increasing *cyp3* copies (Figure 27F).

Based on these results, clone 2 harboring approximately 13 *cyp3* copies was selected as the best 2-HP/ITT producer for the following experiments, henceforth named *U. cynodontis* 2-HP. However, undesired ITA accumulation reaching a maximum concentration of 5.9 g L^{-1} at 144 h and a final concentration of 3.9 g L^{-1} was observed. Apparently, Cyp3 activity poses a bottleneck in the conversion of ITA to its derivatives, even for this best-performing strain. Consequently, we introduced the derivatives specificity as a further KPI in addition to yield, titer, and rate, which is defined as the percentage of the combined concentrations of 2-HP and ITT over the total acid production. This derivatives specificity is a key factor for later downstream processing, which was a target for optimization in this study. 2-HP and ITT can be converted into each other by lactonization or saponification (Guevarra & Tabuchi, 1990b), but ITA will remain as undesired contaminant upon purification.

Glycerol as an alternative carbon source for 2-HP and ITT production

Ustilaginaceae have a slower metabolism on glycerol than on glucose, potentially preventing an ITA overflow caused by the rate-limiting Cyp3-catalyzed conversion of ITA to 2-HP and ITT as illustrated in Figure 28A and B. With the aim of minimizing extracellular ITA accumulation, cultivations on glycerol as an alternative carbon source were directly compared to glucose-based cultivations (Figure 28A-C).

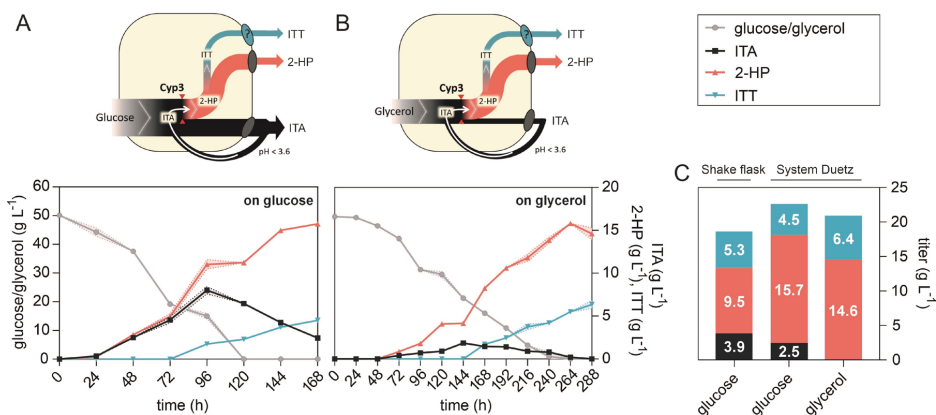


Figure 28: System Duetz microcultivations of *U. cynodontis* 2-HP on two different carbon sources.

Cultivations were performed in System Duetz plates in MTM medium with 15 mM NH₄Cl, 30 mM MES pH 6.5, and (A) 50 g L⁻¹ glucose or (B) 50 g L⁻¹ glycerol (n = 2 biological replicates). For (A) and (B) glucose/glycerol consumption was plotted on the left y-axis, while ITA, 2-HP and ITT titers were plotted on the right y-axis. (C) Mean values of final product titers for direct comparison of different cultures. Product titers obtained on glucose in shake flask cultivations from Figure 27 are shown as well for comparison. Typically, a higher OTR is achieved in System Duetz microcultivations compared to shake flask cultivations with a 10 % filling volume.

Indeed, accumulation of ITA was strongly reduced on glycerol, with its concentration remaining below 1.9 ± 0.1 g L⁻¹ throughout the entire cultivation and a complete conversion to 2-HP and ITT after 288 h resulting in a derivatives specificity of 100 ± 0.0 % (Figure 28B). Although glucose yielded slightly more total acid production, the specificity of derivatives production was only 89 ± 0.2 %. Final cumulative product titers of 2-HP and ITT were even slightly higher on glycerol than on glucose (Figure 28C), but the high derivatives specificity did come at the expense of a lower productivity, which was reduced from 0.12 ± 0.00 g L⁻¹ h⁻¹ on glucose to 0.07 ± 0.00 g L⁻¹ h⁻¹ on glycerol. The substrate-to-product yield was comparable on both carbon sources, amounting to 0.40 ± 0.01 and 0.42 ± 0.02 g_{2-HP+ITT} g_{substrate}⁻¹ on glucose and glycerol, respectively.

Lab-scale fermentation for production of 2-HP and ITT from glycerol

High cell-density batch fermentations with a working volume of 1 L were performed on glycerol (Figure 29B and D) and on glucose as a control (Figure 29A and C) in order to evaluate 2-HP and ITT production at a larger scale, and to obtain larger volumes for initial downstream process development. In all fermentations, the pH was controlled at pH 3.6 during the initial biomass production phase, and then allowed to drop to pH 2.8 through the production of the organic acids (Figure 29A and B). In the glucose fermentation, the pH was further lowered to 2.2 after 120 h in an attempt to further stimulate ITA re-uptake and conversion.

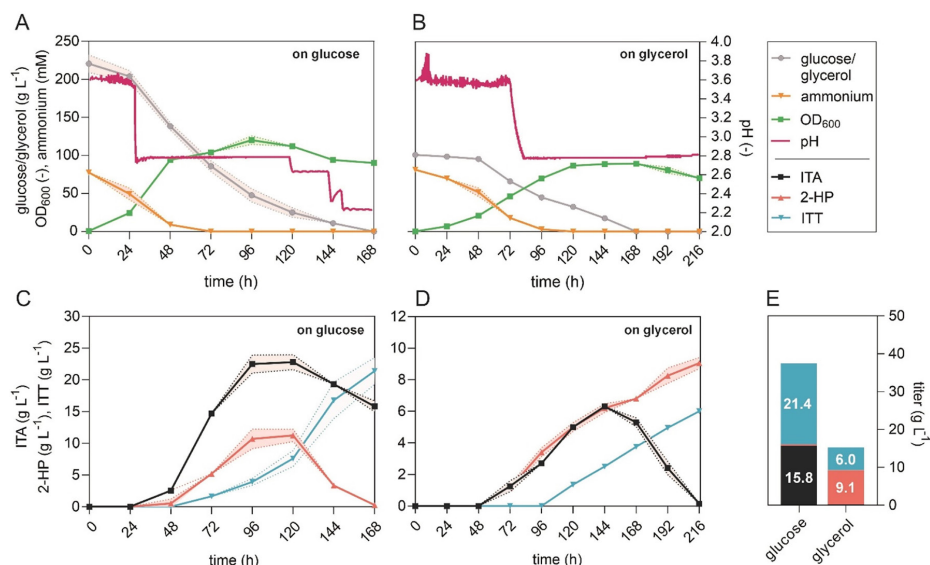


Figure 29: High cell-density batch fermentations of *U. cynodontis* 2-HP on two different carbon sources. Bioreactor cultivations were performed in batch medium with 75 mM NH₄Cl and (A) 200 g L⁻¹ glucose or (B) 100 g L⁻¹ glycerol as carbon source (n = 2 biological replicates). Concentrations for glucose, glycerol and ammonium as well as growth as OD₆₀₀ were plotted on the left y-axis, while pH values were plotted on the right y-axis. Corresponding product titers of ITA, 2-HP and ITT are shown in (C) for glucose-based cultivation and in (D) for glycerol-based cultivation. (E) Mean values of final product titers for direct comparison of different carbon sources. The pH was controlled by automatic titration with 5 M NaOH. After approximately 24 h (A) and 72 h (B), the pH was allowed to drop from pH 3.6 to pH 2.8 through the production of ITA and its two derivatives. Further pH reductions during the fermentation on glucose were performed by the manual addition of 1 M HCl.

The batch fermentation on glucose resulted in the production of a mixture of all three metabolites ITA, 2-HP and ITT (Figure 29C). The highest 2-HP concentration of 11.2 ± 1.0 g L⁻¹ was reached after 120 h, but it was subsequently converted almost completely to ITT. The final ITT concentration was about 21.4 ± 2.1 g L⁻¹. A concentration of 15.8 ± 0.9 g L⁻¹ of ITA was not converted into the other products, resulting in a derivatives specificity of only 58 ± 2.6 % (Figure 29E). Even further decreased pH values, which should facilitate ITA re-uptake, did not result in a complete conversion of ITA to its two downstream products. It is important to note that the equilibrium constant between 2-HP and ITT is theoretically influenced by pH with lower pH values shifting the equilibrium towards 2-HP. However, the time required to reach this equilibrium through non-enzymatic conversion is more than 70 days at conditions comparable to the fermentation (Figure S12), and more than 20 days at neutral pH conditions in Guevarra and Tabuchi (1990a). This is much longer than the fermentation time and we therefore expect biotic effects to be the dominant determinant of 2-HP and ITT concentrations.

Under this high cell-density condition with 200 g L^{-1} glucose, the ITA productivity is apparently too high resulting in an overflow caused by the rate-limiting conversion of ITA to 2-HP and ITT (cf. Figure 28). However, on glycerol, ITA accumulated to a much lesser extent and reached its maximum of only $6.3 \pm 0.1 \text{ g L}^{-1}$ after 144 h (Figure 29D). In contrast to the batch fermentation with glucose, the produced ITA was completely converted to 2-HP and further to ITT yielding $99 \pm 0.3 \%$ derivatives specificity. A similar production pattern was previously observed in System Duetz cultivation (Figure 28). With that, the glycerol fermentation resulted in an ITA-free supernatant with $9.1 \pm 0.4 \text{ g L}^{-1}$ 2-HP and $6.0 \pm 0.0 \text{ g L}^{-1}$ ITT (Figure 29E), making the subsequent purification steps much easier.

Noteworthy, the final cumulative product titers ($21.7 \pm 1.5 \text{ g L}^{-1}$ on glucose and $15.1 \pm 0.3 \text{ g L}^{-1}$ on glycerol), yields ($0.10 \pm 0.00 \text{ g}_{2\text{-HP+ITT}} \text{ g}_{\text{GLC}}^{-1}$ and $0.15 \pm 0.00 \text{ g}_{2\text{-HP+ITT}} \text{ g}_{\text{GLY}}^{-1}$) as well as the volumetric productivity ($0.13 \pm 0.01 \text{ g L}^{-1} \text{ h}^{-1}$ on glucose $0.07 \pm 0.00 \text{ g L}^{-1} \text{ h}^{-1}$ on glycerol) were reduced during the batch fermentations in comparison to System Duetz microcultivations. This might be caused either by differences in medium acidity over time, which was not controlled in the System Duetz microcultivation system, or by lower initial NH_4Cl concentrations in System Duetz cultivations (15 mM) compared to batch fermentations (75 mM). Differences in the OTR between microcultivations and bioreactor cultivations might also contribute to the different product KPIs.

Product purification and characterization

After successful production of larger quantities in glycerol batch fermentations, 2-HP and ITT were purified. Of note, these compounds are not commercially available, and only very small amounts of chemically synthesized 2-HP of unknown purity were thus far available as analytical standard (Geiser et al., 2016b).

Both 2-HP and ITT were successfully obtained from the glycerol fermentation supernatant following a protocol adapted from Guevarra and Tabuchi (1990b) (Figure 30). 2-HP was recovered first through a process of evaporation and lactonization of ITT, followed by 2-HP extraction with ethyl acetate. The obtained 2-HP could subsequently be converted to ITT in the form of its sodium salt by saponification.

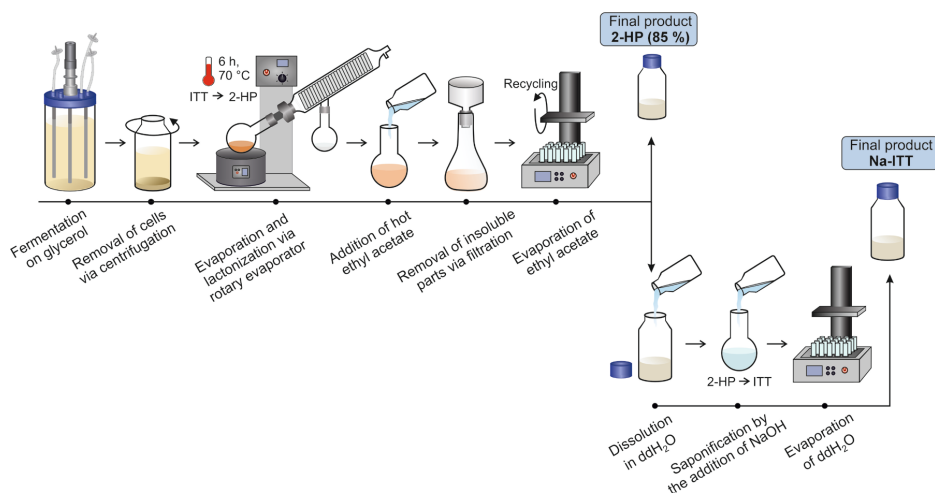


Figure 30: Schematic representation showing the purification procedure of 2-HP and ITT from culture supernatants.

The shown procedure resulted in 2-HP with a purity of 85.3 ± 3.7 % (rounded to 85 % in the scheme) measured via qNMR. The purified 2-HP was saponified with NaOH to Na-ITT.

The concentration of 2-HP that could be identified in the remaining impurities dissolved in ddH₂O was lower than 0.5 g L^{-1} . In total, 91.7 % of the 2-HP initially measured in the fermentation supernatant was recovered. However, when considering the 2-HP produced from ITT lactonization as well, the purification yield was only 49.7 %. This indicates that 2-HP was lost during the purification process, which requires further evaluation in the future.

The obtained products were subsequently characterized by NMR analysis (^1H , ^{13}C , and quantitative), elemental analysis, gas chromatography coupled to time-of-flight mass spectrometry (GC-ToF-MS) and dilute-and-shoot flow-injection-analysis tandem mass spectrometry (DS-FIA-MS/MS) (Reiter et al., 2022). Using ^{13}C NMR analysis, the following carbon atoms of 2-HP were identified: CH_2 at δ 40.43, CH_2 at δ 76.47, C(OH)(COOH) at δ 76.84, COOH at δ 172.30 and C=O at δ 173.81. The ^1H NMR identified the four H atoms of the two CH_2 groups at the following chemical shifts: 2.63 (^1H , d), 3.18 (^1H , d), 4.31 (^1H , d) and 4.61 (^1H , d). The ^{13}C NMR analysis of ITT identified the following carbon atoms: CH_2 at δ 42.42, CH_2 at δ 67.04, C(OH)(COOH) at δ 77.51, COOH at δ 179.08 and COOH at δ 180.27. The ^1H NMR identified also for ITT the four H atoms of the two CH_2 groups at the following chemical shifts: 2.39 (^1H , d), 2.56 (^1H , d), 3.52 (^1H , d) and 3.62 (^1H , d). The ^{13}C NMR spectra of 2-HP and ITT are shown as an example in Figure 31, confirming the structures published by Guevarra and Tabuchi (1990b). 2-HP was further analyzed by qNMR revealing a purity of 85.30 ± 3.7 % ($n = 6$). The identities of both products 2-HP and ITT were also confirmed by GC ToF-MS and DS-FIA-MS/MS.

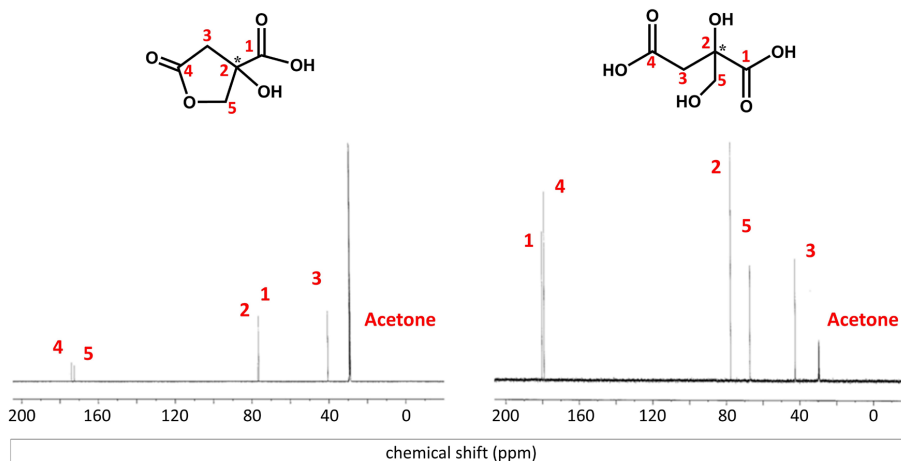


Figure 31: ^{13}C NMR spectra and corresponding structures of 2-HP and ITT. Each peak with different chemical shift and unique shape corresponds to a carbon atom.

Additionally, the elemental composition of 2-HP was determined. Table 9 shows the expected and detected results for 2-HP. The measured composition correlates well with the expected values. The measured percentages of C, H and O add up to about $99.4 \pm 0.3\%$, meaning that there are likely no other elements in the impurities. Potential contaminants could consist of hydrocarbons, given that the 2-HP samples seem to contain a slight excess of C and H. Moreover, no N was detected, thus excluding protein contaminants from the fermentation. The values indicated for N represent detection limits based on sample weight. In the future, additional purification steps such as activated carbon/celite treatment, nanofiltration, or crystallization may be implemented into the purification process to further increase the purity.

Table 9: Elemental analysis of the purified 2-HP.

	% C (w w ⁻¹)	% H (w w ⁻¹)	% O (w w ⁻¹)	% N (w w ⁻¹)
2-HP, expected	41.1	4.1	54.8	0.0
2-HP ($85.3 \pm 3.7\%$), detected (n = 6)	41.7 ± 0.3	4.5 ± 0.1	53.2 ± 1.6	< 0.5

Strain engineering to enhance derivatives specificity

In addition to evaluating the impact of alternative carbon sources on 2-HP and ITT derivatives specificity, we also investigated the effects of additional metabolic engineering approaches (Figure 32). The first approach was the deletion of the *itp1* ITA transporter gene, which could increase the intracellular concentration of ITA and thus its conversion to the products of interest.

Itp1 was also exchanged with the heterologous ITA transporter MfsA from *A. terreus*, which was described to have a higher affinity for 2-HP export than Itp1 (Hosseinpour Tehrani et al., 2019a).

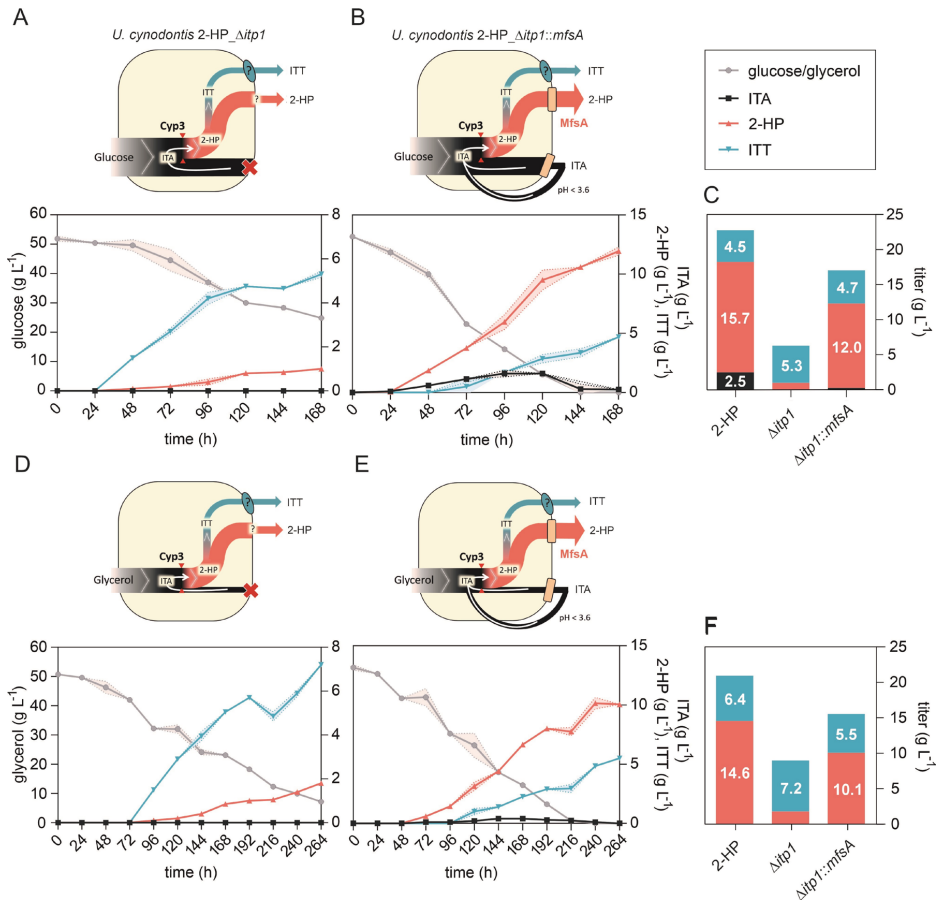


Figure 32: System Duetz microcultivations of *U. cynodontis* 2-HP_Δitp1 and *U. cynodontis* 2-HP_Δitp1::mfsA (henceforth named *U. cynodontis* 2-HP MfsA) on two different carbon sources for analyzing ITA, 2-HP and ITT production.

Cultivations were performed in System Duetz plates in MTM medium with 15 mM NH₄Cl, 30 mM MES pH 6.5, and (A and B) 50 g L⁻¹ glucose or (D and E) 50 g L⁻¹ glycerol (n = 2 biological replicates). Cultivations of *U. cynodontis* 2-HP_Δitp1 (A and D) and *U. cynodontis* 2-HP MfsA (B and E). (C and F) Mean values of final product titers for direct comparison of the different strains. Product titers obtained for *U. cynodontis* 2-HP shown in Figure 28C are again displayed for comparison. For all time courses, carbon source consumption was plotted on the left y-axis, while ITA, 2-HP and ITT titers were plotted on the right y-axis.

The Δitp1 strain was not able to secrete ITA anymore throughout the entire cultivation, and the 2-HP concentration was also significantly reduced (Figure 32A). This confirms its role as ITA and 2-HP exporter as described for *U. maydis*, although the Δitp1 mutant of this strain produced 0.7 ± 0.1 g L⁻¹ ITA (Hosseinpour Tehrani et al., 2019b). This mutant even showed an increased 2-HP

titer in ITA feeding experiments, which points towards an additional 2-HP transport mechanism in *U. maydis* under certain conditions, which is apparently absent in *U. cynodontis*. However, in that previous manuscript ITT could not be quantified due to a lack of a suitable analytical technique and standard. With the produced Na-ITT standard, this was now addressed. Interestingly, the measured ITT concentration of $5.3 \pm 0.1 \text{ g L}^{-1}$ was higher than the one obtained for the control with intact *itp1* gene (Figure 32C), which strongly suggests the existence of a different transport system for ITT. The exchange of *itp1* by *mfsA* in the *U. cynodontis* 2-HP MfsA strain reduced maximum ITA accumulation by approximately $80 \pm 0.7 \%$ compared to the progenitor strain *U. cynodontis* 2-HP (Figure 32B), resulting in an increased derivatives specificity of approximately $99 \pm 0.3 \%$. However, overall derivatives titers were greatly reduced and the knockout also strongly affected substrate uptake rates, likely as a result of the stress of intracellular ITA and 2-HP accumulation. This was ameliorated by the complementation with *mfsA*. Analogous to the $\Delta itp1$ modification, a reduced transport of ITA via MfsA is assumed to result in higher intracellular titers for enhanced conversion into 2-HP and ITT, but this accumulation is less severe. Consequently, there was a greater cumulative production of the derivatives to $17.0 \pm 0.3 \text{ g L}^{-1}$ (Figure 32C), although titers of the two downstream products were reduced compared to the progenitor with *Itp1* transporter. Hence, the improved derivatives specificity came at the expense of a reduced substrate-to-product yield (0.40 ± 0.01 and $0.33 \pm 0.01 \text{ g}_{2\text{-HP+ITT}} \text{ g}_{\text{GLC}}^{-1}$ for *U. cynodontis* 2-HP and *U. cynodontis* 2-HP MfsA, respectively) and a reduced volumetric productivity of $0.10 \pm 0.00 \text{ g L}^{-1} \text{ h}^{-1}$. Here, one can assume that elevated intracellular ITA concentrations may favor its degradation limiting further conversion. Although an ITA degradation pathway has not been published for *Ustilago*, decreasing ITA concentrations have been observed in *U. maydis* during prolonged cultivations (Geiser et al., 2016b; Hosseinpour Tehrani et al., 2019c). Possibly, the degradation occurs through a similar pathway as described for *A. terreus* (Chen et al., 2016). It might also be possible that the higher intracellular ITA concentration reduces production efficiencies. The latter seems likely, given that the $\Delta itp1$ strain has a greatly reduced glucose uptake rate.

Additionally, System Duetz microcultivations of these strains were also performed on glycerol, showing analogous behavior compared to glucose (Figure 32D and E). Deletion of *itp1* caused a strong reduction in ITA and 2-HP accumulation in comparison to the progenitor strain *U. cynodontis* 2-HP (Figure 32F), while ITT levels were increased. Related to glucose as carbon source, performance of *U. cynodontis* 2-HP MfsA on glycerol was slightly worse in terms of the achieved yield ($0.30 \pm 0.01 \text{ g}_{2\text{-HP+ITT}} \text{ g}_{\text{GLC}}^{-1}$) and the calculated productivity ($0.06 \pm 0.00 \text{ g L}^{-1} \text{ h}^{-1}$), favoring cultivation of this improved strain on glucose for specific 2-HP and ITT production in up-scaled fermentations.

Besides a reduction of ITA export, the re-uptake of ITA is also a possible factor that can contribute to 2-HP and ITT production (Geiser et al., 2016b), especially in later production stages when ITA production slows down. To further characterize this effect, additional System Duetz microcultivations were performed with CaCO_3 as buffer (Figure 33). This should prevent ITA re-uptake by avoiding the formation of fully protonated ITA (Hosseinpour Tehrani et al., 2019c; Zambanini et al., 2016b), which may consequently allow to more precisely conclude on initial metabolic fluxes. In addition, calcium carbonate should reduce product inhibition and weak acid stress and thus may allow to reach higher 2-HP and ITT titers.

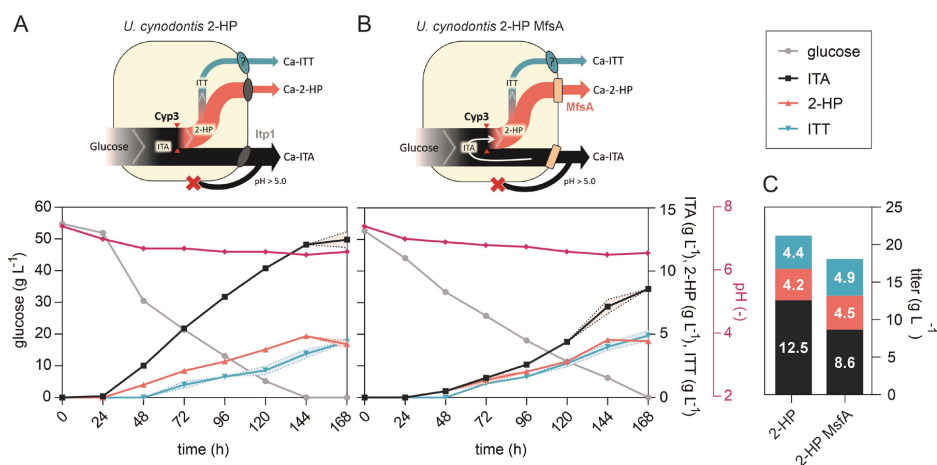


Figure 33: System Duetz microcultivations of *U. cynodontis* 2-HP and *U. cynodontis* 2-HP MfsA on glucose using CaCO_3 as buffer.

Cultivations were performed in System Duetz plates in MTM medium with 15 mM NH_4Cl , 33 g L⁻¹ CaCO_3 pH 7.4, and 50 g L⁻¹ glucose (n = 2 biological replicates). (C) Mean values of final product titers for direct comparison of the different strains.

Cultivation of *U. cynodontis* 2-HP showed similar cumulative end titers of ITA, 2-HP and ITT when using MES (Figure 28C) or CaCO_3 (Figure 33C) as buffer component. For CaCO_3 , all product titers continuously increased until the end of cultivation, which was not the case for cultivation with MES buffer due to re-uptake and further conversion of ITA facilitated by acidic pH values, which are shown in Figure S11. The conversion of ITA to its downstream products was markedly reduced in the presence of CaCO_3 , which prevents acidification of the media (Figure 33A and B). This demonstrates a major contribution of the re-uptake of protonated ITA to 2-HP and ITT production (Figure 28A and C and Figure 33A and C). Compared with the progenitor strain *U. cynodontis* 2-HP, cultivation of *U. cynodontis* 2-HP MfsA on glucose with CaCO_3 buffer showed reduced absolute and relative accumulation of ITA, while more 2-HP and ITT was secreted. This supports the hypothesis that MfsA has a higher affinity for 2-HP and lower affinity for ITA (Hosseinpour Tehrani

et al., 2019a) and it further suggests that it also facilitates ITT transportation (Figure 32C and Figure 33B and C). The fact that these differences are observed with the CaCO_3 buffer proves that the increased specificity of derivatives production is caused by MfsA and not by altered ITA re-uptake dynamics. However, ITA is reduced but not entirely abolished, and therefore a combination of specificity-driving strategies is needed to achieve full conversion.

Bioreactor cultivations on glucose

The exchange of *itp1* with *mfsA* resulted in a substantially increased derivatives specificity, which was further enhanced in cultures with a low pH facilitating ITA re-uptake (Figure 32). We therefore sought to leverage these strategies to maintain the high productivity on glucose compared to glycerol while still achieving full conversion in a high cell-density batch fermentation.

Previous high cell-density batch fermentation of *U. cynodontis* 2-HP resulted in the production of a mixture of all three metabolites (Figure 29). Presumably, the ITA productivity was too high under these conditions resulting in an overflow caused by the rate-limiting conversion of ITA to 2-HP and ITT. Analogous batch fermentation of the newly generated *U. cynodontis* 2-HP MfsA harboring the $\Delta itp1::mfsA$ modification showed a similar production pattern. Although there is overall reduction in extracellular ITA accumulation of 69 ± 0.5 % likely due to the transporter exchange, the ITA is not fully converted even after prolonged incubation and a further decrease of pH (Figure 29C and Figure 34A, B and G). Of note, once the pH value was adjusted to 2.6, a strong decrease in the 2-HP concentration was observed. This decrease most likely resulted from the re-uptake of 2-HP at this pH value, as it is around the pK_a value of 2-HP (2.78 at 20 °C) (Guevarra & Tabuchi, 1990a). While *U. cynodontis* 2-HP metabolized all glucose within 168 h, *U. cynodontis* 2-HP MfsA required an additional 120 h for the complete conversion. The strain also showed a much longer lag phase, indicating that the transporter exchange caused significant stress to the production host especially in this high glucose concentration. However, the final cumulative product titers of 2-HP and ITT were higher with 26.2 ± 0.1 g L⁻¹ compared to *U. cynodontis* 2-HP, resulting in an increased derivatives yield (Table 10).

Since the high cell-density batch fermentations on glucose did not result in the production of pure 2-HP and ITT, a low cell-density fed-batch fermentation with a reduced glucose starting concentration was assessed next (Figure 34C and D). To further reduce stress in the initial biomass production phase, the starting pH value was set to 6.5 (Niehoff et al., 2023). Afterwards, the pH value was allowed to drop through the production of ITA and its two downstream products 2-HP and ITT. However, since the pH value only dropped slowly, it was manually adjusted to 3.6 after 130 h by adding HCl. Despite the low cell-density and reduced glucose concentration, ITA accumulated up to 15.7 ± 1.3 g L⁻¹, comparable to the previous high cell-density batch

fermentation (Figure 29C and Figure 34C, D and G). The high ITA accumulation may be due to the elevated pH value during the initial biomass production phase, preventing secreted ITA from re-entering the cells. Due to the already high ITA concentration, glucose was fed only for a short period of 24 h, and the pH value was further decreased to facilitate the re-uptake of ITA. ITA was continuously converted into its downstream products until it was completely depleted at the end of the fermentation accounting for a derivatives specificity for 2-HP and ITT of $99 \pm 0.2 \%$. After 288 h of fermentation, the ITT concentration remained constant, while the 2-HP concentration increased despite a pH value of 2.2, which theoretically allows 2-HP to be re-uptaken and transformed into ITT. This suggests that a threshold of $30.5 \pm 0.4 \text{ g L}^{-1}$ ITT may exist, beyond which the ITT productivity is strongly reduced, possibly due to feedback inhibition, or precipitation. The final broth contained more ITT than 2-HP with a combined product titer of $44.0 \pm 0.2 \text{ g L}^{-1}$. Guevarra and Tabuchi (1990b) reported higher product titers with the wildtype progenitor of the engineered strains described in this study, but we were unable to reproduce these results due to strong filamentous growth and lower productivities of this non-engineered strain. Perhaps this can be attributed to minor differences in cultivation conditions, such as the use of urea as alternative nitrogen source. Hosseinpour Tehrani et al. (2019d) observed the accumulation of 2-HP during a pulsed fed-batch fermentation of the wildtype *U. cynodontis* $\Delta fuz7$ strain at a concentration of $17.3 \pm 1.1 \text{ g L}^{-1}$ at otherwise comparable cultivation conditions as in the low cell-density fed-batch cultivation presented here, but ITT was not analyzed in this study. Additionally, for all published data potential inaccuracies deriving from standards with unknown purity should be taken into account, further complicating direct comparisons. Apart from 2-HP, high concentrations of ITA ($25.5 \pm 1.1 \text{ g L}^{-1}$) were reported to accumulate during cultivation of *U. cynodontis* $\Delta fuz7$, highlighting the improved derivatives specificity obtained by rational metabolic strain engineering and optimized cultivation conditions described here. Another study reported 2-HP product titers of $21.3 \pm 0.7 \text{ g L}^{-1}$ during high cell-density fed-batch fermentation of the *U. maydis* MB215 wildtype strain after 163 h on 200 g L^{-1} glucose and $75 \text{ mM NH}_4\text{Cl}$. This corresponds to volumetric productivity of $0.13 \pm 0.01 \text{ g L}^{-1} \text{ h}^{-1}$ 2-HP and a comparatively low yield of $0.08 \pm 0.01 \text{ g}_{2\text{-HP}} \text{ g}_{\text{GLC}}^{-1}$, (Geiser et al., 2016b). Comparable to the fermentation results of Hosseinpour Tehrani et al. (2019d), 2-HP production was accompanied by accumulation of ITA, again pointing out the requirement for strain and process optimization to obtain a high 2-HP and ITT derivatives specificity as successfully done in this work.

To evaluate the derivatives specificity of 2-HP and ITT over ITA across the cultivation time on glycerol as a carbon source, an additional fermentation was performed with the newly engineered *U. cynodontis* 2-HP MfsA (Figure 34E, F, and G). Accumulation of ITA during fermentation was substantially lower than on glucose reaching a maximum value of $3.3 \pm 0.4 \text{ g L}^{-1}$, but final

cumulative product titers of 2-HP and ITT were markedly lower during cultivation of *U. cynodontis* 2-HP MfsA on glycerol as well. When compared to the progenitor strain's performance on glycerol, approximately 52 ± 0.5 % reduction in ITA accumulation was observed (Figure 34F). Moreover, whereas product titers of 2-HP and ITT were almost comparable for *U. cynodontis* 2-HP and *U. cynodontis* 2-HP MfsA on glycerol, the latter exhibited a faster conversion of ITA to 2-HP and ITT, achieving complete conversion in just 192 hours, whereas the progenitor strain required 216 hours (Figure 29D and Figure 34F). The growth of both strains was similar, with ammonium depletion occurring after 120 h and glycerol depletion after 168 hours in both fermentations (Figure 29B and Figure 34). This is in contrast to the glucose cultures, where the transporter exchange caused decreased growth and production rates. Likely, the overall reduced metabolic fluxes on glycerol led to a better balancing of substrate uptake, ITA production, and product secretion rates, preventing excessive intracellular ITA accumulation while still improving 2-HP and ITT specificity.

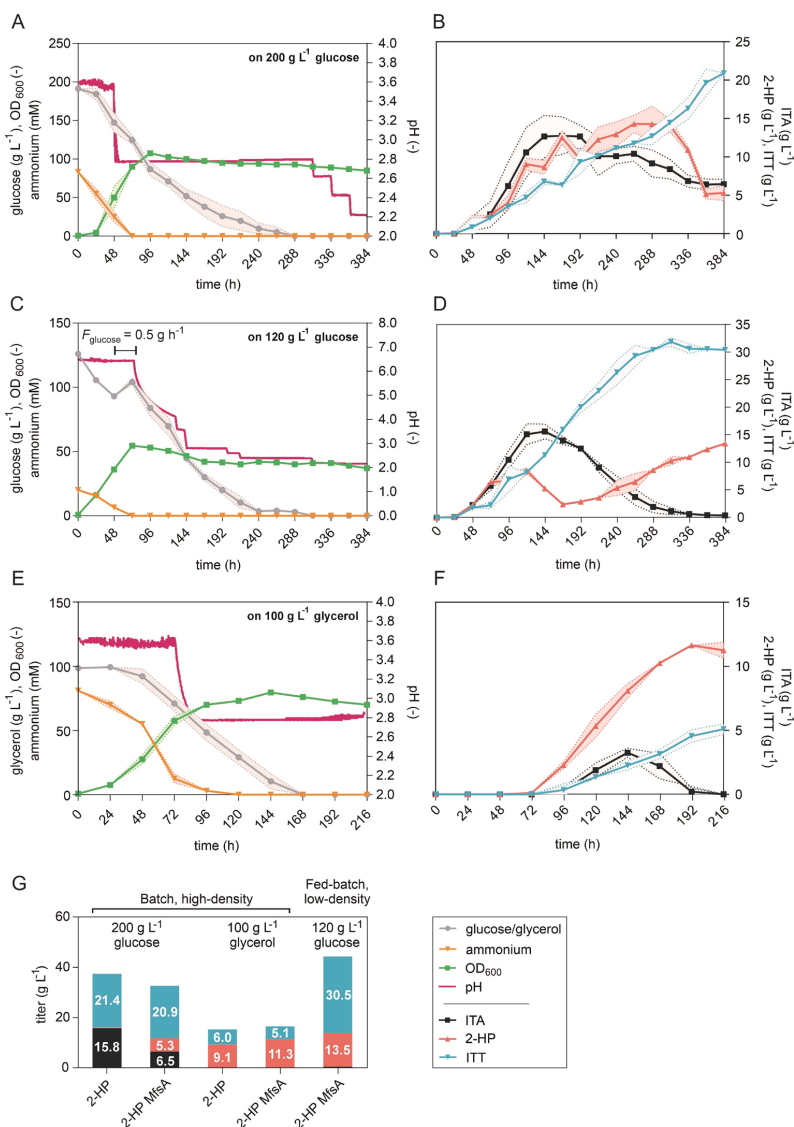


Figure 34: Fermentation approaches of *U. cynodontis* 2-HP MfsA to optimize 2-HP and ITT production.

(A) High cell-density batch fermentation with 75 mM NH₄Cl and 200 g L⁻¹ glucose with corresponding product titers of ITA, 2-HP and ITT shown in (B). (C) Low cell-density fed-batch fermentation with 15 mM NH₄Cl and 120 g L⁻¹ glucose including an additional 12 g glucose fed with corresponding product titers of ITA, 2-HP and ITT shown in (D). (E) High cell-density batch fermentation with 75 mM NH₄Cl and 100 g L⁻¹ glycerol with corresponding product titers of ITA, 2-HP and ITT shown in (F). In case of (A, C and E), carbon source consumption, ammonium concentration and growth were plotted on the left y-axis, while pH values were plotted on the right y-axis. The pH was controlled by automatic titration with 5 M NaOH. After approximately 48 h (A) and 72 h (C and E), the pH was allowed to drop from pH 3.6 to pH 2.8 (A and E) and from 6.5 to 3.6 (C) through the production of ITA and its two derivatives. Further pH reductions during the fermentations on glucose were performed by the manual addition of 1 M HCl. (F) Mean values of final product titers for all performed lab-scale fermentations of strain *U. cynodontis* 2-HP and *U. cynodontis* 2-HP MfsA (n = 2 biological replicates).

3.4.3. Conclusion

This study explores different strategies to increase derivatives specificity for the production of 2-HP and ITT over ITA, including process parameters such as substrate and pH, as well as strain engineering focused on Cyp3 expression and product export. A high copy number of *cyp3* was essential for efficient 2-HP production, but still posed a bottleneck even in the best-performing strain. The linear correlation between copy number of the *P_{etef}Cyp3* cassette and production suggests that Cyp3 activity may still be boosted by further overexpression. Knockout of the exporter gene *itp1* abolished ITA production, but with a drastic reduction in overall production. Exchange of the Itp1 transporter for MfsA from *A. terreus* increased specificity with a much smaller effect on production efficiency, but overall, strain engineering alone could not increase derivatives specificity to 100 % without significantly reducing yield, titer, and rate. Specificity could be driven to 100 ± 0.0 % by a combination of the transporter exchange, low pH to facilitate ITA re-uptake, and use of glycerol to reduce ITA production rate. However, the best yield, titer, and productivity for 2-HP and ITT were achieved when performing a low cell-density fed-batch fermentation on glucose combining high product titers (44.0 ± 0.2 g L⁻¹), high derivatives specificity (99 ± 0.2 %), the highest yield (0.32 ± 0.00 g_{2-HP+ITT} g_{GLC}⁻¹), and one of the highest volumetric productivities (0.11 ± 0.00 g L⁻¹ h⁻¹) (Table 10). Nevertheless, significant amounts of ITA still accumulated during this fermentation, which may be addressed in the future by further strain engineering to optimize Cyp3 expression and activity as a main focus.

In summary, 2-HP and ITT of relatively high purity were produced, building upon the pioneering work of Guevarra and Tabuchi (1990b). This now enables the study of these ITA derivatives for potential pharmaceutical applications, in light of recent discoveries on the anti-bacterial relevance of their ITA precursor (de Witt et al., 2023; Z. Li et al., 2023; O'Neill & Artyomov, 2019; Peace & O'Neill, 2022).

Table 10: KPIs of the different fermentation approaches, calculated for the endpoint titers.

The darker the color, the better the parameter value achieved during cultivation.

Strain	Fermentation	Product	Titer (g L ⁻¹)	Yield (g _{product} g _{substrate} ⁻¹)	Productivity (g L ⁻¹ h ⁻¹)	Derivatives specificity (%)
2-HP	200 g L ⁻¹ glucose	2-HP + ITT	21.7 ± 1.5	0.10 ± 0.00	0.13 ± 0.00	58 ± 2.6
		2-HP	0.3 ± 0.1	0.00 ± 0.00	0.00 ± 0.00	
		ITT	21.4 ± 1.5	0.10 ± 0.00	0.13 ± 0.01	
	100 g L ⁻¹ glycerol	2-HP + ITT	15.1 ± 0.3	0.15 ± 0.00	0.07 ± 0.00	99 ± 0.3
		2-HP	9.1 ± 0.3	0.10 ± 0.00	0.04 ± 0.00	
		ITT	6.0 ± 0.0	0.06 ± 0.00	0.03 ± 0.00	
2-HP MfsA	200 g L ⁻¹ glucose	2-HP + ITT	26.2 ± 0.8	0.14 ± 0.00	0.07 ± 0.00	80 ± 0.6
		2-HP	5.3 ± 0.7	0.03 ± 0.00	0.01 ± 0.00	
		ITT	20.9 ± 0.1	0.11 ± 0.00	0.05 ± 0.00	
	120 g L ⁻¹ glucose	2-HP + ITT	44.0 ± 0.2	0.32 ± 0.01	0.11 ± 0.00	99 ± 0.2
		2-HP	13.5 ± 0.4	0.10 ± 0.00	0.04 ± 0.00	
		ITT	30.5 ± 0.2	0.22 ± 0.01	0.08 ± 0.00	
	100 g L ⁻¹ glycerol	2-HP + ITT	16.4 ± 0.2	0.17 ± 0.00	0.08 ± 0.00	100 ± 0.0
		2-HP	11.3 ± 0.5	0.11 ± 0.01	0.05 ± 0.00	
		ITT	5.1 ± 0.3	0.05 ± 0.00	0.02 ± 0.00	

3.4.4. Materials and methods

Chemicals and strains

All chemicals used in this study were obtained from Sigma-Aldrich (St. Louis, USA), Thermo Fisher Scientific (Waltham, USA), or VWR (Radnor, USA) and were of analytical grade. All strains used in this work are listed in Table 11.

Table 11: *U. cynodontis* strains used in this study.

Strain designation	Resistance	Reference
<i>U. cynodontis</i> NBRC9727 Δ fuz7 (162)	-	(Hosseinpour Tehrani et al., 2019b)
<i>U. cynodontis</i> NBRC9727 Δ fuz7 Δ cyp3 <i>P_{etef}mttA P_{ria1}ria1</i> (223)	Hyg ^R , Cbx ^R	(Hosseinpour Tehrani et al., 2019b)
<i>U. cynodontis</i> NBRC9727 Δ fuz7 Δ cyp3 <i>P_{etef}mttA P_{ria1}ria1 P_{etef}cyp3</i> (1375)	Hyg ^R , Cbx ^R , Nat ^R	this study
<i>U. cynodontis</i> NBRC9727 Δ fuz7 Δ cyp3 <i>P_{etef}mttA P_{ria1}ria1 P_{etef}cyp3 Δitp1</i> (2694)	Hyg ^R , Cbx ^R , Nat ^R , G418 ^R	this study
<i>U. cynodontis</i> NBRC9727 Δ fuz7 Δ cyp3 <i>P_{etef}mttA P_{ria1}ria1 P_{etef}cyp3 Δitp1::mfsA</i> (2695)	Hyg ^R , Cbx ^R , Nat ^R , G418 ^R	this study

Media and culture conditions

U. cynodontis strains were grown in YEPS medium containing 10 g L⁻¹ yeast extract, 10 g L⁻¹ peptone, and 10 g L⁻¹ sucrose. For growth and production experiments, *U. cynodontis* was cultured in 30 mM MES or 33 g L⁻¹ CaCO₃ buffered screening medium according to Geiser et al. (2014) with either 50 g L⁻¹ glucose or glycerol. The medium also contained 15 mM NH₄Cl, 0.2 g L⁻¹ MgSO₄·7H₂O, 0.01 g L⁻¹ FeSO₄·7H₂O, 0.5 g L⁻¹ KH₂PO₄, 1 mL L⁻¹ vitamin solution, and 1 mL L⁻¹ trace element solution. The vitamin solution contained (per liter) 0.05 g D-biotin, 1 g D-calcium pantothenate, 1 g nicotinic acid, 25 g myo-inositol, 1 g thiamine hydrochloride, 1 g pyridoxol hydrochloride, and 0.2 g *para*-aminobenzoic acid. The trace element solution contained (per liter) 1.5 g EDTA, 0.45 g ZnSO₄·7H₂O, 0.10 g MnCl₂·4H₂O, 0.03 g CoCl₂·6H₂O, 0.03 g CuSO₄·5H₂O, 0.04 g Na₂MoO₄·2H₂O, 0.45 g CaCl₂·2H₂O, 0.3 g FeSO₄·7H₂O, 0.10 g H₃BO₃, and 0.01 g KI. Cultivations were conducted in System Duetz plates (24 well plates, Enzymscreen, Netherlands) with a filling volume of 1.5 mL (d = 50 mm, n = 300 rpm, T = 30 °C and Φ = 80 %) (Duetz et al., 2000) or in 500 mL shaking flasks with a filling volume of 50 mL (d=25 mm, n = 200 rpm, T = 30 °C and Φ = 80 %). For growth and production experiments, main cultures were inoculated to an OD₆₀₀ of 0.5 with overnight precultures grown in the same media. When performing System Duetz cultivations,

cultures were simultaneously inoculated into multiple plates. A full plate was designated as a sacrificial sample for each time point to maintain continuous oxygenations.

As previously described in Becker et al. (2021), controlled fed-batch cultivations were carried out in a DASGIP Bioblock (Eppendorf, Germany), controlled using the Eppendorf DASware control software (Eppendorf, Germany). Vessels with a total volume of 2.3 L and a working volume of 1.0 L were used. All cultivations were performed in batch medium according to Geiser et al. (2014) as described above. The medium also contained 1 g L⁻¹ yeast extract (Merck Millipore, Germany) and varying concentrations of glucose, glycerol and NH₄Cl, as indicated. The pH was controlled by automatic addition of 5 M NaOH or 1 M HCl, and the DO was controlled at 30 % by a cascade mode including agitation 800-1200 rpm (0-40 % DOT controller output), air flow 1-2 vvm (40-80 % DOT controller output), and oxygen 21-100 % (80-100 % DOT controller output). The cultivation was performed at 30 °C and the bioreactor was inoculated to a final OD₆₀₀ of 0.75 from an overnight preculture grown in screening medium according to Geiser et al. (2014) containing 50 g L⁻¹ glucose or glycerol, 15 mM NH₄Cl and 100 mM MES pH 6.5. 0.5 mL Antifoam 204 (Sigma, A6426) was added in the beginning of the cultivation and subsequently every 24 h.

Analytical methods

When CaCO₃ was used as buffer, it was dissolved in a 1:1 ratio with 4 M HCl before subsequent measurements, according to the procedure described by Zambanini et al. (2016a). Identification and quantification of products and substrates in the supernatants were performed using a HPLC 1260 Infinity system (Agilent, Waldbronn, Germany) equipped with an ISERA Metab AAC column 300 × 7.8 mm column (ISERA, Germany). Separation was performed using an isocratic elution program at a flow rate of 0.6 mL min⁻¹ and a temperature of 40 °C with 5 mM sulfuric acid as a solvent (Becker et al., 2021). Detection was performed using a diode array detector at 210 nm and a RI detector. All samples were filtered with Rotilabo syringe filters (pore size 0.22 µm) and then diluted with ddH₂O. Analytes were identified on the basis of retention time compared to corresponding standards, and data analysis was performed using the Agilent OpenLAB Data Analysis - Build 2.200.0.528 software (Agilent, Waldbronn, Germany). Ammonium concentrations in culture samples were determined by the colorimetric method described by Willis et al. (1996). In this method, 50 µL culture supernatant was mixed with 1 mL reagent (8 g sodium salicylate, 10 g trisodium phosphate, 0.125 g sodium nitroprusside), followed by rapid addition of 250 µL hypochlorite solution. After color development (at least 15 min at RT), the absorbance was measured at 685 nm using cuvettes and a spectrophotometer. Ammonium concentrations were calculated using an ammonium standard curve. Cell-densities were quantified by measuring the optical density at a wavelength of 600 nm using cuvettes and a spectrophotometer. Samples were

diluted appropriately with the respective medium to fall within the linear measuring range of the photometer between absolute values of 0.2 and 0.4.

Product purification and characterization

Following the successful production of 2-HP and ITT, the corresponding fermentation broths were centrifuged at 10,000 rpm for 30 to 60 min using a Beckman Avanti J-25 Centrifuge from Beckman Instruments (Fullerton, USA). The cell pellet was discarded, and the resulting supernatant was filtered (pore size 0.22 μm). The products 2-HP and ITT were recovered from the fermentation supernatant through a process adapted from Guevarra and Tabuchi (1990b). The lactonization was started with the evaporation of water from the supernatant in a rotary evaporator, resulting in a syrup. Büchi R-210 Rotavapor Evaporator from BÜCHI Labortechnik GmbH (Essen, Germany) was used, which was equipped with a Büchi B-491 Heating Bath and a diaphragm vacuum pump CVC 2 from VACUUBRAND (Wertheim, Germany). The temperature of the water bath was set to 50-60 °C, and the pressure was gradually decreased to approximately 60 mbar, yielding in a concentrated syrup in about 1 h. Subsequently, the temperature of the water bath was gradually raised to 90 °C, the pressure gradually reduced to the minimum of approximately 20 mbar, and the syrup was further heated for at least 6 h to lactonize ITT to 2-HP. The resulting mass was dried with the high vacuum pump TRIVAC D 4 B from Leybold (Köln, Germany) and simultaneously heated with a heating mantle to eliminate residual water over a period of about 2-3 h. The dry mass was dissolved in the same volume of hot ethyl acetate as the initial volume of supernatant. The extraction with ethyl acetate involved continuous stirring and heating (50-60 °C) for approximately 6-7 h, utilizing a reflux condenser to prevent solvent evaporation. Depending on the experiment, 2 to 5 extraction steps were performed with fresh solvent to enhance product recovery. Insoluble impurities were removed through decantation and subsequent filtration (pore size 0.22 μm). The solvent phases from the extraction steps were combined and concentrated using the rotary evaporator. The resulting volume was aliquoted into pre-weighed Eppendorf tubes, and the remaining ethyl acetate was evaporated in the Vacufuge Concentrator Model 5301 from Eppendorf (Hamburg, Germany) to obtain dry 2-HP. The tubes were reweighed to determine the final product quantity. The sodium salt of ITT was obtained by saponifying the 2-HP recovered from the fermentation supernatant, following the procedure described by Guevarra and Tabuchi (1990b). A known mass of 2-HP was dissolved in ddH₂O to obtain a solution of known molarity. The volume of 5 M NaOH required to neutralize the acidic solution was calculated, and twice this volume was added to the 2-HP solution. The mixture was shaken and heated (60-70 °C) for approximately 10-15 min to saponify 2-HP. Finally, the Na-ITT was dried in the Vacufuge Concentrator Model 5301 from Eppendorf (Hamburg, Germany). Several analytical methods were

employed for product characterization. NMR spectroscopy analyses, including ^1H NMR, ^{13}C NMR, and qNMR, were performed with the Avance DRX600 NMR Spectrometer from Bruker Corporation (Billerica, USA). For the NMR analyses, dry 2-HP was dissolved in deuterated acetone, while dry Na-ITT was dissolved in deuterated water. For qNMR, approximately 5 mg of 2-HP and a similar mass of the standard 1,3,5-trimethoxybenzene (to obtain similar molarities) were mixed and dissolved in deuterated acetone. The elemental analysis was conducted with the vario EL cube system from Elementar (Langenselbold, Germany). Small amounts of the products (2 mg) were analyzed in both CHN and O modes. The products were also analyzed by GC-ToF-MS with a method adapted from Paczia et al. (2012). The pH of the samples was adjusted to fall within the neutral range of 6.7 to 7.3 using a NaOH solution and the 766 Laboratory pH Meter from Knick (Berlin, Germany). Dry products were dissolved either in ddH₂O or in 50 mM phosphate buffer with pH 7.0. Samples with volumes of 13 μL or 130 μL and with concentrations not exceeding 5 mM were prepared, shock-frozen in liquid nitrogen and stored at -20°C . The samples were afterwards lyophilized overnight in a Christ LT-105 freeze dryer from Martin Christ Gefriertrocknungsanlagen GmbH (Osterode am Harz, Germany). Following lyophilization, the dried samples were derivatized with 50 μL MeOX (20 mg mL⁻¹ O-methylhydroxylamine in pyridine) for 90 min at 30°C and 600 rpm in a ThermoMixer from Eppendorf (Hamburg, Germany). This was followed by an incubation with 80 μL of MSTFA (*N*-methyl-*N*-(trimethylsilyl)-trifluoroacetamide) for 90 min at 40°C and 600 rpm. The analysis was conducted using an 8890N double SSL gas chromatograph from Agilent (Santa Clara, USA) equipped with a LPAL3-S15 liquid autosampler from LECO (Mönchengladbach, Germany). The gas chromatograph was coupled to a GCxGC HRT+ 4D high-resolution time of flight mass spectrometer from LECO (Mönchengladbach, Germany). A volume of 1 μL of sample was injected into a split/splitless injector at 280°C at varying split modes. The constant helium flow was set to 1 mL min⁻¹ for the active injector and column, and to 0.5 mL min⁻¹ for the passive injector. For peak identification, the Retention time Index value, the baseline noise subtracted fragmentation pattern and the fragment elemental composition were compared to an in-house *m/z* database JuPoD and the commercial database NIST20 (National Institute of Standards and Technology, USA). Purified products were also subjected to analysis by DS-FIA-MS/MS (Reiter et al., 2022). The obtained 2-HP and ITT were dissolved in ddH₂O or in 50 mM phosphate buffer with pH 7.0 prior to analysis. Accurate mass spectra were acquired using the ESI-QqToF MS TripleTOF6600 from AB Sciex (Darmstadt, Germany). An Agilent 1100 system, along with an Agilent 1260 Infinity II Multisampler from Agilent Technologies (Waldbronn, Germany), coupled to an ESI-QqQ API4000 from AB Sciex (Darmstadt, Germany) was employed for the analysis.

Plasmid cloning and strain engineering

Plasmids were constructed via Gibson assembly (Gibson et al., 2009) employing the NEBuilder HiFi DNA Assembly Cloning Kit (New England Biolabs (NEB), Ipswich, MA, USA). DNA oligonucleotides were purchased from Eurofins Genomics (Ebersberg, Germany), and Q5 High-Fidelity DNA Polymerase (NEB) served as the polymerase. Details about the utilized primers and plasmids are shown in Table 12 and Table S5. Standard cloning and plasmid maintenance were carried out using competent *E. coli* DH5 α or PIR2 cells according to Sambrook and Russell (2006). Plasmids were confirmed by PCR, restriction or sequencing. For the generation of protoplasts, transformation, and isolation of genomic DNA of *U. cynodontis* NBRC9727, protocols according to Brachmann et al. (2004) were used. For the integration of *P_{etef}cyp3*, the plasmid was linearized with FspI and integrated randomly into the genome. For the deletion of *itp1*, homologous recombination with 1000 bp flanking regions including FRT-sites and a geneticin G418 resistance cassette were used. For the exchange of *itp1* with *mfsA*, homologous recombination with 1000 bp flanking regions and a geneticin G418 resistance cassette were used. Successful integration, deletion and exchange were confirmed by PCR.

Table 12: Plasmids used in this study.

Plasmid	Description	Reference
<i>P_{etef}</i> 05074_Cbx	Constitutive <i>P_{etef}</i> promotor, <i>cyp3</i> gene from <i>U. maydis</i> MB215, Cbx ^R	(Geiser et al., 2016c)
pUMa3479	FRTm2-NatR-FRTm2 cassette	Kerstin Schipper, Heinrich-Heine University Düsseldorf, Germany
pJET1.2/blunt	Ori Cole1, Amp ^R	Thermo Scientific, Germany
pUMa3414	FRTm7-NatR-FRTm7 cassette	Kerstin Schipper, Heinrich-Heine University Düsseldorf, Germany
<i>P_{etef}gfp</i> _G418	Constitutive <i>P_{etef}</i> promotor, <i>gfp</i> gene, G418 ^R	(Przybilla, Roxense BioSC)
<i>P_{etef}AT_mfsA</i> _Cbx	Constitutive <i>P_{etef}</i> promotor, dicodon-optimized version of <i>A. terreus</i> ATEG 09972 (<i>mfsA</i>), Cbx ^R	(Hosseinpour Tehrani et al., 2019a)
<i>P_{etef}cyp3</i> _Nat	Constitutive <i>P_{etef}</i> promotor, <i>cyp3</i> gene from <i>U. maydis</i> MB215, Nat ^R , FRTm2	this study
Δ <i>itp1</i> _G418	Deletion of the <i>itp1</i> gene in <i>U. cynodontis</i> 2-HP, G418 ^R , FRTm7	this study
Δ <i>itp1::mfsA</i> _G418	Exchange of the <i>itp1</i> gene in <i>U. cynodontis</i> 2-HP with the <i>mfsA</i> gene from <i>A. terreus</i> ATEG 09972, G418 ^R	this study

Determination of the *cyp3* gene copy number was performed via quantitative real-time PCR. After isolation of genomic DNA, concentrations were adjusted to 0.2 ng μ L⁻¹. For qPCR, 5 μ L of the diluted genomic DNA (corresponds to 1 ng) was mixed with 10 μ L 2x Luna Universal qPCR Master

Mix (New England BioLabs, Ipswich, MA, USA) and 1 μ L of each oligonucleotide (Table S5) and adjusted to a final volume of 20 μ L with ddH₂O. Measurements were performed in 96-well plates in the qTOWER 2.2 (Analytik Jena, Jena, Germany). For the determination of *cyp3* copy number, the relative concentration of the *cyp3* gene to two single-copy genes (*tad1* and *rdo1*) was calculated via 'Relative quantification method' of the qPCRsoft 3.1 software (Analytik Jena, Jena, Germany).

Funding

This project has received funding from the Bio-based Industries Joint Undertaking (JU) under the European Union's Horizon 2020 research and innovation program under grant agreement No 887711 for the project Glaukos. The JU receives support from the European Union's Horizon 2020 research and innovation program and the Bio-based Industries Consortium. This project was also funded by the Deutsche Forschungsgemeinschaft (DFG, German Research Foundation) – Project ID 458090666 / CRC1535/1.

Acknowledgements

We thank Prof. Dr. Martina Pohl, Heike Offermann and Lilia Arnold for support during the purification process. We thank Jasmin Wloka for support during the qNMR experiments. We thank Jochem Gätgens for GC-ToF-MS measurements and Dr.-Ing. Alexander Reiter for DS-FIA-MS/MS measurements. We thank Dr. Sabine Willbold and Daniela Gesekus for the elemental analysis. We thank all project partners for fruitful discussions.

Conflict of interest

The authors declare that they have no competing interests.

4. General discussion and perspectives

The world's growing population has led to a corresponding increase in global demand for energy and chemicals. As our economy continues to rely heavily on fossil raw materials, this has resulted in high levels of CO₂ emissions, which are a major contributor to the current climate crisis. To address this issue, a transition from the petrochemical-based industry towards a more sustainable one is necessary (cf. chapter 2.1). Microbial hosts, such as *Ustilago*, can produce platform chemicals like ITA from renewable resources. ITA is considered as a promising alternative to petrochemical-derived acrylic acid and methacrylic acid, and has the advantage of being rapidly degradable by engineered microbial hosts (de Witt et al., 2023; Teleky & Vodnar, 2019). However, its production cost is relatively high compared to its fossil-based counterparts, which limits its usage. To be competitive with the petrochemical-derived analogs, the cost of fermentative production must be significantly reduced. According to Werpy and Petersen (2004), the fermentation cost needs to be lower than 0.5 US\$ kg⁻¹, although the exact number will likely differ in the current economy. Costs can for instance be reduced by improving the microbial host to achieve higher yields, lowering downstream processing costs, and utilizing inexpensive, untreated feedstocks. The overall aim of this thesis is to address these challenges in order to make ITA production with *Ustilago* more economically feasible. In addition, this thesis focuses on the production of 2-HP and ITT, two chiral ITA downstream products in *Ustilago* of potentially higher value, which may serve as stepping stones towards establishing *Ustilago* as a biotechnological production host.

4.1. Itaconic acid hyper-producing *Ustilago* strains: Current limits and optimization approaches

For the model species *U. maydis*, two previously engineered ITA hyper-producing strains are described in literature (cf. chapter 2.3.2) (Becker et al., 2020; Hosseinpour Tehrani et al., 2019c). In order to further optimize ITA production, we consolidated the established modifications of both strains into one strain to stabilize the yeast-like morphology, to alleviate enzymatic bottlenecks and to reduce by-product formation at the same time (Becker et al., 2021). These modifications, especially the overexpression of *mttA*, had a major effect on growth of the final strain *U. maydis* K14, and also reduced the osmotolerance of this strain. However, investigation of ITA production with this strain under industrially relevant conditions in high and low cell-density fed-batch bioreactor experiments revealed no negative effect on the catalytic vigor of the strain, and osmotic stress could be avoided by reducing the glucose concentration with a

continuous feeding strategy. Under these conditions, we achieved ITA production from glucose at 100 % of the theoretical maximal yield during the production phase in a low cell-density fermentation. Since substrate cost is usually the main price-determining factor for commodity products, the high yield achieved in this work will significantly contribute to the establishment of an *Ustilago*-based industrial ITA production process. However, improving the economic feasibility does not just imply the optimization of individual parameters such as yield, but to find the optimum balance between all KPIs as well as to minimize additional main cost drivers such as base consumption and acid usage during fermentation and DSP, respectively (Saur et al., 2023). While *U. maydis*-based ITA production is dependent on pH values above pH 5.0, *U. cynodontis*, a second non-conventional natural ITA producer, is characterized by a high acid tolerance (Hosseinpour Tehrani et al., 2019d), thus making it a superior host for reducing costs associated with pH control reagents and saline waste co-production. *U. cynodontis* ITA MAX pH ($\Delta fuz7 \Delta cyp3 P_{etej}mttA P_{ria1}ria1$) has been previously engineered to higher production efficiencies without significantly affecting the fitness of the strain (Hosseinpour Tehrani et al., 2019b). Although almost identical KPIs were obtained for the deeply engineered strains *U. maydis* K14 and *U. cynodontis* ITA MAX pH using the continuous feeding strategy in low cell-density fed-batch fermentations (Table 13), base consumption was more than 5-fold reduced due to the lower pH value of 3.6 during the production phase in the *U. cynodontis* cultivations. Previous research has shown that *U. cynodontis* can produce ITA even at pH values below 3.6, which further reduces base consumption considering the pK_a values of ITA (3.84 and 5.55 at 20 °C), but also decreases the production yield. A techno-economic analysis based on a detailed characterization of the KPIs at different pH values identified pH 3.6 as the best trade-off between yield, titer, and productivity on the one hand, and base and acid use as well as associated salt waste co-production on the other hand.

Table 13: KPIs obtained during optimized continuous low cell-density fed-batch fermentations.

	<i>U. maydis</i> K14	<i>U. cynodontis</i> ITA MAX pH
Titer _{total} (g L ⁻¹)	75.7 ± 1.3	67.8 ± 0.7
Yield _{max} (g _{ITA} g _{GLC} ⁻¹)	0.72 ± 0.02	0.72 ± 0.01
Productivity _{total} (g L ⁻¹ h ⁻¹)	0.24 ± 0.00	0.22 ± 0.01
5 M NaOH (mL)	340 ± 4	61 ± 1
	(cf. chapter 3.1) (Becker et al., 2021)	(cf. chapter 3.2)

To potentially further reduce costs associated with pH adjusting agents and saline waste, NaOH could be replaced by $\text{Mg}(\text{OH})_2$ for pH control. During the subsequent DSP, acidification of the fermentation broth via HCl would lead to the formation of the co-salt MgCl_2 instead of NaCl, which can be thermally decomposed to recover HCl and $\text{Mg}(\text{OH})_2$ (De Haan et al., 2013; Saur et al., 2023). Thereby, this process would also significantly reduce saline waste co-production. However, an additional techno-economic assessment is needed to evaluate whether the reduction in saline waste can outweigh the higher energy demand for the thermal decomposition.

Despite years of process optimization, the volumetric productivity achieved with the current *Ustilago* strains are still far below the $2.5 \text{ g L}^{-1} \text{ h}^{-1}$, which is required to successfully compete with the petrochemical production (Werpy & Petersen, 2004). One possible solution to increase the productivity would be to shorten the overall process duration. This may be accomplished by changing the microbial production host towards a prokaryotic one, as they typically have shorter generation times and increased growth rates, thereby potentially increasing productivity. However, attempts for heterologous ITA production, e.g. in *E. coli* or *C. glutamicum* failed to compete with the titers and yields achieved with our *Ustilago* strains. This can most likely be traced back to the lack of compartmentalization in prokaryotic cells, which plays a key role for efficient ITA production (Diankristanti & Ng, 2023; Gopaliya et al., 2021). In the following, potential solutions to increase bioprocess efficiency with the natural ITA producing *Ustilago* strains are discussed.

Optimizing nutrient supply and uptake

A potential approach to improve productivity could rely on increasing the carbon uptake rate by metabolic engineering, assuming that an increased substrate uptake rate would result in an increased productivity while maintaining a similar yield. This could not only reduce the overall process time and therefore production cost, but could also be beneficial in reducing exposure time to elevated ITA titers in prolonged production environments. The success of such an approach was already demonstrated in lactate overproducing *S. cerevisiae*. Overproduction of the high-affinity hexose transporter Hxt7 and the transcriptional activator of the low-affinity hexose transporter Hxt1, either in combination or separately of each other, resulted in an increased glucose uptake as well as increased productivity (Kim et al., 2015). Although our knowledge about glucose uptake in *Ustilago* is still limited, the hexose transporter Hxt1 has already been identified as one of overall 19 putative hexose transporters. It is considered to be the major hexose transporter during yeast-like growth and shows high affinity for glucose, fructose and mannose (Schirawski, 2015; Schuler et al., 2015). However, whether its overproduction results in increased glucose uptake and especially in increased ITA production

rates needs to be determined. Liebal et al. (2022) revealed that the growth rate negatively correlates with extracellular glucose concentrations. More precisely, decreasing initial glucose availability leads to an increasing growth rate, substrate uptake rate and biomass yield per carbon with highest values achieved at 50 g L⁻¹. Currently, our fermentations typically start with at least 120 g L⁻¹ glucose. In this context, constitutive expression of the hexose transporter-encoding gene could be favorable under the assumption that increasing protein levels of the transporter would counteract reduced growth rates at elevated glucose concentrations. Besides engineering the host, one could also adjust process conditions during the growth phase by reducing initial glucose concentrations, combined with continuous glucose feeding strategy throughout the entire process to accelerate and increase biomass production and reduce osmotic stress.

Comparing process parameters in high and low cell-density fermentations exposed another dimension to fine-tune the balance between a high productivity and a high yield. As nitrogen is required for protein and DNA metabolism, the availability of nitrogen is the limiting factor for biomass accumulation and its depletion initiates the switch to ITA production (Klement et al., 2012; Maassen et al., 2014). In this context, variations in C/N ratio by adjusting initial nitrogen concentrations might be a further optimization strategy. However, first attempts in this regard have disproved this optimization approach by exposing an unintended reduction in yield (P. Ernst, unpublished). Our results also revealed a non-linear behavior between nitrogen availability and biomass concentration, as indicated by only a 2-fold increase in optical density and productivity at a 5-fold increased nitrogen concentration. This may hint at a potential secondary substrate limitation under high cell-density conditions (Becker et al., 2021) (cf. chapter 3.2). In order to increase biomass accumulation as well as cell fitness and thus productivity, the cultivation medium could be screened for limited compounds. Besides medium optimizations, Ullmann et al. reported an alternative approach to boost KPIs by co-utilizing glucose with the CO₂-derived substrate acetate and formate for *U. maydis* and *U. cynodontis* strains, respectively. This resulted in higher production titers and productivities, and may enable a carbon-neutral ITA production process (Ullmann et al., 2022b; Ullmann et al., 2021). However, it should be kept in mind that co-feeding of formate and its conversion to CO₂ via formate dehydrogenase reduces NAD⁺ to NADH (Ullmann et al., 2021), thereby contributing to a redox imbalance anyway occurring during ITA production as discussed in more detail in chapter 4.3.

Counteracting product inhibition

The ITA productivity is limited by product inhibition. As empirically determined, ITA levels above 80 g L⁻¹ completely inhibit ITA synthesis in the *U. maydis* wildtype (Klement et al., 2012). This is consistent with the presented fermentations of both, *U. maydis* and *U. cynodontis*, where ITA

production either remained below 80 g L^{-1} or was substantially reduced above this threshold. It is assumed that these observations are a result of increased weak acid stress impairing cell vigor (Hosseinpour Tehrani et al., 2019d). In order to improve productivity, product inhibition could be reduced by *in situ* product removal. ITA precipitation by addition of CaCO_3 was already performed during *U. maydis* fermentation, leading to an enormous increase in titer and productivity (Hosseinpour Tehrani et al., 2019c), which even exceeded the product titers obtained with *A. terreus* (Krull et al., 2017a). Nonetheless, a direct comparison of the yields obtained in high cell-density fed-batch fermentation of *U. maydis* K14 in the presence and absence of CaCO_3 revealed a reduction upon calcium ITA precipitation from 0.54 to $0.32 \text{ g}_{\text{ITA}} \text{ g}_{\text{GLC}}^{-1}$, presumably by interference of solids with oxygen supply due to wall adherence and poor mixing. However, this could possibly be counteracted by evolving *Ustilago* towards lower oxygen demands or by heterologous expression of hemoglobin from *Vitreoscilla*, the latter already suggested by Hosseinpour Tehrani (2019) as it was shown to mitigate sensitivity of *A. terreus*-based ITA production towards oxygen fluctuations (Lin et al., 2004). In addition, it could also be interesting to remove the solids by connecting centrifuges for continuous solids discharge to the bioreactor, assuming that these solids can be specifically separated from the biomass. Furthermore, Ca(OH)_2 could be tested as an alternative to CaCO_3 , allowing precipitation of ITA as calcium ITA without releasing CO_2 . However, a general drawback of this approach is that calcium ITA precipitates have to be dissolved with equimolar amounts of HCl (Zambanini et al., 2016a), increasing DSP steps and costs. Moreover, this *in situ* precipitation is not suitable for *U. cynodontis* fermentation processes at acidic pH due to the immediate dissociation of CaCO_3 and Ca(OH)_2 upon lower pH values. Pastoors et al. (2023) successfully proved *in situ* adsorption with activated carbon as an alternative, energy-efficient strategy for ITA recovery at acidic pH values. To this end, an adsorption column with activated carbon was integrated in an external loop. This led to a 1.6-fold increase in ITA titer and a 1.1-fold increase in productivity and yield during *U. cynodontis* ITA MAX pH fermentation when using four ITA separation cycles. Such product removal via adsorption does not just positively affect the production process itself, but also allows easy and cost-effective DSP. However, since the highest affinity to activated carbon was reported for the fully protonated form, this kind of *in situ* product removal is mainly advantageous for low pH fermentations as established for *U. cynodontis* ITA MAX pH. At higher pH values of around 6.0, mainly the fully dissociated form is present, which shows a lower adsorption affinity to activated carbon than glucose (Pastoors et al., 2023). In addition to *in situ* adsorption, reactive extraction represents an additional approach for ITA removal at low pH conditions. It has already been used in *A. terreus* fermentations and was found to increase the final product titer and thus the volumetric productivity. In this setup, ITA reacts with an organic extractant and is transferred to a

biocompatible organic phase that is not miscible with the aqueous phase (Kreyenschulte et al., 2018). In a continuous setting, reactive extraction can be performed in an external loop with prior biomass separation via filtration and nutrient recirculation (Eggert et al., 2019). The corresponding DSP was conducted by pH-controlled back extraction with NaOH and pH-shift crystallization with HCl. An alternative setup for a pH-reversible reactive extraction, which avoids the production of saline waste, involves a direct pH-shift water electrolysis. After the transfer of ITA into the organic phase at low pH, back extraction of ITA into the aqueous phase is induced by an electrochemical pH shift towards alkaline conditions, followed by acidification at the anode for ITA protonation and subsequent cooling crystallization. This concept has already been applied for ITA production with *U. cynodontis* ITA MAX pH after fermentation and has great potential for *in situ* product removal (Gausmann et al., 2021).

Another potential strategy towards circumventing process limitations via product inhibition is an adaptive laboratory evolution experiment of genetically engineered ITA hyper-producing strains towards increased weak acid tolerance, especially at low pH conditions used for *U. cynodontis* ITA MAX pH. This method has already been successfully employed to increase tolerance of *S. cerevisiae* to different organic acids such as L-malic acid or propionic acid (M. Li et al., 2023).

Diploidization of haploid cells

Another interesting approach to increase productivity could aim at the diploidization of haploid yeast cells. Such phenomenon was already systematically studied in *S. cerevisiae* (Harari et al., 2018). Whole-genome duplication, also called endoreduplication, could be triggered in long-term laboratory evolution experiments under different stress conditions, for example in KCl- or ethanol-containing medium. Experimentally, development of diploid cells was monitored by staining pretreated cells from the exponential phase with propidium iodide and analyzing the stain intensity of single cells via flow cytometry, which indicates the DNA amount per cell. Once endoduplicated, the DNA content was stable for hundreds of generations even in absence of the applied stressor. Interestingly, homozygous diploid cells showed faster growth and were able to outcompete their haploid progenitors in various, partly stressful, conditions (Harari et al., 2018). Based on these findings, it may be worth testing whether such stress-induced endoreduplication could also be triggered in *Ustilago*, potentially providing a fitness advantage in fermentation processes. This could allow a faster conversion of glucose to ITA, as well as a reduced sensitivity towards weak acid stress and elevated product titers. Generally, diploid cells of *U. maydis* have already been extensively studied decades ago. These studies showed that diploid, heterozygous cells (*a1a2b1b2*) can be obtained via plate mating, and that they exhibit filamentous, pathogenic growth under certain conditions (Holliday, 1961; Puhalla, 1968). Interestingly, UV irradiation of

these heterozygous diploids can induce mitotic crossing-over, resulting in diploid cells that are homozygous for the *a* or *b* locus, which exhibit more stable, yeast-like growth (Banuett & Herskowitz, 1989; Holliday, 1961, 2004; Kronstad & Leong, 1989). These cells were used to study the importance of *a* and *b* alleles for filamentous growth and pathogenicity (Banuett & Herskowitz, 1989; Kronstad & Leong, 1989), but have not yet been analyzed in the context of production capabilities.

4.2. Implementation of itaconic acid production in a circular bioeconomy concept

The long-term solution for a sustainable bioeconomy implies the use of feedstocks that do not compete with food production, unlike sugary and starchy first generation feedstocks (Figure 35) (Lips, 2022). While initial strain and process development is usually done with the conventional feedstock glucose, transferring this knowledge to alternative, low-cost feedstocks is an important step in reducing overall process costs and increasing sustainability. Around 1.3 billion tons of edible or inedible food waste are annually generated throughout the supply chain from farm to fork, which can contain high amounts of carbohydrates, proteins, lipids, among others (Mamma, 2020; Roy et al., 2023). Valorization of this waste is not just favorable to reduce its environmental impacts, but also represents an opportunity to integrate bio-based production into the circular economy without compromising food availability (Roy et al., 2023).

Recently, industrial starchy by-products have received a growing interest as second generation feedstock for production of value-added compounds (Galhano dos Santos et al., 2016) (Figure 35). In addition to the high abundance and relatively low-cost of starch, its polymeric structure reduces osmotic stress, which is typically caused by high levels of monomeric glucose. In this thesis, we conducted a proof-of-concept study for the usage of gelatinized starch as sole carbon source for ITA production with two engineered *Ustilago* strains. Interestingly, growth and ITA production could exclusively be observed for *U. cynodontis* ITA MAX pH. This was in line with the presence of glucoamylase and α -glucosidase enzymes in its secretome, which degrade starch to single glucose molecules (cf. chapter 3.3). The production efficiency was further optimized by constitutive expression of a α -amylase gene for starch liquefaction, which otherwise seemed silent during yeast-like growth. Accordingly, it is reasonable to assume, that the robustness of *Ustilago* to medium impurities and its hydrolytic potential could make a consolidated bioprocessing with liquefaction, saccharification and fermentation on more complex starchy waste such as potato peel waste feasible. Performance of *U. cynodontis* ITA MAX pH on starch could potentially be further optimized by elevating expression levels of the two detected

saccharification enzymes as well as constitutive overproduction of the genetically-encoded maltase. In case of *U. maydis*, all required enzymes for starch utilization are indeed encoded on the genome, but are not expressed under the tested conditions. However, it was confirmed that the addition of a commercially available α -amylase enables growth and ITA production on starch. In the future, this could be achieved more cost-effectively by activating production of the intrinsic α -amylase in *U. maydis*. ITA production from liquefied corn starch has also been reported for a genetically modified strain of *A. terreus*, which was generated by overproduction of a glucoamylase and exchanging the native signal peptide with a stronger one (Huang et al., 2014), the latter being worth testing in *Ustilago*. However, efficient ITA synthesis from starchy feedstocks like potato starch waste required prior hydrolysis and deionization due to the sensitivity of *A. terreus* to micronutrients like metal ions (Bafana et al., 2019), which is assumed to be expendable for *Ustilago*.

In addition to the metabolization of starch, the knowledge about cultivation and process conditions gained in this PhD thesis (cf. chapter 4.1) has been instrumental for enabling ITA production from other second generation feedstocks such as the low-cost, industrial side stream molasses from the regional sugar industry. While trace elements present in the molasses had to be removed for ITA production with *A. terreus* (Willke & Vorlop, 2001) and citrate production with *A. niger* in submerged fermentations (Shankaranand & Lonsane, 1994), such pretreatment was not necessary during ITA production with our *Ustilago* strains. Sucrose as the main constituent of molasses was successfully converted to ITA during fed-batch fermentation of the ITA hyper-producer *U. maydis* K14 with a yield of $0.38 \text{ g}_{\text{ITA}} \text{ g}_{\text{GLC}}^{-1}$, a productivity of $0.38 \text{ g L}^{-1} \text{ h}^{-1}$, and a final titer of 54.2 g L^{-1} (Helm et al., 2023). ITA production could be further improved through a dual feedstock strategy. By applying molasses in the batch phase and crude glycerol, a low-cost and abundant waste stream from biodiesel industry, during feeding, the productivity was increased 1.4-fold while the yield remained almost constant (Helm et al., 2024). *U. cynodontis* ITA MAX pH was also found to convert molasses to ITA, however with slightly reduced KPIs due to a lower extracellular invertase activity for hydrolysis of sucrose to glucose and fructose (Helm et al., 2023). Both *Ustilago* strains were also able to produce ITA from the sugar industry's side stream thick juice in an extended high cell-density batch fermentation at pH 6.5 with comparable substrate-to-product yields, but improved productivities compared to our glucose-based continuous high cell-density fed-batch fermentations (Niehoff et al., 2023; Saur et al., 2023). This interesting observation could be due to the presence of trace elements in the thick juice, which may be limited in the standard cultivation medium and indicate its optimization potential (cf. chapter 4.1).

The utilization of lignocellulosic biomass as second generation feedstock is generally more complex. It comprises forestry and non-edible agricultural residues (Figure 35) and represents the most abundant and globally distributed terrestrial biomass on earth. It mainly consists of cellulose, hemicellulose like xylan, and lignin. Its complete decomposition is naturally recalcitrant and requires a pretreatment to reduce the structural complexity and increase accessibility to a variety of different enzymes in order to obtain metabolizable monomers (Preethi et al., 2021; Zoghلامي & Paes, 2019). However, as phytopathogenic organisms, *Ustilago* species are genetically equipped with such hydrolytic enzymes as indicated by the detection of a putative exo- α -1,5-L-arabinofuranosidase and a putative aryl-alcohol oxidase in the secretome of yeast-like *U. cynodontis* ITA MAX pH (cf. chapter 3.3), although their expression is usually restricted to filamentous, pathogenic growth (Doehlemann et al., 2008). Geiser et al. (2016a) successfully demonstrated *Ustilago*'s ability to saccharify the main plant cell wall component cellulose and xylan to fermentable sugar by promotor exchanges, which activated enzyme production even during saprophytic growth. Similarly, degradation and further conversion of the main pectin component polygalacturonic acid was enabled by co-expression of intrinsic and foreign endo- and exoenzymes, respectively (Stoffels et al., 2020). Besides broadening the substrate range by homologous or also heterologous overexpression, co-cultivation with organisms specialized in hydrolysis of such alternative feedstocks was revealed as an alternative option for a consolidated bioprocess. While the fungus *Trichoderma reesei* as sophisticated producer of plant cell wall hydrolyzing enzymes was used for degrading cellulose to single glucose molecules, *U. maydis* could focus on conversion of glucose to ITA (Schlembach et al., 2020). Although the performance of *Ustilago* species on these more complex feedstocks is usually not yet comparable to that on pure glucose as carbon source, these initial studies can serve as a basis for further process optimization. A subsequent techno-economic assessment will determine whether the reduction in substrate cost as the main cost factor of bio-based bulk chemicals can outweigh the cost of the required lignocellulose pretreatment and the increased effort in product purification (Preethi et al., 2021).

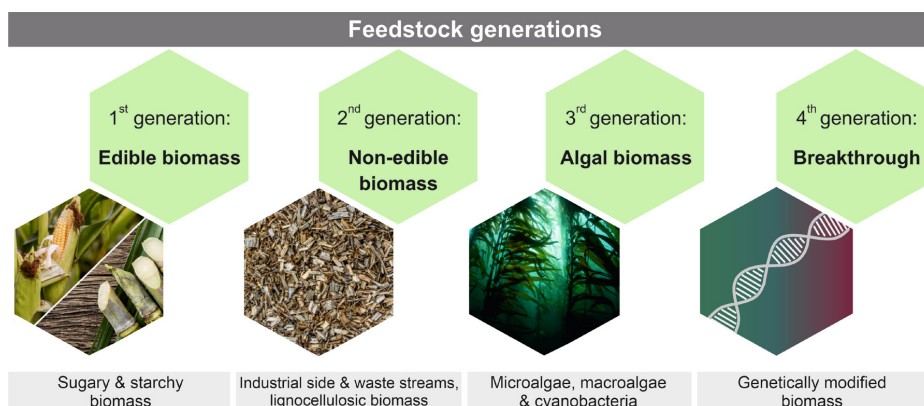


Figure 35: Overview of feedstock generations for bio-based production. Images of first to third generation feedstocks were taken from Lips (2022).

Facing the issues associated with the recalcitrance of lignocellulosic biomass and the removal of lignin, microalgae or cyanobacteria as third generation feedstock represents an emerging alternative (Figure 35). Besides their ability to grow on non-arable land and wastewater, their high biomass productivity and lignin-free cell walls, these photosynthetic microorganisms are able to convert CO₂, H₂O and sunlight into carbohydrates more efficiently than plants (Singh et al., 2019). This capacity is particularly important in light of the current climate crisis. Even if anthropogenic CO₂ emission can be completely eliminated, its atmospheric longevity will affect our climate for generations and highlights the need for additional measures in order to capture CO₂ from the atmosphere (Moreira & Pires, 2016). CO₂-derived, photosynthesized carbohydrates can either be incorporated into the microalgal cell wall, in the case of cellulose, hemicellulose and pectin, or accumulate intracellularly, mainly in the form of starch in microalgae or glycogen and sucrose in cyanobacteria (Levasseur et al., 2020). The general ability of *Ustilago* to hydrolyze the respective carbohydrates and convert the monomers to ITA was already discussed above. In addition, *U. maydis* encodes a variety of further enzymes like, for instance, lysozyme, lipases and proteases (Mueller et al., 2008). Accordingly, the use of algal extracts for *Ustilago*-based ITA synthesis is expected to allow simultaneous saccharification and fermentation in a net CO₂-reduced manner. Assuming that such process can eventually be carried out efficiently without prior pretreatment, co-cultivation approaches of phototrophic cyanobacteria or microalgae with heterotrophic *Ustilago* species might provide a promising long-term solution (ACCeSS project: Active Carbon Capture for Sustainable Synthesis, <https://www.access.hhu.de/>). However, although attractive from an environmental perspective, the development of large-scale cultivation platforms is costly and the use of third generation biomass has not yet been economically feasible. Genetic modifications of algae as fourth generation biomass, e.g. to

increase photosynthetic efficiency or to enable production of value-added compounds prior to its utilization as feedstock, may have the potential to overcome some of these issues, but come with its own technical challenges and legislative limitations due to environmental and health concerns (Abdullah et al., 2019; Kumar et al., 2020).

4.3. Production of value-added compounds beyond itaconic acid

In addition to expanding the substrate range, the ITA hyper-producing *U. cynodontis* ITA MAX pH strain was further engineered to produce additional compounds such as the two ITA downstream products 2-HP and ITT (2-HP: $pK_a = 2.78$; ITT: $pK_{a1} = 3.14$ and $pK_{a2} = 4.92$ at 20 °C) (Guevarra & Tabuchi, 1990b). The functional groups within 2-HP can be manipulated in various ways to produce a diverse range of high-value and novel chemicals (Brandt et al., 2017; Mori & Fukamatsu, 2010). Hence, these chemicals have potential applications in fields such as medicine, agriculture, and even quantum computing (Brandt et al., 2017). By overexpressing the ITA-oxidizing P450 monooxygenase *cyp3* in this strain, ITA was converted to its chiral lactone 2-HP (cf. chapter 3.4). The second product ITT is most likely the result of the hydrolysis of 2-HP, resulting from either enzymatic conversion by a putative 2-HP lactonase or abiotic conversion in aqueous solutions (Geiser et al., 2016b; Guevarra & Tabuchi, 1990a, 1990b).

Notably, despite the overexpression of *cyp3*, significant amounts of ITA accumulated during cultivation, suggesting Cyp3-mediated conversion as rate-limiting step. The qPCR on pre-selected clones showed a clear correlation between genomic *cyp3* copies and 2-HP synthesis. Consequently, it needs to be investigated if a further increase in copy numbers and/or expression levels by using a stronger promotor such as *P_{oma}* would allow a complete conversion of ITA. Interestingly, the initial screening for *cyp3* integration via colony PCR revealed positive results for several clones without any detectable conversion of ITA to 2-HP. This may be due to locus-dependent negative effects of the random genomic integration and potentially hint towards silent integration of single copies. This could be circumvented by newly establishing a targeted integration protocol for *U. cynodontis*. Besides limiting laborious screenings, this approach could potentially even further increase Cyp3-mediated 2-HP synthesis by elevating promotor activity and thus transcription levels, as it was shown in another context for targeted gene integration into the *ip*-locus of *U. maydis* (Schmitz et al., 2020). Alternatively, as demonstrated for *S. cerevisiae*, the introduction of synthetic DNA landing pads can enable targeted multi-copy gene integration in a single transformation with a tight control of gene copy number (Bourgeois et al., 2018). In contrast to constitutive expression of target genes, the Tet-on/Tet-off systems can be used for tunable gene expression and have already been established in *U. maydis* (Ingole et al.,

2022; Zarnack et al., 2006). The Tet-off system utilizes tetracycline to prevent the binding of a constitutively expressed Tet-responsive transactivator to its target promotor, thereby switching off transcription initiation of a GOI (Zarnack et al., 2006). Conversely, the Tet-on system employs a reverse Tet-responsive transactivator that can only bind to a Tet-responsive promotor and thus activate gene expression upon the addition of tetracycline (Ingole et al., 2022). Such a system could also be established in *U. cynodontis*, allowing the controlled expression of selected ITA and 2-HP biosynthetic genes upon transition from growth to production phase, thereby reducing for example growth defects during the initial biomass accumulation phase caused by constitutive *P_{eter}*-driven *mttA* overexpression (cf. chapter 3.1 and 3.4).

Interestingly, the yield of all *cyp3*-overexpressing strains was significantly lower when cultivations were scaled up from System Duetz or shake flask cultivations to bioreactor experiments. This could be conditioned by differences in the acidification. While the pH value during the production phase in bioreactors was controlled mostly at pH 2.8, the uncontrolled pH value during small-scale cultivations reached final values of around pH 2.1, which might be beneficial for 2-HP and ITT production. In order to rule out negative effects of the applied pH control on production parameters, follow-up studies should investigate the pH optimum for 2-HP and ITT producing strains, as it was already done for ITA production (Hosseinpour Tehrani et al., 2019d) (cf. chapter 3.2). Furthermore, it cannot be excluded that MES buffer used in small-scale cultivations positively influences ITA conversion via Cyp3. Such differences in production capabilities were already reported by Hosseinpour Tehrani et al. (2019b), when comparing different morphological mutant strains regarding organic acid production. During this screening, it also became apparent that a $\Delta ras2$ strain lacking another component of the same MAPK signaling cascade than Fuz7 achieved higher 2-HP titers. Accordingly, deleting *ras2* instead of *fuz7* in an optimized producer strain seemed to be a reasonable approach in the first place. Yet, it has to be noted that this strain showed filamentous growth on elevated glucose concentrations and glycerol (Hosseinpour Tehrani et al., 2019b), making the handling during bioprocessing more challenging.

Another important aspect for high-level production is an appropriate cofactor balancing. In case of ITA production, a surplus of NADH is generated through glycolysis and the TCA cycle (Hartmann et al., 2018), whose depletion is dependent on an electron acceptor. In *U. maydis*, ITA production is usually accompanied by production of malate (Hosseinpour Tehrani et al., 2019c), which is assumed to originate from the NADH-dependent reduction of oxaloacetate and contributes to cofactor regeneration (Zambanini et al., 2017b). In contrast, cultivations with *U. cynodontis* revealed lower malate production than *U. maydis* (Hosseinpour Tehrani et al., 2019b), thereby potentially having a higher activity of other regeneration paths. Besides the NADH-dependent

cytosolic malate dehydrogenase, the primary NAD⁺ regeneration during the ITA production phase in *Ustilago* is assumed to occur via the alternative electron transport chain consisting of an external NADH dehydrogenase (NDH-2) and an alternative oxidase (AOX). Unlike the regular mitochondrial respiratory chain, this alternative electron transport chain is not coupled to ATP synthesis (Juárez et al., 2004; Juárez et al., 2006). However, as pH homeostasis requires more ATP at low pH values due to increased weak acid stress (Kane, 2016), it may be beneficial for *U. cynodontis* to have an active regular electron transport chain during ITA production phase to generate this ATP from NADH. Consequently, there could be a dynamic system where the activity of the alternative electron transport chain NDH-2/AOX predominates in the initial production phase, potentially transitioning to the regular mitochondrial respiratory chain in response to increased weak acid stress at higher ITA concentrations. The exact mechanisms of cofactor regeneration could be investigated in follow-up studies to potentially further improve ITA production, and thus also 2-HP and ITT production. In the 2-HP overproducing *U. cynodontis* strain, the NAD⁺/NADH cofactor balancing is likely supported by the conversion of ITA to 2-HP via Cyp3, which is expected to utilize NAD(P)H as a specific cofactor (Geiser et al., 2016b). The simultaneous overexpression of a putative redox partner *cypOR* (cytochrome P450 oxidoreductase, UMAG_06273) did not significantly alter titers of 2-HP and ITT (data not shown). However, Cyp3 is reported to belong to the family of CYP504, which is known to be responsible for the oxidation of the plant growth hormone phenyl acetate in a NADPH-dependent manner (Mingot et al., 1999). Since oxidation of ITA to 2-HP is a rather unusual reaction for this P450 monooxygenase family, further studies are required to evaluate if conversion via Cyp3 is indeed dependent on a redox partner. If so, CypOR might not be the appropriate redox partner and additional ones should be screened in the future to potentially improve cofactor balancing and thus production. Nevertheless, it should be kept in mind that some monooxygenases can directly interact with NADH in absence of any redox partner or do not need NADH at all (Črešnar & Petrič, 2011; Lamb & Waterman, 2013), which could be elucidated by *in vitro* assays. Notably, 2-HP accumulation has also been observed in *A. terreus* (Guevarra & Tabuchi, 1990a), but its biosynthesis has not yet been sufficiently studied to draw any conclusions about 2-HP synthesis for *Ustilago*.

Currently, this limited knowledge hampers targeted optimizations in this direction and requires alternative measures to increase product specificity. To this end, the native ITA transporter *Itp1* was 1) eliminated and 2) substituted with the *A. terreus* ITA transporter *MfsA*, which is anticipated to exhibit a higher affinity for exporting 2-HP (Hosseinpour Tehrani et al., 2019a). Both modifications yielded an increased product specificity as they either completely abolished ($\Delta itp1$) or strongly reduced ITA accumulation ($\Delta itp1::mfsA$). Interestingly, the $\Delta itp1$ mutant strain of

U. maydis MB215 produced 0.7 ± 0.1 g L⁻¹ ITA (Hosseinpour Tehrani et al., 2019a), and even showed an increased 2-HP titer in ITA feeding experiments (Geiser et al., 2016b). This hints towards an alternative 2-HP transport mechanism in *U. maydis* under certain conditions, which is not present in *U. cynodontis*. The overall product titers and yields of the new transporter mutant strains of *U. cynodontis* were reduced compared to *cyp3* overexpressing progenitor strain, potentially due to feedback inhibition or triggered ITA degradation upon elevated intracellular product levels. The latter could be tackled by deleting the potential degradation pathway (cf. chapter 2.3.1). In addition to genetic engineering approaches, utilization of glycerol as alternative carbon source turned out to increase product specificity, probably due to an overall reduced metabolism on this non-preferred carbon source, and a direct conversion of ITA to 2-HP. Although this came at the expense of a lower productivity, the high product specificity obtained on this low-cost industrial waste stream will most likely be an important aspect for future 2-HP production processes.

Given the high product specificity obtained on glycerol, both products could be recovered with a purity of 85 % from the fermentation supernatants according to a protocol adapted from Guevarra and Tabuchi (1990b). The remaining impurities could be due to the co-extraction of other compounds from the fermentation broth via ethyl acetate. To enhance the purity, one could try to crystallize 2-HP from ethyl acetate by adding chloroform, a solvent that is miscible with ethyl acetate but does not dissolve 2-HP. Alternatively, additional solvents for extraction could be tested to increase 2-HP selectivity and solubility, as the latter seemed to be low during the extraction experiments. However, no appropriate solvent could be identified in a first screening. Moreover, removing pigments and colorants in the fermentation broth via prior nanofiltration did not improve the purity as evidenced by preliminary HPLC results. A cooling crystallization step prior to the lactonization did also not improved the purity (data not shown). Accordingly, follow-up studies could focus on the integration of additional purification techniques such as chromatography into the current DSP workflow.

4.4. Bioactivity of *Ustilago*-derived organic acids: An ecological perspective

Besides its relevance as a platform chemical for production of bio-based plastics and various other applications, ITA is a macrophage-produced immunometabolite and shows strong anti-bacterial properties by inhibiting the isocitrate lyase in the glyoxylate shunt (cf. chapter 2.2.1). However, several pathogenic bacteria have evolved resistance to ITA through its degradation and use as a sole carbon source (Martin et al., 1961; Sasikaran et al., 2014). This gives an indication for an ongoing evolutionary arms race between ITA-producing cells and ITA-degrading pathogenic

microorganisms such as *P. aeruginosa*. Whereas initial studies disproved production of 2-HP and ITT by LPS-activated macrophages (P. Ernst and D. Hiller, unpublished), production of the ITA derivatives 2-HP and ITT in *Ustilago* could be a strategy to compete with and combat resistant bacteria in the same ecological niche. To test this hypothesis, we supplemented supernatants from *U. cynodontis* 2-HP fermentations on glycerol containing a mixture of 2-HP and ITT to cultivations of *P. putida* KT2440 harboring an ITA-degrading cluster from *P. aeruginosa*. Indeed, this mixture was shown to interfere with the ITA degradation of this strain, and to inhibit growth on glucose and acetate. The anti-microbial effect is assumed to derive from 2-HP and was substantially more pronounced under acetate-metabolizing conditions. A similar growth inhibition has also been detected in the pathogenic yeast *Candida albicans* (de Witt et al., 2023).

Interestingly, growth phenotypes comparable to those of the ITA-degrading *P. putida* in the presence of 2-HP were observed for the *P. putida* KT2440 wildtype upon addition of ITA (de Witt et al., 2023). ITA is known to be a competitive inhibitor of the isocitrate lyase as key enzyme of the glyoxylate cycle required for acetate metabolization (McFadden & Purohit, 1977). Accordingly, results gained for growth-inhibiting activity of 2-HP might reflect a comparable point of attack. Considering the structural differences between ITA and 2-HP, a non-competitive inhibition of the isocitrate lyase by 2-HP could be assumed. Further C2 substrates like ethanol as carbon source could be tested in the future to confirm the hypothesis of an inhibited glyoxylate shunt. Moreover, to unravel the mechanism of action of 2-HP as a promising drug candidate, *in vitro* enzymes assays with the isocitrate lyase and 2-HP as potential inhibitor could be performed using ITA-mediated inhibition as positive control. In the same way, one could try to identify a possible enzymatic target in the inhibited ITA degradation pathway. Moreover, identification of suppressor mutants in an adaptive laboratory evolution experiment under 2-HP pressure might expose its bacterial or fungal interaction partners.

Another aspect to consider is that 2-HP is a chiral molecule. GC-ToF-MS analysis of the fermentation broth from *U. cynodontis* 2-HP already revealed the presence of two compounds with the same *m/z* ratio, but whether these indicate the presence of both enantiomers of 2-HP or a reaction intermediate is currently under investigation. According to previous reports, P450 monooxygenases are generally capable of producing both enantiomers (Tang et al., 2010), but contribution of a further, yet unknown enzyme cannot be excluded as well. Given the presence of two compounds with the identical *m/z* ratio, it remains to be clarified whether the anti-bacterial activity is associated with one or both enantiomers of 2-HP, or potentially with an intermediate compound. Interestingly, ITA-degrading *P. putida* KT2440 was already found to convert 2-HP to ITT in an enantioselective manner, whereas the other enantiomer remained in

the culture supernatant (de Witt et al., 2023). Although it was anticipated that conversion of 2-HP to ITT is mediated by the Rdo1 present in the ITA-degrading cluster, ongoing research with the respective *P. putida* KT2440 strain provided preliminary evidence that 2-HP can also be converted to ITT in absence of Rdo1. In line with that, deletion and overexpression of the *Ustilago*-derived Rdo1 in the *cyp3* overexpressing 2-HP producer strain did not significantly affect product distribution of 2-HP and ITT (data not shown). A complementary approach by purifying Rdo1 of *U. maydis* from *E. coli* showed no enzymatic conversion of purified 2-HP as well (data not shown). Accordingly, further investigations are required to analyze the enzymatic participation in ITT production.

5. Conclusion

This thesis focused on *Ustilago* as a biotechnological workhorse for the production of value-added compounds such as ITA, an important bio-based industrial building block and therapeutic agent (cf. chapter 2.2.1). Using a combinatorial approach of strain and process engineering, we have optimized ITA production with *U. maydis* K14 and *U. cynodontis* ITA MAX pH in terms of the substrate-to-product yield and the production pH (cf. chapter 3.1 and 3.2), thereby bringing *Ustilago*-based industrial ITA production closer to reality. In addition, we have opened up ITA production from the readily available and low-cost substrate starch (cf. chapter 3.3), which is expected to further improve economic viability of the ITA production process in the future. Finally, the production and purification of the two ITA downstream products 2-HP and ITT (cf. chapter 3.4) provides the basis for investigating these derivatives regarding their potential pharmaceutical applications, and serves as an important step towards establishing *Ustilago* as a biotechnological production host.

6. References

- Abdullah, B., Syed Muhammad, S. A. F. a., Shokravi, Z., Ismail, S., Kassim, K. A., Mahmood, A. N., & Aziz, M. M. A. (2019). Fourth generation biofuel: A review on risks and mitigation strategies. *Renew Sust Energy Rev*, 107, 37-50. <https://doi.org/10.1016/j.rser.2019.02.018>
- Aguilar, L. R., Pardo, J. P., Lomeli, M. M., Bocardo, O. I. L., Juarez Oropeza, M. A., & Guerra Sanchez, G. (2017). Lipid droplets accumulation and other biochemical changes induced in the fungal pathogen *Ustilago maydis* under nitrogen-starvation. *Arch Microbiol*, 199(8), 1195-1209. <https://doi.org/10.1007/s00203-017-1388-8>
- Altschul, S. F., Madden, T. L., Schäffer, A. A., Zhang, J., Zhang, Z., Miller, W., & Lipman, D. J. (1997). Gapped BLAST and PSI-BLAST: a new generation of protein database search programs. *Nucleic Acids Res*, 25(17), 3389-3402. <https://doi.org/10.1093/nar/25.17.3389>
- Bafana, R., & Pandey, R. A. (2018). New approaches for itaconic acid production: bottlenecks and possible remedies. *Crit Rev Biotechnol*, 38(1), 68-82. <https://doi.org/10.1080/07388551.2017.1312268>
- Bafana, R., Sivanesan, S., & Pandey, R. A. (2019). Optimization and scale up of itaconic acid production from potato starch waste in stirred tank bioreactor. *Biotechnology Progress*, 35(3), e2774. <https://doi.org/10.1002/btpr.2774>
- Bambouskova, M., Gorvel, L., Lampropoulou, V., Sergushichev, A., Loginicheva, E., Johnson, K., Korenfeld, D., Mathyer, M. E., Kim, H., Huang, L. H., Duncan, D., Bregman, H., Keskin, A., Santeford, A., Apte, R. S., Sehgal, R., Johnson, B., Amarasinghe, G. K., Soares, M. P., . . . Artyomov, M. N. (2018). Electrophilic properties of itaconate and derivatives regulate the I κ B ζ -ATF3 inflammatory axis. *Nature*, 556(7702), 501-504. <https://doi.org/10.1038/s41586-018-0052-z>
- Banuett, F. (1995). Genetics of *Ustilago maydis*, a fungal pathogen that induces tumors in maize. *Annu. Rev. Genet.*, 29(1), 179-208. <https://doi.org/10.1146/annurev.ge.29.120195.001143>
- Banuett, F., & Herskowitz, I. (1989). Different α alleles of *Ustilago maydis* are necessary for maintenance of filamentous growth but not for meiosis. *PNAS*, 86(15), 5878-5882. <https://doi.org/10.1073/pnas.86.15.5878>
- Banuett, F., & Herskowitz, I. (1994). Identification of Fuz7, a *Ustilago maydis* MEK/MAPKK homolog required for α -locus-dependent and-independent steps in the fungal life cycle. *Genes & Dev.*, 8, 1367-1378. <https://doi.org/10.1101/gad.8.12.1367>
- Baup, S. (1836). Ueber eine neue Pyrogen-Citronensäure, und über Benennung der Pyrogen-Säuren überhaupt. *Annalen der Pharmacie*, 19(1), 29-38. <https://doi.org/10.1002/jlac.18360190107>
- Becker (b. Loevenich), J. (2019). *Optimization of itaconic acid production by U. maydis through metabolic engineering & adaptive laboratory evolution*. RWTH Aachen, Doctoral Thesis. <https://publications.rwth-aachen.de/record/781564/files/781564.pdf>
- Becker, J., Hosseinpour Tehrani, H., Ernst, P., Blank, L. M., & Wierckx, N. (2021). An Optimized *Ustilago maydis* for Itaconic Acid Production at Maximal Theoretical Yield. *J Fungi (Basel)*, 7(1), 20. <https://doi.org/10.3390/jof7010020>
- Becker, J., Hosseinpour Tehrani, H., Gauert, M., Mampel, J., Blank, L. M., & Wierckx, N. (2020). An *Ustilago maydis* chassis for itaconic acid production without by-products. *Microb Biotechnol*, 13(2), 350-362. <https://doi.org/10.1111/1751-7915.13525>

- Becker, J., Liebal, U. W., Phan, A. N., Ullmann, L., & Blank, L. M. (2023). Renewable carbon sources to biochemicals and -fuels: contributions of the smut fungi Ustilaginaceae. *Curr Opin Biotechnol*, 79, 102849. <https://doi.org/10.1016/j.copbio.2022.102849>
- Bentley, R., & Thiessen, C. P. (1957). Biosynthesis of Itaconic Acid in *Aspergillus terreus*. I. Tracer studies with C^{14} -labeled substrates. *J Biol Chem*, 226(2), 673-687. [https://doi.org/10.1016/s0021-9258\(18\)70850-8](https://doi.org/10.1016/s0021-9258(18)70850-8)
- Biselli, A., Echtermeyer, A., Reifsteck, R., Materla, P., Mitsos, A., Viell, J., & Jupke, A. (2022). Investigation of the elution behavior of dissociating itaconic acid on a hydrophobic polymeric adsorbent using in-line Raman spectroscopy. *J Chromatogr A*, 1675, 463140. <https://doi.org/10.1016/j.chroma.2022.463140>
- Bölker, M. (2001). *Ustilago maydis* – a valuable model system for the study of fungal dimorphism and virulence. *Microbiol*, 147(6), 1395-4001. <https://doi.org/10.1099/00221287-147-6-1395>
- Bölker, M., Basse, C. W., & Schirawski, J. (2008). *Ustilago maydis* secondary metabolism-from genomics to biochemistry. *Fungal Genet Biol*, 45 Suppl 1, S88-93. <https://doi.org/10.1016/j.fgb.2008.05.007>
- Bonnarme, P., Gillet, B., Sepulchre, A. M., Role, C., Beloeil, J. C., & Ducrocq, C. (1995). Itaconate biosynthesis in *Aspergillus terreus*. *J Bacteriol*, 177(12), 3573-3578. <https://doi.org/10.1128/jb.177.12.3573-3578.1995>
- Bösch, K., Frantzeskakis, L., Vraneš, M., Kämper, J., Schipper, K., & Göhre, V. (2016). Genetic Manipulation of the Plant Pathogen *Ustilago maydis* to Study Fungal Biology and Plant Microbe Interactions. *J Vis Exp*(115), e54522. <https://doi.org/10.3791/54522>
- Bourgeois, L., Pyne, M. E., & Martin, V. J. J. (2018). A Highly Characterized Synthetic Landing Pad System for Precise Multicopy Gene Integration in Yeast. *ACS Synth Biol*, 7(11), 2675-2685. <https://doi.org/10.1021/acssynbio.8b00339>
- Bozell, J. J., & Petersen, G. R. (2010). Technology development for the production of biobased products from biorefinery carbohydrates—the US Department of Energy's "Top 10" revisited. *Green Chemistry*, 12(4), 539-554. <https://doi.org/10.1039/b922014c>
- Brachmann, A., König, J., Julius, C., & Feldbrügge, M. (2004). A reverse genetic approach for generating gene replacement mutants in *Ustilago maydis*. *Mol Genet Genomics*, 272(2), 216-226. <https://doi.org/10.1007/s00438-004-1047-z>
- Brandt, J. R., Salerno, F., & Fuchter, M. J. (2017). The added value of small-molecule chirality in technological applications. *Nat Rev Chem*, 1(6), 0045. <https://doi.org/10.1038/s41570-017-0045>
- Brefort, T., Doehlemann, G., Mendoza-Mendoza, A., Reissmann, S., Djamei, A., & Kahmann, R. (2009). *Ustilago maydis* as a Pathogen. *Annu Rev Phytopathol*, 47(1), 423-445. <https://doi.org/10.1146/annurev-phyto-080508-081923>
- Calam, C. T., Oxford, A. E., & Raistrick, H. (1939). Studies in the biochemistry of micro-organisms: Itaconic acid a metabolic product of a strain of *Aspergillus terreus* Thom. *Biochem J*, 33(9), 1488-1495. <https://doi.org/10.1042/bj0331488>
- Carapito, R., Imberty, A., Jeltsch, J. M., Byrns, S. C., Tam, P. H., Lowary, T. L., Varrot, A., & Phalip, V. (2009). Molecular basis of arabinobio-hydrolase activity in phytopathogenic fungi: crystal structure and catalytic mechanism of *Fusarium graminearum* GH93 exo- α -L-arabinanase. *J Biol Chem*, 284(18), 12285-12296. <https://doi.org/10.1074/jbc.M900439200>

- Celińska, E., Nicaud, J. M., & Bialas, W. (2021). Hydrolytic secretome engineering in *Yarrowia lipolytica* for consolidated bioprocessing on polysaccharide resources: review on starch, cellulose, xylan, and inulin. *Appl Microbiol Biotechnol*, 105(3), 975-989. <https://doi.org/10.1007/s00253-021-11097-1>
- Cervantes-Chávez, J. A., Valdés-Santiago, L., Bakkeren, G., Hurtado-Santiago, E., León-Ramírez, C. G., Esquivel-Naranjo, E. U., Landeros-Jaime, F., Rodríguez-Aza, Y., & Ruiz-Herrera, J. (2016). Trehalose is required for stress resistance and virulence of the Basidiomycota plant pathogen *Ustilago maydis*. *Microbiol.*, 162(6), 1009-1022. <https://doi.org/10.1099/mic.0.000287>
- Chen, M., Huang, X., Zhong, C., Li, J., & Lu, X. (2016). Identification of an itaconic acid degrading pathway in itaconic acid producing *Aspergillus terreus*. *Appl Microbiol Biotechnol*, 100(17), 7541-7548. <https://doi.org/10.1007/s00253-016-7554-0>
- Chen, Y., & Nielsen, J. (2016). Biobased organic acids production by metabolically engineered microorganisms. *Curr Opin Biotechnol*, 37, 165-172. <https://doi.org/10.1016/j.copbio.2015.11.004>
- Chiba, S. (1988). α -Glucosidases. In Amylase Research Society of Japan (Ed.), *Handbook of Amylases and Related Enzymes: Their Sources, Isolation Methods, Properties and Applications*. Pergamon Press, Oxford. <https://doi.org/10.1016/C2009-0-00364-X>
- Chiba, S. (1997). Molecular Mechanism in α -Glucosidase and Glucoamylase. *Biosci. Biotech. Biochem.*, 61(8), 1233-1239. <https://doi.org/10.1271/bbb.61.1233>
- Choi, H., Park, J., & Lee, J. (2022). Sustainable Bio-Based Superabsorbent Polymer: Poly(itaconic acid) with Superior Swelling Properties. *ACS Appl Polym Mater*, 4(6), 4098-4108. <https://doi.org/10.1021/acsapm.2c00021>
- Christensen, J. J. (1963). *Corn smut caused by Ustilago maydis*. American Phytopathological Society. <https://www.biodiversitylibrary.org/item/126222>
- Couturier, M., Mathieu, Y., Li, A., Navarro, D., Drula, E., Haon, M., Grisel, S., Ludwig, R., & Berrin, J. G. (2016). Characterization of a new aryl-alcohol oxidase secreted by the phytopathogenic fungus *Ustilago maydis*. *Appl Microbiol Biotechnol*, 100(2), 697-706. <https://doi.org/10.1007/s00253-015-7021-3>
- Couturier, M., Navarro, D., Olivé, C., Chevret, D., Haon, M., Favel, A., Lesage-Meessen, L., Henrissat, B., Coutinho, P. M., & Berrin, J.-G. (2012). Post-genomic analyses of fungal lignocellulosic biomass degradation reveal the unexpected potential of the plant pathogen *Ustilago maydis*. *BMC genomics*, 13, 57. Retrieved 2012/02//, from
- Črešnar, B., & Petrič, Š. (2011). Cytochrome P450 enzymes in the fungal kingdom. *Biochim Biophys Acta*, 1814(1), 29-35. <https://doi.org/10.1016/j.bbapap.2010.06.020>
- Cunha da Cruz, J., Machado de Castro, A., & Camporese Sérvulo, E. F. (2018). World market and biotechnological production of itaconic acid. *3 Biotech*, 8(3). <https://doi.org/10.1007/s13205-018-1151-0>
- de Witt, J., Ernst, P., Gätgens, J., Noack, S., Hiller, D., Wynands, B., & Wierckx, N. (2023). Characterization and engineering of branched short-chain dicarboxylate metabolism in *Pseudomonas* reveals resistance to fungal 2-hydroxyparaconate. *Metab Eng*, 75, 205-216. <https://doi.org/10.1016/j.ymben.2022.12.008>
- De Haan, André B., Van Breugel, J., van der Weide, P. L. J., Jansen, P. P., Vidal Lancis, J. M., & Cerdá Baró, A. (2013). *Recovery of carboxylic acid from their magnesium salts by precipitation using hydrochloric acid, useful for fermentation broth work-up* Patent No. WO2013025107A1. <https://patents.google.com/patent/WO2013025107A1/en>

- Diankristanti, P. A., & Ng, I. S. (2023). Microbial itaconic acid bioproduction towards sustainable development: Insights, challenges, and prospects. *Bioresour Technol*, 384, 129280. <https://doi.org/10.1016/j.biortech.2023.129280>
- Doehlemann, G., Wahl, R., Vranes, M., de Vries, R. P., Kämper, J., & Kahmann, R. (2008). Establishment of compatibility in the *Ustilago maydis*/maize pathosystem. *J Plant Physiol*, 165(1), 29-40. <https://doi.org/10.1016/j.jplph.2007.05.016>
- Drula, E., Garron, M. L., Dogan, S., Lombard, V., Henrissat, B., & Terrapon, N. (2022). The carbohydrate-active enzyme database: functions and literature. *Nucleic Acids Res*, 50(D1), D571-D577. <https://doi.org/10.1093/nar/gkab1045>
- Duchenne-Moutien, R. A., & Neetoo, H. (2021). Climate Change and Emerging Food Safety Issues: A Review. *J Food Prot*, 84(11), 1884-1897. <https://doi.org/10.4315/JFP-21-141>
- Duetz, W. A., Rüedi, L., Hermann, R., O'Connor, K., Büchs, J., & Witholt, B. (2000). Methods for intense aeration, growth, storage, and replication of bacterial strains in microtiter plates. *Appl. Environ. Microbiol*, 66(6), 2641-2646. <https://doi.org/10.1128/aem.66.6.2641-2646.2000>
- Ebrahimian, F., Denayer, J. F. M., & Karimi, K. (2022). Potato peel waste biorefinery for the sustainable production of biofuels, bioplastics, and biosorbents. *Bioresource Technology*, 360. <https://doi.org/10.1016/j.biortech.2022.127609>
- Eggert, A., Maßmann, T., Kreyenschulte, D., Becker, M., Heyman, B., Büchs, J., & Jupke, A. (2019). Integrated in-situ product removal process concept for itaconic acid by reactive extraction, pH-shift back extraction and purification by pH-shift crystallization. *Sep Purif Technol*, 215, 463-472. <https://doi.org/10.1016/j.seppur.2019.01.011>
- EIA (U.S. Energy Information Administration). (2023). *Consumption of primary fossil fuel energy in the United States from 1990 to 2022, by sector (in trillion British thermal units)*. Statista. Retrieved 07. February 2024 from <https://www.statista.com/statistics/244429/us-fossil-fuel-energy-consumption-by-sector/>
- European Commission. (2019). Communication from the Commission to the European Parliament, the European Council, the Council, the European Economic and Social Committee and the Committee of the Regions: The European green deal. *COM(2019) 640*. <https://eur-lex.europa.eu/legal-content/EN/TXT/?uri=CELEX%3A52019DC0640>
- Feldbrügge, M., Kämper, J., Steinberg, G., & Kahmann, R. (2004). Regulation of mating and pathogenic development in *Ustilago maydis*. *Curr Opin Microbiol*, 7(6), 666-672. <https://doi.org/10.1016/j.mib.2004.10.006>
- Feldbrügge, M., Kellner, R., & Schipper, K. (2013). The biotechnological use and potential of plant pathogenic smut fungi. *Appl Microbiol Biotechnol*, 97(8), 3253-3265. <https://doi.org/10.1007/s00253-013-4777-1>
- Gabrielli, P., Gazzani, M., & Mazzotti, M. (2020). The Role of Carbon Capture and Utilization, Carbon Capture and Storage, and Biomass to Enable a Net-Zero-CO₂ Emissions Chemical Industry. *Ind. Eng. Chem. Res*, 59(15), 7033-7045. <https://doi.org/10.1021/acs.iecr.9b06579>
- Gabrielli, P., Rosa, L., Gazzani, M., Meys, R., Bardow, A., Mazzotti, M., & Sansavini, G. (2023). Net-zero emissions chemical industry in a world of limited resources. *One Earth*, 6(6), 682-704. <https://doi.org/10.1016/j.oneear.2023.05.006>
- Galhano dos Santos, R., Ventura, P., Bordado, J. C., & Mateus, M. M. (2016). Valorizing potato peel waste: an overview of the latest publications. *Rev Environ Sci Biotechnol*, 15(4), 585-592. <https://doi.org/10.1007/s11157-016-9409-7>

- García-Guzmán, G., & Burdon, J. J. (1997). Impact of the Flower Smut *Ustilago cynodontis* (Ustilaginaceae) on the Performance of the Clonal Grass *Cynodon dactylon* (Gramineae). *Am. J. Bot.* 84(11), 1565-1571. <https://doi.org/10.2307/2446618>
- Gausmann, M., Kocks, C., Pastoors, J., Büchs, J., Wierckx, N., & Jupke, A. (2021). Electrochemical pH-T-Swing Separation of Itaconic Acid for Zero Salt Waste Downstream Processing. *ACS Sustain Chem Eng*, 9(28), 9336-9347. <https://doi.org/10.1021/acssuschemeng.1c02194>
- Geiser, E., Hosseinpour Tehrani, H., Meyer, S., Blank, L. M., & Wierckx, N. (2018). Evolutionary freedom in the regulation of the conserved itaconate cluster by Ria1 in related Ustilaginaceae. *Fungal Biol Biotechnol*, 5, 14. <https://doi.org/10.1186/s40694-018-0058-1>
- Geiser, E., Przybilla, S. K., Engel, M., Kleineberg, W., Büttner, L., Sarikaya, E., Hartog, T. d., Klankermayer, J., Leitner, W., Bölker, M., Blank, L. M., & Wierckx, N. (2016b). Genetic and biochemical insights into the itaconate pathway of *Ustilago maydis* enable enhanced production. *Metab Eng* 38, 427-435. <https://doi.org/10.1016/j.ymben.2016.10.006>
- Geiser, E., Przybilla, S. K., Friedrich, A., Buckel, W., Wierckx, N., Blank, L. M., & Bölker, M. (2016c). *Ustilago maydis* produces itaconic acid via the unusual intermediate *trans*-aconitate. *Microb Biotechnol*, 9(1), 116-126. <https://doi.org/10.1111/1751-7915.12329>
- Geiser, E., Reindl, M., Blank, L. M., Feldbrügge, M., Wierckx, N., & Schipper, K. (2016a). Activating Intrinsic Carbohydrate-Active Enzymes of the Smut Fungus *Ustilago maydis* for the Degradation of Plant Cell Wall Components. *Appl Environ Microbiol*, 82(17), 5174-5185. <https://doi.org/10.1128/AEM.00713-16>
- Geiser, E., Wiebach, V., Wierckx, N., & Blank, L. M. (2014). Prospecting the biodiversity of the fungal family Ustilaginaceae for the production of value-added chemicals. *Fungal Biol Biotechnol*, 1, 2. <https://doi.org/10.1186/s40694-014-0002-y>
- Geiser, E., Wierckx, N., Zimmerman, M., & Blank, L. M. (2013). Identification of an endo-1,4-beta-xylanase of *Ustilago maydis*. *BMC Biotechnol*, 13, 59. <https://doi.org/10.1186/1472-6750-13-59>
- Gerland, P., Hertog, S., Wheldon, M., Kantorova, V., Gu, D., Gonnella, G., Williams, I., Zeifman, L., Bay, G., Castanheira, H., Kamiya, Y., Bassarsky, L., Gaigbe-Togbe, V., & Spoorenberg, T. (2022). *World Population Prospects 2022: Summary of results*. <https://www.researchgate.net/publication/361944109>
- Gertz, E. M., Yu, Y.-K., Agarwala, R., Schäffer, A. A., & Altschul, S. F. (2006). Composition-based statistics and translated nucleotide searches: Improving the TBLASTN module of BLAST. *BMC Biology*, 4(1), 41. <https://doi.org/10.1186/1741-7007-4-41>
- Gibson, D. G., Young, L., Chuang, R. Y., Venter, J. C., Hutchison, C. A., 3rd, & Smith, H. O. (2009). Enzymatic assembly of DNA molecules up to several hundred kilobases. *Nat Methods*, 6(5), 343-345. <https://doi.org/10.1038/nmeth.1318>
- Glose, A., Chatterjee, B. S., & Das, A. (1990). Characterization of glucoamylase from *Aspergillus terreus* 4. *FEMS Microbiol Lett*, 66(1-3), 345-349. <https://doi.org/10.1111/j.1574-6968.1990.tb04024.x>
- Goldberg, I., & Rokem, J. S. (2009). Organic and Fatty Acid Production, Microbial. In M. Schaechter (Ed.), *Encyclopedia of Microbiology (Third Edition)* (pp. 421-442). Academic Press. <https://doi.org/10.1016/B978-012373944-5.00156-5>
- González, M., Álvarez-Blanco, S., Riera, F., & Alvarez, R. (2006). Purification of Lactic Acid from Fermentation Broths by Ion-Exchange Resins. *Ind. Eng. Chem. Res*, 45(9), 3243-3247. <https://doi.org/10.1021/ie051263a>

- Gopaliya, D., Kumar, V., & Khare, S. K. (2021). Recent advances in itaconic acid production from microbial cell factories. *Biocatal Agric Biotechnol*, 36, 102130. <https://doi.org/10.1016/j.bcab.2021.102130>
- Guevarra, E. D., & Tabuchi, T. (1990a). Accumulation of Itaconic, 2-Hydroxyparaconic, Itatartaric, and Malic Acids by Strains of the Genus *Ustilago*. *Agric biol chem*, 54(9), 2353-2358. <https://doi.org/10.1080/00021369.1990.10870333>
- Guevarra, E. D., & Tabuchi, T. (1990b). Production of 2-Hydroxyparaconic and Itatartaric Acids by *Ustilago cynodontis* and Simple Recovery Process of the Acids. *Agric biol chem*, 54(9), 2359-2365. <https://doi.org/10.1080/00021369.1990.10870334>
- Gyamerah, M. (1995). Factors affecting the growth form of *Aspergillus terreus* NRRL 1960 in relation to itaconic acid fermentation. *Appl Microbiol Biotechnol*, 44(3), 356-361. <https://doi.org/10.1007/BF00169929>
- Harari, Y., Ram, Y., Rappoport, N., Hadany, L., & Kupiec, M. (2018). Spontaneous Changes in Ploidy Are Common in Yeast. *Curr Biol*, 28(6), 825-835 e824. <https://doi.org/10.1016/j.cub.2018.01.062>
- Hartmann, S. K., Stockdreher, Y., Wandrey, G., Hosseinpour Tehrani, H., Zambanini, T., Meyer, A. J., Büchs, J., Blank, L. M., Schwarzlander, M., & Wierckx, N. (2018). Online in vivo monitoring of cytosolic NAD redox dynamics in *Ustilago maydis*. *Biochim Biophys Acta Bioenerg*, 1859(10), 1015-1024. <https://doi.org/10.1016/j.bbabi.2018.05.012>
- Hegde, K., Prabhu, A., Sarma, S. J., Brar, S. K., & Venkata Dasu, V. (2016). Chapter 10 - Potential Applications of Renewable Itaconic Acid for the Synthesis of 3-Methyltetrahydrofuran. In S. Kaur Brar, S. Jyoti Sarma, & K. Pakshirajan (Eds.), *Platform Chemical Biorefinery* (pp. 181-200). <https://doi.org/10.1016/b978-0-12-802980-0.00010-9>
- Helm, T., Niehoff, P. J., Gätgens, J., Stausberg, T., Pichler, B., Hassler, T., Wiechert, W., Büchs, J., Wierckx, N., & Noack, S. (2023). Introducing molasses as an alternative feedstock into itaconate production using *Ustilago* sp. *N Biotechnol*, 77, 30-39. <https://doi.org/10.1016/j.nbt.2023.06.003>
- Helm, T., Stausberg, T., Previati, M., Ernst, P., Klein, B., Busche, T., Kalinowski, J., Wibberg, D., Wiechert, W., Claerhout, L., Wierckx, N., & Noack, S. (2024). Itaconate Production from Crude Substrates with *U. maydis*: Scale-up of an Industrially Relevant Bioprocess. *Microb Cell Factories*, 23, 29. <https://doi.org/10.1186/s12934-024-02295-3>
- Hernandez-Ortega, A., Ferreira, P., & Martinez, A. T. (2012). Fungal aryl-alcohol oxidase: a peroxide-producing flavoenzyme involved in lignin degradation. *Appl Microbiol Biotechnol*, 93(4), 1395-1410. <https://doi.org/10.1007/s00253-011-3836-8>
- Hevekerl, A., Kuenz, A., & Vorlop, K.-D. (2014). Influence of the pH on the itaconic acid production with *Aspergillus terreus*. *Appl Microbiol Biotechnol*, 98(24), 10005-10012. <https://doi.org/10.1007/s00253-014-6047-2>
- Hewald, S., Josephs, K., & Bölker, M. (2005). Genetic Analysis of Biosurfactant Production in *Ustilago maydis*. *Appl. Environ. Microbiol*, 71(6), 3033-3040. <https://doi.org/10.1128/AEM.71.6.3033-3040.2005>
- Hewald, S., Linne, U., Scherer, M., Marahiel, M. A., Kämper, J., & Bölker, M. (2006). Identification of a gene cluster for biosynthesis of mannosylerythritol lipids in the basidiomycetous fungus *Ustilago maydis*. *Appl Environ Microbiol*, 72(8), 5469-5477. <https://doi.org/10.1128/AEM.00506-06>
- Hoffman, C. S., & Winston, F. (1987). A ten-minute DNA preparation from yeast efficiently releases autonomous plasmids for transformation of *Escherichia coli*. *Gene*, 57(2-3), 267-272. [https://doi.org/10.1016/0378-1119\(87\)90131-4](https://doi.org/10.1016/0378-1119(87)90131-4)

- Holliday, R. (1961). Induced mitotic crossing-over in *Ustilago maydis*. *Genetical Research*, 2(2), 231-248. <https://doi.org/10.1017/S0016672300000720>
- Holliday, R. (2004). Early studies on recombination and DNA repair in *Ustilago maydis*. *DNA Repair* 3(6), 671-682. <https://doi.org/10.1016/j.dnarep.2004.02.002>
- Holtz, A., Görtz, J., Kocks, C., Junker, M., & Jupke, A. (2021). Automated measurement of pH-dependent solid-liquid equilibria of itaconic acid and protocatechuic acid. *Fluid Phase Equilibria*, 532, 112893. <https://doi.org/10.1016/j.fluid.2020.112893>
- Hosseinpour Tehrani, H. (2019). *Engineering the morphology and metabolism of Ustilago to expand the process window for itaconic acid production*. RWTH Aachen, Doctoral Thesis. <https://publications.rwth-aachen.de/record/765515/files/765515.pdf>
- Hosseinpour Tehrani, H., Becker, J., Bator, I., Saur, K., Meyer, S., Rodrigues Loia, A. C., Blank, L. M., & Wierckx, N. (2019c). Integrated strain- and process design enable production of 220 g L⁻¹ itaconic acid with *Ustilago maydis*. *Biotechnol Biofuels Bioprod*, 12, 263. <https://doi.org/10.1186/s13068-019-1605-6>
- Hosseinpour Tehrani, H., Geiser, E., Engel, M., Hartmann, S. K., Hossain, A. H., Punt, P. J., Blank, L. M., & Wierckx, N. (2019a). The interplay between transport and metabolism in fungal itaconic acid production. *Fungal Genet Biol*, 125, 45-52. <https://doi.org/10.1016/j.fgb.2019.01.011>
- Hosseinpour Tehrani, H., Saur, K., Tharmasothirajan, A., Blank, L. M., & Wierckx, N. (2019d). Process engineering of pH tolerant *Ustilago cynodontis* for efficient itaconic acid production. *Microb Cell Factories*, 18(1), 213. <https://doi.org/10.1186/s12934-019-1266-y>
- Hosseinpour Tehrani, H., Tharmasothirajan, A., Track, E., Blank, L. M., & Wierckx, N. (2019b). Engineering the morphology and metabolism of pH tolerant *Ustilago cynodontis* for efficient itaconic acid production. *Metabolic engineering*, 54, 293-300. <https://doi.org/10.1016/j.ymben.2019.05.004>
- Huang, X., Chen, M., Lu, X., Li, Y., Li, X., & Li, J.-J. (2014). Direct production of itaconic acid from liquefied corn starch by genetically engineered *Aspergillus terreus*. *Microb Cell Factories*, 13, 108. <https://doi.org/10.1186/s12934-014-0108-1>
- Hünnefeld, M., Viets, U., Sharma, V., Wirtz, A., Hardy, A., & Frunzke, J. (2021). Genome Sequence of the Bacteriophage CL31 and Interaction with the Host Strain *Corynebacterium glutamicum* ATCC 13032. *Viruses*, 13(3), 495. <https://www.mdpi.com/1999-4915/13/3/495>
- Ingle, K. D., Nagarajan, N., Uhse, S., Giannini, C., & Djamei, A. (2022). Tetracycline-controlled (TetON) gene expression system for the smut fungus *Ustilago maydis*. *Front Fungal Biol*, 3, 1029114. <https://doi.org/10.3389/ffunb.2022.1029114>
- Jagadeesan, S., Govindaraju, I., & Mazumder, N. (2020). An Insight into the Ultrastructural and Physiochemical Characterization of Potato Starch: a Review. *Am J Potato Res*, 97(5), 464-476. <https://doi.org/10.1007/s12230-020-09798-w>
- Jaklitsch, W. M., Kubicek, C. P., & Scrutton, M. C. (1991). The subcellular organization of itaconate biosynthesis in *Aspergillus terreus*. *Microbiol*, 137(3), 533-539. <https://doi.org/10.1099/00221287-137-3-533>
- Janecek, S., Svensson, B., & MacGregor, E. A. (2003). Relation between domain evolution, specificity, and taxonomy of the α -amylase family members containing a C-terminal starch-binding domain. *Eur. J. Biochem.*, 270(4), 635-645. <https://doi.org/10.1046/j.1432-1033.2003.03404.x>

- Ji, H., Yang, H., Zhou, X., Sun, C., Li, L., Zhao, S., Yu, J., Li, S., Wang, R., & Zhang, L. (2023). Preparation of bio-based elastomer and its nanocomposites based on dimethyl itaconate with versatile properties. *Composites Part B: Engineering*, 248, 110383. <https://doi.org/10.1016/j.compositesb.2022.110383>
- Juárez, O., Guerra, G., Martínez, F., & Pardo, J. P. (2004). The mitochondrial respiratory chain of *Ustilago maydis*. *Biochim Biophys Acta*, 1658(3), 244-251. <https://doi.org/10.1016/j.bbabi.2004.06.005>
- Juárez, O., Guerra, G., Velázquez, I., Flores-Herrera, O., Rivera-Pérez, R. E., & Pardo, J. P. (2006). The physiologic role of alternative oxidase in *Ustilago maydis*. *FEBS J*, 273(20), 4603-4615. <https://doi.org/10.1111/j.1742-4658.2006.05463.x>
- Kahmann, R., & Kämper, J. (2004). *Ustilago maydis*: how its biology relates to pathogenic development. *New Phytol*, 164(1), 31-42. <https://doi.org/10.1111/j.1469-8137.2004.01156.x>
- Kahmann, R., Steinberg, G., Basse, C., Feldbrügge, M., & Kämper, J. (2000). *Ustilago maydis*, the Causative Agent of Corn Smut Disease. In J. W. Kronstad (Ed.), *Fungal Pathology* (pp. 347-371). Springer Netherlands. https://doi.org/10.1007/978-94-015-9546-9_12
- Kämper, J., Kahmann, R., Bölker, M., Ma, L. J., Brefort, T., Saville, B. J., Banuett, F., Kronstad, J. W., Gold, S. E., Müller, O., Perlin, M. H., Wösten, H. A., de Vries, R., Ruiz-Herrera, J., Reynaga-Pena, C. G., Sneltselaar, K., McCann, M., Perez-Martin, J., Feldbrügge, M., . . . Birren, B. W. (2006). Insights from the genome of the biotrophic fungal plant pathogen *Ustilago maydis*. *Nature*, 444(7115), 97-101. <https://doi.org/10.1038/nature05248>
- Kane, J. H., Finlay, A. C., & Amann, P. F. (1945). *Production of itaconic acid* (US Patent No. US2385283A). <https://patents.google.com/patent/US2385283A/en>
- Kane, P. M. (2016). Proton Transport and pH Control in Fungi. In J. Ramos, H. Sychrová, & M. Kschischo (Eds.), *Yeast Membrane Transport* (pp. 33-68). Springer International Publishing. https://doi.org/10.1007/978-3-319-25304-6_3
- Karaffa, L., Díaz, R., Papp, B., Fekete, E., Sándor, E., & Kubicek, C. P. (2015). A deficiency of manganese ions in the presence of high sugar concentrations is the critical parameter for achieving high yields of itaconic acid by *Aspergillus terreus*. *Appl Microbiol Biotechnol*, 99(19), 7937-7944. <https://doi.org/10.1007/s00253-015-6735-6>
- Karaffa, L., & Kubicek, C. P. (2019). Citric acid and itaconic acid accumulation: variations of the same story? *Appl Microbiol Biotechnol*, 103(7), 2889-2902. <https://doi.org/10.1007/s00253-018-09607-9>
- Khan, K., Zhang, J., Gul, F., & Li, T. (2022). The “carbon curse”: Understanding the relationship between resource abundance and emissions. *Extr Ind Soc*, 11, 101119. <https://doi.org/10.1016/j.exis.2022.101119>
- Khrunyk, Y., Munch, K., Schipper, K., Lupas, A. N., & Kahmann, R. (2010). The use of FLP-mediated recombination for the functional analysis of an effector gene family in the biotrophic smut fungus *Ustilago maydis*. *New Phytol*, 187(4), 957-968. <https://doi.org/10.1111/j.1469-8137.2010.03413.x>
- Kim, D., Song, J. Y., & Hahn, J. S. (2015). Improvement of glucose uptake rate and production of target chemicals by overexpressing hexose transporters and transcriptional activator Gcr1 in *Saccharomyces cerevisiae*. *Appl Environ Microbiol*, 81(24), 8392-8401. <https://doi.org/10.1128/AEM.02056-15>
- Kim, M. S., Chang, H., Zheng, L., Yan, Q., Pflieger, B. F., Klier, J., Nelson, K., Majumder, E. L. W., & Huber, G. W. (2023). A Review of Biodegradable Plastics: Chemistry, Applications,

- Properties, and Future Research Needs. *Chem Rev*, 123(16), 9915-9939. <https://doi.org/10.1021/acs.chemrev.2c00876>
- Kinoshita, K. (1931). Über eine neue *Aspergillus* Art, *A. itaconicus*. *Bot. Mag. Tokyo*, 45, 45-50.
- Kircher, M. (2021). Bioeconomy - present status and future needs of industrial value chains. *N Biotechnol*, 60, 96-104. <https://doi.org/10.1016/j.nbt.2020.09.005>
- Klement, T., & Büchs, J. (2013). Itaconic acid-a biotechnological process in change. *Bioresour Technol*, 135, 422-431. <https://doi.org/10.1016/j.biortech.2012.11.141>
- Klement, T., Milker, S., Jäger, G., Grande, P. M., Domínguez de María, P., & Büchs, J. (2012). Biomass pretreatment affects *Ustilago maydis* in producing itaconic acid. *Microb Cell Factories*, 11, 43. <https://doi.org/10.1186/1475-2859-11-43>
- Klose, J., de Sa, M. M., & Kronstad, J. W. (2004). Lipid-induced filamentous growth in *Ustilago maydis*. *Mol Microbiol*, 52(3), 823-835. <https://doi.org/10.1111/j.1365-2958.2004.04019.x>
- Kretschmer, M., Croll, D., & Kronstad, J. W. (2017). Maize susceptibility to *Ustilago maydis* is influenced by genetic and chemical perturbation of carbohydrate allocation. *Mol Plant Pathol*, 18(9), 1222-1237. <https://doi.org/10.1111/mpp.12486>
- Kreyenschulte, D., Heyman, B., Eggert, A., Maßmann, T., Kalvelage, C., Kossack, R., Regestein, L., Jupke, A., & Büchs, J. (2018). In situ reactive extraction of itaconic acid during fermentation of *Aspergillus terreus*. *Biochem Eng J*, 135, 133-141. <https://doi.org/10.1016/j.bej.2018.04.014>
- Kronstad, J. W., & Leong, S. A. (1989). Isolation of two alleles of the *b* locus of *Ustilago maydis*. *PNAS*, 86(3), 978-982. <https://doi.org/10.1073/pnas.86.3.978>
- Krull, S., Hevekerl, A., Kuenz, A., & Prusse, U. (2017a). Process development of itaconic acid production by a natural wild type strain of *Aspergillus terreus* to reach industrially relevant final titers. *Appl Microbiol Biotechnol*, 101(10), 4063-4072. <https://doi.org/10.1007/s00253-017-8192-x>
- Krull, S., Lünsmann, Prüße, U., & Kuenz, A. (2020). *Ustilago Rabenhorstiana*—An Alternative Natural Itaconic Acid Producer. *Fermentation*, 6(1), 4. <https://doi.org/10.3390/fermentation6010004>
- Kuenz, A., & Krull, S. (2018). Biotechnological production of itaconic acid-things you have to know. *Appl Microbiol Biotechnol*, 102(9), 3901-3914. <https://doi.org/10.1007/s00253-018-8895-7>
- Kühnel, S., Westphal, Y., Hinz, S. W., Schols, H. A., & Gruppen, H. (2011). Mode of action of *Chrysosporium lucknowense* C1 α -L-arabinohydrolases. *Bioresour Technol*, 102(2), 1636-1643. <https://doi.org/10.1016/j.biortech.2010.09.029>
- Kumar, G., Shekh, A., Jakhu, S., Sharma, Y., Kapoor, R., & Sharma, T. R. (2020). Bioengineering of Microalgae: Recent Advances, Perspectives, and Regulatory Challenges for Industrial Application [Review]. *Front Bioeng Biotechnol*, 8, 914. <https://doi.org/10.3389/fbioe.2020.00914>
- Kumar, J. A., Sathish, S., Prabu, D., Renita, A. A., Saravanan, A., Deivayanai, V. C., Anish, M., Jayaprabakar, J., Baigzenhenov, O., & Hosseini-Bandegharai, A. (2023). Agricultural waste biomass for sustainable bioenergy production: Feedstock, characterization and pre-treatment methodologies. *Chemosphere*, 331, 138680. <https://doi.org/10.1016/j.chemosphere.2023.138680>
- Kumar, P., & Satyanarayana, T. (2009). Microbial glucoamylases: characteristics and applications. *Crit Rev Biotechnol*, 29(3), 225-255. <https://doi.org/10.1080/07388550903136076>

- Lamb, D. C., & Waterman, M. R. (2013). Unusual properties of the cytochrome P450 superfamily. *Philos Trans R Soc B*, 368(1612), 20120434. <https://doi.org/10.1098/rstb.2012.0434>
- Lampropoulou, V., Sergushichev, A., Bambouskova, M., Nair, S., Vincent, E. E., Loginicheva, E., Cervantes-Barragan, L., Ma, X., Huang, S. C., Griss, T., Weinheimer, C. J., Khader, S., Randolph, G. J., Pearce, E. J., Jones, R. G., Diwan, A., Diamond, M. S., & Artyomov, M. N. (2016). Itaconate Links Inhibition of Succinate Dehydrogenase with Macrophage Metabolic Remodeling and Regulation of Inflammation. *Cell Metab*, 24(1), 158-166. <https://doi.org/10.1016/j.cmet.2016.06.004>
- Lavigne, R., Ceyssens, P.-J., & Robben, J. (2009). Phage Proteomics: Applications of Mass Spectrometry. In M. R. J. Clokie & A. M. Kropinski (Eds.), *Bacteriophages: Methods and Protocols, Volume 2 Molecular and Applied Aspects* (pp. 239-251). Humana Press. https://doi.org/10.1007/978-1-60327-565-1_14
- Lee, B.-H., Yan, L., Phillips, R. J., Reuhs, B. L., Jones, K., Rose, D. R., Nichols, B. L., Quezada-Calvillo, R., Yoo, S.-H., & Hamaker, B. R. (2013). Enzyme-Synthesized Highly Branched Maltodextrins Have Slow Glucose Generation at the Mucosal α -Glucosidase Level and Are Slowly Digestible In Vivo. *PLOS ONE*, 8(4), e59745. <https://doi.org/10.1371/journal.pone.0059745>
- Leong, H. Y., Chang, C. K., Khoo, K. S., Chew, K. W., Chia, S. R., Lim, J. W., Chang, J. S., & Show, P. L. (2021). Waste biorefinery towards a sustainable circular bioeconomy: a solution to global issues. *Biotechnol Biofuels Bioprod*, 14(1), 87. <https://doi.org/10.1186/s13068-021-01939-5>
- Levasseur, W., Perre, P., & Pozzobon, V. (2020). A review of high value-added molecules production by microalgae in light of the classification. *Biotechnol Adv*, 41, 107545. <https://doi.org/10.1016/j.biotechadv.2020.107545>
- Levi, P. G., & Cullen, J. M. (2018). Mapping Global Flows of Chemicals: From Fossil Fuel Feedstocks to Chemical Products. *Environ Sci Technol*, 52(4), 1725-1734. <https://doi.org/10.1021/acs.est.7b04573>
- Levinson, W. E., Kurtzman, C. P., & Kuo, T. M. (2006). Production of itaconic acid by *Pseudozyma antarctica* NRRL Y-7808 under nitrogen-limited growth conditions. *Enzyme Microb Technol*, 39(4), 824-827. <https://doi.org/10.1016/j.enzmictec.2006.01.005>
- Li, L., Ji, H., Yang, H., Zhang, L., Zhou, X., & Wang, R. (2020). Itaconate Based Elastomer as a Green Alternative to Styrene-Butadiene Rubber for Engineering Applications: Performance Comparison. *Processes*, 8(12), 1527. <https://doi.org/10.3390/pr8121527>
- Li, M., Chu, Y., Dong, X., & Ji, H. (2023). General mechanisms of weak acid-tolerance and current strategies for the development of tolerant yeasts. *World J Microbiol Biotechnol*, 40(2), 49. <https://doi.org/10.1007/s11274-023-03875-y>
- Li, Z., Zheng, W., Kong, W., & Zeng, T. (2023). Itaconate: A Potent Macrophage Immunomodulator. *Inflammation*, 46(4), 1177-1191. <https://doi.org/10.1007/s10753-023-01819-0>
- Liebal, U. W., Ullmann, L., Lieven, C., Kohl, P., Wibberg, D., Zambanini, T., & Blank, L. M. (2022). *Ustilago maydis* Metabolic Characterization and Growth Quantification with a Genome-Scale Metabolic Model. *J Fungi (Basel)*, 8(5), 524. <https://doi.org/10.3390/jof8050524>
- Lin, Y.-H., Li, Y.-F., Huang, M.-C., & Tsai, Y.-C. (2004). Intracellular expression of *Vitreoscilla* hemoglobin in *Aspergillus terreus* to alleviate the effect of a short break in aeration during culture. *Biotechnology Letters*, 26(13), 1067-1072. <https://doi.org/10.1023/B:BILE.0000032964.15178.7c>

- Liobikienė, G., & Miceikienė, A. (2023). Contribution of the European Bioeconomy Strategy to the Green Deal Policy: Challenges and Opportunities in Implementing These Policies. *Sustainability*, 15(9). <https://doi.org/10.3390/su15097139>
- Lips, D. (2022). Fuelling the future of sustainable sugar fermentation across generations. *Engineering Biology*, 6(1), 3-16. <https://doi.org/10.1049/enb2.12017>
- López-Garzón, C.S., & Straathof, A. J. J. (2014). Recovery of carboxylic acids produced by fermentation. *Biotechnol Adv*, 32(5), 873-904. <https://doi.org/10.1016/j.biotechadv.2014.04.002>
- Lovely, C. B., Aulakh, K. B., & Perlin, M. H. (2011). Role of Hsl7 in morphology and pathogenicity and its interaction with other signaling components in the plant pathogen *Ustilago maydis*. *Eukaryot Cell*, 10(7), 869-883. <https://doi.org/10.1128/EC.00237-10>
- Lovely, C. B., & Perlin, M. H. (2011). Cla4, but not Rac1, regulates the filamentous response of *Ustilago maydis* to low ammonium conditions. *Commun Integr Biol*, 4(6), 670-673. <https://doi.org/10.4161/cib.17063>
- Maassen, N., Panakova, M., Wierckx, N., Geiser, E., Zimmermann, M., Bölker, M., Kliner, U., & Blank, L. M. (2014). Influence of carbon and nitrogen concentration on itaconic acid production by the smut fungus *Ustilago maydis*. *Eng Life Sci*, 14(2), 129-134. <https://doi.org/10.1002/elsc.201300043>
- Magalhães, A. I., de Carvalho, J. C., Thoms, J. F., Medina, J. D. C., & Soccol, C. R. (2019). Techno-economic analysis of downstream processes in itaconic acid production from fermentation broth. *J Clean Prod*, 206, 336-348. <https://doi.org/10.1016/j.jclepro.2018.09.204>
- Mamma, D. (2020). Food Wastes: Feedstock for Value-Added Products. *Fermentation*, 6(2), 47. <https://doi.org/10.3390/fermentation6020047>
- Manjunath, P., Shenoy, B. C., & Raghavendra Rao, M. R. (1983). Fungal glucoamylases. *J Appl Biochem*, 5(4-5), 235-260. <http://europepmc.org/abstract/MED/6434506>
- Martin, W. R., Frigan, F., & Bergman, E. H. (1961). Noninductive metabolism of itaconic acid by *Pseudomonas* and *Salmonella* species. *J Bacteriol*, 82(6), 905-908. <https://doi.org/10.1128/jb.82.6.905-908.1961>
- Martinez-Espinoza, A. D., Ruiz-Herrera, J., León-Ramírez, C. G., & Gold, S. E. (2004). MAP Kinase and cAMP Signaling Pathways Modulate the pH-Induced Yeast-to-Mycelium Dimorphic Transition in the Corn Smut Fungus *Ustilago maydis*. *Curr Microbiol*, 49, 274-281. <https://doi.org/10.1007/s00284-004-4315-6>
- McFadden, B. A., & Purohit, S. (1977). Itaconate, an isocitrate lyase-directed inhibitor in *Pseudomonas indigofera*. *J Bacteriol*, 131(1), 136-144. <https://doi.org/10.1128/jb.131.1.136-144.1977>
- Michelucci, A., Cordes, T., Ghelfi, J., Pailot, A., Reiling, N., Goldmann, O., Binz, T., Wegner, A., Tallam, A., Rausell, A., Buttini, M., Linster, C. L., Medina, E., Balling, R., & Hiller, K. (2013). Immune-responsive gene 1 protein links metabolism to immunity by catalyzing itaconic acid production. *PNAS*, 110(19), 7820-7825. <https://doi.org/10.1073/pnas.1218599110>
- Miller, G. L. (1959). Use of Dinitrosalicylic Acid Reagent for Determination of Reducing Sugar. *Anal. Chem*, 31(3), 426-428. <https://doi.org/10.1021/ac60147a030>
- Mills, E. L., Ryan, D. G., Prag, H. A., Dikovskaya, D., Menon, D., Zaslona, Z., Jedrychowski, M. P., Costa, A. S. H., Higgins, M., Hams, E., Szpyt, J., Runtsch, M. C., King, M. S., McGouran, J. F., Fischer, R., Kessler, B. M., McGettrick, A. F., Hughes, M. M., Carroll, R. G., . . . O'Neill,

- L. A. (2018). Itaconate is an anti-inflammatory metabolite that activates Nrf2 via alkylation of KEAP1. *Nature*, 556(7699), 113-117. <https://doi.org/10.1038/nature25986>
- Mingot, J. M., Peñalva, M. A., & Fernández-Cañón, J. M. (1999). Disruption of *phacA*, an *Aspergillus nidulans* Gene Encoding a Novel Cytochrome P450 Monooxygenase Catalyzing Phenylacetate 2-Hydroxylation, Results in Penicillin Overproduction*. *J Biol Chem*, 274(21), 14545-14550. <https://doi.org/10.1074/jbc.274.21.14545>
- Moon, H. J., Jeya, M., Kim, I. W., & Lee, J. K. (2010). Biotechnological production of erythritol and its applications. *Appl Microbiol Biotechnol*, 86(4), 1017-1025. <https://doi.org/10.1007/s00253-010-2496-4>
- Moreira, D., & Pires, J. C. M. (2016). Atmospheric CO₂ capture by algae: Negative carbon dioxide emission path. *Bioresour Technol*, 215, 371-379. <https://doi.org/10.1016/j.biortech.2016.03.060>
- Mori, K., & Fukamatsu, K. (2010). ChemInform Abstract: Pheromone Synthesis. Part 144. A Synthesis of (1R,5S)-(+)-Frontalin from (S)-(-)-2-Hydroxyparaconic Acid. *ChemInform*, 24(12). <https://doi.org/10.1002/chin.199312267>
- Morita, T., Konishi, M., Fukuoka, T., Imura, T., & Kitamoto, D. (2008). Identification of *Ustilago cynodontis* as a New Producer of Glycolipid Biosurfactants, Mannosylerythritol Lipids, Based on Ribosomal DNA Sequences. *J Oleo Sci*, 57(10), 549-556. <https://doi.org/10.5650/jos.57.549>
- Mueller, O., Kahmann, R., Aguilar, G., Trejo-Aguilar, B., Wu, A., & de Vries, R. P. (2008). The secretome of the maize pathogen *Ustilago maydis*. *Fungal Genet Biol*, 45 Suppl 1, S63-70. <https://doi.org/10.1016/j.fgb.2008.03.012>
- Müller, M. J., Stachurski, S., Stoffels, P., Schipper, K., Feldbrügge, M., & Büchs, J. (2018). Online evaluation of the metabolic activity of *Ustilago maydis* on (poly)galacturonic acid. *J Biol Eng*, 12, 34. <https://doi.org/10.1186/s13036-018-0128-1>
- Murphy, C., Powlowski, J., Wu, M., Butler, G., & Tsang, A. (2011). Curation of characterized glycoside hydrolases of Fungal origin. *Database*, 2011, bar020. <https://doi.org/10.1093/database/bar020>
- Nascimento, M. F., Marques, N., Correia, J., Faria, N. T., Mira, N. P., & Ferreira, F. C. (2022). Integrated perspective on microbe-based production of itaconic acid: From metabolic and strain engineering to upstream and downstream strategies. *Process Biochemistry*, 117, 53-67. <https://doi.org/10.1016/j.procbio.2022.03.020>
- Niehoff, P. J., Müller, W., Pastoors, J., Miebach, K., Ernst, P., Hemmerich, J., Noack, S., Wierckx, N., & Büchs, J. (2023). Development of an itaconic acid production process with Ustilaginaceae on alternative feedstocks. *BMC Biotechnol*, 23(1), 34. <https://doi.org/10.1186/s12896-023-00802-9>
- O'Neill, L. A. J., & Artyomov, M. N. (2019). Itaconate: the poster child of metabolic reprogramming in macrophage function. *Nat Rev Immunol*, 19(5), 273-281. <https://doi.org/10.1038/s41577-019-0128-5>
- Ogundero, V. W., & Osunlaja, S. O. (1986). Glucoamylase production and activity by *Aspergillus clavatus* Des., a toxigenic fungus from malting barley. *Mycopathologia*, 96(3), 153-156. <https://doi.org/10.1007/BF00437381>
- Okabe, M., Lies, D., Kanamasa, S., & Park, E. Y. (2009). Biotechnological production of itaconic acid and its biosynthesis in *Aspergillus terreus*. *Appl Microbiol Biotechnol*, 84(4), 597-606. <https://doi.org/10.1007/s00253-009-2132-3>

- Okuyama, M., Saburi, W., Mori, H., & Kimura, A. (2016). α -Glucosidases and α -1,4-glucan lyases: structures, functions, and physiological actions. *Cell Mol Life Sci*, 73(14), 2727-2751. <https://doi.org/10.1007/s00018-016-2247-5>
- Olagnier, D., Farahani, E., Thyrsted, J., Blay-Cadanet, J., Herengt, A., Idorn, M., Hait, A., Hernaez, B., Knudsen, A., Iversen, M. B., Schilling, M., Jorgensen, S. E., Thomsen, M., Reinert, L. S., Lappe, M., Hoang, H. D., Gilchrist, V. H., Hansen, A. L., Ottosen, R., . . . Holm, C. K. (2020). SARS-CoV2-mediated suppression of NRF2-signaling reveals potent antiviral and anti-inflammatory activity of 4-octyl-itaconate and dimethyl fumarate. *Nat Commun*, 11(1), 4938. <https://doi.org/10.1038/s41467-020-18764-3>
- Olicón-Hernández, D. R., Araiza-Villanueva, M. G., Pardo, J. P., Aranda, E., & Guerra-Sánchez, G. (2019). New Insights of *Ustilago maydis* as Yeast Model for Genetic and Biotechnological Research: A Review. *Curr Microbiol*, 76(8), 917-926. <https://doi.org/10.1007/s00284-019-01629-4>
- Ortíz-de-Lira, A., Reynel-Ávila, H. E., Díaz-Muñoz, L. L., Mendoza-Castillo, D. I., Aminabhavi, T. M., Badawi, M., & Bonilla-Petriciolet, A. (2022). Sustainable Downstream Separation of Itaconic Acid Using Carbon-Based Adsorbents. *Adsorp Sci Technol* 2022, 7333005. <https://doi.org/10.1155/2022/7333005>
- Paczia, N., Nilgen, A., Lehmann, T., Gätgens, J., Wiechert, W., & Noack, S. (2012). Extensive exometabolome analysis reveals extended overflow metabolism in various microorganisms. *Microb Cell Factories*, 11, 122. <https://doi.org/10.1186/1475-2859-11-122>
- Pandey, A., Nigam, P., Soccol, C. R., Soccol, V. T., Singh, D., & Mohan, R. (2000). Advances in microbial amylases. *Biotechnol Appl Biochem*, 31(2), 135-152. <https://doi.org/10.1042/ba19990073>
- Pastors, J., Deitert, A., Michel, C., Gunster, K., Finger, M., Hofstede, J., Deischter, J., Biselli, A., Viell, J., Palkovits, R., Jupke, A., & Büchs, J. (2023). In situ adsorption of itaconic acid from fermentations of *Ustilago cynodontis* improves bioprocess efficiency. *Biotechnol Biofuels Bioprod*, 16(1), 181. <https://doi.org/10.1186/s13068-023-02433-w>
- Paulino, B. N., Pessoa, M. G., Molina, G., Kaupert Neto, A. A., Oliveira, J. V. C., Mano, M. C. R., & Pastore, G. M. (2017). Biotechnological production of value-added compounds by ustilaginomycetous yeasts. *Appl Microbiol Biotechnol*, 101(21), 7789-7809. <https://doi.org/10.1007/s00253-017-8516-x>
- Peace, C. G., & O'Neill, L. A. (2022). The role of itaconate in host defense and inflammation. *J Clin Invest*, 132(2), e148548. <https://doi.org/10.1172/JCI148548>
- Pfaffl, M. W. (2001). A new mathematical model for relative quantification in real-time RT-PCR. *Nucleic Acids Res*, 29(9), e45. <https://doi.org/10.1093/nar/29.9.e45>
- Philp, J. (2023). Bioeconomy and net-zero carbon: lessons from Trends in Biotechnology, volume 1, issue 1. *Trends Biotechnol*, 41(3), 307-322. <https://doi.org/10.1016/j.tibtech.2022.09.016>
- Preethi, M. G., Kumar, G., Karthikeyan, O. P., Varjani, S., & J, R. B. (2021). Lignocellulosic biomass as an optimistic feedstock for the production of biofuels as valuable energy source: Techno-economic analysis, Environmental Impact Analysis, Breakthrough and Perspectives. *Environ Technol Innov*, 24, 102080. <https://doi.org/10.1016/j.eti.2021.102080>
- Puhalla, J. E. (1968). Compatibility reactions on solid medium and interstrain inhibition in *Ustilago maydis*. *Genetics*, 60(3), 461-474. <https://doi.org/10.1093/genetics/60.3.461>

- Rappsilber, J., Mann, M., & Ishihama, Y. (2007). Protocol for micro-purification, enrichment, pre-fractionation and storage of peptides for proteomics using StageTips. *Nat Protoc*, 2(8), 1896-1906. <https://doi.org/10.1038/nprot.2007.261>
- Regestein, L., Klement, T., Grande, P., Kreyenschulte, D., Heyman, B., Massmann, T., Eggert, A., Sengpiel, R., Wang, Y., Wierckx, N., Blank, L. M., Spiess, A., Leitner, W., Bolm, C., Wessling, M., Jupke, A., Rosenbaum, M., & Büchs, J. (2018). From beech wood to itaconic acid: case study on biorefinery process integration. *Biotechnol Biofuels Bioprod*, 11, 279. <https://doi.org/10.1186/s13068-018-1273-y>
- Reiter, A., Asgari, J., Wiechert, W., & Oldiges, M. (2022). Metabolic Footprinting of Microbial Systems Based on Comprehensive In Silico Predictions of MS/MS Relevant Data. *Metabolites*, 12(3), 257. <https://doi.org/10.3390/metabo12030257>
- Ribó-Molina, P., Weiss, H., Susma, B., van Nieuwkoop, S., Persoons, L., Zheng, Y., Ruzek, M., Daelemans, D., Fouchier, R. A. M., O'Neill, L. A. J., & van den Hoogen, B. G. (2023). 4-Octyl itaconate reduces influenza A replication by targeting the nuclear export protein CRM1. *J Virol*, 97(10), e0132523. <https://doi.org/10.1128/jvi.01325-23>
- Rissman, J., Bataille, C., Masanet, E., Aden, N., Morrow, W. R., Zhou, N., Elliott, N., Dell, R., Heeren, N., Huckestein, B., Cresko, J., Miller, S. A., Roy, J., Fennell, P., Cremmins, B., Koch Blank, T., Hone, D., Williams, E. D., de la Rue du Can, S., . . . Helseth, J. (2020). Technologies and policies to decarbonize global industry: Review and assessment of mitigation drivers through 2070. *Applied Energy*, 266, 114848. <https://doi.org/10.1016/j.apenergy.2020.114848>
- Roa Engel, C. A., van Gulik, W. M., Marang, L., van der Wielen, L. A. M., & Straathof, A. J. J. (2011). Development of a low pH fermentation strategy for fumaric acid production by *Rhizopus oryzae*. *Enzyme Microb Technol*, 48(1), 39-47. <https://doi.org/10.1016/j.enzmictec.2010.09.001>
- Robertson, G. H., Wong, D. W. S., Lee, C. C., Wagschal, K., Smith, M. R., & Orts, W. J. (2006). Native or Raw Starch Digestion: A Key Step in Energy Efficient Biorefining of Grain. *J Agric Food Chem*, 54(2), 353-365. <https://doi.org/10.1021/jf051883m>
- Rodríguez-Martínez, B., Coelho, E., Gullón, B., Yáñez, R., & Domingues, L. (2023). Potato peels waste as a sustainable source for biotechnological production of biofuels: Process optimization. *Waste Manag*, 155, 320-328. <https://doi.org/10.1016/j.wasman.2022.11.007>
- Roy, P., Mohanty, A. K., Dick, P., & Misra, M. (2023). A Review on the Challenges and Choices for Food Waste Valorization: Environmental and Economic Impacts. *ACS Environ Au*, 3(2), 58-75. <https://doi.org/10.1021/acsenvironau.2c00050>
- Rychtera, M., & Wase, D. A. J. (2007). The growth of *Aspergillus terreus* and the production of itaconic acid in batch and continuous cultures. The influence of pH. *J Chem Technol Biotechnol*, 31(1), 509-521. <https://doi.org/10.1002/jctb.503310168>
- Sakamoto, T., Ihara, H., Shibano, A., Kasai, N., Inui, H., & Kawasaki, H. (2004). Molecular characterization of a *Penicillium chrysogenum* exo-1,5- α -L-arabinanase that is structurally distinct from other arabinan-degrading enzymes. *FEBS Letters*, 560(1-3), 199-204. [https://doi.org/10.1016/s0014-5793\(04\)00106-1](https://doi.org/10.1016/s0014-5793(04)00106-1)
- Salmerón-Santiago, K. G., Pardo, J. P., Flores-Herrera, O., Mendoza-Hernández, G., Miranda-Arango, M., & Guerra-Sánchez, G. (2011). Response to osmotic stress and temperature of the fungus *Ustilago maydis*. *Arch. Microbiol.*, 193(10), 701-709. <https://doi.org/10.1007/s00203-011-0706-9>

- Sambrook, J., & Russell, D. W. (2006). Preparation and Transformation of Competent *E. coli* Using Calcium Chloride. *CSH Protoc*, 2006(1). <https://doi.org/10.1101/pdb.prot3932>
- Sasikaran, J., Ziemski, M., Zadora, P. K., Fleig, A., & Berg, I. A. (2014). Bacterial itaconate degradation promotes pathogenicity. *Nat Chem Biol*, 10(5), 371-377. <https://doi.org/10.1038/nchembio.1482>
- Saur, K. M., Kiefel, R., Niehoff, P. J., Hofstede, J., Ernst, P., Brockkötter, J., Gätgens, J., Viell, J., Noack, S., Wierckx, N., Büchs, J., & Jupke, A. (2023). Holistic Approach to Process Design and Scale-Up for Itaconic Acid Production from Crude Substrates. *Bioengineering (Basel)*, 10(6), 723. <https://doi.org/10.3390/bioengineering10060723>
- Saville, B., Donaldson, M., & Doyle, C. (2012). Investigating Host Induced Meiosis in a Fungal Plant Pathogen. In *Meiosis - Molecular Mechanisms and Cytogenetic Diversity*. <https://doi.org/10.5772/30032>
- Scarcia, P., Gorgoglione, R., Messina, E., Fiermonte, G., Blank, L. M., Wierckx, N., Palmieri, L., & Agrimi, G. (2020). Mitochondrial carriers of *Ustilago maydis* and *Aspergillus terreus* involved in itaconate production: same physiological role but different biochemical features. *FEBS Lett*, 594(4), 728-739. <https://doi.org/10.1002/1873-3468.13645>
- Schirawski, J. (2015). Invasion is sweet. *New Phytol*, 206(3), 892-894. <https://doi.org/10.1111/nph.13397>
- Schlembach, I., Hosseinpour Tehrani, H., Blank, L. M., Büchs, J., Wierckx, N., Regestein, L., & Rosenbaum, M. A. (2020). Consolidated bioprocessing of cellulose to itaconic acid by a co-culture of *Trichoderma reesei* and *Ustilago maydis*. *Biotechnol Biofuels Bioprod*, 13(1), 207. <https://doi.org/10.1186/s13068-020-01835-4>
- Schmitz, L., Kronstad, J. W., & Heimel, K. (2020). Conditional gene expression reveals stage-specific functions of the unfolded protein response in the *Ustilago maydis*-maize pathosystem. *Mol Plant Pathol*, 21(2), 258-271. <https://doi.org/10.1111/mpp.12893>
- Schuler, D., Wahl, R., Wippel, K., Vranes, M., Munsterkotter, M., Sauer, N., & Kämper, J. (2015). Hxt1, a monosaccharide transporter and sensor required for virulence of the maize pathogen *Ustilago maydis*. *New Phytol*, 206(3), 1086-1100. <https://doi.org/10.1111/nph.13314>
- Shankaranand, V. S., & Lonsane, B. K. (1994). Ability of *Aspergillus niger* to tolerate metal ions and minerals in a solid-state fermentation system for the production of citric acid. *Process Biochemistry*, 29(1), 29-37. [https://doi.org/10.1016/0032-9592\(94\)80056-1](https://doi.org/10.1016/0032-9592(94)80056-1)
- Shi, X., Zhou, H., Wei, J., Mo, W., Li, Q., & Lv, X. (2022). The signaling pathways and therapeutic potential of itaconate to alleviate inflammation and oxidative stress in inflammatory diseases. *Redox Biol*, 58, 102553. <https://doi.org/10.1016/j.redox.2022.102553>
- Singh, A., Prajapati, P., Vyas, S., Gaur, V. K., Sindhu, R., Binod, P., Kumar, V., Singhania, R. R., Awasthi, M. K., Zhang, Z., & Varjani, S. (2022). A Comprehensive Review of Feedstocks as Sustainable Substrates for Next-Generation Biofuels. *BioEnergy Research*, 16(1), 105-122. <https://doi.org/10.1007/s12155-022-10440-2>
- Singh, H., Varanasi, J. L., Banerjee, S., & Das, D. (2019). Production of carbohydrate enrich microalgal biomass as a bioenergy feedstock. *Energy*, 188, 116039. <https://doi.org/10.1016/j.energy.2019.116039>
- Sohail, A., Iqbal, A. A., Sahini, N., Chen, F., Tantawy, M., Waqas, S. F. H., Winterhoff, M., Ebensen, T., Schultz, K., Geffers, R., Schughart, K., Preusse, M., Shehata, M., Bahre, H., Pils, M. C., Guzman, C. A., Mostafa, A., Pleschka, S., Falk, C., . . . Pessler, F. (2022). Itaconate and

- derivatives reduce interferon responses and inflammation in influenza A virus infection. *PLoS Pathog*, 18(1), e1010219. <https://doi.org/10.1371/journal.ppat.1010219>
- Sollka, L., & Lienkamp, K. (2021). Progress in the Free and Controlled Radical Homo- and Copolymerization of Itaconic Acid Derivatives: Toward Functional Polymers with Controlled Molar Mass Distribution and Architecture. *Macromol Rapid Commun*, 42(4), 2000546. <https://doi.org/10.1002/marc.202000546>
- Stegmann, P., Londo, M., & Junginger, M. (2020). The circular bioeconomy: Its elements and role in European bioeconomy clusters. *Resour Conserv Recycl*, X, 6, 100029. <https://doi.org/10.1016/j.rcrx.2019.100029>
- Steiger, M. G., Punt, P. J., Ram, A. F. J., Mattanovich, D., & Sauer, M. (2016). Characterizing MttA as a mitochondrial cis-aconitic acid transporter by metabolic engineering. *Metabolic engineering*, 35, 95-104. <https://doi.org/10.1016/j.ymben.2016.02.003>
- Steiger, M. G., Wierckx, N., Blank, L. M., Mattanovich, D., & Sauer, M. (2017). Itaconic Acid – An Emerging Building Block. In *Industrial Biotechnology* (pp. 453-472). <https://doi.org/10.1002/9783527807833.ch15>
- Stoffels, P., Müller, M. J., Stachurski, S., Terfrüchte, M., Schröder, S., Ihling, N., Wierckx, N., Feldbrügge, M., Schipper, K., & Büchs, J. (2020). Complementing the intrinsic repertoire of *Ustilago maydis* for degradation of the pectin backbone polygalacturonic acid. *J Biotechnol*, 307, 148-163. <https://doi.org/10.1016/j.jbiotec.2019.10.022>
- Straathof, A. J. J., Wahl, S. A., Benjamin, K. R., Takors, R., Wierckx, N., & Noorman, H. J. (2019). Grand Research Challenges for Sustainable Industrial Biotechnology. *Trends Biotechnol*, 37(10), 1042-1050. <https://doi.org/10.1016/j.tibtech.2019.04.002>
- Strelko, C. L., Lu, W., Dufort, F. J., Seyfried, T. N., Chiles, T. C., Rabinowitz, J. D., & Roberts, M. F. (2011). Itaconic acid is a mammalian metabolite induced during macrophage activation. *J Am Chem Soc*, 133(41), 16386-16389. <https://doi.org/10.1021/ja2070889>
- Tabuchi, T., Sugisawa, T., Ishidori, T., Nakahara, T., & Sugiyama, J. (1981). Itaconic Acid Fermentation by a Yeast Belonging to the Genus *Candida*. *Agric biol chem*, 45(2), 475-479. <https://doi.org/10.1080/00021369.1981.10864534>
- Tan, E. C. D., & Lamers, P. (2021). Circular Bioeconomy Concepts—A Perspective. *Front Sustain*, 2, 701509. <https://doi.org/10.3389/frsus.2021.701509>
- Tanaka, Y., Aki, T., Hidaka, Y., Furuya, Y., Kawamoto, S., Shigeta, S., Ono, K., & Suzuki, O. (2002). Purification and Characterization of a Novel Fungal α -Glucosidase from *Mortierella alliaacea* with High Starch-hydrolytic Activity. *Biosci Biotechnol Biochem*, 66(11), 2415-2423. <https://doi.org/10.1271/bbb.66.2415>
- Tang, W. L., Li, Z., & Zhao, H. (2010). Inverting the enantioselectivity of P450pyr monooxygenase by directed evolution. *Chem Commun (Camb)*, 46(30), 5461-5463. <https://doi.org/10.1039/c0cc00735h>
- Teichmann, B., Linne, U., Hewald, S., Marahiel, M. A., & Böcker, M. (2007). A biosynthetic gene cluster for a secreted cellobiose lipid with antifungal activity from *Ustilago maydis*. *Mol Microbiol*, 66(2), 525-533. <https://doi.org/10.1111/j.1365-2958.2007.05941.x>
- Teleky, B. E., & Vodnar, D. C. (2019). Biomass-Derived Production of Itaconic Acid as a Building Block in Specialty Polymers. *Polymers (Basel)*, 11(6), 1035. <https://doi.org/10.3390/polym11061035>
- Teufel, F., Almagro Armenteros, J. J., Johansen, A. R., Gislason, M. H., Pihl, S. I., Tsigirigos, K. D., Winther, O., Brunak, S., von Heijne, G., & Nielsen, H. (2022). SignalP 6.0 predicts all five

- types of signal peptides using protein language models. *Nat Biotechnol*, 40(7), 1023-1025. <https://doi.org/10.1038/s41587-021-01156-3>
- Thakur, A., Sharma, K., & Goyal, A. (2019). α -L-Arabinofuranosidase: A Potential Enzyme for the Food Industry. In B. Parameswaran, S. Varjani, & S. Raveendran (Eds.), *Green Bio-processes: Enzymes in Industrial Food Processing* (pp. 229-244). Springer Singapore. https://doi.org/10.1007/978-981-13-3263-0_12
- Tsukamoto, S., Yoshida, T., Hosono, H., Ohta, T., & Yokosawa, H. (2006). Hexylitaconic acid: a new inhibitor of p53-HDM2 interaction isolated from a marine-derived fungus, *Arthrinium* sp. *Bioorg Med Chem Lett*, 16(1), 69-71. <https://doi.org/10.1016/j.bmcl.2005.09.052>
- Ullmann, L., Guntermann, N., Kohl, P., Schrodgers, G., Musgens, A., Francio, G., Leitner, W., & Blank, L. M. (2022b). Improved Itaconate Production with *Ustilago cynodontis* via Co-Metabolism of CO₂-Derived Formate. *J Fungi (Basel)*, 8(12), 1277. <https://doi.org/10.3390/jof8121277>
- Ullmann, L., Phan, A. N. T., Kaplan, D. K. P., & Blank, L. M. (2021). Ustilaginaceae Biocatalyst for Co-Metabolism of CO₂-Derived Substrates toward Carbon-Neutral Itaconate Production. *J Fungi (Basel)*, 7(2). <https://doi.org/10.3390/jof7020098>
- Ullmann, L., Wibberg, D., Busche, T., Rückert, C., Müsgens, A., Kalinowski, J., & Blank, L. M. (2022a). Seventeen Ustilaginaceae High-Quality Genome Sequences Allow Phylogenomic Analysis and Provide Insights into Secondary Metabolite Synthesis. *J Fungi (Basel)*, 8(3), 269. <https://doi.org/10.3390/jof8030269>
- van Maris, A. J., Konings, W. N., van Dijken, J. P., & Pronk, J. T. (2004). Microbial export of lactic and 3-hydroxypropanoic acid: implications for industrial fermentation processes. *Metabolic engineering*, 6(4), 245-255. <https://doi.org/10.1016/j.ymben.2004.05.001>
- Verified Market Research. (2022). *Itaconic Acid Market Size And Forecast*. Retrieved 27.11.2023 from <https://www.verifiedmarketresearch.com/product/itaconic-acid-market/> (Internet)
- Vihinen, M., & Mantsiila, P. (1989). Microbial Amylolytic Enzyme. *Crit Rev Biochem Mol Biol*, 24(4), 329-418. <https://doi.org/10.3109/10409238909082556>
- Vollmeister, E., Schipper, K., Baumann, S., Haag, C., Pohlmann, T., Stock, J., & Feldbrügge, M. (2012). Fungal development of the plant pathogen *Ustilago maydis*. *FEMS Microbiol Rev*, 36(1), 59-77. <https://doi.org/10.1111/j.1574-6976.2011.00296.x>
- Wan, J., He, M., Hou, Q., Zou, L., Yang, Y., Wei, Y., & Chen, X. (2021). Cell wall associated immunity in plants. *Stress Biol*, 1(1), 3. <https://doi.org/10.1007/s44154-021-00003-4>
- Watson, R., Carraro, C., Canziani, P., Nakicenovic, N., McCarthy, J., Goldemberg, J., & Hisas, L. (2016). *The Truth About Climate Change*. https://www.researchgate.net/publication/308750455_The_Truth_About_Climate_Change
- Wege, S. M., Gejer, K., Becker, F., Bölker, M., Freitag, J., & Sandrock, B. (2021). Versatile CRISPR/Cas9 Systems for Genome Editing in *Ustilago maydis*. *J Fungi (Basel)*, 7(2), 149. <https://doi.org/10.3390/jof7020149>
- Werpy, T., & Petersen, G. (2004). *Top value added chemicals from biomass: volume I--results of screening for potential candidates from sugars and synthesis gas*. U.S. Department of Energy (DOE). <https://doi.org/10.2172/926125>
- Wierckx, N., Agrimi, G., Lübeck, P. S., Steiger, M. G., Mira, N. P., & Punt, P. J. (2020). Metabolic specialization in itaconic acid production: a tale of two fungi. *Curr Opin Biotechnol*, 62, 153-159. <https://doi.org/10.1016/j.copbio.2019.09.014>

- Wierckx, N., Miebach, K., Ihling, N., Hussnaetter, K. P., Büchs, J., & Schipper, K. (2021). Perspectives for the application of Ustilaginaceae as biotech cell factories. *Essays in Biochemistry*, 65(2), 365-379. <https://doi.org/10.1042/ebc20200141>
- Willis, R. B., Montgomery, M. E., & Allen, P. R. (1996). Improved Method for Manual, Colorimetric Determination of Total Kjeldahl Nitrogen Using Salicylate. *J Agric Food Chem*, 44(7), 1804-1807. <https://doi.org/10.1021/jf950522b>
- Willke, T., & Vorlop, K. D. (2001). Biotechnological production of itaconic acid. *Appl Microbiol Biotechnol*, 56(3-4), 289-295. <https://doi.org/10.1007/s002530100685>
- Wong, D. W. S., Robertson, G. H., Lee, C. C., & Wagschal, K. (2007). Synergistic Action of Recombinant α -Amylase and Glucoamylase on the Hydrolysis of Starch Granules. *The Protein Journal*, 26(3), 159-164. <https://doi.org/10.1007/s10930-006-9057-9>
- Xiao, Z., Storms, R., & Tsang, A. (2006). A quantitative starch-iodine method for measuring alpha-amylase and glucoamylase activities. *Anal Biochem*, 351(1), 146-148. <https://doi.org/10.1016/j.ab.2006.01.036>
- Xu, D.-B., Madrid, C. P., Röhr, M., & Kubicek, C. P. (1989). The influence of type and concentration of the carbon source on production of citric acid by *Aspergillus niger*. *Appl Microbiol Biotechnol*, 30, 553-558. <https://doi.org/10.1007/BF00255358>
- Yeoman, C. J., Han, Y., Dodd, D., Schroeder, C. M., Mackie, R. I., & Cann, I. K. O. (2010). Chapter 1 - Thermostable Enzymes as Biocatalysts in the Biofuel Industry. In *Adv Appl Microbiol* (Vol. 70, pp. 1-55). Academic Press. [https://doi.org/10.1016/S0065-2164\(10\)70001-0](https://doi.org/10.1016/S0065-2164(10)70001-0)
- Zambanini, T., Hartmann, S. K., Schmitz, L. M., Buttner, L., Hosseinpour Tehrani, H., Geiser, E., Beudels, M., Venc, D., Wandrey, G., Büchs, J., Schwarzlander, M., Blank, L. M., & Wierckx, N. (2017c). Promoters from the itaconate cluster of *Ustilago maydis* are induced by nitrogen depletion. *Fungal Biol Biotechnol*, 4, 11. <https://doi.org/10.1186/s40694-017-0040-3>
- Zambanini, T., Hosseinpour Tehrani, H., Geiser, E., Merker, D., Schleese, S., Krabbe, J., Buescher, J. M., Meurer, G., Wierckx, N., & Blank, L. M. (2017a). Efficient itaconic acid production from glycerol with *Ustilago vetiveriae* TZ1. *Biotechnol Biofuels Bioprod*, 10, 131. <https://doi.org/10.1186/s13068-017-0809-x>
- Zambanini, T., Hosseinpour Tehrani, H., Geiser, E., Sonntag, C. K., Buescher, J. M., Meurer, G., Wierckx, N., & Blank, L. M. (2017b). Metabolic engineering of *Ustilago trichophora* TZ1 for improved malic acid production. *Metab Eng Commun*, 4, 12-21. <https://doi.org/10.1016/j.meten.2017.01.002>
- Zambanini, T., Kleineberg, W., Sarikaya, E., Buescher, J. M., Meurer, G., Wierckx, N., & Blank, L. M. (2016b). Enhanced malic acid production from glycerol with high-cell density *Ustilago trichophora* TZ1 cultivations. *Biotechnol Biofuels Bioprod*, 9, 135. <https://doi.org/10.1186/s13068-016-0553-7>
- Zambanini, T., Sarikaya, E., Kleineberg, W., Buescher, J. M., Meurer, G., Wierckx, N., & Blank, L. M. (2016a). Efficient malic acid production from glycerol with *Ustilago trichophora* TZ1. *Biotechnol Biofuels Bioprod*, 9, 67. <https://doi.org/10.1186/s13068-016-0483-4>
- Zarnack, K., Maurer, S., Kaffarnik, F., Ladendorf, O., Brachmann, A., Kämper, J., & Feldbrügge, M. (2006). Tetracycline-regulated gene expression in the pathogen *Ustilago maydis*. *Fungal Genet Biol*, 43(11), 727-738. <https://doi.org/10.1016/j.fgb.2006.05.006>
- Zoghلامي, A., & Paes, G. (2019). Lignocellulosic Biomass: Understanding Recalcitrance and Predicting Hydrolysis. *Front Chem*, 7, 874. <https://doi.org/10.3389/fchem.2019.00874>

7. Appendix

7.1. Appendix to 3.1: An Optimized *Ustilago maydis* for Itaconic Acid Production at Maximal Theoretical Yield

Table S1: Oligonucleotides used for deletion and overexpression constructs.

Primer name	Sequence (5'-3') and description
JB-89	ctcgagttttcagcaagatCCGATCGTGTTAGGACAC Amplification of 5'-UTR flank for generation of <i>fuz7</i> deletion construct
JB-90	acttcgtgccCGTGAAACGTTGCAAAACAG Amplification of 5'-UTR flank for generation of <i>fuz7</i> deletion construct
JB-91	acgtttcacgGGCCAGAAGTTCCTATTC Amplification of FRT_m1-HygR-FRT_m1 cassette for generation of <i>fuz7</i> deletion construct
JB-92	tctcagtcggCCCGGGAAGTTCCTATAC Amplification of FRT_m1-HygR-FRT_m1 cassette for generation of <i>fuz7</i> deletion construct
JB-93	acttcccgggCCGACTGAGAGATTATGGTC Amplification of 3'-UTR flank for generation of <i>fuz7</i> deletion construct
JB-94	aggagatctttagaaagataATCGGAACCGTGACCTG Amplification of 3'-UTR flank for generation of <i>fuz7</i> deletion construct
JB-126_fwd	ATGGCTTCTCAATCGCAC Amplification of reference gene UMAG_02592 during qRT-PCR
JB-127_rev	CCTGGTGTGAGGATGAG Amplification of reference gene UMAG_02592 during qRT-PCR
JB-128_fwd	ACATCGTCAAGGCTATCG Amplification of reference gene UMAG_03726 during qRT-PCR
JB-129_rev	AAAGAACACCGGACTTGG Amplification of reference gene UMAG_03726 during qRT-PCR
JB-132_fwd	AACACGTTCAACTGCGTCAA Amplification of <i>mttA</i> during qRT-PCR
JB-133_rev	GAACATGATGGCCGAGGTG Amplification of <i>mttA</i> during qRT-PCR
HT-4a_rev	ACAGACGTCGCGGTGAGTTC Verification of FRT-HygR-cassette based insertions
HT-202_fwd	TCCTGCGTCAGTCGTCCAAC Verification of P_{etef} <i>mttA</i> integration
HT-203_fwd	GTCCGAGGGCAAAGGAATAG Verification of <i>fuz7</i> deletion
HT-210_fwd	TCGCTGTTAGACACAACCTG Amplification of <i>fuz7</i> deletion construct
HT-210a	TCGGTGTGCGGCGATTCTG Verification of <i>fuz7</i> deletion
HT-211	CCGTGTACCTGGCTGTGTAG Amplification of <i>fuz7</i> deletion construct
HT-220	GATTCTGTGGGACAAGAAGC Verification of <i>fuz7</i> deletion
T_{nos}	CAAGACCGGCAACAGGATTC Verification of P_{etef} <i>mttA</i> integration

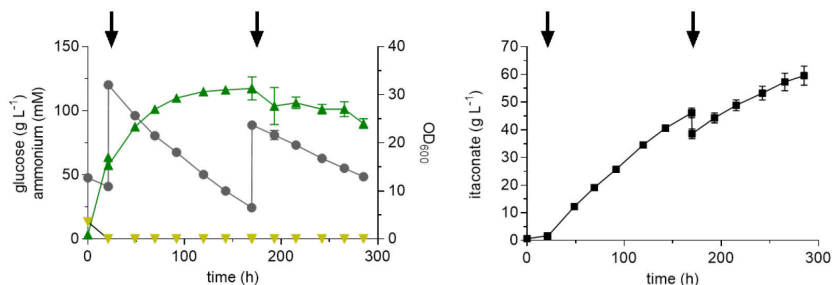


Figure S1: Low cell-density pulsed fed-batch fermentations of *U. maydis* strain K14.

(A) Concentration of glucose (●), ammonium (▼), and OD₆₀₀ (▲) and (B) concentration of itaconate (■) during fermentation in bioreactors containing batch medium with 15 mM NH₄Cl and 50 g L⁻¹ glucose (n = 3 biological replicates). The pH was kept at 6.5 by automatic titration with 5 M NaOH. Arrows indicate the addition of 80 g glucose.

Table S2: Production parameters of two engineered *U. maydis* MB215 strains in two different types of fed-batch fermentations.

Fermentations with 75 mM NH₄Cl, 200 g L⁻¹ glucose, and CaCO₃ as buffer (n = 2 biological replicates) and fermentations with 15 mM NH₄Cl, 50 g L⁻¹ glucose, and NaOH as pH control reagent (n = 3 biological replicates). a) maximum ITA titer; b) overall ITA productivity; c) yield ITA per consumed glucose.

Cultivation condition	Feed	Strain	Titer _{max} ^a (g L ⁻¹)	q _p ^b (g L ⁻¹ h ⁻¹)	Y _{P/S} ^c (g _{ITA} g _{GLC} ⁻¹)
200 g L ⁻¹ glucose, 75 mM NH ₄ Cl, CaCO ₃	Pulsed	<i>U. maydis</i> MB215 $\Delta cyp3$ $\Delta fuz7 \Delta P_{ria1}::P_{etef} P_{etef} mttA$	220.3	0.46	0.33
	Pulsed	<i>U. maydis</i> strain K14	205.6 ± 1.1	0.43 ± 0.00	0.32 ± 0.00
50 g L ⁻¹ glucose, 15 mM NH ₄ Cl, NaOH	Pulsed	<i>U. maydis</i> MB215 $\Delta cyp3$ $\Delta fuz7 \Delta P_{ria1}::P_{etef} P_{etef} mttA$	35.9 ± 1.5	0.12 ± 0.00	0.20 ± 0.01
	Pulsed	<i>U. maydis</i> strain K14	59.6 ± 5.9	0.21 ± 0.02	0.42 ± 0.02
	Continuous	<i>U. maydis</i> strain K14	75.7 ± 1.3	0.24 ± 0.01	0.66 ± 0.02

7.2. Appendix to 3.2: Balancing pH and Yield: Exploring Itaconic Acid Production in *Ustilago cynodontis* from an Economic Perspective

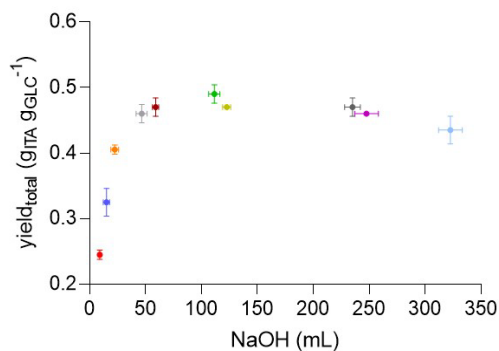


Figure S2: Scatter plot of yield versus volumes of 5 M NaOH.

The colors indicate fermentations at the pH values as shown in Figure 16 A-C.

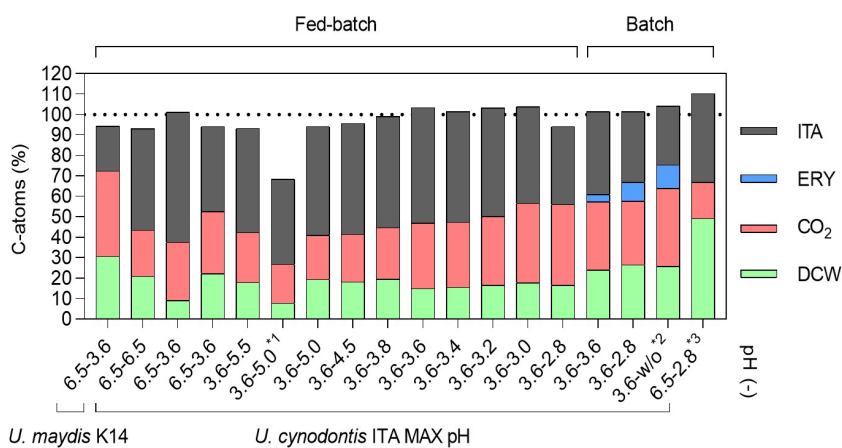


Figure S3: Carbon balance of all fermentations.

*1: with a prolonged feeding phase. *2: without pH control after the growth phase; final pH value of 2.1.

*3: with thick juice as a sole carbon source.

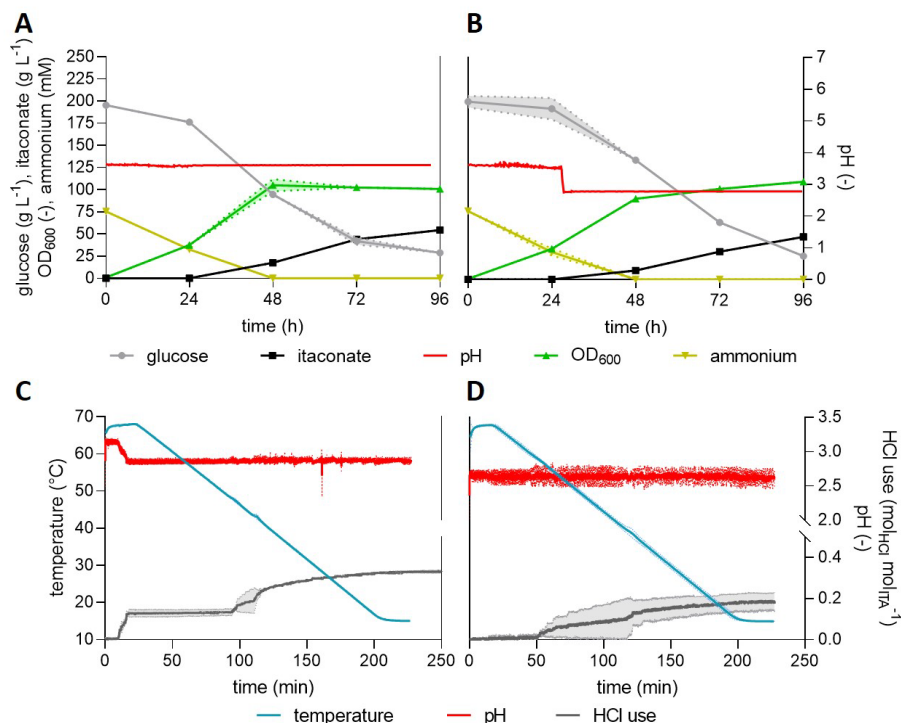


Figure S4: Crystallization of ITA from batch fermentations conducted at pH 3.6 and pH 2.8.

Bioreactor cultivations of *U. cynodontis* ITA MAX pH were performed in batch medium with 75 mM NH₄Cl and approximately 200 g L⁻¹ glucose (n = 2 biological replicates). During the fermentation at pH 3.6, the pH was maintained at a constant level throughout the entire fermentation process (A). For the fermentation at pH 2.8, the pH was controlled at 3.6 for approximately 30 h and was then allowed to naturally decrease to 2.8 (B). Following fermentation, the cell-free broths with pH 3.6 (C) and pH 2.8 (D) were concentrated by rotary evaporation using an IKA RV10 auto Hb rotary evaporator and an IKA VACSTAR digital vacuum pump (IKA Werke GmbH & Co. KG, Staufen, Germany) at 60–65 °C and 100 mbar. Afterwards, the crystallization was performed with an EasyMax 102 Titration calorimeter (Mettler Toledo, Columbus, OH, USA) equipped with a SIMDOS O2 FEM 1.02 S pump (KNF Holding AG, Sursee, Switzerland) and an InLab Semi Micro pH electrode (Mettler Toledo, Columbus, OH, USA) (n = two technical replicates). The cooling rate of 0.3 K starting from 68 °C to reach 15 °C was applied and the pH was controlled at 2.8 by addition of 5 M HCl. Crystals were filtered from mother liquor with a Whatman Grade 50 Thin filter (Cytiva Europa GmbH, Freiburg im Breisgau, Germany) and afterwards dried in a VT 6060 VACUTHERM vacuum oven (Fisher Scientific GmbH, Schwerte, Germany) at 200 mbar vacuum and 40 °C for 72 h.

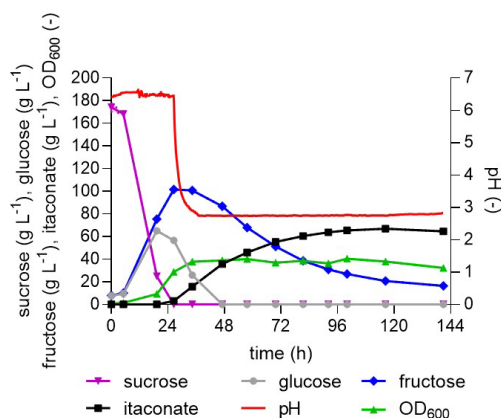


Figure S5: High cell-density batch fermentation of *U. cynodontis* ITA MAX pH with thick juice as a sole carbon source.

Bioreactor cultivation was performed in batch medium with 75 mM NH₄Cl and approximately 200 g L⁻¹ sucrose from thick juice (n = 1 biological replicate measured as technical triplicates). The pH was controlled by automatic titration with 5 M NaOH. After approximately 28 h, the pH was allowed to naturally drop from pH 6.5 to pH 2.8 through the production of ITA. Upon reaching this highly acidic pH value, ITA production continued up to a titer of approximately 65 g L⁻¹ at a productivity of 0.46 g L⁻¹ h⁻¹ and a yield of 0.4 g_{ITA} g_{GLC}⁻¹. These values are higher than the ones achieved on pure glucose. This might be due to the fact that thick juice includes some other compounds such as amino acids resulting in fitter biomass and a higher carbon load.

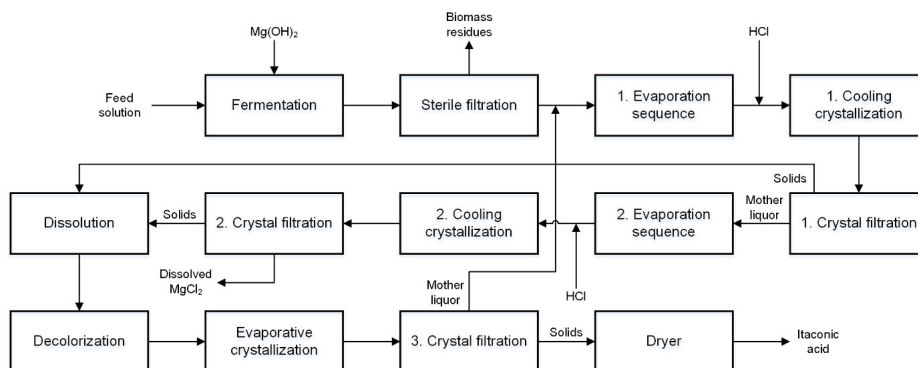


Figure S6: Block flow diagram of multiple crystallization process (simplified from Saur et al. (2023)).

Table S3: Feeding profile with 70 % w/v glucose solution during high cell-density fed-batch fermentation with a prolonged feeding phase of *U. cynodontis* ITA MAX pH (Figure 17).

Time (h)	Feed rate (g h ⁻¹)
32-53	2.2
53-120	1.5
120-144	1.0
144-173	0.75
173-316	0.5
316-648	0.25

7.3. Appendix to 3.3: Establishing an Itaconic Acid Production Process with *Ustilago* species on the Low-cost Substrate Starch

MTRPTSQRRSKPMVLLGSAGLALLLICLCAFSSNANA³⁸ ASVARSLIGLDKETNRLEPRAVSSSYAYQR
 MIANIGGASSAGGSQVNPVQTGAVIASPSTAGPDYFYSWVRDAALTMKVVISQPTLDRTLVTNYANA
 EKVHQQNAAKSSSSQGEKFNADGSLFTGPWGRPQLDAGLRASSLMFAKRIGLNDPFTTSTLYQ
 SSLSGGSLIKTDLEYVAHNWQSSGFDLWEEVQGTHTFFTLIVQYRSLIDGAKFATSMNDPGAATYYNQ
 AAIAKAKLQAFWDSNNGYIQAYQVSGRSGLDSCSVMLGALKGWDTTNTAAVDASVFGPASDKVLAT
 HRKYVDSFRSLYSINKNAAPPAAGTGRYAEDVFNGVSTSGQNPWYICTLAAAEVLNTAVAVSNSRGS
 LSVTSTSLPFYKQFSSATTGTFNSSGSSQYTALTSGMRAMAKGFVDIVNSHAWPNGSLNEEFNRDTG
 FNQGGARDLTWSYAAFVSNDLASQGFYLV

Molecular weight	= 53.3 kDa, 502 aa (9 Trp, 20 Tyr and 4 Cys)
Potential N-linked glycosylation sites	= 2 (bold/underlined)
Theoretical pI	= 8.95
-/+ aa	= 33/39

Figure S7: Amino acid sequence of putative glucoamylase encoded by the gene with the GenBank accession number CAKMX010000014 (region: 83686 to 85185) in *U. cynodontis* ITA MAX pH identified by LC-MS/MS.

The peptide confidences are ranged by a color code - black: no match; red: 0-50; yellow: 50-95; green: 95-100. The first 38 aa are predicted as the signal peptide according to Teufel et al. (2022).

MRFFAKALGLVSLAMSASATPLQKR²⁶ DLGPVTIYTPPSNYTSDRSLYARTLMLTVNDNTGTLSTWE
 NYSGGKTWFPPIRSTDHGYTWPSPSAVTDQVNGWGLRYQPFLEYLKQSFAGYPAGSILLAGNSIPED
 LSKTQLDLYSTDKGKTWKFLSHIAAGGKAVPNNGETPVWEPFLLVNNGQLICYSDORDPKYGQKL
 VHQTTSDLKNWGSVVDVTEFSYARPGMPVVAQMGDGNVIMTFEYGGAGEGNFAVYYKISNDPFS
 WADKKQQLVKATDGTGTPRSPYVMTWPIGSRSGATANGTVVVSAYTDTGLYLNRANGAPNAWTRL
 VSNAPAAYSREVTGKFNPKDIMIAGSGAIGQGSTNRVTFESARDVNGCATC

Molecular weight	= 41.8 kDa, 385 aa (10 Trp, 22 Tyr and 3 Cys)
Potential N-linked glycosylation sites	= 3 (bold/underlined)
Theoretical pI	= 8.72
-/+ aa	= 29/33

Figure S8: Amino acid sequence of putative exo- α -1,5-L-arabinofuranosidase encoded by the gene with the GenBank accession number CAKMX010000018 (region 665749 to 665919, 666077 to 666352, and 666447 to 667148) in *U. cynodontis* ITA MAX pH identified by LC-MS/MS.

The peptide confidences are ranged by a color code - black: no match; red: 0-50; yellow: 50-95; green: 95-100. The first 26 aa are predicted as the signal peptide according to Teufel et al. (2022).

MTRLRLRAVVVGLVASFSDVLT²³ YPVQDDHVNRRLLPGLGGSTDDTYDYVVVGGGSGMTLAARLSENKGV
 VAVLEAGIDYRSNLVNQQLVDTPGYDTFGVGASPSDWVNGNIDWGFVTEGEPGYDNRKVKYAR**GK**CIGGSSAR
 NFMLYHRPPKDAQQTWVSLTGDNQWSFDNLPYYQKSFTAFGPR**HD**IRKDDPPAQYNPAFFGNPGPVSVGF
 NYAQPFSGPLLSNLEVGVPSTSDMSSGNILGAQYSTVTVEATNGKRATSRSFYQQAQDEKRANLVIFEALAK
 KVVFDTSGRQPTAVAVDYTLPGFVKKT**IK**ARKEIIISAGAFQSPQLLMVSGIGPADQLKAQNPVLVENSNGQH
 QDHVFFGPPTYTVNIDPTKEANDPFLAASIADFNLRNRGIFTNNVADLIGFEKW**NT**YLDSDIAGALK**NP**SDWP
 EIEYLSGPGYIGDFTNLVINNIIVNGLTQQFASLLVAIVAPISEGSVTLKSADTADLPAIRPNWLSSPYDQQVAIAAFK
 RARQVFAANAMKSTRTSD**NET**FPGFVATDDQILASIRKNLMTVWHAASTCR**AR**NAQSGVLDNSFKVFGVDG
 LRVVDASSFPRLLPGHPQAVCYMIAERAADIIAANK

Molecular weight	= 68.4 kDa, 632 aa (8 Trp, 20 Tyr and 3 Cys)
Potential N-linked glycosylation sites	= 3 (bold/underlined)
Theoretical pI	= 6.04
-/+ aa	= 58/54

Figure S9: Amino acid sequence of putative aryl-alcohol oxidase encoded by the gene with GenBank accession number CAKMX010000011 (region 416218 to 416544 and 416702 to 418270) in *U. cynodontis* ITA MAX pH identified by LC-MS/MS.

The peptide confidences are ranged by a color code - black: no match; red: 0-50; yellow: 50-95; green: 95-100. The first 23 aa are predicted as the signal peptide according to Teufel et al. (2022).

Table S4: Oligonucleotides used for the generation of deletion and overexpression constructs.

Primer name	Sequence (5'-3') and description
PE1_fwd	gttcttctagGATCACTCTCGGCATGGAC Amplification of pJET1.2 backbone for the generation of <i>U. cynodontis</i> α -amylase overexpression construct
PE2_rev	gcgagacgaaGATAATAATGGTTTCTTAGACGTCAG Amplification of pJET1.2 backbone for the generation of <i>U. cynodontis</i> α -amylase overexpression construct
PE3_fwd	cattattatcTTCGTCTCGCGCTTTCG Amplification of the <i>P_{etef}</i> promotor for the generation of <i>U. cynodontis</i> α -amylase overexpression construct
PE4_rev	aggaagccatGATCCCGTGGATGATGTTGTC Amplification of the <i>P_{etef}</i> promotor for the generation of <i>U. cynodontis</i> α -amylase overexpression construct
PE5_fwd	ccacgggatcATGGCTTCTCTGCCAAC Amplification of the α -amylase gene for the generation of <i>U. cynodontis</i> α -amylase overexpression construct
PE6_rev	gagagtgcctCTAGAAGAACTGACGGTGC Amplification of the α -amylase gene for the generation of <i>U. cynodontis</i> α -amylase overexpression construct
PE7_fwd	cagactgactggATCTTTCTAGAAGATCTCCTAC Amplification of pJET1.2 backbone for the generation of UMAG_04064 deletion construct
PE8_rev	tgaattgattctATCTTGCTGAAAACTCG Amplification of pJET1.2 backbone for the generation of UMAG_04064 deletion construct
PE9_fwd	tttcagcaagatAGAATCAATTCAAGCGGTG Amplification of 5'-UTR flank for the generation of UMAG_04064 deletion construct
PE10_rev	ggcaagcttcgCGGCTTCAAGATCGTGGTTAAC Amplification of 5'-UTR flank for the generation of UMAG_04064 deletion construct
PE11_fwd	gatcttgaagccCGCGAAGCTTGCCGGCAG Amplification of G418R cassette for the generation of UMAG_04064 deletion construct
PE12_rev	aagtggagatgcGCCGACTCCTACAGCTTG Amplification of G418R cassette for the generation of UMAG_04064 deletion construct
PE13_fwd	taggagtgcggcGATATCTCCACTTGCCGG Amplification of 3'-UTR flank for the generation of UMAG_04064 deletion construct
PE14_rev	ctctagaaagatCCAGTCAGTCTGTCAGTC Amplification of 3'-UTR flank for the generation of UMAG_04064 deletion construct
PE15_fwd	tgttttgcctaATCTTTCTAGAAGATCTCCTAC Amplification of pJET1.2 backbone for the generation of UMAG_02740 deletion construct
PE16_rev	ttgcgatgcttctATCTTGCTGAAAACTCG Amplification of pJET1.2 backbone for the generation of UMAG_02740 deletion construct
PE17_fwd	tttcagcaagatAGAAGCATCGCAACGCAAG Amplification of 5'-UTR flank for the generation of UMAG_02740 deletion construct
PE18_rev	gcaagcttcgAAGATTCCACGATGCTATAAC Amplification of 5'-UTR flank for the generation of UMAG_02740 deletion construct
PE19_fwd	tcgtgggaatctCGCGAAGCTTGCCGGCAG Amplification of G418R cassette for the generation of UMAG_02740 deletion construct
PE20_rev	ggcctcctcaagGCCGACTCCTACAGCTTG Amplification of G418R cassette for the generation of UMAG_02740 deletion construct
PE21_fwd	taggagtgcggcCTTGAGGAGGCCCAATC Amplification of 3'-UTR flank for the generation of UMAG_02740 deletion construct
PE22_rev	ctctagaaagatTAGGCAAAACCAAGACATGC Amplification of 3'-UTR flank for the generation of UMAG_02740 deletion construct

7.4. Appendix to 3.4: Production and Characterization of the Itaconic Acid-derived Compounds 2-Hydroxyparaconic and Itatartaric Acid

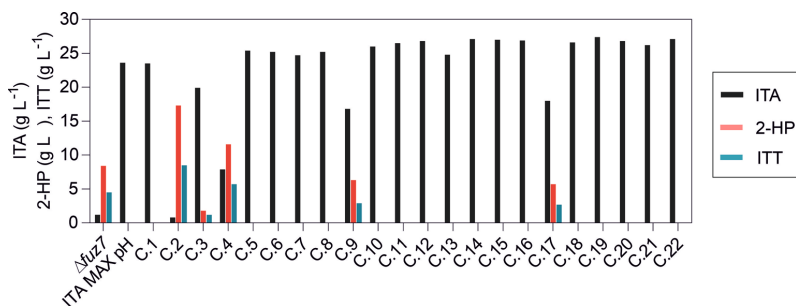


Figure S10: Initial screening of 22 clones in System Duetz plates – endpoint measurement after 240 h. Several clones (22) were cultivated in System Duetz plates in MTM with 15 mM NH_4Cl , 30 mM MES pH 6.5, and 50 g L^{-1} glucose (n = 1 biological replicate). ITA (black bar), 2-HP (green bar) and ITT (orange bar).

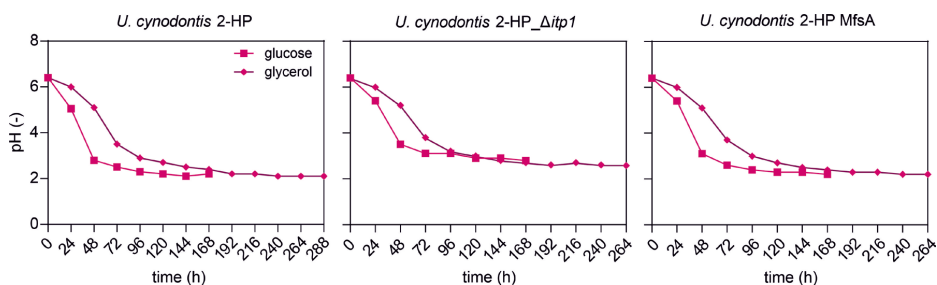


Figure S11: pH values during System Duetz microcultivations of *U. cynodontis* 2-HP, *U. cynodontis* 2-HP_Δitp1, and *U. cynodontis* 2-HP MfsA.

Cultivations were performed in System Duetz plates in MTM medium with 15 mM NH_4Cl , 30 mM MES pH 6.5, and 50 g L^{-1} glucose or 50 g L^{-1} glycerol (n = 2 biological replicates).

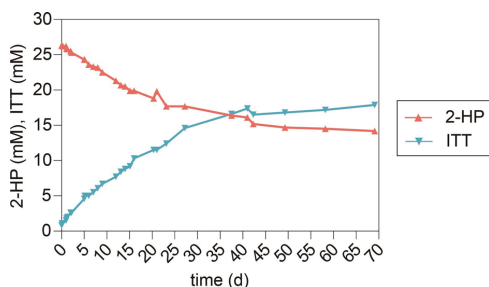


Figure S12: Non-enzymatic equilibration between 2-HP and ITT under acidic conditions (pH 2.3) at room temperature.

The purified 2-HP was dissolved in ddH₂O to approximately 26 mM. No other products were observed by HPLC during this equilibration.

Table S5: Oligonucleotides used for deletion, exchange and overexpression constructs.

Primer name	Sequence (5'-3') and description
PE23_fwd	gcctgagtggccTCTTGATATATCATATCGTTCTTTCC Amplification of <i>cyp3</i> cassette for the generation of <i>cyp3</i> overexpression construct
PE24_rev	gaactctggccGGTCGGTGATGTATG Amplification of <i>cyp3</i> cassette for generation the of <i>cyp3</i> overexpression construct
PE25_fwd	atccacaccgaccGGCCAGAAGTCTCTATTCTCAAG Amplification of FRT_M2-NatR cassette for the generation of <i>cyp3</i> overexpression construct
PE26_rev	tgatatatcaagaGGCCACTCAGGCCAGAAG Amplification of FRT_M2-NatR cassette for the generation of <i>cyp3</i> overexpression construct
PE27_fwd	ctgagtggccTCTCTTCTCGCCTCTG Amplification of 5'-UTR flank for the generation of <i>itp1</i> deletion construct
PE28_rev	ctagaaagatTGCCAGCAGAGTCAGAGAG Amplification of 5'-UTR flank for the generation of <i>itp1</i> deletion construct
PE29_fwd	tcagcaagatGCTGGTGCCAGCTCTGTATATG Amplification of 3'-UTR flank for the generation of <i>itp1</i> deletion construct
PE30_rev	actctggccGTCGAGGACGTTGTTGTG Amplification of 3'-UTR flank for the generation of <i>itp1</i> deletion construct
PE31_fwd	tctgtcgcaATCTTTCTAGAAGATCTCCTAC Amplification of pJET1.2 backbone for the generation of <i>itp1</i> deletion construct
PE32_rev	tggcaccagcATCTTGCTGAAAACTCG Amplification of pJET1.2 backbone for the generation of <i>itp1</i> deletion construct
PE33_fwd	cgtcctcgacGGCCAGAAGTCTATTCTCTATAAAG Amplification of FRT_M7 cassette for the generation of <i>itp1</i> deletion construct
PE34_rev	aggaagaggaGGCCACTCAGGCCAGAAG Amplification of FRT_M7 cassette for the generation of <i>itp1</i> deletion construct
PE35_fwd	accatggcgtCGCGAAGCTTGCCGGCAG Amplification of G418R cassette for the generation of <i>itp1</i> deletion construct
PE36_rev	tctgacttgcGCCCACTCTACAGCTTG Amplification of G418R cassette for the generation of <i>itp1</i> deletion construct
PE37_fwd	cgtcctcgacATGGGTACGGCGACACC Amplification of <i>mfsA</i> cassette for the generation of <i>itp1::mfsA</i> exchange construct
PE38_rev	aagcttcgcaACTATAGGGAGACGGCAGATC Amplification of <i>mfsA</i> cassette for the generation of <i>itp1::mfsA</i> exchange construct
PE39_fwd	ggagtgcggcTCCTCTTCTCGCCTCTG Amplification of backbone for the generation of <i>itp1::mfsA</i> exchange construct
PE40_rev	cgtgacccatGTCGAGGACGTTGTTGTG Amplification of backbone for the generation of <i>itp1::mfsA</i> exchange construct
PE41_fwd	tcctatagtCGCGAAGCTTGCCGGCAG Amplification of G418R cassette for the generation of <i>itp1::mfsA</i> exchange construct
PE42_rev	aggaagaggaGCCGCACTCTACAGCTTG Amplification of G418R cassette for the generation of <i>itp1::mfsA</i> exchange construct
PE43_fwd	acgctaaaagtaagccgct Amplification of <i>cyp3</i> during qPCR
PE44_rev	ggatggcgatttctcaca Amplification of <i>cyp3</i> during qPCR
PE45_fwd	cgtctacattcacgcttgcg Amplification of reference gene <i>tad1</i> during qPCR
PE46_rev	agtgcagccgaagtccaatt Amplification of reference gene <i>tad1</i> during qPCR
PE47_fwd	ttgatcttgcgagccgaa Amplification of reference gene <i>rdx1</i> during qPCR
PE48_rev	agcgcgatctatccgtcaag Amplification of reference gene <i>rdx1</i> during qPCR

Acknowledgements

An erster Stelle möchte ich mich bei Prof. Dr. Nick Wierckx bedanken, der mir die Möglichkeit gegeben hat, an diesem spannenden und aktuellen Projekt zu arbeiten und mich stets mit Ideen und anregenden Diskussionen unterstützt hat. Weiterhin möchte ich mich bei Prof. Dr. Michael Feldbrügge für die Übernahme der Zweitbetreuung bedanken.

Des Weiteren möchte ich mich bei allen Kooperationspartnern des Glaukos und UpRePP Projektes für die hervorragende Zusammenarbeit und die vielen aufschlussreichen Projekttreffen bedanken. Ein besonderer Dank geht auch an Dr. Benedikt Wynands, der mir immer mit Rat und Tat zur Seite stand.

Danke auch an meine Studenten Leona Deuster und Felicia Zlati für ihre Unterstützung im Rahmen ihrer Abschlussarbeiten. Außerdem möchte ich mich bei meiner Arbeitsgruppe für die super Arbeitsatmosphäre bedanken. Ein ganz besonderer Dank geht dabei an Yannic Ackermann, Jan de Witt, Thorsten Lechtenberg und Thomas Konjetzko, die in den letzten vier Jahren zu guten Freunden und Sportkameraden geworden sind.

Zu guter Letzt möchte ich von ganzem Herzen meiner Familie danken, die mich auf allen meinen Wegen unterstützt und an mich geglaubt hat. Ein besonderer Dank gilt auch meiner Freundin Larissa für die vielen fachlichen Diskussionen, motivierenden Worte und die Unterstützung in allen anderen Lebensbereichen.

Eidesstattliche Erklärung

Hiermit versichere ich an Eides Statt, dass die Dissertation von mir selbständig und ohne unzulässige fremde Hilfe unter Beachtung der „Grundsätze zur Sicherung guter wissenschaftlicher Praxis an der Heinrich-Heine-Universität Düsseldorf“ erstellt worden ist. Die Dissertation wurde in der vorgelegten oder in ähnlicher Form noch bei keiner anderen Institution eingereicht. Ich habe bisher keine erfolglosen Promotionsversuche unternommen.

Philipp Ernst

Band / Volume 279

Rare-earth atoms on two-dimensional materials: ab initio investigation of magnetic properties

J. P. Carbone (2024), 235 pp

ISBN: 978-3-95806-740-0

Band / Volume 280

Communities of Niche-optimized Strains (CoNoS) – a novel concept for improving biotechnological production

R. Zuchowski (2024), VIII, 168 pp

ISBN: 978-3-95806-743-1

Band / Volume 281

Enabling mixed microbial upcycling of plastic monomers

Y. S. Ackermann (2024), XVI, 203 pp

ISBN: 978-3-95806-749-3

Band / Volume 282

Folding and structural studies of *saccharomyces cerevisiae* Phosphoglycerate Kinase

N. Bustorff (2024), xxvi, 126 pp

ISBN: 978-3-95806-754-7

Band / Volume 283

The role of cellular development in multicellular antiphage defense of *Streptomyces*

T. Luthe (2024), vi, 173 pp

ISBN: 978-3-95806-768-4

Band / Volume 284

Probing the Transformation from Transition Metal Complexes to Extended Two-Dimensional Nanostructures

D. Baranowski (2024), XII, 103 pp

ISBN: 978-3-95806-772-1

Band / Volume 285

Neutron Scattering

Lectures of the JCMS Laboratory Course held at Forschungszentrum Jülich and at the Heinz-Maier-Leibnitz Zentrum Garching

edited by S. Förster, K. Friese, M. Kruteva, S. Nandi, M. Zobel, R. Zorn (2024), ca. 365 pp

ISBN: 978-3-95806-774-5

Band / Volume 286

Ab initio investigation of intrinsic antiferromagnetic solitons

Amal Jawdat Nayef Aldarawsheh (2024), xv, 164 pp

ISBN: 978-3-95806-785-1

Band / Volume 287

Understanding the dynamics of Plant-Bacteria-Bacteriophage interactions as a means to improve plant performance

S. H. Erdrich (2024), ix, 176 pp

ISBN: 978-3-95806-791-2

Band / Volume 288

**Prediction of Magnetic Materials for Energy and Information
Combining Data-Analytics and First-Principles Theory**

R. Hilgers (2024), xv, 215 pp

ISBN: 978-3-95806-795-0

Band / Volume 289

Biodegradation and microbial upcycling of plastics

J. de Witt (2025), XVI, 259 pp

ISBN: 978-3-95806-804-9

Band / Volume 290

Practical Methods for Efficient Analytical Control in Superconducting Qubits

B. Li (2025), 202 pp

ISBN: 978-3-95806-807-0

Band / Volume 291

Ab initio investigation of topological magnetism in two-dimensional van der Waals heterostructures

N. Abuawwad (2025), xviii, 135 pp

ISBN: 978-3-95806-808-7

Band / Volume 292

Tolerance engineering of Pseudomonas for the efficient conversion and production of aldehydes

T. Lechtenberg (2025), XVI, 185 pp

ISBN: 978-3-95806-817-9

Band / Volume 293

Exploring the process window for production of itaconic, 2-hydroxyparaconic, and itatartaric acid with engineered *Ustilago* strains

P. Ernst (2025), x, 145 pp

ISBN: 978-3-95806-825-4

Schlüsseltechnologien / Key Technologies
Band / Volume 293
ISBN 978-3-95806-825-4